Static Electric Dipole Polarizabilities of Atoms and Molecules

A thesis presented in partial fulfillment of the requirements
for the degree of
Doctor of Philosophy
in
Chemistry

at Massey University, Albany
New Zealand.

Ivan S. Lim

2004

Candidate's Declaration

This is to certify that research carried out for my Doctoral thesis entitled "*Static Electric Dipole Polarizabilities of Atoms and Molecules*" in the Institute of Fundamental Sciences, Massey University at Albany, New Zealand is my work and that the thesis material has not been used in part or in whole for any other qualification.

Candidate's Name: Ivan S. Lim

Signature: 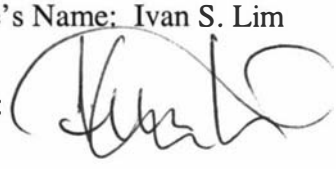

Date: July 20, 2004

Supervisor's Declaration

This is to certify that research carried out for the Doctoral thesis entitled "*Static Electric Dipole Polarizabilities of Atoms and Molecule*" was done by Mr. Ivan S. Lim in the Institute of Fundamental Sciences, Massey University at Albany, New Zealand. The thesis material has not been used in part or in whole for any other qualification, and I confirm that that the candidate has pursued the course of study in accordance with the requirements of the Massey University regulations.

Supervisor's Name: Prof. Peter Schwerdtfeger

Signature: 

Date: July 20, 2004

Abstract

The static dipole polarizabilities and ionization potentials of the first and second main group elements, including the charged ions, are obtained from all-electron relativistic coupled-cluster theory using a scalar relativistic Douglas-Kroll Hamiltonian. Spin-orbit coupling effects are investigated using a fully relativistic four-component Dirac-Coulomb-Hartree-Fock scheme followed by a second-order many-body perturbation treatment to account for electron correlation. Periodic trends in the dipole polarizabilities and the ionization potentials are discussed. In each case, a detailed discussion on electron correlation and relativistic effects are given. A relationship for relativistic and electron correlation effects between the dipole polarizability and the ionization potential is established. Particular attention is paid to the evaluation of a near basis set limit quality of the dipole polarizabilities. This is accomplished by the evaluation of all-electron basis sets used, followed by an extensive study on the convergence behavior of the dipole polarizabilities with respect to a finite basis set expansion. The present all-electron dipole polarizabilities are believed to be very precise, especially for charged ions where the availability of experimental values are limited. Scalar relativistic small-core pseudopotentials are fitted and their performance is tested in terms of static dipole polarizabilities and ionization potentials. It is demonstrated that the small-core definition of the pseudopotential (nine-valence electron for the main group 1 and ten-valence electron for the main group 2 elements) enables us to safely omit core-valence correlation without scarifying accuracy. Following atomic dipole polarizabilities, applications are made to molecules starting with alkali dimers and their singly charged ions. The scalar relativistic pseudopotentials of this study are used to calculate equilibrium bond lengths, dissociation energies, vibrational frequencies and the dipole polarizabilities of these dimers. The change in the molecular dipole polarizabilities from the corresponding atomic dipole polarizabilities are discussed in terms of molecular bonding models. Simple ammonia complexes of the alkali-metals and their singly charged ions are studied. The equilibrium geometries, dissociation energies, harmonic vibrational frequencies as well as the dipole polarizabilities of these complexes are given.

Acknowledgments

The biggest thanks goes to Prof. Peter A. Schwerdtfeger for his encouragement and patience. Also, big thanks to Prof. Hermann Stoll and Prof. Peter Botschwina for inviting me to work in their research group and to a lot of people including Dr. Markus Pernpointner, Dr. Jon K. Laerdahl, Dr. Ralf Wesendrup, Dr. Holger Hermann, Dr. Robert Krawczyk, Nicola Gaston, and Behnam Assadollahzadeh. And of course to my parents for their continuing support and love and for never giving up on me. I also like to thank my partners in crime, Richard Selby Inkster and Mason Kailahi for being my only brothers. Last but not least I thank my other half, Carey F. Garland for being the true inspiration of my life.

Contents

Some of the work described in this thesis has been published already. The relevant references are:

[1] Ivan S. Lim, Markus Pernpointner, Michael Seth, Jon K. Laerdahl, and Peter Schwerdtfeger, *Relativistic coupled-cluster static dipole polarizabilities of the alkali metals from Li to element 119*, Phys. Rev. A **60**, 2822-2828 (1999).

[2] Ivan S. Lim, Jon K. Laerdahl, and Peter Schwerdtfeger, *The static electric dipole polarizability of* Rb^+, J. Phys. B **33**, L91-L96 (2000).

[3] Ivan S. Lim, Jon K. Laerdahl, and Peter Schwerdtfeger, *Fully relativistic coupled-cluster static dipole polarizabilities of the positively charged alkali ions from* Li^+ *to element* 119^+, J. Chem. Phys. **116**, 172-178 (2002).

[4] Ivan S. Lim and Peter Schwerdtfeger, *Four-component and scalar relativistic Douglas-Kroll calculations for static dipole polarizabilities of the alkaline-earth elements and their ions from* Ca^n *to* Ra^n *(n=0, +1, +2)*, Phys. Rev. A **70**, 062501-1 (2004).

[5] Ivan S. Lim, Bernhard Metz, Hermann Stoll, and Peter Schwerdtfeger, *All-electron and relativistic pseudopotentials studies for the group 1 element polarizabilities from K to element 119*, J. Chem. Phys. accepted, Dec (2004).

[6] Ivan S. Lim, Peter Schwerdtfeger, Tilo Söhnel, and Hermann Stoll, *Ground state properties and static dipole polarizabilities of the alkali dimers from* K_2^n *to* Fr_2^n *(n=0, +1) from relativistic pseudopotential coupled-cluster and density functional studies*, J. Chem. Phys. submitted (2004).

[7] Ivan S. Lim, Bernhard Metz, Hermann Stoll, and Peter Schwerdtfeger, *Relativistic small-core energy-consistent pseudopotentials for the group 2 elements from Ca to Ra*, J. Chem. Phys. in preparation (2004).

[8] Ivan S. Lim, Peter Botschwina, Hermann Stoll, and Peter Schwerdtfeger, *The ground state properties and static dipole polarizabilities of the alkali metal ammonia complexes from* $(K\text{-}NH_3)^n$ *to* $(Fr\text{-}NH_3)^n$ *(n=0, +1)*, J. Chem. Phys. in preparation (2004).

Chapter 1
INTRODUCTION

When an atom or a molecule interacts with an external electric field the atom (or the molecule) is polarized and the resulting charge distribution is characterized by induced electric multipole moments. Of these multipole moments, the induced dipole moment is related to the electric field through the dipole polarizability whereas the quadrupole moment is related to the electric field gradient through the field-gradient polarizability. The higher order polarizabilities also arise through similar relations involving higher-order derivatives of the electric field. The static electric dipole polarizability, α_D of an atom or a molecule, therefore, describes the changes in the charge distribution when it interacts with an external electric field. It is a linear response property and is defined as the second derivative of the total energy with respect to the external homogenous electric field. As the majority of interactions in nature are governed by electric forces, the dipole polarizability is undoubtedly an important quantity, especially for the description of intermolecular forces [1], electron-atom scattering [2], and optical properties of materials [3] and clusters [4] to name a few. Its use extends to broad areas of chemistry and physics including refractive indices [5], ion mobility in gases, dielectric constants, and van der Waals constants [6] as well as accounting for electron correlation effects in pseudopotential methods [7-9] and transition moment calculations [10]. In particular, because of their close relationship to the dielectric constants, the study of dipole polarizabilities has a long history. The relationship between polarizabilities and various physical quantities could be found in Ref. [11].

Of particular interest is the article published by Dalgarno in 1962 in Advances in Physics entitled "*Atomic Polarizabilities and Shielding Factors*" [12]. It contained a comprehensive review of calculations of atomic polarizabilities and shielding factors at the time. This article is considered to be a citation classic. Dalgarno had worked on atomic perturbation theory for many

years and had been impressed with the confusion in describing the response of an atomic or a molecular system to a static electric field. The confusion mainly rested on the effects of the perturbation originating from the inaccuracies in the description of the unperturbed system. Dalgarno noted that the perturbed and unperturbed systems could be treated simultaneously at the same level of approximation and the theory of perturbation could be expressed in variational terms. He formulated an expression for the dipole polarizabilities and shielding factors for closed shell systems within the coupled Hartree-Fock approximation. Through the calculations of helium and beryllium sequences, he noted that environmental effects significantly modify polarizabilities and also electron correlation effects usually reduce polarizabilities. Only in the last few years have fully relativistic procedures including coupled-cluster (CC) techniques become available for the calculation of various response properties.

In the last 40 years, the experimental determination of dipole and multipole polarizabilities has improved significantly. These advances include dielectric constant measurements [13], Rayleigh scattering [14], molecular beam methods [15-18], atom interferometry [19], position sensitive time-of-flight [20], Kerr-effect experiments [21], collision-induced scattering of light [22-24], and electric field-induced second and third harmonic generation experiments [25-27]. One of the most frequently used methods of obtaining dipole polarizabilities was by the determination of dielectric constants for a gas from the bulk. This was also considered to be the most accurate method up to 15 years ago. Many such measurements were performed at the Brown University in the late 1960s and early 1970s. On the other hand, measurements of the refractive index enabled one to obtain dynamic polarizabilities. The application and the accuracy of the experimental methods are, however, subject to specific cases. Further difficulties arise when dealing with charged ions, as dipole polarizabilities are not subject to direct experimental determination. In this case, resources are made to purely theoretical, empirical, or semiempirical determination of crystal polarizabilities containing the ion of interest. Even so, complications arise due to the nonadditive nature of individual free ionic polarizabilities in its crystalline environment and the results can only be shown according to the polarizabilities of the ionic counterpart in the crystalline structure [28].

Despite the long history of experimental developments, experimental polarizability data are available for a few elements, namely alkali, alkaline-earth, and noble gases. In particular, it was noted by Miller and Bederson [3] that due to the early attempts of calculating polarizabilities by Dalgarno and Kingston

[29], experimentalists are lagging behind theoreticians especially for atomic dipole polarizabilities.

Indeed, the theoretical evaluation of dipole polarizabilities has been an active field of research. Dipole polarizabilities can be determined analytically by using, for example, the coupled Hartree-Fock approximation first proposed by Dalgarno [30]. This method has been used to obtain dipole polarizabilities of atoms and ions with two valence electrons [31]. Numerical determination of dipole polarizabilities is done mostly by the finite field perturbation method. Density dependent potentials have been used to calculate the dipole polarizabilities of closed shell atoms and ions [32]. Density functional theory, however, does not seem to be the method of choice due to large deviations from the known experimental values. The configuration interaction approach has been used to determine the dipole polarizabilities of the alkali metals [33]. The pseudopotential approximation has been used extensively especially for the group 1 elements due to their simple valence electron configuration. Further, as the dipole polarizabilities result mostly from the interaction of the valence electrons with an external field, determination of dipole polarizabilities has been used to characterize the accuracy and the transferability of pseudopotentials [34, 35].

There are important issues to consider in theoretical determination of dipole polarizabilities. Firstly, basis sets in *ab-initio* calculations. It is well known that dipole polarizabilities are extremely sensitive to the choice of basis sets used. As dipole polarizabilities largely result from the valence electrons, sufficient diffuse functions must be included in the basis sets. A careful consideration of polarization functions is also necessary. The importance of basis sets for the accurate determination of dipole polarizabilities is discussed in numerous papers. Of particular interest is the generation of purpose oriented basis sets such as so-called first-order polarized basis sets of Sadlej and co-workers [36].

Secondly, electron correlation effects should be treated at the highest level of theory possible. Such a consideration arises from the inadequacy of the Many-Body-Perturbation theory in correctly estimating electron correlation contributions to dipole polarizabilities.

Thirdly, relativistic effects. It is now well known that relativistic effects are important not only for the inner atomic shells, but also for the valence electrons through direct, indirect, and/or spin-orbit effects [37]. As demonstrated by Desclaux and co-workers [38], relativistic effects make one of the most dominating contributions to the dipole polarizabilities, especially for heavy elements. The well known Z^2 (Z is the nuclear charge) dependence of relativistic

effects in dipole polarizabilities means that such effects are important even for the lighter elements. For example, Dalgarno and co-workers gave a precise nonrelativistic dipole polarizability of Li of 164.111 a.u. [39] which compares well with the experimental value of 164.0(34) a.u. [40]. Relativistic effects for Li has been recently estimated to reduce the dipole polarizability by 0.06 a.u., which gives a relativistic dipole polarizability of 164.05 a.u. [41]. Finally, large effects of relativity lead to anomalous trends in dipole polarizabilities such as those of the group 1 elements [41].

An accurate determination of atomic and molecular static and dynamic dipole and hyper polarizabilities is an active and challenging field of research. Due to its sensitivity to basis sets, electron correlation and relativistic effects, and the vibrational structure in the case of molecules, it is by no means an easy task to accurately determine polarizabilities [42]. An extensive review on atomic polarizabilities has been given by Miller and Bederson [3] and more recently by Schwerdtfeger [42]. Reviews on experimental methods can be found in articles by van Wijngaarden [43, 44].

1.1 Thesis Overview

In the following chapter, a general discussion on static dipole polarizabilities and various theoretical and experimental methods of determination are presented.

This is followed by chapter 3 which briefly discusses relativistic effects in chemistry.

Chapter 4 contains details of the pseudopotential approximation and the fitting procedure employed in this study. The pseudopotential parameters obtained in the present study are listed in appendix A.

Chapters 5 to 9 present atomic valence properties, namely the static dipole polarizabilities and the ionization potentials of the neutral group 1 elements and their singly positive ions, followed by the neutral group 2 elements and their singly and doubly charged ions, respectively. The details of the basis sets developed in this study are discussed, in appropriate chapters, for each periodic group studied. The basis set exponents together with the contraction coefficients are listed in appendix B. The dipole polarizabilities and the ionization potentials determined by an all-electron method are presented first in each chapter followed by those determined by the pseudopotential approximation. Periodic trends in the

dipole polarizabilities and the ionization potentials as well as those in electron correlation and relativistic effects are discussed and compared across different periodic groups of varying valence electron configuration.

In Chapter 10, molecular applications of the adjusted pseudopotentials are made to a number of spectroscopic properties of the neutral and singly charged alkali dimers. This addresses the accuracy and the transferability of these pseudopotentials. Also presented are the dipole polarizabilities of these molecules. The resulting values are compared with other theoretical and experimental values.

In chapter 11, the molecular application is extended to the ammonia complexes of the group 1 elements. The optimized geometries, dissociation energies, vibrational frequencies as well as the dipole polarizabilities of these complexes are discussed.

The thesis is concluded in chapter 12.

References

[1] A. D. Buckingham, Adv. Chem. Phys. **12**, 107 (1976).

[2] C. J. Kleinman, Y. Hahn, and L. Spruch, Phys. Rev. **165**, 53 (1968).

[3] T. M. Miller and B. Bederson, Adv. At. Mol. Phys. **25**, 37 (1988).

[4] W. A. de Herr, Rev. Mod. Phys. **65**, 611 (1993).

[5] A. Dalgarno and A. E. Kingston, Proc. R. Soc. London Ser. A **259**, 424 (1960).

[6] C. A. Coulson, Proc. R. Soc. Edinburgh Sect. A **61**, 20 (1941).

[7] C. Bottcher, J. Phys. B **8**, 1140 (1971).

[8] J. C. Weisheit, Phys. Rev. A **5**, 1671 (1972).

[9] W. Müller, J. Flesch, and W. Meyer, J. Chem. Phys. **80**, 3297 (1984).

[10] D. W. Norcross, Phys. Rev. A **7**, 606 (1973).

[11] K. D. Bonin and V. V. Kresin, *Electric-Dipole polarizabilities of Atoms, Molecules, and Clusters* (World Scientific, Singapore, 1997).

[12] A. Dalgarno, Adv. Phys. **11**, 281 (1962).

[13] H. Sutter and R. H. Cole, J. Chem. Phys. **52**, 132 (1970).

[14] V. A. Maltsev, O. A. Nerushev, S. A. Novopashin, and B. A. Selivanov, Chem. Phys. Lett. **212**, 480 (1993).

[15] A. Salop, E. Pollack, and B. Benderson, Phys. Rev. **124**, 1431 (1961).

[16] E. Pollack, E. J. Robinson, and B. Benderson, Phys. Rev. A **134**, 1210 (1964).

[17] B. Benderson and E. J. Robinson, Adv. Chem. Phys. **10**, 1 (1961).

[18] G. E. Chamberlain and J. C. Zorn, Phys. Rev. **129**, 677 (1963).

[19] C. R. Ekstrom, J. Schmiedmayer, M. S. Chapman, T. D. Hammond, and D. E. Pritchard, Phys. Rev. A **51**, 3883 (1995).

[20] W. Heer, P. Milani, and A. Chatelain, Phys. Rev. Lett. **63**, 2834 (1989).

[21] L. L. Boyle, A. D. Buckingham, R. L. Disch, and D. A. Dummur, J. Chem. Phys. **45**, 1318 (1996).

[22] J. P. C. McTague and G. Birnbaum, Phys. Rev. Lett. **21**, 661 (1968).

[23] J. P. C. McTague and G. Birnbaum, Phys. Rev. A **3**, 1376 (1971).

[24] L. Frommhold, Adv. Chem. Phys. **46**, 1 (1981).

[25] R. S. Finn and J. F. Ward, Phys. Rev. Lett. **26**, 285 (1971).

[26] R. S. Finn and J. F. Ward, J. Chem. Phys. **60**, 454 (1974).

[27] I. J. Bigio and J. F. Ward, Phys. Rev. A **9**, 35 (1974).

[28] H. Coker, J. Phys. Chem. **80**, 2078 (1976).

[29] A. Dalgarno and A. E. Kingston, Proc. Roy. Soc. (London) A **73**, 455 (1959).

[30] A. Dalgarno, Proc. R. Soc. London Ser. A **251**, 282 (1959).

[31] E. Markiewicz, R. P. McEachran, and A. D. Stauffer, J. Phys. B **14**, 949 (1981).

[32] G. D. Mahan, Phys. Rev. A **22**, 1780 (1980); J. Chem. Phys. **76**, 493 (1982).

[33] P. S. Christiansen and K. S. Pitzer, Chem. Phys. Lett. **85**, 434 (1982).

[34] A. Filippetti, D. Vanderbilt, W. Zhong, Y. Cai, and G. B. Bachelet, Phys. Rev. B **52**, 11793 (1995).

[35] P. Fuentealba, J. Phys. B **15** L555 (1982).

[36] I. Miadoková, V. Kellö, and A. Sadlej, Theor. Chem. Acc. 96, **166** (1997).

[37] P. Pyykkö, Chem. Rev. **88**, 563 (1988).

[38] J. P. Desclaux, L. Laaksonen, and P. Pyykkö, J. Phys. B. **14**, 419 (1981).

[39] Z.-C. Yan, J. F. Babb, A. Dalgarno, and G. W. F. Drake, Phys. Rev. A **54**, 2824 (1996).

[40] R. W. Molof, H. L. Schwartz, T. M. Miller, and B. Bederson, Phys. Rev. A **10**, 1131 (1974).

[41] I. S. Lim, M. Pernpointner, M. Seth, J. K. Laerdahl, and P. Schwerdtfeger, Phys. Rev. A **60**, 2822 (1999).

[42] P. Schwerdtfeger, to be submitted.

[43] W. A. Wijngaarden, Adv. At. Mol. Opt. Phys. **36**, 141 (1996).

[44] W. A. Wijngaarden, At. Phys. **16**, 305 (1999).

Chapter 2
DIPOLE POLARIZABILITIES

The interaction of a particle with an external electric field is characterized by induced electric multipole moments. The induced dipole moment is related to the electric field through the atomic dipole polarizability. The higher order polarizabilities also arise through similar relations involving higher-order derivatives of the electric field. From this, the static electric dipole polarizability can be defined as a measure of the distortion of the electronic density under the effect of a static external electric field.

Dipole polarizabilities are important in many areas of chemistry and physics. In electromagnetic field-matter interactions, for example, the response of a neutral particle to an applied field such as a laser is determined by polarizabilities.

Quantity	Relation to α
Dielectric constant[a]	$\varepsilon = 1 + 4\pi\alpha$
Refractive index[a]	$\eta = 1 + 2\pi\alpha$
Ion mobility in gas[b]	$K = 13.876\sqrt{\alpha\mu}\ \mathrm{cm}^2$ /volt sec
van der Waals constant between system a and b	$C_6 = \frac{3}{2}\left(\frac{\alpha_a\alpha_b}{\sqrt{\alpha_a/n_a} + \sqrt{\alpha_b/n_b}}\right)$
Long-range electron- or ion-atom interaction potential[c]	$U = -e^2\alpha/2r^4$

[a]For a dilute nonpolar gas.
[b]μ is the reduced mass and α is in units of Å^3.
[c]For singly charged ions and r is the separation between colliding pair of particles. e is the charge on an electron.

Table 2.1. The relationship between the dipole polarizability, α and other physical quantities.

Polarizabilities determine the behavior of neutral particles in the interaction with other particles such as in collision phenomena. Some of the important relationships between polarizabilities and other physical properties are listed in Table 2.1.

2.1 The Electric Dipole Polarizability

In this section the explicit expressions for the static and time-dependent dynamic dipole polarizability are derived from perturbation theory.

2.1.1 The Static Dipole Polarizability

The expression for the static dipole polarizability follows from perturbation theory. The perturbation expression for the energy, E for the ground state $|0\rangle$ is

$$E_0 = E_0^{(0)} + \langle 0|H^{(1)}|0\rangle + \sum_n{}' \frac{\langle 0|H^{(1)}|n\rangle\langle n|H^{(1)}|0\rangle}{E_0 - E_n} + \ldots \qquad \text{Eq. 2.1}$$

A homogeneous electric field perturbation along the z-axis, $H^{(1)} = -\mu_z F$ (see section 2.2.2 and Eq. 2.26) gives

$$E_0 = E_0^{(0)} - \langle 0|\mu_z|0\rangle F + \left\{ \sum_n{}' \frac{\langle 0|\mu_z|n\rangle\langle n|\mu_z|0\rangle}{E_0 - E_n} \right\} F^2 + \ldots \qquad \text{Eq. 2.2}$$

The dipole polarizability is defined as the second derivative of the above expression with respect to the field strength, F at $F = 0$ such that

$$\alpha_{zz} = -\left(\frac{\mathrm{d}^2 E}{\mathrm{d}F^2}\right)_0 = 2\sum_n{}' \frac{\langle 0|\mu_z|n\rangle\langle n|\mu_z|0\rangle}{E_0 - E_n} \qquad \text{Eq. 2.3}$$

Note that the first derivative results in the expectation value of the dipole moment operator, $\langle 0|\mu_z|0\rangle$ which gives the permanent electric dipole moment.

Eq. 2.3 shows the dipole polarizability, α_{zz} with two subscripts. This is because the dipole polarizability is regarded as a second rank tensor. When an external field is applied along the z-axis, a dipole may be induced with components, μ_x, μ_y, and μ_z, where

$$\mu_\alpha = \alpha_{\alpha z} F_z \qquad \alpha = x, y, z \qquad \text{Eq. 2.4}$$

In general, the diagonal element, α_{zz} dominates the other two when the electric field is along the z-axis, as the induced dipole moment is usually almost parallel to the applied electric field [1]. For example, in a closed-shell atom the dipole polarizability can be reduced to a scalar quantity in which the only surviving polarizability tensor component is the one parallel to the applied electric field.

Eq. 2.3 gives an explicit expression for the static dipole polarizability. Similar expressions can be written for polarizabilities with a field applied along the x- or y-axis. Before proceeding further, $E_0 - E_n$ in Eq. 2.3 is expressed as ΔE_{n0} and the matrix element $\langle m|\mu_z|n\rangle$ is written as $\mu_{z,mn}$. Then, Eq. 2.3 is simplified to

$$\alpha_{zz} = 2\sum_n{}' \frac{\mu_{z,n0}^2}{\Delta E_{n0}} \qquad \text{Eq. 2.5}$$

The mean polarizability α is a property observed when a molecule presents all orientations to the applied field and is given by

$$\begin{aligned} \alpha &= \frac{1}{3}\left(\alpha_{xx} + \alpha_{yy} + \alpha_{zz}\right) \\ &= \frac{2}{3}\sum_n{}' \frac{\mu_{x,n0}^2 + \mu_{y,n0}^2 + \mu_{z,n0}^2}{\Delta E_{n0}} \end{aligned} \qquad \text{Eq. 2.6}$$

The numerator on the right hand side of Eq. 2.6 can be expressed as a scalar product of two vectors

$$\boldsymbol{\mu}_{0n} \cdot \boldsymbol{\mu}_{n0} = \mu_{x,n0}^2 + \mu_{y,n0}^2 + \mu_{z,n0}^2 \qquad \text{Eq. 2.7}$$

The dipole moment operator is a Hermitian operator, $\mu_{0n} = \mu_{n0}^{*}$ so that the left hand side of Eq. 2.7 can be expressed as $|\mu_{n0}|^2$. Then the Eq. 2.6 becomes

$$\alpha = \frac{2}{3}\sum_{n}{}' \frac{|\mu_{n0}|^2}{\Delta E_{n0}} \qquad \text{Eq. 2.8}$$

2.1.2 The Dynamic Dipole Polarizability

In order to derive the expression for the dynamic dipole polarizability, an alternate approach is taken. That is, the expectation value of the dipole moment operator is used, utilizing the first-order perturbed wavefunctions.

The perturbation due to an external field along the z-direction with an oscillating frequency, ω is

$$H^{(1)}(t) = -2\mu_z F \cos\omega t \qquad \text{Eq. 2.9}$$

The expectation value of the z-component of the dipole moment is

$$\langle \mu_z \rangle = \int \Psi^{*}(t)\mu_z \Psi(t)\mathrm{d}\tau \qquad \text{Eq. 2.10}$$

where the time dependent wavefunction is given by

$$\Psi(t) = \psi_0 e^{-iE_0 t/\hbar} + \sum_{n}{}' a_n(t)\psi_n e^{-iE_0 t/\hbar} \qquad \text{Eq. 2.11}$$

Here, the prime signifies the omission of the term $n = 0$, and to first order $a_0(t) = 1$. It must be noted that when the perturbation is applied it may result in the generation of transient oscillations of the electron density. These are eliminated by leaving the oscillating field on for a long time and allowing it to reach its full strength slowly:

$$H^{(1)}(t) = \begin{cases} 0 & \text{for } t < 0 \\ H^{(1)}\left(1 - e^{-kt}\right) & \text{for } t \geq 0 \end{cases} \qquad \text{Eq. 2.12}$$

with a small and positive k. Using Eq. 2.12, Eq. 2.9 is modified to

$$\begin{aligned} H^{(1)}(t) &= -2\mu_z F\left(1-e^{-t/\tau}\right)\cos\omega t \\ &= -\mu_z F\left(1-e^{-t/\tau}\right)\left(e^{i\omega t}+e^{-i\omega t}\right) \end{aligned} \qquad \text{Eq. 2.13}$$

where τ is the time-constant for switching on the perturbation.

Now a task remains to evaluate the coefficients $a_n(t)$ in Eq. 2.11. Assuming that t >> τ and that the perturbation is switched on very slowly in a sense that $\left|\tau(\omega \pm \omega_{n0})\right| >> 1$, one obtains for $a_n(t)$

$$\begin{aligned} a_n(t) &= \frac{1}{i\hbar}\int_0^t H_{n0}^{(1)}(t)\, e^{i\omega_{n0}t}\, dt \\ &= \frac{\mu_{z,n0}F}{\hbar}\left\{\frac{e^{i(\omega+\omega_{n0})t}}{\omega+\omega_{n0}} - \frac{e^{-i(\omega+\omega_{n0})t}}{\omega-\omega_{n0}}\right\} \end{aligned} \qquad \text{Eq. 2.14}$$

It then follows that

$$\langle \mu_z \rangle = \mu_{0z} + \frac{2}{\hbar}\sum_n{}' \left(\frac{\omega_{n0}\left|\mu_{z,n0}\right|^2}{\omega_{n0}^2-\omega^2}\right) \times 2F\cos\omega t \qquad \text{Eq. 2.15}$$

Then the expression for the dynamic dipole polarizability is

$$\alpha_{zz}(\omega) = \frac{2}{\hbar}\sum_n{}' \left(\frac{\omega_{n0}\left|\mu_{z,n0}\right|^2}{\omega_{n0}^2-\omega^2}\right) \qquad \text{Eq. 2.16}$$

and the mean polarizability is given by

$$\alpha(\omega) = \frac{2}{3\hbar}\sum_n{}' \left(\frac{\omega_{n0}\left|\boldsymbol{\mu}_{n0}\right|^2}{\omega_{n0}^2-\omega^2}\right) \qquad \text{Eq. 2.17}$$

where $\left|\boldsymbol{\mu}_{n0}\right|^2 = \boldsymbol{\mu}_{0n}\cdot\boldsymbol{\mu}_{n0}$ as before. The above expression reduces to the static polarizability when $\omega \rightarrow 0$.

2.2 Theory

When a uniform external field, **F** is applied to an atom (or a molecule) the interaction of the field with the atom is given by the perturbed Hamiltonian:

$$H^{(1)} = -\boldsymbol{\mu}\cdot\mathbf{F} \qquad \boldsymbol{\mu} = \sum_i q_i \mathbf{r}_i \qquad \text{Eq. 2.18}$$

where q_i is the charge of the particle i at the location $\mathbf{r}_i$. It is therefore important to calculate the dipole moment, i.e. the expectation value:

$$\boldsymbol{\mu} = \langle \Psi | \sum_i \mu_i | \Psi \rangle \qquad \text{Eq. 2.19}$$

where Ψ is the wavefunction of the full Hamiltonian. As the dipole polarizability is a linear response property one is interested in the lowest-order result of the polarization. In principle, various theoretical methods of evaluating the dipole polarizability are equivalent to one another. In practice, however, they rely on different implementations and approximations. Two of the most widely used theoretical methods of evaluating the dipole polarizability are discussed in this section, followed by experimental methods in section 2.3.

2.2.1 The Oscillator Strengths and Sum Rules

The dipole polarizability of the kth state can be expressed in terms of the dipole oscillator strength distribution, noting that the polarizabilities depend on the square of transition dipole moments. The square of this kind appears in terms of the intensities of spectroscopic transitions. One of the useful measures of absorption intensity is the oscillator strength. The oscillator strength formula for the transition $k \rightarrow l$ is

$$f_{kl} = \left(\frac{4\pi m_e}{3e^2\hbar}\right) \nu_{kl} |\boldsymbol{\mu}_{kl}|^2 \qquad \text{Eq. 2.20}$$

It follows that

$$\alpha = \frac{\hbar^2 e^2}{m_e} \sum_{l \neq k} \frac{f_{kl}}{\Delta E_{kl}^2} \qquad \text{Eq. 2.21}$$

where the summation runs over all integrals including the continuum.

The oscillator strengths can be determined from the band intensities and their energies from their locations on a frequency scale. Eq. 2.21 provides a prediction of the polarizability in relation to spectroscopy. That is, large contributions to the polarizability come from low energy, high intensity electronic transitions. In general, this implies that if a molecule absorbs strongly at low frequencies, then it can be expected to be highly polarizable. Intensely colored molecules should therefore be more polarizable. In contrast, for molecules that absorb weakly or at high frequencies such as colorless hydrocarbons, which weakly absorb and only in the ultraviolet region, low polarizabilities are expected.

Both experiments or calculations of the excited electronic spectrum can provide the necessary oscillator strengths. Even if it is not feasible to obtain all f_{kl}, the above expression for the dipole polarizability is useful in establishing the bounds of the dipole polarizability. This is based on the Thomas-Reiche-Kuhn (TRK) sum rule [2]:

$$\sum_{l \neq k} f_{kl} = N_e \qquad \text{Eq. 2.22}$$

where N_e is the total number of electrons. It follows that if only l' transitions are known as a sub set of all transitions, $k \rightarrow l$, then a lower bound of the dipole polarizability is given by

$$\alpha \geq \alpha_{\min} = \frac{\hbar^2 e^2}{m_e} \sum_{l' \neq k} \frac{f_{kl'}}{\Delta E_{kl'}^2} \qquad \text{Eq. 2.23}$$

Consequently, the upper bound is found by assigning the remaining oscillator strength, $N_e - \sum_{l' \neq k} f_{kl'}$ to the smallest possible energy difference $E_{\min}$ [3]

$$\alpha \leq \alpha_{\min} + \frac{\hbar^2 e^2}{m_e}\left[\frac{N_e - \sum_{l' \neq k} f_{kl'}}{E_{\min}^2}\right] \qquad \text{Eq. 2.24}$$

If the dipole transition strength is concentrated around a strong resonance at a frequency, $\tilde{\omega}$, then a simple estimate of the dipole polarizabilities is given by

$$\alpha \approx \frac{\hbar^2 N_e e^2}{m_e \tilde{\omega}^2} \qquad \text{Eq. 2.25}$$

The key feature of this formula is the relationship between the dynamic and the static properties of any quantum mechanical system. That is, if the frequencies and the strength of its principal transitions are known, the response to a static field can be derived.

2.2.2 The Finite Field Method

Using a generalized Buckingham notation [4] to denote response tensors, the static dipole polarizability of a molecule is expressed as

$$\mu_\alpha = \alpha_{\alpha\beta} F_\beta \qquad \text{Eq. 2.26}$$

where μ_α is the induced dipole moment and F_β is the magnitude of the electric field. Alternatively, the static dipole polarizability can be expressed as partial derivatives in the limit of vanishing fields as

$$\alpha_{\alpha\beta} = -\left(\frac{\partial^2 E}{\partial F_\alpha \partial F_\beta}\right)_0 \qquad \text{Eq. 2.27}$$

where E denotes the total energy. This can be derived from perturbation theory as follows:

The perturbation caused by an electric field $\mathbf{F}$ is expressed as

$$H^{(1)} = -\boldsymbol{\mu} \cdot \mathbf{F} \qquad \boldsymbol{\mu} = \sum_i q_i \mathbf{r}_i \qquad \text{Eq. 2.28}$$

where q_i is the charge of the particle i at the location $\mathbf{r}_i$.

The key to the derivation of the dipole polarizability expression in Eq. 2.27 is the Hellmann-Feynman theorem [5, 6]:

$$\frac{dE}{d\lambda} = \left\langle \frac{\partial H}{\partial \lambda} \right\rangle \qquad \text{Eq. 2.29}$$

The Hellmann-Feynman theorem describes how the energy, E of a system varies as the Hamiltonian of the system varies with respect to the interacting parameter λ. In the present case, the total Hamiltonian, H is the sum of the unperturbed Hamiltonian, $H^{(0)}$ and the perturbed Hamiltonian, $H^{(1)}$ and the interacting parameter is the electric field strength, F_α. Since the unperturbed Hamiltonian $H^{(0)}$ is independent of the electric field it follows from Eq. 2.28 and Eq. 2.29 that

$$\frac{\partial E}{\partial F_\alpha} = \left\langle \frac{\partial H}{\partial F_\alpha} \right\rangle = \left\langle \frac{\partial H^{(1)}}{\partial F_\alpha} \right\rangle = -\langle \mu_\alpha \rangle \qquad \text{Eq. 2.30}$$

Note also that the static response properties of a molecule can be defined by expanding the field dependent energy $E(F)$ in a Taylor expansion:

$$\begin{aligned} E = E(0) + \left(\frac{\partial E}{\partial F_\alpha}\right)_0 F_\alpha + \frac{1}{2!}\left(\frac{\partial^2 E}{\partial F_\alpha \partial F_\beta}\right)_0 F_\alpha F_\beta \\ + \frac{1}{3!}\left(\frac{\partial^3 E}{\partial F_\alpha \partial F_\beta \partial F_\gamma}\right)_0 F_\alpha F_\beta F_\gamma + \ldots \end{aligned} \qquad \text{Eq. 2.31}$$

Differentiation of Eq. 2.31 with respect to F_α yields

$$\frac{\partial E}{\partial F_\alpha} = \left(\frac{\partial E}{\partial F_\alpha}\right)_0 + \left(\frac{\partial^2 E}{\partial F_\alpha \partial F_\beta}\right)_0 F_\beta + \frac{1}{2}\left(\frac{\partial^2 E}{\partial F_\alpha \partial F_\beta \partial F\gamma}\right)_0 F_\beta F_\gamma + \ldots \qquad \text{Eq. 2.32}$$

The expectation value of the dipole moment in the presence of the electric field is the sum of the permanent dipole moment and the contribution induced by the field:

$$\langle \mu_\alpha \rangle = \mu_0 + \alpha_{\alpha\beta} F_\beta + \frac{1}{2} \beta_{\alpha\beta\gamma} F_\beta F_\gamma + \ldots \qquad \text{Eq. 2.33}$$

where $\alpha_{\alpha\beta}$ is the dipole polarizability and $\beta_{\alpha\beta\gamma}$ is the first hyperpolarizability. Note the subscripts associated with the polarizabilities as explained in Eq. 2.4.

Eq. 2.32 and 2.33 are equivalent with each other as it follows from the Hellmann-Feynman theorem as shown in Eq. 2.30. Then, Eq. 2.32 and 2.33 are combined to give

$$\langle \mu_\alpha \rangle = -\frac{\partial E}{\partial F_a} = -\left(\frac{\partial E}{\partial F_\alpha}\right) - \left(\frac{\partial^2 E}{\partial F_\alpha \partial F_\beta}\right) F_\beta - \frac{1}{2}\left(\frac{\partial^2 E}{\partial F_\alpha \partial F_\beta \partial F\gamma}\right) F_\beta F_\gamma - \ldots \qquad \text{Eq. 2.34}$$

A comparison between Eq. 2.33 and 2.34 gives the expression for the dipole polarizability as in Eq. 2.27

$$\alpha_{\alpha\beta} = -\left(\frac{\partial^2 E}{\partial F_\alpha \partial F_\beta}\right)_0$$

For a spherically symmetric system the dipole polarizability is a scalar quantity i.e. $\alpha_{xx} = \alpha_{yy} = \alpha_{zz}$.

2.3 Experimental Methods

There is a variety of experimental methods of determining the polarizability. Some of the traditional methods include dielectric constant measurement, refractive index, and beam deflection. There are also new techniques available such as atom interferometry. Although the experimental study of polarizabilities is outside the scope of this thesis, a brief description of some of these methods is presented in this section.

2.3.1 Dielectric Constant Measurement

The dipole polarizability is related to the dielectric constant by the Debye equation:

$$\alpha = \frac{3}{4\pi n}\left(\frac{\varepsilon - 1}{\varepsilon + 2}\right) - \frac{\mu_0^2}{3kT} \qquad \text{Eq. 2.35}$$

where n is the gas number density, μ_0 is the permanent electric dipole moment of the molecule, k is the Boltzmann constant, and T is the absolute temperature in Kelvin [7]. A special case is obtained for $\mu_0 = 0$, which gives the so-called Clausius-Mossotti relation. The dielectric constant is close to unity for a dilute gas so that Eq. 2.35 reduces to (see Table 2.1)

$$\varepsilon \approx 1 + 4\pi n\left[\alpha + \mu_0^2/(3kT)\right] \qquad \text{Eq. 2.36}$$

The dielectric constant measurements are made by constructing a capacitor such that the volume between the plates can be either evacuated or filled with the material to be measured. The change in resonance frequency when the material is introduced between the capacitor plates yields dielectric constants [8]. A more common way is by building an ac-bridge circuit to compare a unknown capacitance to a capacitance standard [9, 10].

Dielectric constant measurements for the dipole polarizability is the most useful for a gas at room temperature. The measurements can be very accurate. For example, the dipole polarizability of argon was measured with accuracy of 0.05% [11]. For materials that cannot be isolated in a gas form (i.e. those which need to be heated to form the gas), one must consider systematic errors originating from dissociation, excitation, ionization, and temperature gradients.

2.3.2 Refractive Index

The refractive index is the ratio of the speed of light in vacuum to that in a material and is related to the dipole polarizability by Lorentz-Lorenz relation

$$\alpha = \frac{3}{4\pi n}\left(\frac{\eta^2 - 1}{\eta^2 + 2}\right) \qquad \text{Eq. 2.37}$$

where n is the number density of the gas or liquid [7]. Note that the above equation and Eq. 2.35 are related by the Maxwell relation $\varepsilon = \eta^2$. Eq. 2.37 is valid for non-polar molecules, or at high enough frequencies so that the permanent dipole cannot follow the electric field. Measurements of the refractive index yield the most accurate values of the dipole polarizability for low-density gases. Although the dipole polarizability can be deduced for a liquid, the polarizability values are often imprecise due to the local field correction used [12]. For a solid, the refractive index provides only an estimate for the polarizability.

For accurate measurements of the refractive index for a gas, one can use interferometry. For example, an evacuated cell is placed in one arm of a Michelson interferometer. The fringe shift, N^* is measured as this cell is filled. The relationship between the refractive index and the fringe shift is

$$2l(\eta - 1) = N^* \lambda \qquad \text{Eq. 2.38}$$

where l is the length of the cell and λ is the wavelength of the light. Interferometric measurements have been used for species where a capacitance measurement of the dielectric constant is impractical. For example, the dipole polarizability of atomic nitrogen and oxygen has been measured by Alpher and White [13], using a shock tube to dissociate N_2 and O_2.

2.3.3 Beam Deflection

One of the most straightforward methods of determining the dipole polarizability is by the beam deflection method where the deflection of a collimated molecular beam passing through a static electric field is measured.

When the field is defined to be along the z-axis, the force on a molecule in the field is

$$F_F = \alpha_{zz} F_z \frac{dF_z}{dz} z \qquad \text{Eq. 2.39}$$

where F_F is the electric force, α_{zz} is the dipole polarizability along the z-axis and F_z is the magnitude of the electric field. The spatial deflection of a molecule is approximately proportional to $1/v^2$, where v is the speed of the molecule. To detect the deflection, a hot wire is used. This is particularly useful for alkali-metals. For other materials a different detector may be required [14].

The first use of this technique to measure dipole polarizabilities dates back to 1934 by Scheffers and Stark [15]. They have measured the dipole polarizabilities of alkali metals to accuracies of 20% to 50%. The large errors associated with this measurement are largely attributed to a lack of knowledge of the velocity distribution. This was taken care of by Hall and Zorn in 1974 who used a velocity selector in their electric deflection measurements with an improved accuracy of around 10% [16].

2.4 Relationship with Ionization Potential

In 1959, Dalgarno and Kingston [17] first employed the oscillator strength formula to obtain reliable values of the ground-state dipole polarizabilities of the alkali-metals. They noted that for one-valence electron systems like the alkali-metals, the dipole polarizability, α_D can be obtained by using the oscillator strength formula for the transition of $0 \rightarrow k$ as

$$\alpha_D = \frac{e^2\hbar^2}{m_e}\sum\frac{f_{k0}}{(E_k - E_0)^2} \qquad \text{Eq. 2.40}$$

where f_{k0} is the oscillator strength and E_k and E_0 are the energy of excited and ground states, respectively. The integral in Eq. 2.40 runs over all discrete and continuum states. For a one valence electron system such as the alkali atoms, most contribution to the oscillator strengths comes from the strong nS → nP transition of the valence electron and the oscillator strength is essentially unity [18]. Therefore, the dipole polarizability can be approximated by (in a.u.)

$$\alpha_D = \sum\frac{f_{0,k}}{(E_k - E_0)^2} \approx \frac{1}{(E_1 - E_0)^2} \qquad \text{Eq. 2.41}$$

where E_1 refers to the first excited state and E_0 to the ground state. Alternatively, Eq. 2.41 can be written in atomic units as

$$\begin{aligned}\alpha_D &= c_1(E_1 - E_0)^{-2} + c_2 \\ &= c_1((E_\infty - E_0) - (E_\infty - E_1))^{-2} + c_2 \\ &= c_1(IP_0 - IP_1)^{-2} + c_2 \\ &= c_1\left(IP_0\left(1 - \frac{IP_1}{IP_0}\right)\right)^{-2} + c_2 \\ &\cong c_1 IP_0^{-2} + c_2 \qquad (\because IP_0 >> IP_1)\end{aligned} \qquad \text{Eq. 2.42}$$

where IP_0 and IP_1 are the first and second ionization potentials, respectively. This equation implies that dipole polarizability increase with decreasing ionization potential and decreases with increasing ionization potential. It was shown that Eq. 2.42 works reasonably well for the alkali-metals [17] and for the group 11 metals [19].

It is now possible to approximate relativistic effects based on a near linear relationship between the dipole polarizability and the ionization potential as in Eq. 2.42 by

$$\begin{aligned}\frac{\alpha_D^{NR}}{\alpha_D^{R}} &= a\left(\frac{IP_{NR}}{IP_R}\right)^{-2} + b \\ &= a\frac{IP_R^2}{IP_{NR}^2} + b\end{aligned} \qquad \text{Eq. 2.43}$$

where a and b are constants to be determined. The consequence of this relationship is that if relativistic (or electron correlation) effects cause an increase in the ionization potential then they will cause a decrease in the dipole polarizability. It is also important to note the quadratic dependency of IP_R/IP_{NR} on $\alpha_D^{NR}/\alpha_D^{R}$, which implies that the relativistic (or electron correlation) effects in dipole polarizabilities are larger than those in ionization potentials.

References

[1] P. W. Atkins and R. S. Friedman, *Molecular Quantum Mechanics*, 3rd ed. (Oxford University Press, New York, 1997).

[2] H. A. Bethe and R. Jackiw, *Intermediate Quantum Mechanics*, 3rd ed. (Benjamin, Menlo Park, 1986).

[3] T. M. Miller and B. Bederson, Adv. At. Mol. Phys. **13**, 1 (1977).

[4] A. D. Buckingham, Adv. Chem. Phys. **12**, 107 (1967).

[5] H. Hellmann, *Einführung in die Quantenchemie*, Franz Deuticke, Leipzig, Germany, (1937).

[6] R. P. Feynman, Phys. Rev. **41**, 721 (1939).

[7] C. Böttcher, O. van Bell, P. Bordewijk, and A. Rip, *Theory of Electric Polarization*, 2nd ed. (Elsevier, Amsterdam, 1973), Vol. 1.

[8] A. N. M. Barnes, D. J. Turner, and L.E. Sutton, Trans. Faraday Soc. **67**, 2902 (1971).

[9] H. Sutter and R. H. Cole, J. Chem. Phys. **52**, 132 (1970).

[10] C. M. Meyer and G. Morrison, J. Phys. Chem. **95**, 3860 (1991).

[11] R. H. Orcutt and R. H. Cole, J. Chem. Phys. **46**, 697 (1967); A. C. Newell and R. C. Baird J. Appl. Phys. **36** 3751 (1965).

[12] V. A. Zamkov, in *Molecular Liquids*: *New Perspectives in Physics and Chemistry*, Vol. 379 of NATO ASI, edited by J. J. C. Teixeira-Dias (Kluwer, Dordrecht, 1992).

[13] R.A. Alpher and D. R. White, Phys. Fluids **2**, 153 (1959).

[14] K. D. Bonin and V. V. Kresin, *Electric-Dipole Polarizabilities of Atoms, Molecules, and Clusters*, (World Scientific, 1997).

[15] H. Scheffers and J. Stark, Phys. Z. **35**, 625 (1934).

[16] W. D. Hall and J. C. Zorn, Phys. Rev. A **51**, 3883 (1995).

[17] A. Dalgarno and A. E. Kingston, Proc. Roy. Soc. (London) A **73**, 455 (1959).

[18] T. M. Miller and B. Bederson, Adv. At. Mol. Phys. **25**, 37 (1988).

[19] P. Schwerdtfeger and G. A. Bowmaker, J. Chem. Phys. **100**, 4487 (1994).

Chapter 3
RELATIVISTIC EFFECTS

Relativity and quantum mechanics are two basic theories of modern physics. The theory of relativity was proposed by Einstein in 1905, but its impact on chemistry came to be known only in the 1970s. In the framework of nonrelativistic mechanics, the velocity of light is assumed to be infinite. This theory works reasonably well as long as the speed of an electron in an atom or a molecule is far smaller than the speed of light such as those in light atoms. For heavy atoms, however, the velocity of the inner electrons approaches the speed of light. Although it is the core electrons that experience substantial relativistic effects, it is now well known that the valence electrons undergo significant alterations as well.

Relativistic effects are defined as the difference in any observable properties that arises from the true, finite velocity of light as opposed to the assumed infinite velocity. One of the effects of relativity is the relativistic mass increase:

$$m = \frac{m_0}{\left(1 - \frac{v}{c}\right)^{\frac{1}{2}}} \qquad \text{Eq. 3.1}$$

where m_0 is the rest mass and v is the speed of the particle. Consider a core electron which moves at 60% of the speed of light, e.g. the 1*s* electron of gold. According to Eq. 3.1, the mass of the 1*s* electron moving at 58% of the speed of light is 23% heavier than the rest mass. This increase in the kinetic energy of the 1*s* electron is balanced by the contraction of the 1*s* orbital. In general, this leads to a decrease in the effective Bohr radius:

$$a_0 = (4\pi\varepsilon_0)\left(\frac{\hbar^2}{m_e^2}\right) \qquad \text{Eq. 3.2}$$

for inner electrons with large average speed. This affects properties associated with the electron distribution near the nucleus. Although most of relativistic effects are experienced by the core electrons, the valence orbitals do undergo a contraction as they are subjected to nuclear charge to a greater extent. For very precise calculations, relativistic corrections are already needed for systems such as H_2^+ or H_2 [1].

3.1 The Dirac Equation

In 1928, Dirac proposed a relativistic wave equation as the Lorentz invariant counterpart of the Schrödinger equation. The so-called Dirac equation is a first-order differential equation in both the time and spatial coordinates. For a free particle in the absence of any external field, the Dirac equation is given by (in a.u.) [2]

$$h_D\psi = \left[c\boldsymbol{\alpha}\cdot\mathbf{p} + c^2\beta\right] \qquad \text{Eq. 3.3}$$

where Dirac matrices $\boldsymbol{\alpha}$ and β are expressed in terms of the Pauli matrices. For a many-electron system in the presence of an external field, the free Dirac equation of Eq. 3.3 becomes

$$H_D = \sum_i h_D(i) + \sum_{i<j} g_{ij} \qquad \text{Eq. 3.4}$$

where $h_D(i)$ is the one-electron Dirac Hamiltonian as in Eq. 3.3 with a potential energy term for the external field:

$$h_D(i) = \boldsymbol{\alpha}_i\cdot\mathbf{p}_i + \beta_i c^2 + V_{ext}(i) \qquad \text{Eq. 3.5}$$

The last term in Eq. 3.4 describes the electron-electron interaction and is given by

$$g_{ij} = \frac{1}{r_{ij}} - \left\{ \frac{\boldsymbol{\alpha}_i \boldsymbol{\alpha}_j}{r_{ij}} \cos\left(\omega_{ij} r_{ij}\right) \right\} + \left(\boldsymbol{\alpha}_i \nabla_i\right)\left(\boldsymbol{\alpha}_j \nabla_j\right) \frac{1 - \cos\left(\omega_{ij} r_{ij}\right)}{\omega_{ij}^2 r_{ij}} \qquad \text{Eq. 3.6}$$

where ω_{ij} is the frequency of the virtual exchange photon between electron i and j. In the low frequency limit ($\omega_{ij} = 0$), the dominant term is the classical Coulomb and Gaunt term

$$g_{ij} = \frac{1}{r_{ij}} - \left(1 - \boldsymbol{\alpha}_i \boldsymbol{\alpha}_j\right) \qquad \text{Eq. 3.7}$$

If quantum electrodynamic effects (QED) are ignored we have $g_{ij} = 1/r_{ij}$.

3.2 The Douglas-Kroll Transformation

The four-component Dirac spinors can be expressed in the large and small components using the Pauli 2-spinors. The Dirac equation can then be written in a 'split notation' as (for a single particle without the electron-electron interaction term)

$$\begin{aligned} \left(V_{ext} - E\right)\psi + c\boldsymbol{\alpha} \cdot \mathbf{p}\varphi = 0 \\ c\boldsymbol{\alpha} \cdot \mathbf{p}\psi + \left(V_{ext} - 2c^2 - E\right)\varphi = 0 \end{aligned} \qquad \text{Eq. 3.8}$$

The coupling between the large and small components can be seen from Eq. 3.8 via the odd (off diagonal) operator, $c\boldsymbol{\alpha} \cdot \mathbf{p}$. The even operators like β and V_{ext} do not cause any coupling between the large and small components. The four-component wavefunctions present a practical barrier due to the large number of integral calculations involved. As a good approximation, methods that decouple the positronic and electronic solutions have been developed by a unitary transformation which annihilate the coupling between the electronic and positronic degrees of freedom. In other words, the odd terms in the Hamiltonian that couple the large and small components are removed to a certain order. In this way the cost of computation is reduced with the decreased number of degrees of freedom.

One of the well established transformation of the four-component Dirac spinors to a two-component form is the Douglas-Kroll (DK) transformation used in this thesis. The DK method was first presented by Douglas and Kroll [3] in 1974 and has been extensively discussed and tested by Heß and coworkers [4, 5]. The DK transformation defines a transformation of the external-field Dirac Hamiltonian to a two-component form by a systematic expansion of the Hamiltonian in ascending powers of the external potential, V_{ext}, removing odd terms step by step. This leads to operators which are bound from below and can be used variationally.

The DK method begins with a first order Foldy-Wouthuysen (FW) transformation performed in momentum space [2]. The momentum space for a single particle is given by

$$h_D = \boldsymbol{\alpha} \cdot \mathbf{p} + \beta m + V_{ext} \qquad \text{Eq. 3.9}$$

where the external potential V_{ext} acting on a momentum space state vector, $\phi(p)$ is given by the expression

$$V_{ext}\phi(p) = \int d^3p' V(p,p')\phi(p') \qquad \text{Eq. 3.10}$$

The unitary operator used in the first-order transformation is given by

$$U = \left(\frac{E_p + m}{2E_p}\right)^{\frac{1}{2}} \left[1 + \beta\left(\frac{\boldsymbol{\alpha} \cdot \mathbf{p}}{E_p + m}\right)\right] \qquad \text{Eq. 3.11}$$

where E_p is the positive energy eigenvalues given by

$$E_p = \sqrt{p^2 + m^2} \qquad \text{Eq. 3.12}$$

When the unitary operator in Eq. 3.11 is applied to the single particle Dirac Hamiltonian, h_D, using the following definitions

$$A_p = \sqrt{\frac{E_p + m}{2E_p}}$$
$$R_p = \frac{\boldsymbol{\alpha} \cdot \mathbf{p}}{E_p + m} \qquad \text{Eq. 3.13}$$

the result is

$$Uh_D U^\dagger = \beta E_p + \mathsf{E} + \mathsf{O} = h'_D \qquad \text{Eq. 3.14}$$

with the even and odd operators as

$$\mathsf{E} = A_p (V_{ext} + R_p V_{ext} R_p) A_p$$
$$\mathsf{O} = \beta A_p \left[R_p, V_{ext} \right] \qquad \text{Eq. 3.15}$$

From this point, Douglas and Kroll proposed the use of a second unitary transformation of the form

$$U' = \sqrt{1 + W_1^2} + W_1 \qquad \text{Eq. 3.16}$$

where W is anti-Hermitian obeying the equation

$$\left[W_1, E_p \right]_+ = \beta \mathsf{O} \qquad \text{Eq. 3.17}$$

Because the operator O is linear in V_{ext} as in Eq. 3.15, an integral operator W_1 must be expressed in terms of its kernel as

$$W_1(p, p') = \beta \frac{\mathsf{O}}{E_{p'} + E_p} \qquad \text{Eq. 3.18}$$

A more explicit expression for the anti-Hermitian operator $W_1(p, p')$ may be obtained using the functional form of O,

$$W_1(p,p') = A_{p'}A_p(R_p - R_{p'})\frac{V_{ext}(p,p')}{E_{p'} + E_p} \qquad \text{Eq. 3.19}$$

This transformation removes all coupling of the upper and the lower halves of the transformed wavefunction to first order in V_{ext}. Through the repeated application of the n^{th} order transformation, further separation to arbitrary orders in the external potential is achieved:

$$U_n = (1 + W_n)^{1/2} W_n \qquad \text{Eq. 3.20}$$

Separation to second order in the external potential should be sufficient for the description of the valence electronic structure, as higher order contributions should only be important for the proper treatment of the lowest lying electrons.

The large component of the single-particle Hamiltonian which has been decoupled to second order in V_{ext} is given by

$$h_D'' = E_p + \mathsf{E}_1 + 1/2\left(\left[E_p, W_1^2\right]_+ + W_1 E_p W_1\right) \qquad \text{Eq. 3.21}$$

This Hamiltonian may be employed in conjunction with the Coulomb inter-electron repulsion operator to define a many-electron Hamiltonian as (without the QED term)

$$H_{DK} = \sum_i^n h_D'' + 1/2 \sum_{i<j}^n \frac{1}{r_{ij}} \qquad \text{Eq. 3.22}$$

The Hamiltonian in Eq. 3.22 is frequently referred to as the no-pair Douglas-Kroll Hamiltonian. It has been shown that the scalar relativistic DK operator performs extremely well for superheavy elements like element 111 [6].

Methods based on the DK operator rely on the assumption that the contribution from the small components is much smaller than that from the large components. This assumption is a good for the valence orbitals. For this reason, methods employing the DK Hamiltonian have been used extensively for the calculation of dipole polarizabilities [7].

3.3 Relativistic Effects in Chemistry

In practice, relativistic effects in a given property may be defined as the difference between the results obtained in a nonrelativistic and relativistic calculation. There are excellent review articles dealing with relativistic effects in chemistry [1, 8-9].

The importance of relativistic effects in atomic orbital energies and spatial extent can be realized by the Bohr model of the hydrogenic atom of charge Z. In a semi-classical sense, an electron in an orbital with principal quantum number n would travel at a distance r_n at a velocity υ_n with a total energy E_n:

$$\begin{aligned} r_n &= \frac{n^2}{mZ} \\ \upsilon_n &= Z/n \\ E_n &= -\frac{mZ^2}{2n^2} \end{aligned} \qquad \text{Eq. 3.23}$$

By replacing m with the velocity-dependent mass, one obtains

$$m = \frac{m_e}{\sqrt{1-\upsilon^2/c^2}} = \frac{m_e}{\sqrt{1-Z^2/n^2c^2}} \qquad \text{Eq. 3.24}$$

This relationship is illustrated in Figure 3.1. The relativistic correction of the mass variation is typically referred to as a direct relativistic effect. These effects are most easily seen by the contraction of *s*- and *p*-type orbitals. In other words, the *s* orbitals, which have zero angular momentum, have a greater density near the nucleus and thus experience a greater fraction of the nuclear charge. For heavy elements, the velocity of the inner 1*s* and 2*s* electrons reaches close to that of light and this results in a significant lowering of the orbital energies. Increasing relativistic effects for heavy elements are accompanied by the increasingly strong Coulomb field of the highly charged atomic nucleus. The contraction of the *p*-type orbitals is smaller than that of *s*-type orbitals because the angular momentum prevents the electrons in the *p*-type orbitals approaching the nucleus very closely.

A greater density in the nuclear vicinity caused by the *s* and *p* orbital contraction results in an increased shielding of the nuclear charge. This has an

effect on the higher angular momentum *d* and *f* orbitals, as the nucleus is more efficiently screened. The resulting expansion of the *d* and *f* orbitals and the associated shift of the orbital energies are referred to as an indirect relativistic effect. The more diffuse *d* and *f* electrons experience a relativistic energetic destabilization.

The electrons with angular momentum *l* greater than zero (i.e. *p*, *d*, *f*, ...) undergo spin-orbit splitting into $\mathbf{j} = \mathbf{l} \pm \mathbf{s}$ ($j = l \pm ½$). Spin-orbit effects are significant for the lower *j* value (l - ½), usually giving a small mean radius and a larger ionization energy than the higher *j* value (l + ½). Also, the spin-orbit interaction splits and mixes different excited states that would not mix in the absence of spin-orbit splitting.

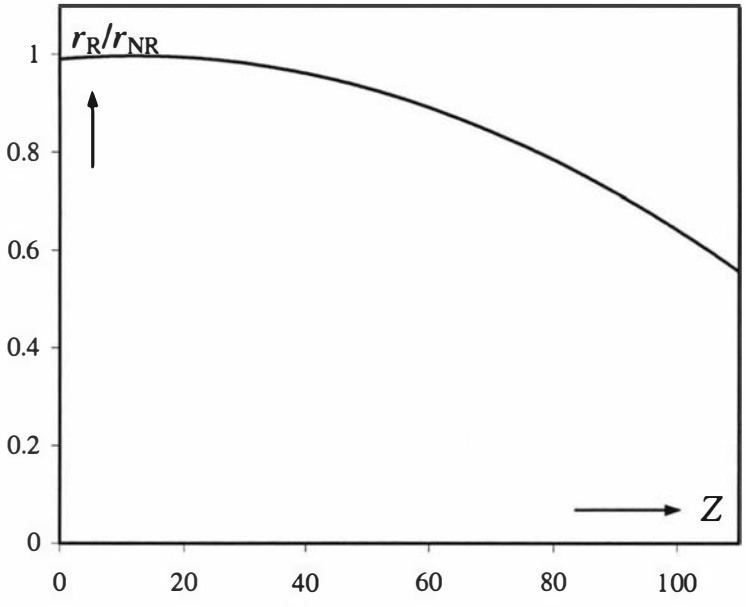

Figure 3.1. Ratio of the relativistic to non-relativistic Bohr orbit.

The chemical consequences of relativity become evident in the fifth row, and occasionally in the forth row elements. In the first and second column of the periodic table, the relativistic contraction of the outer *s* shell is so great for Fr and Ra that their atomic radii are smaller than the lighter Cs and Ba, respectively [10]. So far no evidence is given for the possible contraction of the σ-bond involving the valence *s* orbital of these elements.

References

[1] P. Pyykkö, Chem. Rev. **88**, 563 (1988).

[2] P. Schwerdtfeger, *Relativistic Electronic Structure Theory Part 1. Fundamentals* (Elsevier, 2002).

[3] M. Douglas and N. M. Kroll, Ann. Phys. **82**, 89 (1974).

[4] B. A. Heß, Phys. Rev. A **39**, 3742 (1986).

[5] R. Samzov, B. A. Heß, and G. Jansen, J. Chem. Phys. **96**, 1227 (1992).

[6] M. Seth, M. Dolg, K. Faegri, B. A. Heß, U. Kaldor, and P. Schwerdtfeger, Chem. Phys. Lett. **250**, 461 (1996).

[7] I. Miadoková, V. Kellö, and A. J. Sadlej, Theor. Chem. Acc. **96**, 166 (1977).

[8] P. Pyykkö, J. -P. Desclaux, Acc. Chem. Res. **12**, 276 (1979).

[9] B. A. Heß, C. M. Marian, and S. Peyerimhoff, *Advanced Series in Physical Chemistry: Modern Electronic Structure Theory*, Vol. 2 (World Scientific, 1995).

[10] J. B. Fricke and D. T. Waber, J. Chem. Phys. **56**, 3246 (1972).

Chapter 4
THE PSEUDOPOTENTIAL APPROXIMATION

The way of developing a valence only formalism for atoms and molecules by the use of pseudopotentials has been widely applied over the past decades since its development [1, 2]. The use of pseudopotentials is based on the assumption that most chemical properties are determined by valence orbitals where the atomic core is largely inactive in chemical processes. Although the improvement made in computer technology and hence the CPU power has been exponential over the last 20 years, the need to further approximate the commonly used Hartree-Fock (HF), post-HF, and Dirac-Coulomb-Hartree-Fock (DCHF) methods is ever increasing, especially for large and heavy molecules. Pseudopotential methods significantly reduce the number of electrons in the Hamiltonian by replacing core electrons by an effective potential, assuming a frozen core and applying a core-valence separation. One of the biggest advantages of the pseudopotential method is therefore attributed to the computational saving in integral calculations between core and core-valence electrons. There are, however, important issues to be considered.

Firstly, it is difficult to decide how and at what level of approximation (i.e. Hartree-Fock or correlated level) the pseudopotentials are introduced. This is because electrons are indistinguishable and a n-particle Hamiltonian cannot be separated into a core and a valence part. However, in the framework of a one-particle approximation such as HF or DCHF theory, core and valence orbitals can be defined on the basis of energetic or spatial arguments such as orbital energies or expectation values of orbitals. The pseudopotentials are therefore introduced at the independent particle model. Even at this level, the Pauli exclusion of the core has to be satisfied. To this effect, Phillips and Kleinman provided a modified valence Hamiltonian which replaces the explicit core-valence orthogonalilty constraints for the one valence electron cases.

Secondly, a question of transferability arises. That is, when pseudopotentials are introduced at the *ab-initio* level, the pseudopotentials must be applicable to different valence states in atoms and molecules. Therefore, pseudopotential parameters are derived from a multitude of atomic states of a neutral atom and low-charge ions that might be of relevance in, for example, chemical bonding. Difficulties still remain as the atomic core might become polarized by the other electrons and nuclei. Core repulsion might be important at small internuclear distances.

Thirdly, the theoretical level employed for the generation of atomic reference data for a pseudopotential fitting procedure should be close to the level of theory (such as correlation and relativistic theories) at which the pseudopotentials are used in molecular calculations.

Computational saving by the reduction of basis sets to represent the valence orbital can only be achieved by elimination of core orbitals and radial nodes, and if the shape of the resulting pseudo valence orbital is as smooth as possible in the core region. Therefore the pseudo-orbital transformation should be modeled so as to minimize the difference to the all-electron case.

Nevertheless, the pseudopotential approximations do have distinctive features that are advantageous over all-electron methods. As mentioned earlier, one of the more immediate advantages is in computational savings by reducing the number of basis functions by replacing the core with pseudopotentials resulting in nodeless pseudoorbitals. Numerical noise associated with finite field methods can be reduced by the ability of pseudopotentials to evaluate small perturbations with a reduced total electronic energy. Perhaps more importantly, relativistic effects can be implicitly incorporated into the pseudopotential approximation [3-5].

4.1 The Pseudopotential Approximation

In pseudopotential approximations, one starts with an effective model valence Hamiltonian:

$$H_v = \sum_{i}^{n_v} h_v(i) + \sum_{i<j}^{n_v} g_v(i,j) + V_{cc} + V_{CPP} \qquad \text{Eq. 4.1}$$

where c and v denote core and valence, and h_v and g_v are effective one- and two-electron operators, respectively. V_{cc} represents core repulsion between core and nuclei and V_{CPP} is a core polarization potentials (CPP). n_v is the number of valence electrons treated explicitly in the calculations and is defined by

$$n_v = \sum_{\lambda}^{N} (Z_\lambda - Q_\lambda) \qquad \text{Eq. 4.2}$$

Here Q_λ is the charge of the core λ. Relativistic effects are treated implicitly for a reasonable compromise between accuracy and efficiency. That is, relativistic effects are treated by a nonrelativistic kinetic energy operator. Thus a standard scheme uses the inclusion of relativistic effects via parameterization of the pseudopotentials at a one-component (scalar relativistic) or a two-component (including spin-orbit coupling) level. In other words, the relativistic one- and two-component pseudopotentials use a nonrelativistic model Hamiltonian for the one- and two-electron operator (in a.u.):

$$h_v(i) = -\frac{1}{2}\Delta_i + V_v(i) \quad \text{and} \quad g_v(i,j) = \frac{1}{r_{ij}} \qquad \text{Eq. 4.3}$$

Here, V_v describes the interaction of a valence electron with all nuclei and cores in the system, and the relativistic contribution results from the parameterization of the potential, V_v. The molecular pseudopotential is assumed to be a superposition of atomic pseudopotentials which is led by the Coulomb attraction between point charges:

$$V_v(i) = \sum_{\lambda}^{N} \left(-\frac{Q_\lambda}{r_{\lambda i}} + \Delta V_v^\lambda (r_{\lambda i}) \right) + \ldots \qquad \text{Eq. 4.4}$$

Finally, the interaction between nuclei and the core is

$$V_{cc} = \sum_{\lambda<\mu}^{N} \left(\frac{Q_\lambda Q_\mu}{r_{\lambda\mu}} + \Delta V_{cc}^{\lambda\mu} (r_{\lambda\mu}) \right) + \ldots \qquad \text{Eq. 4.5}$$

4.1.1 Selecting the Core

Needless to say, one of the first steps in the pseudopotential approximation is to define an approximate core. The accuracy of the pseudopotential approximation is critically dependent on the size of core, and in turn the number of valence electrons. As usual, one must find a balance between the desired accuracy and the computational saving. There are some important points to consider when selecting a core.

The static dipole polarizability of the core should be small, for example, less than 1 a.u. The core usually consists of filled *p*, *d*, and *f* outermost orbitals. However, care must be taken as relativistic effects, especially the indirect and spin-orbit coupling effects may increase the core polarizability. In this case, the choice of the nonrelativistic core may not be suitable for relativistic calculations of heavy elements. Also, the frozen-core approximation needs to be kept intact. That is, the core density should not change significantly by either adding or removing valence electrons important in chemical bonding.

4.1.2 The Model Potential (MP)

Model potentials are based on the transfer of operators and potentials from an all-electron *ab-initio* scheme. In other words, by adding a core level-shift operator to the usual Hamiltonian. The most successful kind is the *ab-initio* model potential (AIMP) by Huzinaga *et al.* [6-9]. These MP's retain the nodal structure of the valence orbitals in the core. This means that basis functions are required to model these nodes. However, it still offers computational savings since only additional overlap integrals are needed.

4.1.3 The Effective Core Potential (ECP)

Historically, pseudopotentials were first defined as a one-electron operator simulating the frozen core-valence interaction by means of a local potential [10]. It was soon realized that the initial idea of a local potential could be improved by a semi-local or a non-local form of the pseudopotential as it was apparent that a local potential is less accurate in describing different states of angular symmetry

[11, 12]. That is, for example, the sequence in the angular momentum symmetries cannot be altered in a one-valence electron case, i.e. one always obtains $\varepsilon_s \leq \varepsilon_p \leq \varepsilon_d \ldots$ for the lowest eigenstates of each symmetry. In Ca^+, for example, the $4s \rightarrow 3d$ transition (13650 cm^{-1}) is below the $4s \rightarrow 4p$ transition (25192 cm^{-1}) and a local potential cannot correctly describe such a change in symmetry. One therefore chooses semi-local pseudopotentials [13].

For relativistic calculations including spin-orbit coupling, the semi-local ansatz in a two-component form may be written as

$$\Delta V_v^\lambda(\vec{r}_{\lambda i}) = \sum_{l=0}^{L-1} \sum_{j=|l-1/2|}^{l+1/2} \left(V_{lj}^\lambda(r_{\lambda i}) - V_L^\lambda(r_{\lambda i})\right) P_{lj}^\lambda(i) + V_L^\lambda(r_{\lambda i}) \qquad \text{Eq. 4.6}$$

Here, P_{lj}^λ is a projection operator at atom λ:

$$P_{lj}^\lambda(i) = P_{l,l\pm1/2}^\lambda(i) = \sum_{m_j=-j}^{j} \left|\lambda l j m_j(i)\right\rangle\left\langle\lambda l j m_j(i)\right| \qquad \text{Eq. 4.7}$$

For scalar relativistic calculations, a one-component form is obtained by averaging over the spin,

$$\Delta V_{v,av}^\lambda(\vec{r}_{\lambda i}) = \sum_{l=0}^{L-1}\left(V_l^\lambda(r_{\lambda i}) - V_L^\lambda(r_{\lambda i})\right) P_l^\lambda(i) + V_L^\lambda(r_{\lambda i}) \qquad \text{Eq. 4.8}$$

In this case the projection operator refers to

$$P_l^\lambda(i) = \sum_{m_l=-l}^{l} \left|\lambda l m_l(i)\right\rangle\left\langle\lambda l m_l(i)\right| \qquad \text{Eq. 4.9}$$

A spin-orbit operator may be defined as

$$\Delta V_{v,so}^\lambda(\vec{r}_{\lambda i}) = \sum_{l=1}^{L-1} \frac{\Delta V_l^\lambda(r_{\lambda i})}{2l+1}\left[l P_{l,l+1/2}^\lambda(i) - (l+1) P_{l,l-1/2}^\lambda(i)\right] \qquad \text{Eq. 4.10}$$

The potentials V_{lj}^{λ} and V_{l}^{λ} are represented as a linear combination of Gaussian functions:

$$V_{lj}^{\lambda}(r_{\lambda i}) = \sum_{k} A_{ljk}^{\lambda} r_{\lambda i}^{n_{ljk}^{\lambda}} \exp\left(-a_{ljk}^{\lambda} r_{\lambda i}^{2}\right) \qquad \text{Eq. 4.11}$$

In shape-consistent pseudopotentials [14, 15], the pseudopotential parameters in Eq. 4.11 are adjusted to the valence orbitals of a specific symmetry to high accuracy above a certain cut off radius, r_c. One way of achieving this is to modify the all-electron orbitals such that they are nodeless in the core region below $r < r_c$. In other words, the pseudo-orbitals are generated by keeping the valence orbital outside r_c unchanged while the nodal structure inside the radius r_c is replaced by a smooth and nodeless polynomial expansion. The pseudopotential parameters are then adjusted to reproduce these nodeless pseudo-orbitals. These so-called shape-consistent pseudopotentials including spin-orbit operators have been generated by Christiansen and Ermler [16].

In energy-consistent pseudopotentials, the pseudopotential parameters are fitted to an atomic valence spectrum in a least-square fit so that the following function is minimized:

$$S = \sum_{m} \sum_{n} w_{n,m} \left[E_{nm}^{\mathrm{PP}} - E_{val,nm}^{\mathrm{AE}} \right]^{2} \qquad \text{Eq. 4.12}$$

The energy-consistent pseudopotentials are appealing in that the pseudopotential parameters are fitted to quantum mechanical observables such as the total valence energy instead of relying on quantities such as orbitals or orbital energies, which are only meaningful in the framework of the one-particle approximation. In recent advances, reference data are obtained in all-electron numerical Dirac-Coulomb-Hartree-Fock calculations. Such techniques are widely used by the Stuttgart group [17].

4.2 The Details of the Pseudopotential Adjustment

In the present study, the following valence model Hamiltonian (in atomic units) was used for an atom:

$$H_v = -\frac{1}{2}\sum_i \Delta_i + \sum_i V_{pp}(i) + \sum_{i<j} \frac{1}{r_{ij}} + V_{CPP} \qquad \text{Eq. 4.13}$$

where i, j are valence electron indices and V_{pp} (i) is a semi-local pseudopotential. For a j-dependent two-component spin-orbit pseudopotentials (SOPP), the following ansatz for the pseudopotential $V_{pp}(i)$ was used:

$$V_{\text{SOPP}} = -\frac{Q_c}{r_i} + \sum_{klj} B_{klj} \exp\left(-\beta_{ljk} r_i^2\right) P_{lj} \qquad \text{Eq. 4.14}$$

where Q_c denotes the core charge, and P_{lj} is the projection operator acting on the Hilbert subspace of angular symmetry l and $j = l \pm 1/2$. For a j-averaged pseudopotential (ARPP), the above ansatz largely remains the same with the j-dependence dropped out:

$$V_{\text{ARPP}} = -\frac{Q_c}{r_i} + \sum_{kl} C_{lk} \exp\left(-\gamma_{lk} r_i^2\right) P_l \qquad \text{Eq. 4.15}$$

In both cases, these essentially form a linear combination of Gaussian functions with adjustable parameters, B and β (C and γ).

In order to construct a series of reference data to which the pseudopotential parameters are adjusted, the all-electron reference valence energies (defined as $E^{\text{AE}}_{val,nm} = E_{total} - E_{core}$) of a number of different electronic states of the group 1 and group 2 elements (K to E119 and Ca to Ra) were obtained numerically in an all-electron multi-configuration Dirac-Coulomb-Hartree-Fock (DCHF) calculation, using a modified version of the finite-difference atomic GRASP code [18]. Here, relativistic effects are included at a four-component level using the Dirac-Coulomb Hamiltonian, with Breit interaction terms correct to the first order [19]. Average level type of calculations were performed with GRASP, which includes all configurations state functions resulting from a given nonrelativistic

configuration. For the case of SOPP, individual j-dependent energies were used, whereas the j-averaged energies were taken in the case of ARPP.

The pseudopotentials were then fitted in a least-square sense so that the function in Eq. 4.12 is minimized with respect to the pseudopotential parameters.

$$S = \sum_{m}\sum_{n} w_{n,m}\left[E_{nm}^{\mathrm{PP}} - E_{val,nm}^{\mathrm{AE}}\right]^2$$

Here, m and n are orbital configurations and relativistic states of a given orbital configuration, and E_{nm}^{PP} and $E_{val,nm}^{\mathrm{AE}}$ are valence energies from the pseudopotential and all-electron calculations, respectively. $w_{n,m}$ are individual and configurational weights. By an augmented-Hessian like procedure based on the derivatives of E_{nm}^{PP} with respect to B_{klj} and β_{ljk}, a new set of parameters resulting in a smaller value of S is obtained. This typically involves some hundreds of iterations, achieving a near minimum value of S. Such methods have been used in the generation of energy-consistent pseudopotentials for the group 13 [20], 14, and 15 elements [21], using a small core definition of $(n\text{-}1)spd(n)sp$.

In order to address the transferability of pseudopotentials to the subsequent molecular application, the singly and doubly charged cations and the anion were included in the reference energy data spectrum for s-, p-, and d-projectors. The f- and g-projectors were adjusted to the valence energies arising from various configurations of 7^+ ions with a single f- or g-electron outside the core to obtain a better convergence for the group 1 pseudopotentials. (8^+ ions for the group 2 pseudopotentials) As a demonstration, the reference states used for the generation of the Cs pseudopotentials are listed below:

Cs	$5s^25p^66s^1$	$5s^25p^66p^1$	$5s^25p^67s^1$	$5s^25p^67p^1$
	$5s^25p^56s^2$	$5s^25p^56s^16p^1$	$5s^25p^56p^2$	$5s^25p^65d^1$
	$5s^25p^66d^1$	$5s^25p^55d^16s^1$	$5s^25p^55d^2$	$5s^25p^55d^16p^1$
Cs^+	$5s^25p^6$	$5s^25p^56s^1$	$5s^25p^56p^1$	$5s^25p^55d^1$
Cs^{2+}	$5s^25p^5$	$5s^25p^46s^1$	$5s^25p^46p^1$	$5s^25p^45d^1$
Cs^-	$5s^25p^66s^2$			
Cs^{7+}	$4f^1$ - $7f^1$			
Cs^{7+}	$5g^1$ - $7g^1$			

For the group 1 elements, the valence shell consists of nine electrons. The maximum value of parameter l has been chosen to be 3 for K and Rb, and 4 for Cs, Fr, and E119. The expansion parameter, k was allowed to vary up to 4. For the group 2 elements, the valence shell consists of ten electrons. The present pseudopotential parameters of ARPP and SOPP are listed in appendix A.

Up to this point, correlation effects of the core electrons on the valence electrons are taken into account in a frozen core approximation. However, this is not always a good approximation, especially for the alkali atoms due to their easily polarizable core. Therefore, the last term in Eq. 4.13, V_{CPP} is introduced to account for the dynamic polarization of the atomic core by the valence electrons. The following form of the effective core polarization potential (CPP) is used as demonstrated by Müller *et al.*[22]:

$$V_{CPP} = -\frac{1}{2}\alpha_{\mathrm{D}}\mathbf{f}_{\lambda}^{2} \qquad \text{Eq. 4.16}$$

$$\mathbf{f}_{\lambda} = -\sum_{i}\frac{\mathbf{r}_{i\lambda}}{r_{i\lambda}^{3}}\left[1-\exp(-\delta_{e}^{\lambda}r_{i\lambda}^{2})\right]^{n_e} + \sum_{\mu\neq\lambda}Q_{\mu}\frac{\mathbf{r}_{\mu\lambda}}{r_{\mu\lambda}^{3}}\left[1-\exp(-\delta_{c}^{\lambda}r_{\mu\lambda}^{2})\right]^{n_c} \qquad \text{Eq. 4.17}$$

α_{D} is the static dipole polarizability of the core λ and $\mathbf{f}$ is the electric field generated by the valence electrons. A cut-off parameter for the electric field is used to avoid divergence caused by valence electrons too close to the core.

Following the small core definition of M^{9+} for the group 1 pseudopotentials and M^{10+} for the group 2, it is argued that the majority of core-valence correlation is incorporated into the valence correlation. The effects of core-valence correlation is therefore only considered in selected cases where there is obvious suspicion that valence correlation alone leads to improper accounts of the correlation effects. The details of the CPP parameters used in the present study are described in appendix A.

So far any errors due to finite basis set expansion have been avoided by the numerical calculations in the generation of the pseudopotentials. These pseudopotentials, however, need to be accompanied with valence basis sets for subsequent molecular calculations. The exponents for these valence basis sets are taken from the relativistic all-electron basis sets developed in this study. These valence basis sets are presented in appendix A.

4.3 The Accuracy of Pseudopotentials

In order to demonstrate the accuracy of the present pseudopotentials, the HF valence energies of a few selected states of the group 1 and 2 elements calculated by numerical all-electron and pseudopotential methods are listed in Table 4.1 and Table 4.2, respectively. The radial distribution functions of the outer most valence orbital estimated by these pseudopotentials are compared with numerical all-electron DCHF results in Figures 4.1 to 4.9.

It is easily seen from Table 4.1 that the pseudopotential errors, ΔE^{PP} are well below 0.01 eV for K and Rb. From Cs, the pseudopotential error of some states starts to exceed 0.01 eV. The problematic configurations for elements up to Cs seem to be the doubly charged configuration of $(n\text{-}1)s^2p^5$. For the heavier elements, the pseudopotential error of the negatively charged ns^2 configuration exceeds that of the doubly charged $(n\text{-}1)s^2p^5$ configuration.

Also evident from Table 4.1 is the large pseudopotential errors associated with E119. In particular, the pseudopotential valence energy of the ground state configuration of $7s^27p^68s^1$ for E119 deviates from the all-electron case by more than 0.026 eV. Three other states listed in Table 4.1 for E119 have pseudopotential errors in excess of 0.01 eV. As a result the 8*s* radial distribution calculated with these pseudopotentials deviates slightly from the all-electron case as shown in Figure 4.5. For all the other group 1 elements, the radial distribution functions of the valence *ns* orbital from the pseudopotential calculations are virtually identical to the all-electron cases in the valence region. It was noted in this study that Seth's original pseudopotentials [23] for E119 performs no better than the present ones.

For the group 2 elements, the agreement between the pseudopotential and all-electron methods tends to be better than for the group 1 elements. The pseudopotential errors in Table 4.2 are smaller than 0.01 eV for all elements except for Ca where the upper bound of the pseudopotential error is found to be 0.02 eV. The largest pseudopotential errors for all elements are associated with the doubly charged $(n\text{-}1)s^2p^6$, except for Ra. The resulting pseudopotential radial distribution functions of the valence orbital are virtually identical to the all-electron cases for all elements as shown in Figures 4.6 to 4.9.

	Valence state	E^{AE}	E^{PP}	ΔE^{PP}
K	$3s^2 3p^6 4s^1$	-28.0389393898	-28.0390180359	-0.00214
K	$3s^2 3p^6 4p^1$	-27.9867725965	-27.9866007673	0.00468
K^+	$3s^2 3p^6$	-27.1647046848	-27.1648661183	-0.00439
K^{2+}	$3s^2 3p^5$	-26.7660098531	-26.7657764303	0.00635
K^-	$3s^2 3p^6 4s^2$	-28.0360669598	-28.0361601926	-0.00254
Rb	$4s^2 4p^6 5s^1$	-23.7993090499	-23.7993671083	-0.00158
Rb	$4s^2 4p^6 5p^1$	-23.7499301499	-23.7498409748	0.00243
Rb^+	$4s^2 4p^6$	-23.6596681499	-23.6595669494	0.00275
Rb^{2+}	$4s^2 4p^5$	-22.6833674832	-22.6832661965	0.00276
Rb^-	$4s^2 4p^6 5s^2$	-23.7967601499	-23.7968268091	-0.00181
Cs	$5s^2 5p^6 6s^1$	-19.8592853847	-19.8599167280	-0.01718
Cs	$5s^2 5p^6 6p^1$	-19.8159058180	-19.8158617550	0.00120
Cs^+	$5s^2 5p^6$	-19.7315150847	-19.7315428791	-0.00076
Cs^{2+}	$5s^2 5p^5$	-18.8943171180	-18.8935987469	0.01955
Cs^-	$5s^2 5p^6 6s^2$	-19.8570811847	-19.8577194171	-0.01737
Fr	$6s^2 6p^6 7s^1$	-18.9222635243	-18.9221610895	0.00279
Fr	$6s^2 6p^6 7p^1$	-18.8727041910	-18.8731867126	-0.01313
Fr^+	$6s^2 6p^6$	-18.7904545243	-18.7907764075	-0.00876
Fr^{2+}	$6s^2 6p^5$	-18.0005851910	-18.0004419630	0.00390
Fr^-	$6s^2 6p^6 7s^2$	-18.9205545243	-18.9203523210	0.00550
E119	$7s^2 7p^6 8s^1$	-18.6899133687	-18.6889545053	0.02609
E119	$7s^2 7p^6 8p^1$	-18.6155323687	-18.6157207896	-0.00513
$E119^+$	$7s^2 7p^6$	-18.5343393687	-18.5339205866	0.01140
$E119^{2+}$	$7s^2 7p^5$	-17.7565830354	-17.7554372576	0.03118
$E119^-$	$7s^2 7p^6 8s^2$	-18.6932323687	-18.6918103164	0.03870

Table 4.1. Valence HF energies (in a.u.) of the group 1 elements obtained in numerical DCHF all-electron calculations, E^{AE} and numerical pseudopotential calculations, E^{PP}. ΔE^{PP} is the pseudopotential error in eV. All values are spin-orbit averaged.

	Valence state	E^{AE}	E^{PP}	ΔE^{PP}
Ca	$3s^2 3p^6 4s^2$	-36.4470295688	-36.4476959336	-0.01813
Ca	$3s^2 3p^6 4s^1 4p^1$	-36.3864441730	-36.3870022802	-0.01519
Ca^+	$3s^2 3p^6 4s^1$	-36.2581305088	-36.2583726896	-0.00659
Ca^{2+}	$3s^2 3p^6$	-35.8409013188	-35.8403794438	0.01420
Sr	$4s^2 4p^6 5s^2$	-30.3428904304	-30.3430295874	-0.00379
Sr	$4s^2 4p^6 5s^1 5p^1$	-30.2865018387	-30.2866688840	-0.00455
Sr^+	$4s^2 4p^6 5s^1$	-30.1683388304	-30.1683870101	-0.00131
Sr^{2+}	$4s^2 4p^6$	-29.7846510997	-29.7846492304	-0.00005
Ba	$5s^2 5p^6 6s^2$	-25.1021400471	-25.1023213203	-0.00493
Ba	$5s^2 5p^6 6s^1 6p^1$	-25.0540060388	-25.0541782130	-0.00469
Ba^+	$5s^2 5p^6 6s^1$	-24.9448598471	-24.9449381745	-0.00213
Ba^{2+}	$5s^2 5p^6$	-24.6007437471	-24.6005277745	0.00588
Ra	$6s^2 6p^6 7s^2$	-23.7485331551	-23.7481657126	0.01000
Ra	$6s^2 6p^6 7s^1 7p^1$	-23.6913495718	-23.6914182731	-0.00187
Ra^+	$6s^2 6p^6 7s^1$	-23.5884391551	-23.5882634675	0.00478
Ra^{2+}	$6s^2 6p^6$	-23.2412961551	-23.2409540329	0.00931

Table 4.2. Valence HF energies (in a.u.) of the group 2 elements obtained in numerical DCHF all-electron calculations, E^{AE} and numerical pseudopotential calculations, E^{PP}. ΔE^{PP} is the pseudopotential error in eV. All values are spin-orbit averaged.

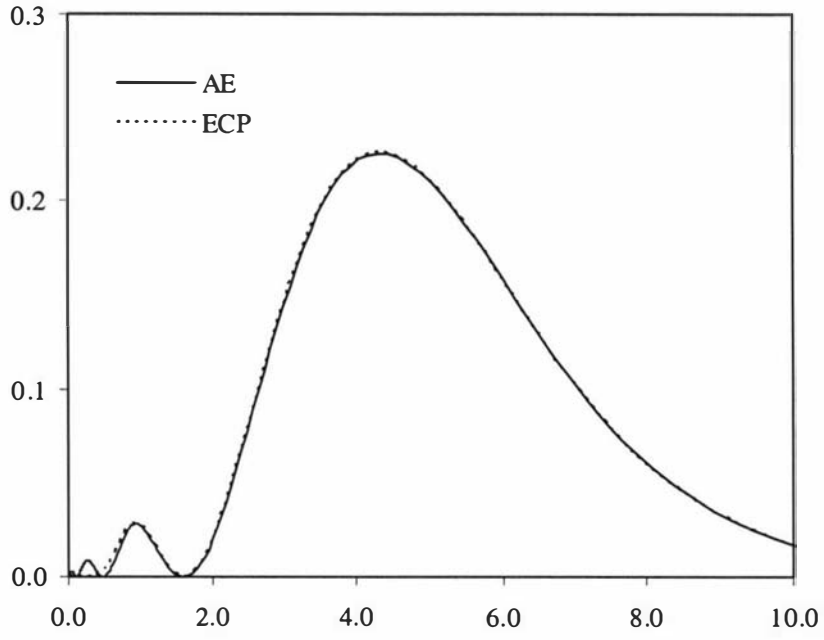

Figure 4.1. The 4*s* radial distribution function of K estimated in a numerical Dirac-Coulomb-Hartree-Fock and a pseudopotential calculation.

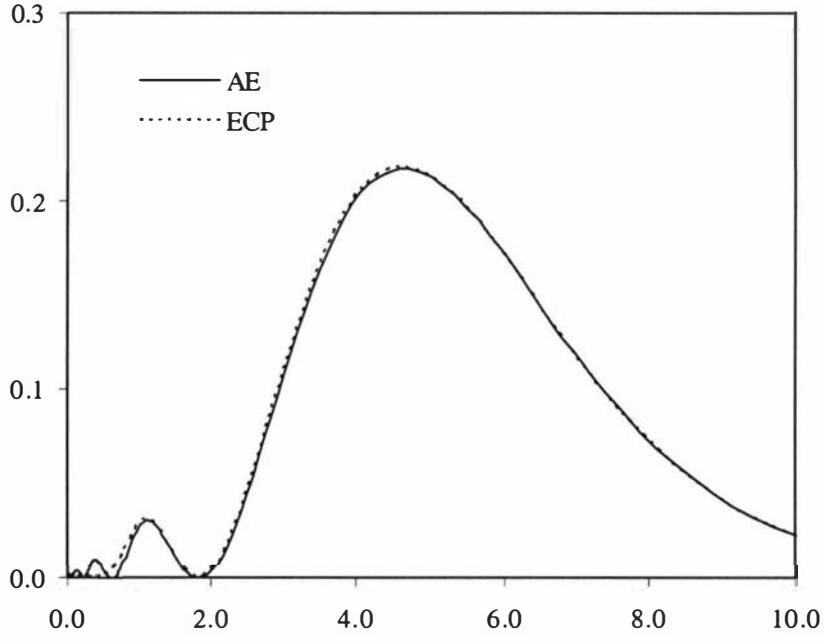

Figure 4.2. The 5*s* radial distribution function of Rb estimated in a numerical Dirac-Coulomb-Hartree-Fock and a pseudopotential calculation.

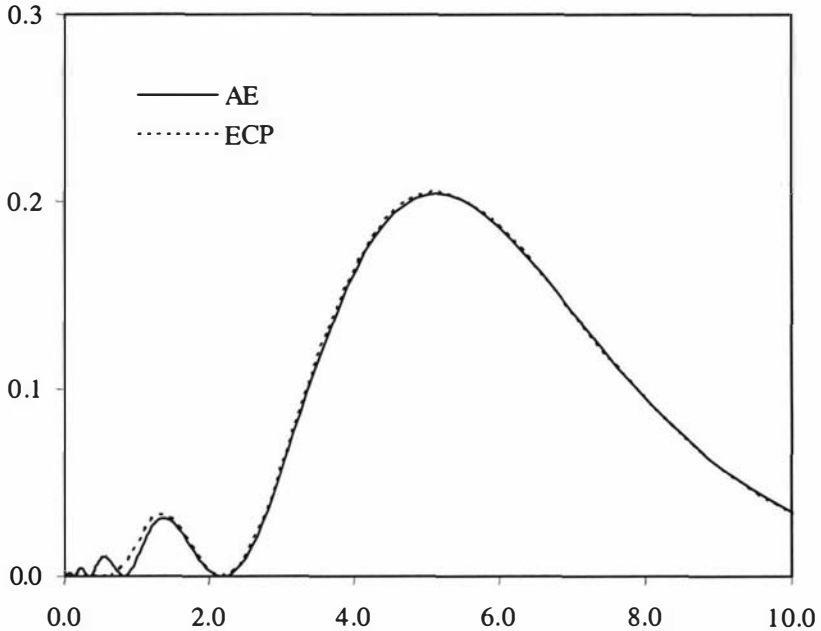

Figure 4.3. The 6*s* radial distribution function of Cs estimated in a numerical Dirac-Coulomb-Hartree-Fock and a pseudopotential calculation.

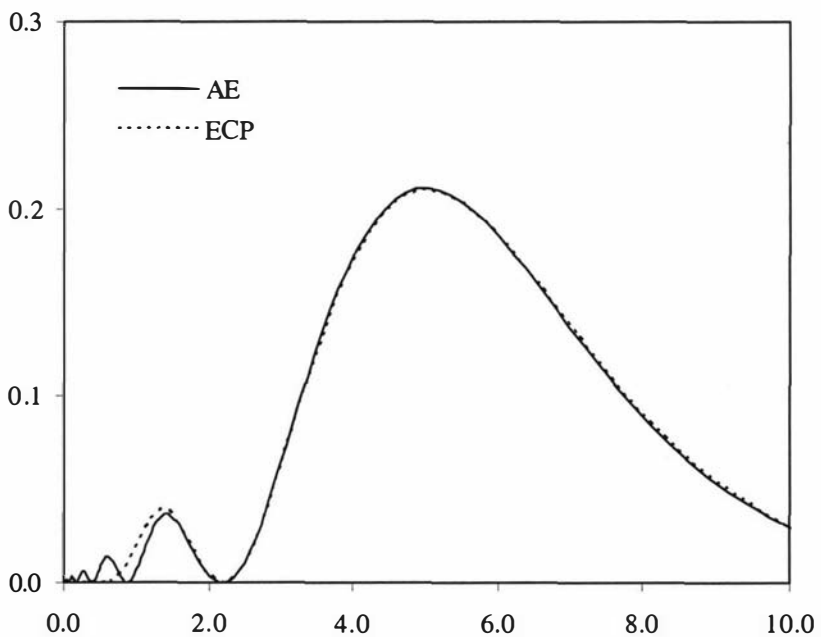

Figure 4.4. The 7*s* radial distribution function of Fr estimated in a numerical Dirac-Coulomb-Hartree-Fock and a pseudopotential calculation.

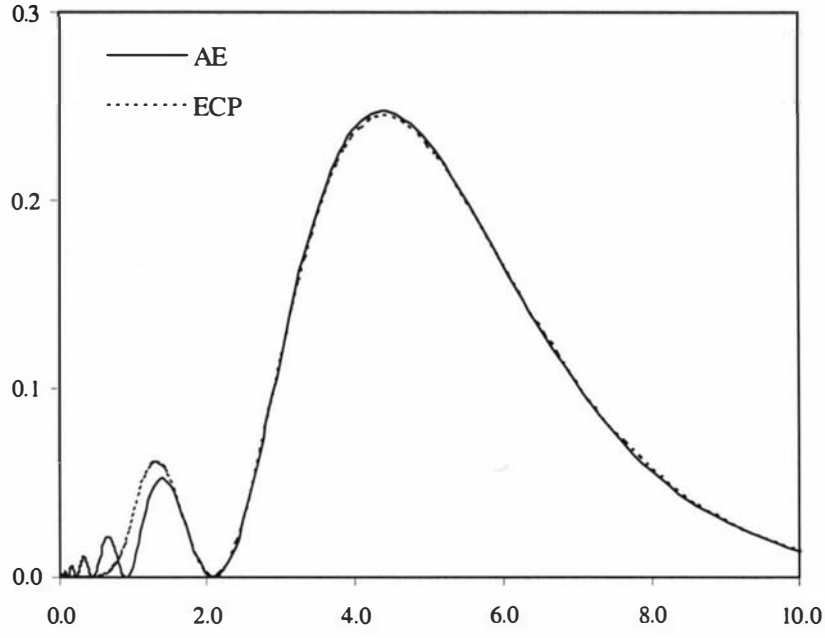

Figure 4.5. The 8*s* radial distribution function of E119 estimated in a numerical Dirac-Coulomb-Hartree-Fock and a pseudopotential calculation.

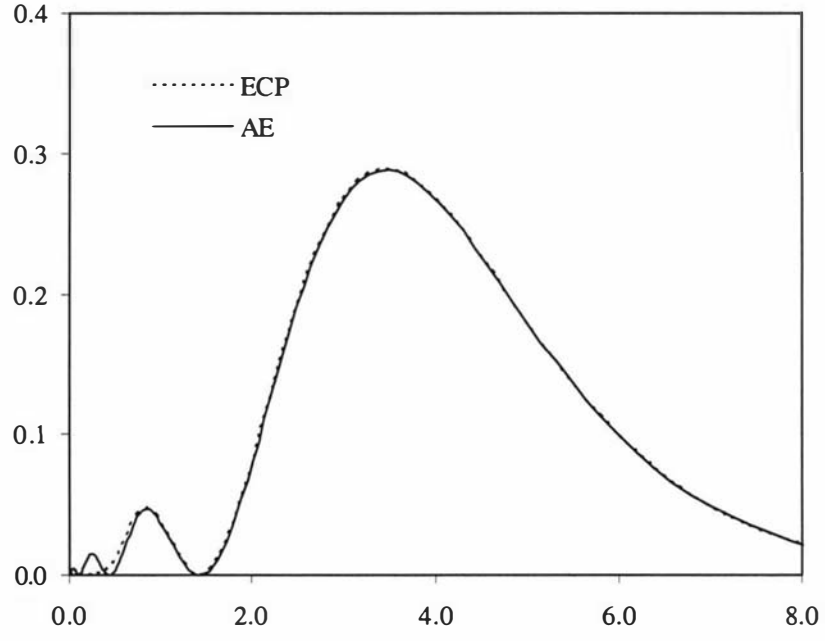

Figure 4.6. The 4*s* radial distribution function of Ca estimated in a numerical Dirac-Coulomb-Hartree-Fock and a pseudopotential calculation.

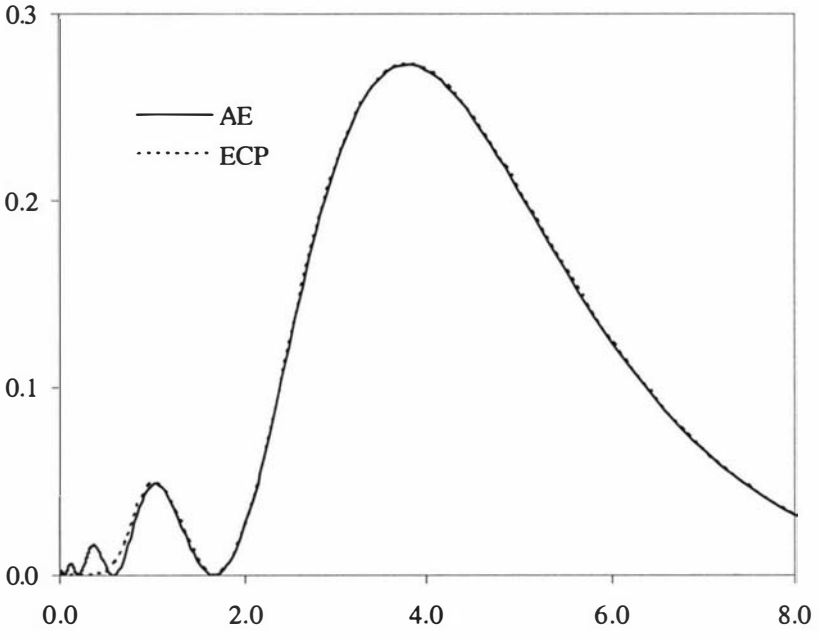

Figure 4.7. The 5*s* radial distribution function of Sr estimated in a numerical Dirac-Coulomb-Hartree-Fock and a pseudopotential calculation.

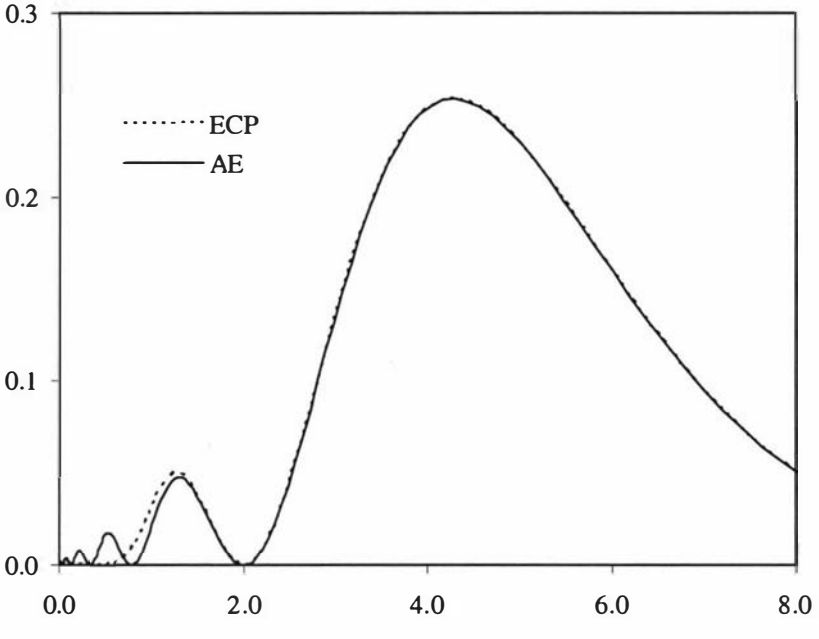

Figure 4.8. The 6*s* radial distribution function of Ba estimated in a numerical Dirac-Coulomb-Hartree-Fock and a pseudopotential calculation.

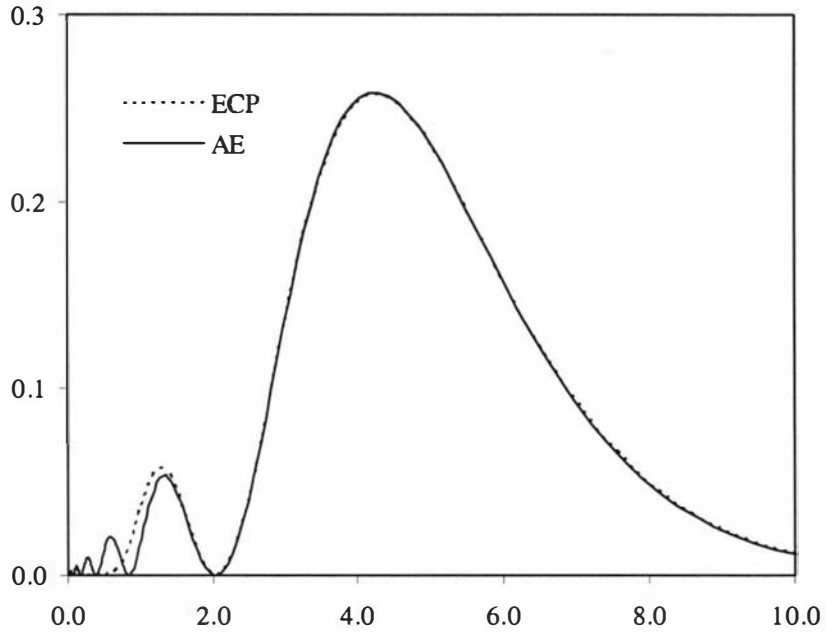

Figure 4.9. The 7*s* radial distribution function of Ra estimated in a numerical Dirac-Coulomb-Hartree-Fock and a pseudopotential calculation.

References

[1] H. Hellmann, J. Chem. Phys. **3**, 61 (1935).

[2] P. Gombás, Z. Phys. **94**, 473 (1935).

[3] G. Frenking, I. Antes, M. Böhme, S. Dapprich, A. W. Ehlers, V. Jonas, A. Neuhaus, M. Otto, R. Stegmann, A. Veldkamp, and S. F. Vyboishikov, in *Reviews in Computational Cemistry*, edited by K. B. Lipkowitz and D. B. Boyd (VCH, New York, 1996), vol. 8 p. 63.

[4] Y. Ishikawa and G. Malli, J. Chem. Phys. **75**, 5423 (1981).

[5] A. Shukla and A. Banerjee, J. Chem. Phys. **100**, 3695 (1994).

[6] S. Huzinaga, L. Seijo, Z. Barandiaran, and M. Klobukowski J. Chem. Phys. **86**, 2132 (1987).

[7] S. Katsuki and S. Huzinaga, Chem. Phys. Lett. **147**, 597 (1998).

[8] L. Seijo, Z. Barandiaran, and S. Huzinaga, J. Chem. Phys. **91**, 7011 (1989).

[9] Z. Barandiaran, L. Seijo, and S. Huzinaga, J. Chem. Phys. **93**, 5843 (1990).

[10] V. Fock, M. Vesslow, and M. Petraschen, Zh. Eksp. Teor. Fiz. **10**, 723 (1940).

[11] W. H. E. Schwarz, Theor. Chim. Acta **11**, 307 (1968).

[12] W. H. E. Schwarz, Theor. Chim. Acta **11**, 377 (1968).

[13] L. R. Kahn and W. A. Goddard, J. Chem. Phys. **56**, 2685 (1972).

[14] P. Durand and J. C. Barthelat, Theor. Chim Acta. **38**, 283 (1975).

[15] P. A. Christiansen, Y. S. Lee, and K. S. Pitzer, J. Chem. Phys. **71**, 4445 (1979).

[16] W. C. Ermler, R. B. Ross, and P. A. Christiansen, J. Quant. Chem. **40**, 829 (1991).

[17] The Stuttgart group pseudopotentials of Stoll and co-worker are available in http://www.theochem.uni-stuttgart.de/pseudopotentials/index.html

[18] K. G. Dyall, I. P. Grant, C. T. Johnson, F. A. Parpia, E. P. Plummer, Comput. Phys. Commun **55**, 425 (1989).

[19] G. Breit, Phys. Rev. **34**, 553 (1929); ibid. **39**, 616 (1932).

[20] B. Metz, M. Schweizer, H. Stoll, M. Dolg, and W. Liu, Theor. Chem. Acc. **104**, 22 (2000).

[21] B. Metz, H. Stoll, and M. Dolg, J. Chem. Phys. **113**, 2563 (2000).

[22] W. Müller, J. Flesch, and W. Meyer, J. Chem. Phys. **80**, 3297 (1984).

[23] M. Seth, PhD thesis (1998) The University of Auckland.

Chapter 5
THE NEUTRAL GROUP 1 ELEMENTS

An accurate calculation of the static or dynamic multipole polarizabilities for atoms and molecules including heavy atoms remains a great challenge to theoreticians. This is largely associated with electron correlation and relativistic effects, as they become increasingly more important for heavy elements [1, 2].

Concerning the static dipole polarizabilities of the neutral alkali-metal atoms, there are two sets of experimental data by Molof *et al.* [3] and Zorn *et al.* [4, 5], which have error bars of a few percent. Recently, a very accurate experimental value of the Cs static dipole polarizability (α_D(Cs) = 401.0 ± 0.6 a.u.) has been published by Amini *et al.* [6]. They have reported that the uncertainty associated with their measurement is improved by a factor of 14 over previous measurements.

There are a number of theoretical studies [7, 8] for H [9, 10], Li [8, 10-17], Na [8, 10, 13, 15, 16], K [1, 10, 13], Rb [1, 13, 18], Cs [1, 18], and Fr [1]. Particularly noteworthy are the calculations by Kellö *et al.* [1] for K, Rb, Cs, and Fr at the complete active space second-order perturbation (CASPT2) level of theory, using the mass-velocity and Darwin (MVD) terms of the Pauli Hamiltonian [19] to account for scalar relativistic effects. The perturbative MVD method employed in their study, however, accounts only for the first order corrections of the Pauli Hamiltonian and is shown to perform rather poorly when applied to superheavy elements [20]. This is because it relies on the assumption that the perturbation is relatively small.

As for the accuracy of static dipole polarizabilities obtained by all-electron methods, the quality of the basis sets is critically important, especially in the estimation of electron correlation effects. In order to obtain highly accurate dipole polarizabilities, basis set effects on the static dipole polarizabilities of the neutral group 1 elements are investigated at the coupled-cluster (CC) level using large basis sets derived in this study.

Relativistic effects in dipole polarizabilities are investigated in detail within a relativistic Douglas-Kroll (DK) formalism [21] discussed in chapter 3. While it has been shown that the first-order Pauli Hamiltonian is not adequate for the heaviest elements, the scalar relativistic DK operator performs extremely well even for superheavy elements such as E111 [20].

The performance of the present pseudopotentials for the alkali-metals, together with the optimized valence basis sets, was tested for the static dipole polarizabilities and the ground state ionization potentials of the neutral group 1 elements from K to E119. The results are compared with all-electron (AE) values.

5.1 Basis Sets

The importance of basis sets in calculating dipole polarizabilities are well documented [1, 13]. Much effort has gone into devising standardized basis sets for high level calculations by Sadlej *et al.* [22]. They have developed a technique for the generation of the so-called first-order polarized basis sets. Although their basis sets are relatively compact and seem to offer reasonable computational savings, they tend to lack in accuracy. The authors, however, noted that their basis sets are primarily for molecular applications where a further extension of their basis sets is rather impractical for routine calculations.

5.1.1 Basis Set Modification

In order to minimize errors caused by the use of finite basis sets, the convergence behavior of the group 1 dipole polarizabilities with respect to a basis set expansion was studied both at the DK Hartree-Fock (DKHF) and DK second-order many-body-perturbation (DKMP2) level. This was carried out by modifying the relativistic DK all-electron basis sets of Ref. [23]. Particular attention was given in the expansion of polarization functions up to a maximum angular momentum, l_{max} of 4, i.e. *g*-type functions. l_{max} was chosen to be 4 as a basis set expansion beyond the *g*-type functions presents computational difficulties for high level (coupled-cluster) electron correlation treatment. The

influence of *h*-type functions was, therefore, investigated at the DKMP2 level only and will be discussed later in the chapter.

The present basis set modification is as follows: For K, the original DK set was extended by one *s*-type function (0.07) and three *d*-type functions (4.1168, 1.556, 0.08126), leading to a (17*s*14*p*7*d*) GTO set. This GTO set was further augmented by five *f*-type functions (4.1168, 1.556, 0.61219, 0.22305, 0.08126), giving a final (17*s*14*p*7*d*5*f*) GTO set.

For Rb, the original DK basis set was modified by replacing six *s*-type functions (3.130680, 1.423036, 0.646835, 0.31, 0.15, 0.08) with five (3.946150, 1.844039, 0.692172, 0.276767, 0.0791) and by deleting one function (0.006404) in order primarily to eliminate linear dependencies. This (22*s*15*p*11*d*4*f*) GTO set was further augmented by four additional *f*-type functions (0.21126, 0.071, 0.02549, 0.00886). In order to test the influence of *g*-type functions, five functions (17.65946, 6.359740, 2.431531, 0.7215166, 0.21126) were added to the *g* sub-set, giving a (22*s*15*p*11*d*8*f*5*g*) GTO set.

The original DK basis set of Cs was extended with one *d*-type function (0.0498) and six *f*-type functions (30.342, 0.3469, 0.13384, 0.049804, 0.0199217, 0.0076859). This (27*s*19*p*13*d*10*f*) GTO set was extended by five *g*-type functions (5.6225, 2.37308, 0.91618, 0.3469, 0.13384), leading to a final (27*s*19*p*13*d*10*f*5*g*) GTO set.

For Fr, an additional *d*-type function (0.052867) and four additional diffuse *f*-type functions (0.361091, 0.134774, 0.0528672, 0.022028) were added to the original DK basis set. The influence of *g*-type functions was tested more extensively than previously carried out [23] by an addition of seven *g*-type functions. The resulting GTO set was (31*s*22*p*19*d*14*f*7*g*).

	Basis set contraction schemes
K	(17*s*14*p*7*d*5*f*)/[12*s*12*p*7*d*5*f*]
Rb	(22*s*15*p*11*d*8*f*5*g*)/[15*s*12*p*9*d*8*f*5*g*]
Cs	(27*s*19*p*13*d*10*f*5*g*)/[13*s*11*p*9*d*10*f*5*g*]
Fr	(31*s*22*p*19*d*14*f*7*g*)/[15*s*13*p*11*d*11*f*7*g*]
E119	(31*s*29*p*23*d*17*f*11*g*)/[17*s*16*p*14*d*17*f*11*g*]

Table 5.1. All-electron basis sets and the contraction schemes of the neutral group 1 elements from K to E119.

For E119, a new (31*s*29*p*23*d*17*f*11*g*) GTO set was obtained by an energy minimization using the 4-component fully relativistic GRASP code [24]. This GTO set was contracted to a [17*s*16*p*14*d*17*f*11*g*] CGTO set.

All present GTO sets were generally contracted. The contraction coefficients were obtained from a relativistic DKHF calculation. The optimized final basis sets along with the contraction schemes are summarized in Table 5.1.

5.2 Static Dipole Polarizabilities of the Neutral Group 1 Elements

The calculated static dipole polarizabilities of the neutral group 1 elements together with the corresponding atomic basis sets are presented in Table 5.2. In order to clearly demonstrate the effects of the basis set modifications described in chapter 5.1.1, the present dipole polarizabilities are compared with the values resulting from the original basis sets [23], as shown in the first row (rows marked [23]) for each element in Table 5.2. The values are shown to two decimal places to make small changes more transparent.

5.2.1 Basis Set Effects of the Dipole Polarizabilities

Table 5.2 summarizes the effects of the present basis set modification at the scalar relativistic DK level.

At the HF level, the basis set modification shows a negligible increase in dipole polarizabilities for all elements, except for E119. (E119 is excluded from this discussion, as the basis exponents for this element was newly optimized, rather than extended.) That is to say that the previous basis sets already bear the converged values of dipole polarizabilities with respect to the basis set expansion up to angular momentum, $l_{max} = 4$.

Table 5.2 shows that, at the HF level, the inclusion of polarization functions has little effect on dipole polarizabilities. This can be rationalized by understanding the primary role of the polarization functions. The presence of polarization functions allows polarization of the valence shells. However in the HF case, the uncorrelated wavefunctions, described by a one-electron

Table 5.2. The calculated scalar relativistic all-electron static dipole polarizabilities of the group 1 elements. All values are in a.u. (1 a.u. = 0.148 18 Å^3).

		Basis set	DKHF	DKMP2	DKCCSD	DKCCSD(T)
K	[23]	(16*s*14*p*4*d*)/[12*s*12*p*4*d*]	409.05	277.47	307.22	301.28
		(17*s*14*p*7*d*)/[12*s*12*p*7*d*]	410.29	273.19		
		(17*s*14*p*7*d*5*f*)/[12*s*12*p*7*d*5*f*]	410.17	261.35	303.24	291.12
Rb	[23]	(24*s*15*p*11*d*4*f*)/[17*s*12*p*9*d*4*f*]	483.77	267.32	341.14	324.24
		(22*s*15*p*11*d*8*f*)/[15*s*12*p*9*d*8*f*]	484.28	257.50		
		(22*s*15*p*11*d*8*f*5*g*)/[15*s*12*p*9*d*8*f*5*g*]	484.28	253.60	335.81	316.17
Cs	[23]	(27*s*19*p*12*d*4*f*)/[13*s*11*p*8*d*4*f*]	670.88	279.64	444.09	432.71
		(27*s*19*p*13*d*10*f*)/[13*s*11*p*8*d*10*f*]	671.52	254.97		
		(27*s*19*p*13*d*10*f*5*g*)/[13*s*11*p*9*d*10*f*5*g*]	671.52	245.78	435.27	396.02
Fr	[23]	(31*s*22*p*18*d*10*f*)/[15*s*13*p*10*d*7*f*]	542.99	193.51	355.44	329.17
		(31*s*22*p*19*d*14*f*)/[15*s*13*p*11*d*11*f*]	543.41	177.73		
		(31*s*22*p*19*d*14*f*7*g*)/[15*s*13*p*11*d*11*f*7*g*]	543.42	165.38	347.59	315.23
E119	[23]	(27*s*22*p*17*d*11*f*)/[17*s*13*p*10*d*7*f*]	252.76	130.45	191.34	184.83
		(31*s*29*p*23*d*17*f*)/[17*s*16*p*14*d*17*f*]	244.36	114.15		
		(31*s*29*p*23*d*17*f*11*g*)/[17*s*16*p*14*d*17*f*11*g*]	244.38	101.94	176.52	165.97

Hamiltonian, do not properly account for the core polarization and the atomic core does not significantly alter the valence region. As the valence region remains largely unchanged, the polarization functions have little effect on the dipole polarizabilities in the HF case. In other words, once the valence region is sufficiently relaxed by proper diffuse functions for the occupied orbitals, the uncorrelated dipole polarizabilities stabilize and a convergence is reached with respect to the basis sets without excessive use of polarization functions.

Although the magnitude of change in the dipole polarizability by the present basis set modification is negligible, the direction of change is in accordance with one's expectation. That is, as more diffuse functions are added, the valence tail of electronic density decays more slowly and as a result the valence region becomes more easily polarizable by an external electric field. Since the major contribution to the dipole polarizability comes from the polarization of the valence shell, this leads to an increased dipole polarizability (however small it might be) as shown in Table 5.2. This remains however a qualitative effect rather than a quantitative one as shown by a negligible amount of change.

At the correlated level, the present basis set modification leads to a significant decrease in dipole polarizabilities, in contrast to the HF case (Table 5.2) It is, therefore, evident that the convergence of the dipole polarizability with respect to the basis set expansion is slower at the correlated level than at the uncorrelated HF level. As electron correlation significantly alters the valence region more polarization functions are needed to allow the polarization of the valence region and to account for the effects of electron correlation. Consequently, a large number of *f*- and *g*-type functions were necessary for the evaluation of dipole polarizabilities of a basis set limit quality.

Indeed, the effects of additional *f*- and *g*-type functions in dipole polarizabilities are somewhat striking. For K, for example, the contribution from the *f*-type function is three fold higher than that from the additional *s*- and *d*-type functions. The influence of the *g*-type functions grow from Rb to E119. For E119, the *g*-type functions reduce the dipole polarizability by 11% at the DKMP2 level.

For E119, the new, larger basis set yields a dipole polarizability smaller than the original basis set even at the HF level. This clearly demonstrates the deficiencies in the original basis set. The influence of higher angular momenta functions is such that the dipole polarizability is reduced by 1.69 a.u at the DKMP2 level upon inclusion of nine *h*-type functions. This is further reduced by

0.40 a.u. when seven *i*-type functions were added. The convergence pattern in the dipole polarizability is therefore clearly demonstrated in terms of polarization functions. As mentioned earlier due to a very high computational demand with these extensive basis sets, the influence of *h*- and *i*-type functions were investigated at the MP2 level only.

5.2.2 Electron Correlation Contribution to the Dipole Polarizability

The data in Table 5.2 show that electron correlation effects reduce the dipole polarizability substantially. In the correlated case, the valence shell contracts and therefore the valence electrons are more tightly bound by the nucleus. This leads to a smaller change in the total electronic energy as a function of the applied external electric field in the correlated case than in the uncorrelated case as shown below:

$$\Delta E_{0,F}^{\text{correlated}} < \Delta E_{0,F}^{\text{uncorrelated}}$$

where E_0 and E_F are the total electronic energies at zero field and at the field strength of F, respectively. As a result, when the change in total electronic energy is plotted as a function of the external electric field strength, the resulting polynomial fit reveals a smaller curvature around zero field in the correlated case as depicted in Figure 5.1. The dipole polarizability essentially results from a second derivative of such a polynomial at zero field. Hence, the smaller the curvature, the smaller the dipole polarizability. This confirms that electron correlation leads to a decrease in the dipole polarizability and clearly demonstrates the overestimation of the dipole polarizability at the HF level. The reduction of dipole polarizabilities at the correlated level is, therefore, attributed to the valence shell contraction, which dominates over the slight core expansion caused by electron correlation [25]. The largest correlation effect is expected for the heaviest element, E119. This is however not supported in Table 5.2, where the dipole polarizability of Fr shows the largest correlation effect. This is because the values in Table 5.2 incorporate relativistic effects, which significantly alter electron correlation. Clearly, the two effects are not additive.

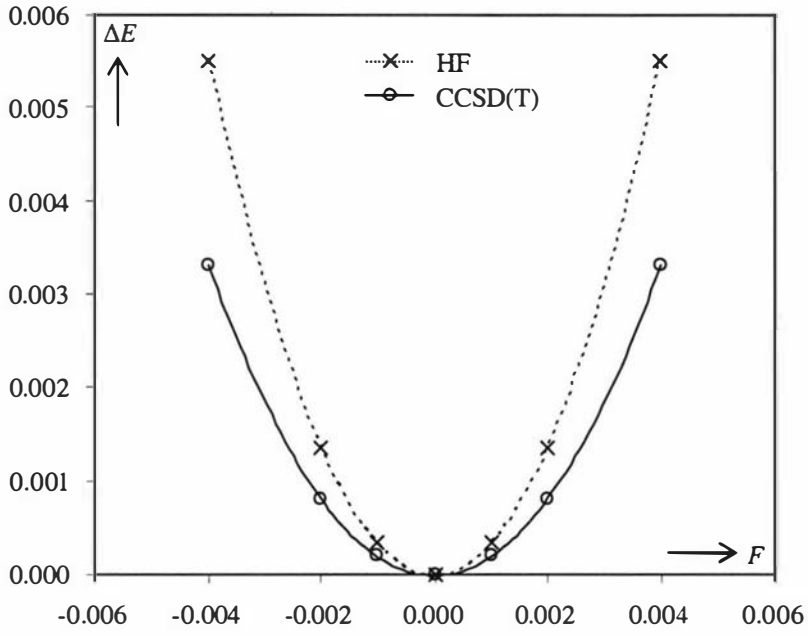

Figure 5.1. A plot of change in total electronic energy, ΔE as a function of electric field strength, F at uncorrelated and correlated level. The plot is taken from the present results for Cs. All values are in a.u.

5.2.3 Active Space in Electron Correlation for the Dipole Polarizability

Although it is the diffuse region of the electronic density that is of most importance in the polarization caused by an external electric field, it is critical to take into consideration the inner shell polarization, which significantly alters the polarization of the valence region. For example, it has been suggested by Sadlej *et al.* that for Cs, the inclusion of the $(n\text{-}2)d$ shell in the electron correlation procedure is important and the omission of this shell leads to an overestimated dipole polarizability by as much as 9 a.u. at the CASPT2 level of theory [1]. In order to extend this investigation to the case of Fr, the dipole polarizability of Fr was calculated with various sizes of active space in the correlation step. The results are shown in Table 5.3.

Frozen core	DKMP2	DKCCSD	DKCCSD(T)
KLMNO	234.04	356.12	331.67
KLMN	172.50	347.59	315.23
KLM	165.30	348.34	315.18
None	164.81	-	-

Table 5.3. The static dipole polarizability of Fr resulting from various active spaces. All values are in a.u.

At the DKMP2 level, the dipole polarizability shows a strong dependency on the choice of the active space. Upon inclusion of the (n-3) shell in electron correlation (compare frozen core KLMN and KLM), the dipole polarizability decreases by 4%. As many as 59 electrons need to be correlated in order to obtain a converged dipole polarizability. In contrast to Sadlej *et al.*'s earlier findings for Cs, it is clear that for Fr, the (n-3) shell as well as the (n-2) shell is of a significant importance in electron correlation at the DKMP2 level.

This dependency of the dipole polarizability on the size of the active correlating space is somewhat less profound at the DKCCSD/DKCCSD(T) level. Correlation of the (n-3) shell (i.e. KLM frozen core) has a negligible effect on the dipole polarizability compared with the smaller correlation space of frozen KLMN core. However, correlation of the (n-2) shell decreases the dipole polarizability by 5%. In other words, as many as 27 electrons need to be correlated at the DKCCSD/DKCCSD(T) step in order to obtain a dipole polarizability independent of the active correlation space. This is somewhat comforting since a DKCCSD/DKCCSD(T) calculation with a lager active space than KLM frozen core is currently not feasible with the large basis set used in this study. Nonetheless, the importance of correlating the (n-2) shell is clearly demonstrated for Fr.

5.2.4 Comparison with other Values

Overall, the present DKCCSD(T) dipole polarizabilities show an excellent agreement with the best available experimental values as shown in Table 5.4. Noteworthy is the calculation by Derevianko *et al.* [26] and Safronova *et al.* [27]. They have performed accurate calculations of dipole polarizabilities, adopting

high precision experimental values of the dipole matrix elements of the principal transitions. They have estimated error bars from the experimental accuracy of the matrix elements. Their theoretical approach utilized the explicit expression of the dipole polarizability shown in Eq. 2.5, noting the overwhelming contribution of the principal transitions to the sum-over-states, a fact made possible by the one valence electron configuration of the alkali-metals. Their values for the heavier elements, with smaller error bars than experimental values, are in excellent agreement with the present DKCCSD(T) values. The present dipole polarizabilities for Cs and Fr seem to be slightly smaller in comparison with the values of Derevianko *et al.* [26]. One source of the discrepancy is the spin-orbit coupling effects, where an increase in the dipole polarizabilities is expected due to a splitting of the next-to-valence p orbital into $p_{1/2}$ and $p_{3/2}$.

Coincidently, the purely theoretical dipole polarizabilities of Derevianko *et al.* [26] agree better with the present values than their values adopting experimental dipole matrix elements.

Basis set	K	Rb	Cs	Fr	E119
This work	291.1	316.2	396.0	315.2	166.0
Theor./Expt. [26]	290.2 ± 8	318.6 ± 6	399.9 ± 1.9	317.8 ± 2.4	-
Expt. [3, 6]	293 ± 6	319 ± 6	401 ± 0.6	-	-

Table 5.4. The static dipole polarizabilities of the neutral group 1 elements compared with other values. All values are in a.u.

Due to the relativistic contraction of the valence s orbital, there is an anomaly in the trend of the dipole polarizability for the heavier elements. That is, the dipole polarizability increases with increasing nuclear charge up to Cs as expected but decreases thereon to Fr and further to E119 as shown in Figure 5.2.

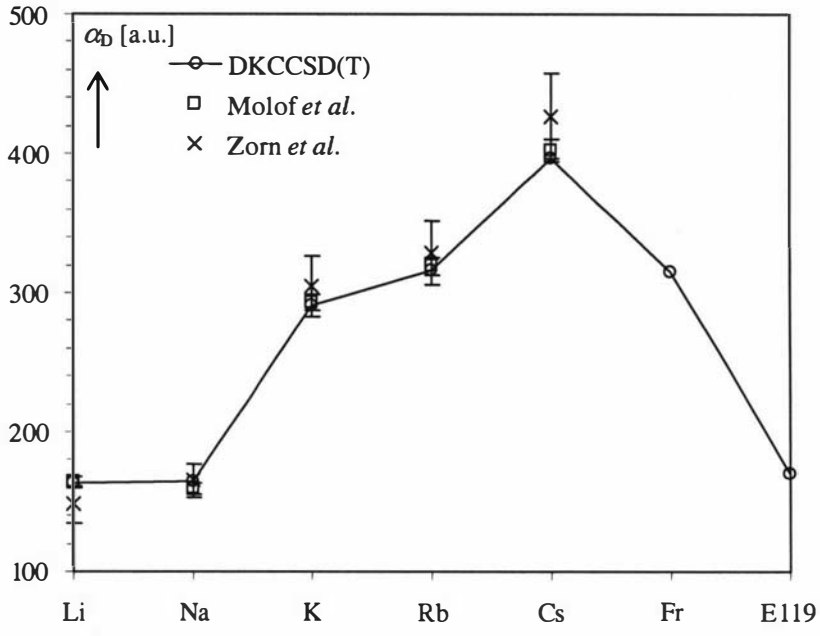

Figure 5.2. The static dipole polarizabilities of the neutral group 1 elements. The values for Li and Na taken from Ref. [23] were included for completeness. All values are in a.u.

5.3 Ionization Potentials

The present all-electron DKCCSD(T) values of the ground state first ionization potentials for the neutral group 1 elements are presented in Table 5.5, together with the results from the previous basis sets [23] and experimental values for comparison. The theoretical values were taken from the work by Eliav *et al.* [28].

The data in Table 5.5 show that the ionization potential decreases monotonically from K to Cs. Due to relativistic effects, this downward trend is reversed with increasing nuclear charge as the first ionization potential increases for the two heaviest elements, namely Fr and E119.

The present basis set modification outlined in section 5.1.1 significantly improves the agreement with the experimental values. The values are, however, still underestimated compared with the experimental values but the discrepancy is small, only 0.01 eV for elements up to Cs and becomes slightly larger for Fr to 0.04 eV.

	K	Rb	Cs	Fr	E119
Present Basis Set	4.336	4.167	3.881	4.038	4.713
Previous Basis Set [23]	4.284	4.137	3.821	3.975	4.540
[a]Theor. [28]	4.343	4.181	3.898	4.072	-
Expt. [29]	4.341	4.177	3.894	4.073	-

[a]Relativistic Fock-space coupled-cluster singles and doubles approximation starting from a Dirac-Coulomb-Breit Hamiltonian.

Table 5.5. The calculated values of the ground state ionization potentials at the all-electron DKCCSD(T). The present values are compared with the previous values from Ref. [23], other theoretical, and experimental values. All values are in eV.

5.3.1. The Relationship between the Dipole Polarizability and the Ionization Potential

The relationship between the ionization potential and the static dipole polarizability was first pointed out by Fricke [30]. That is, the polarizability increases with decreasing ionization potential. This relationship is easily seen by the sum-over-state formula. Dalgarno and Kingston noted that for one-valence *s*-electron systems like the alkali-metal atoms, the sum-over-state formula for the dipole polarizability, α_D can be approximated by (in a.u.)

$$\alpha_D = \sum \frac{f_{0,k}}{\left(E_k - E_0\right)^2} \approx f_{^2s\rightarrow{}^2p} \frac{1}{\left(E_{^2s} - E_{^2p}\right)^2} \qquad \text{Eq. 5.1}$$

The summation runs over all discrete and continuum states and $f_{0,k}$ is the oscillator strength between the ground state, $|0\rangle$ and the excited state, $|k\rangle$, and E_k is the corresponding eigenvalue. More precisely, Eq. 2.42 gives

$$\alpha_D \cong c_1 IP_0^{-2} + c_2 \qquad \text{Eq. 5.2}$$

where IP_0 is the first ionization potential of the atom in its electronic ground state. Dalgarno and Kingston noted that Eq. 5.2 works well for the alkali-metal atoms

and it was shown recently that this approximation works reasonably well for the group 11 metals, Cu, Ag, and Au [31]. Eq. 5.2 suggests a relationship between the polarizability and the first ionization potential as mentioned earlier: the polarizability increases with decreasing ionization potential.

A monotonic decrease in the ionization potential from K to Cs is in accordance with the increasing dipole polarizability for these elements. As the maximum dipole polarizability is observed for Cs, the ionization potential reaches the minimum for Cs. A decrease in the dipole polarizability for Fr and E119 is followed by an increase in the ionization potential for these elements.

5.3.2 Comparison with other Values

The improvement made in the ionization potentials by the present basis set modification is clear as shown in Table 5.5. The discrepancy between the calculated and the experimental values is reduced by as much as a factor of five.

In comparison with the theoretical values of Eliav *et al.* [28] estimated at the DCHF-CCSD(T) level, the present scalar relativistic ionization potentials are underestimated due to the neglect of spin-orbit coupling effects. Overall, the ionization potentials show an excellent agreement with the experimental values.

5.4 The Pseudopotential Results

In this section, the dipole polarizabilities and the ionization potentials calculated with the new nine-valence-electron scalar relativistic pseudopotentials are discussed. The calculated group 1 dipole polarizabilities are presented and compared with all-electron values in Table 5.6. The results incorporating a core polarization potential are also listed in Table 5.6 for Cs to E119. The pseudopotential results for the ionization potentials are listed in Table 5.7.

		ARPP	ARPP+CPP	AE(DK)
K	HF	406.37	-	410.17
	CCSD	301.89	-	303.24
	CCSD(T)	290.68	-	291.12
Rb	HF	482.27	-	484.28
	CCSD	337.09	-	335.81
	CCSD(T)	319.09	-	316.17
Cs	HF	654.27	613.80	671.52
	CCSD	429.04	415.65	435.27
	CCSD(T)	395.10	390.79	396.02
Fr	HF	547.80	490.42	543.42
	CCSD	356.52	333.93	347.59
	CCSD(T)	328.39	316.81	315.23
E119	HF	229.74	209.35	244.38
	CCSD	172.49	164.81	176.52
	CCSD(T)	164.76	160.13	165.97

Table 5.6. The static dipole polarizabilities of the group 1 elements using the present scalar relativistic pseudopotentials (ARPP) and core polarization potentials (CPP). All-electron values are scalar relativistic Douglas-Kroll values of this study. All values are in a.u.

5.4.1 Static Dipole Polarizabilities

The ARPP dipole polarizabilities at the CCSD(T) level agree with the AE values within 1% for elements up to Cs. The agreement between ARPP+CPP and AE values for Cs becomes somewhat worse with the use of a CPP. Nonetheless, the pseudopotential errors seem to remain at just over 1%.

For Fr, however, the ARPP results agree with the AE results rather poorly. It is, therefore, evident that the present core definition of nine-valence-electrons is not sufficient to account for electron correlation effects. This is not surprising since the all-electron DKCCSD(T) calculations (Table 5.3, section 5.2.3) clearly demonstrate that far more than nine valence-electrons need to be correlated to obtain an accurate dipole polarizability. For this reason the ARPP dipole polarizability with nine valence-electrons should be compared with the AE results of KLMNO frozen core in the correlation step. In this case, the agreement is

better than 1%. For a comparison with AE results which correlate more than nine electrons, it is necessary to include core-valence correlation in the pseudopotential calculation. Indeed, the use of a CPP reduces the ARPP dipole polarizability of Fr much like the correlation of (n-2) shell in the AE calculation does. Evidently, the ARPP+CPP dipole polarizability agrees well with the AE results within 0.5%.

For E119, the dipole polarizability seems to be underestimated by the ARPP, with a discrepancy of less than 1% from the AE result at the CCSD(T) level. The agreement becomes poorer with the use of a CPP as the dipole polarizability is further reduced.

Relativistic effects estimated by the present ARPPs are in line with the all-electron scalar relativistic Douglas-Kroll results, where a maximum dipole polarizability is observed for Cs.

5.4.2 Ionization Potentials

At the HF level, the ARPP ionization potentials agree with the AE results within 0.02 eV for the elements up to Fr. For E119, the agreement becomes worse with a discrepancy of 0.05 eV. At the CCSD(T) level, the discrepancy between the ARPP and the AE ionization potentials is even smaller than in the HF case for K to Cs, but larger for Fr and E119, amounting up to 0.03 eV.

The agreement between ARPP+CPP and AE for Cs at the CCSD(T) level is slightly poorer than that without the use of a CPP. However, the agreement with the experimental value improves with the use of the CPP. This seems somewhat fortunate though, as the ionization potential is underestimated by both ARPP and AE methods, while the inclusion of core-valence contribution overestimates the ionization potential in comparison with the experimental value.

For Fr, inclusion of core-valence correlation clearly improves the agreement with the AE result. Also, the ARPP+CPP result for Fr shows a good agreement with the experimental value within 0.02 eV.

	ARPP		ARPP+CPP	[a]Other PP	AE(DK)		Expt.
	HF	CCSD(T)	CCSD(T)	CCSD(T)/CISD	HF	CCSD(T)	
K	4.029	4.333	-	4.278	4.020	4.336	4.341
Rb	3.805	4.161	-	4.135	3.801	4.167	4.177
Cs	3.488	3.884	3.901	3.880	3.473	3.881	3.894
Fr	3.559	4.011	4.054	-	3.565	4.038	4.073
E119	4.183	4.716	4.761	-	4.134	4.713	-

[a]Nine-valence-electron pseudopotentials were used. Correlation was treated at the CCSD(T) level for K and Rb and at the CISD level for Cs. See Ref. [32, 33].

Table 5.7. The ionization potentials of the group 1 elements from the ARPP and ARPP+CPP calculations. The values are compared with the present all-electron Douglas-Kroll [AE(DK)] values and other pseudopotential results. The experimental values are taken from Ref. [29]. All values are in eV.

For E119, the use of a CPP makes the agreement with the AE result worse as the positive core-valence contribution increases the already overestimated ARPP result. This also follows the trend observed in the dipole polarizability, where the underestimated ARPP result becomes even smaller by core-valence correlation, worsening the agreement with the AE result. Nonetheless, the present pseudopotentials seem to give more accurate ionization potentials than other pseudopotentials as shown in Table 5.7.

References

[1] V. Kellö , A. J. Sadlej, and K. Faegri, Jr., Phys. Rev. A **47**, 1715 (1993).

[2] S. Kirpekar, J. Oddershede, and H. J. Aa. Jensen, J. Chem. Phys. **103**, 2983 (1995); C.Hättig and B. A. Heß, *ibid.* **108**, 3863 (1998); L. Visscher, T. Saue, and J. Oddershede, Chem. Phys. Lett. **274**, 181 (1997).

[3] R. W. Molof, H. L. Schwartz, T. M. Miller, and B. Bederson, Phys. Rev. A **10**, 1131 (1974).

[4] W. D. Hall and J. C. Zorn, Phys. Rev. A **10**, 1141 (1974).

[5] G. E. Chamberlain and J. C. Zorn, Phys. Rev. **129**, 677 (1963).

[6] J. Amini and H. Gould, Phys. Rev. Lett. **91**, 153001-1 (2003).

[7] Only the all-electron correlated results are cited. For a complete review of the calculations of dipole polarizabilities from He to Kr, see Ref. 8.

[8] J. Stiehler and J. Hinze, J. Phys. B **28**, 4055 (1995).

[9] M. L. Bartlett and E. A. Power, J. Phys. A **2**, 419 (1969); S. Kaneko, J. Phys. B **10**, 3347 (1977); E. Fischbach, B. S. Free-man, and W. -K. Cheng, Phys. Rev. D **23**, 2157 (1981); S.P. Goldman, Phys. Rev. A **39**, 976 (1989); D. M. Bishop and J. Pipin, Int. J. Quantum Chem. **45**, 349 (1993); L. A. Thu, L. V. Hoang, L. I. Komarov, and T. S. Romanova, J. Phys. B **27**, 4083 (1994); D. M. Bishop and J. Pipin, Chem. Phys. Lett. **236**, 15 (1995).

[10] D. Spelsberg, T. Lorenz, and W. Meyer, J. Chem. Phys. **99**, 7845 (1993).

[11] P. Fuentealba and Y. Simón-Manso, J. Phys. Chem. **101**, 4231 (1997).

[12] H. Gollisch, J. Phys. B **17**, 1463 (1984).

[13] A. J. Sadlej and M. Urban, J. Mol. Struct.: THEOCHEM **234**, 147 (1991).

[14] N. El-Bakali Kassimi and A. Thakkar, Phys. Rev. A **50**, 2948 (1994).

[15] H. -J. Werner and W. Meyer, Phys. Rev. A **13**, 13 (1976).

[16] D. R. Beck and C. A. Nicolaides, Chem. Phys. Lett. **49**, 357 (1977).

[17] G. Maroulis and A. J. Thakkar, J. Phys. B **22**, 2439 (1989).

[18] P. A. Christianssen and K. S. Pitzer, Chem. Phys. Lett. **85**, 434 (1982).

[19] T. Itoh, Rev. Mod. Phys. **37**, 159 (1963).

[20] M. Seth, P. Schwerdtfeger, M. Dolg, K. Fægri, B. A. Heß and U. Kaldor, Chem. Phys. Lett. **250**, 461 (1996).

[21] M. Douglas and N. M. Kroll, Ann. Phys. N.Y. **82**, 89 (1974); B. A. Heß, Phys. Rev. A **39**, 3742 (1986).

[22] I. Miadoková, V. Kellö, and A. J. Sadlej, Theor. Chem. Acc. **96**, 166 (1997).

[23] I. S. Lim, M. Pernpointner, M. Seth, J. K. Laerdahl, and P. Schwerdtfeger, Phys. Rev. A **60**, 2822 (1999).

[24] K. G. Dyall, I. P. Grant, C. T. Johnson, F. A. Parpia, E. P. Plummer, Comput. Phys. Commun **55**, 425 (1989).

[25] W. Müller, J. Flesch, and W. Meyer, J. Chem. Phys. **80**, 3297 (1984).

[26] A. Derevianko, W. R. Johnson, M. S. Safronova, and J. F. Babb, Phys. Rev. Lett. **82**, 3589 (1999).

[27] M. S. Safronova, W. R. Johnson, and A. Derevianko, Phys. Rev. A **60**, 4476 (1999).

[28] E. Eliav, U. Kaldor, and Y. Ishikawa, Phys. Rev. A **50**, 1121 (1994).

[29] C. E. Moore, *Atomic Energy Levels*, Natl. Bur. Stand. Circ. No.467, U.S. Government Printing Office, Washington, D.C.,1958. [(b)]E. Arnold, W. Brochers, H. T. Duong, P. Juncar, J. Lerme, P. Lievens, W. Neu, R. Neugart, M. Pellarin, J. Pinard, J. L. Vialle, K. Wendt, and the ISOLDE collaboration, J. Phys. B **23**, 3511 (1990).

[30] B. Fricke, J. Chem. Phys. **84**, 862 (1986).

[31] P. Schwerdtfeger and G. A. Bowmaker, J. Chem. Phys. **100**, 4487 (1994).

[32] K. Doll and H. Stoll, Phys. Rev. B **57**, 4327 (1998).

[33] P. Fuentealba, O. Reyes, H. Stoll, and H. Preuss, J. Chem. Phys. **87**, 5338 (1987).

Chapter 6
THE SINGLY CHARGED GROUP 1 ELEMENTS

Dipole polarizabilities of free or gaseous ions are not susceptible to direct experimental measurements. In this case one must make resources to some type of empirical or purely theoretical methods. Over the years, many attempts have been made to devise models that best fit the data obtained from refractive indices or dielectric constants for ionic crystals in order to estimate free ion polarizabilities [1, 2]. These methods, in general, only yield the dipole polarizabilities per ion pair, which are not equal to the sum of constant polarizabilities for the constituent ions [3, 4]. That is, the dipole polarizabilities are diminished in the field of positive charge and are enhanced in the field of negative charge. This lack of additivity together with the sensitive nature of dipole polarizabilities to the crystal environment has proven to be a challenging aspect of the accurate determination of free ion polarizabilities.

For alkali ions, a simple model for obtaining free ion polarizabilities was introduced by Fowler and Pyper [2]. Their model was based on their earlier conclusion that in-crystal polarizabilities can be taken equal to the free ion polarizabilities, as the environmental influences resulting from overlap compressions of alkali cations and the electrostatic potential are expected to be of the same magnitude but with opposite signs [5]. They have employed previously known values of dipole polarizabilities for lighter ions and deduced the dipole polarizabilities of Rb^+ and Cs^+ to be 9.05 ± 0.15 a.u. and 15.28 ± 0.27 a.u., respectively [6]. These values were similar to Wilson and Curtis' 9.245 a.u. and 15.59 a.u. for respective Rb^+ and Cs^+ [1]. The dipole polarizabilities obtained by Coker [7] were higher than these values, 9.515 a.u. for Rb^+ and 16.33 a.u. for Cs^+. Coker's values are, however, based on the presumption that the ions retain their identity in the crystal phase and that the perturbation can be described in some functional manner.

For the accurate determination of free ion dipole polarizabilities unaffected by the crystal environment or by some pre-fixed values of dipole polarizabilities, attempts have been made employing density functional theories [8-10]. The dipole polarizabilities obtained, however, span over a wide range, depending critically on the particular functional chosen. For example, 1.16 - 1.31 a.u. for Na^+, 4.56 - 5.837 for K^+, 4.67 - 10.09 for Rb^+, and 14.6 - 17.64 for Cs^+. The dipole polarizability of Cs^+ has also been estimated from high-lying Rydberg states of neutral Cs to yield 15.819(30) [11] and 15.544(30) [12] a.u.

On the theoretical side, all-electron *ab-initio* calculations were performed on positively charged alkali atoms. Most of the early calculations used the (coupled) Hartree-Fock method [13, 14]. Relativistic coupled Hartree-Fock calculations have reported [15] $\alpha_D(Rb^+)$ of 9.08 and $\alpha_D(Cs^+)$ of 15.8 a.u. The importance of suitable basis sets in *ab-initio* calculations was demonstrated by Sadlej *et al.* [16] who calculated the dipole polarizabilities of Li^+ to Fr^+ at the relativistic coupled-cluster Douglas-Kroll level.

There is no doubt that accurate static dipole polarizabilities will serve as calibrating values and lead to deeper understanding of the in-crystal behavior of the ions. In this chapter, the static dipole polarizabilities of the positively charged alkali ions from Li^+ to $E119^+$ are presented and discussed. The dipole polarizabilities were determined using a spin-free (scalar) relativistic Douglas-Kroll Hamiltonian within closed-shell coupled-cluster theory. Spin-orbit coupling was accounted for by employing a fully relativistic four-component Dirac-Coulomb-Hartree-Fock (DCHF) scheme, followed by second-order many body perturbation theory (DCMP2) to account for electron correlation. Even-tempered basis sets were developed in this study. A detailed description of these basis sets are provided in the following section.

6.1 Basis Sets

Despite a great effort into devising suitable basis sets for the calculations of dipole polarizabilities, especially for the neutral group 1 atoms [17, 18], there seems to be less experience for the basis set dependency of the dipole polarizability for the cations. Only for Li^+, Hartree-Fock limit estimates are available [19].

A systematic investigation into the importance of the quality of basis sets in obtaining reliable dipole polarizabilities was carried out by studying the basis set dependence of the dipole polarizability, employing even-tempered Gaussian type basis sets. The generation of the even-tempered basis sets for the dipole polarizabilities of singly charged group 1 elements and a discussion on their performances are presented in the following section.

6.1.1 Even-Tempered Basis Sets and Notation

For the present even-tempered basis sets, the exponents for all angular momentum functions (*s*-, *p*-, *d*-type etc) were taken from the same master list of exponents generated by the even-tempered prescription:

$$\lambda_i = \lambda_1 \beta^{i-1} \qquad \text{where } i = 1, 2, \ldots, N \qquad \text{Eq. 6.1}$$

Here, λ_1 is the most diffuse (i.e. the smallest) exponent and β is the ratio parameter with $\beta > 1.0$. The basis set notation $\{n^s_a{:}n^s_b, n^p_a{:}n^p_b, n^d_a{:}n^d_b, \ldots\}$ gives the range of the value, i in Eq. 6.1 for each angular type. For example, {1:21, 3:16, ...} designate λ_1 to λ_{21} for the *s*-type sub-set and λ_3 to λ_{16} for the *p*-type sub-set.

The advantage of using even-tempered basis sets is that one may straightforwardly improve the quality of the basis set and thus the quality of the one-electron description by reducing the basis set ratio parameter, β, using a greater number of basis functions for each angular type or by employing higher angular momentum basis functions. In principle, one may in this fashion converge the one-electron description to the basis set limit for any property, in the present case, the dipole polarizability, while for example energy optimized basis sets are only optimized with respect to the total electronic energy.

6.1.2 Optimization of Even-Tempered Basis Sets: Test Case of Rb^+

As a starting point of devising a suitable basis set, a number of uncontracted basis sets including only *s*-, *p*-, and *d*-type functions were constructed by varying β

while a fixed value of λ_1 was chosen. A very wide range of exponents was chosen for these basis sets, ensuring that the basis sets are essentially converged with respect to the range of the exponents used for all angular momentum functions. This enables one to study the convergence of the dipole polarizability, depending on the single factor, β. Once suitable values of λ_1 and β are determined, more basis sets are constructed, this time, by varying the range of exponents (i.e. i in Eq. 6.1) until a convergence is reached in terms of the dipole polarizability. The underlying idea here is to find a balance between accuracy and computational economy so that the final basis set contains enough basis functions to produce a converged dipole polarizability and yet is the most economical one for high level calculations. In order to test the influence of polarization functions on the dipole polarizability, higher angular momentum functions are then added.

With the experience gained from the basis set study for the dipole polarizabilities of the neutral alkali elements, the most diffuse function, λ_1 was chosen to be 0.001. As for the ratio parameter, β, the forth-row element Rb^+ was chosen as a test case to study the behavior of the dipole polarizability as a function of β, from which a suitable value of β was determined.

6.1.3 Static Dipole Polarizability of Rb^+ as a Function of the Ratio Parameter, β

The calculated dipole polarizabilities resulting from the initial uncontracted $\{s, p, d\}$ basis sets are presented in Table 6.1. The values are shown to four decimal places to make small changes more transparent, which reflects the precision of the numerical procedure. A plot of the dipole polarizabilities as a function of β is depicted in Figure 6.1.

At both the HF and MP2 level, the dipole polarizabilities are underestimated with a large value of β. This indicates that basis sets with large gaps in-between each successive pair of exponents are not suitable to describe the polarization of orbitals in an external electric field, as insufficient orbital mixing is allowed. As β decreases and in turn the basis sets become more dense, the dipole polarizability reaches a peak around $\beta = 3.8$ and 3.6 at the respective HF and MP2 level. The dipole polarizability then starts to decrease before a

Basis set	β	E_{tot}		α_D	
		NRHF	NRMP2	NRHF	NRMP2
{1:15,1:12,1:10}	4.5	-2922.99602526	-2923.82413773	8.7246	8.6136
{1:16,1:13,1:11}	4.0	-2930.22379460	-2931.03759512	9.1516	9.0629
{1:18,1:14,1:12}	3.5	-2935.63390894	-2936.49857439	9.1860	9.1571
{1:20,1:16,1:14}	3.0	-2937.68905189	-2938.59440720	9.1155	9.0850
{1:22,1:18,1:15}	2.7	-2938.09834798	-2939.01895369	9.1266	9.0916
{1:24,1:19,1:16}	2.5	-2938.18950381	-2939.11597789	9.1318	9.0952
{1:26,1:21,1:17}	2.3	-2938.21205947	-2939.14195256	9.1359	9.0984
{1:29,1:23,1:19}	2.1	-2938.21626665	-2939.14878445	9.1354	9.0968
{1:31,1:25,1:20}	2.0	-2938.21685009	-2939.14969842	9.1352	9.0963
{1:37,1:29,1:24}	1.8	-2938.21830392	-2939.15291262	9.1352	9.0959
HF-limit		-2938.21993123			

Table 6.1. The total electronic energies, E_{tot} and the dipole polarizabilities, α_D of Rb^+ resulting from varying values of β at the nonrelativistic HF and MP2 level. The HF limit is obtained from numerical nonrelativistic calculations [20]. All values are given in a.u.

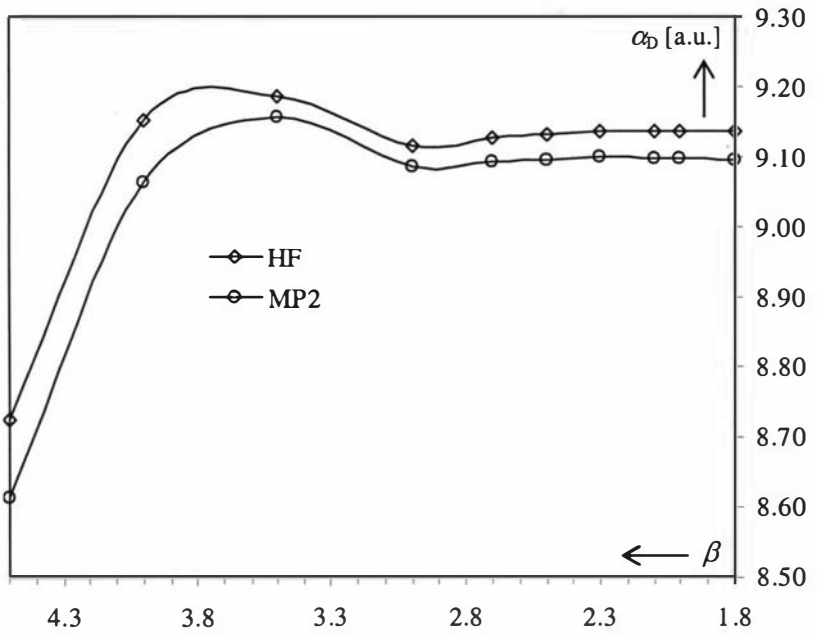

Figure 6.1. The static dipole polarizability, α_D of Rb^+ as a function of β at the nonrelativistic HF and MP2 level.

converged value is obtained. As shown in Table 6.1 and Figure 6.1, the dipole polarizability is converged to 9.135 and 9.096 a.u. at the HF and MP2 level, respectively. The $\beta = 2.3$ basis set offers the smallest $\{s, p, d\}$ basis set, which deviates insignificantly from the HF and MP2 limit. The convergence limit in this case is $\Delta\alpha_D = 0.01$ a.u. Consequently, it was decided to employ $\beta = 2.3$ for the subsequent calculations, which extend to all the other singly charged group 1 elements and to high level correlation calculations as well as higher angular momenta polarization functions.

6.1.4 Determination of the Range of Exponents for Rb^+

So far, the optimization of the even-tempered basis sets was carried out in terms of a single parameter β. The next step is to test the range of exponents needed to achieve the smallest basis set, yet converged dipole polarizability. Given that a sufficiently wide range of exponents were used in the determination of the ratio parameter β, tailoring of the range of exponents usually involves deletion of

exponents to reduce the size of the basis set without affecting the dipole polarizability.

Indeed, for $\beta = 2.3$, it was found that a number of high and low exponent functions could be removed with no significant change in the dipole polarizability either at the HF or the MP2 level. The resulting {6:26,6:20,6:16} (α_D = 9.136 and 9.098 a.u. at the HF and MP2 level, respectively) set was used for the remaining calculations including the higher level correlation treatment.

6.1.5 Polarization Functions for Rb^+

The influence of adding polarization functions to the above {6:26,6:20,6:16} set was tested by augmenting the basis set with higher angular momentum type functions, starting with *f*, until no significant change was observed in the calculated dipole polarizability either at the HF or MP2 level. The exponents were chosen such that they covered the whole necessary range for each angular momentum type but at the same time offer the most computationally economical basis set for the coupled-cluster treatment. It was also checked that the basis sets were converged in the relativistic calculations.

Table 6.2 summarizes the dipole polarizabilities upon inclusion of polarization functions at the nonrelativistic HF and MP2 level. The rows labeled *d*, *f*, *g*, etc are the basis sets which offer the optimum range of exponents up to that angular symmetry and thus the final choice of the range of exponents. The next two rows, i.e. the rows labeled -hrd and -dff in each angular momentum type, give the basis sets with either the highest or the most diffuse function removed from the optimum range of the exponents in that angular momentum type, respectively. The purpose of this is to offer a clear threshold for the optimum range of exponents needed and to demonstrate that the final choice of exponents offers the most time efficient basis set in a given angular momentum type.

As can be seen from Table 6.2, the influence of *f*-type functions is clear as the dipole polarizability increases by 0.073 a.u. at the MP2 level. The exponents of the optimum *f*-type polarization functions, with a converged dipole polarizability range from i = 7-11.

l	Basis set	NRHF	NRMP2
d	{6:26,6:20,6:16}	9.136	9.098
f	{6:26,6:20,6:16,7:11}	9.144	9.171
-hrd	{6:26,6:20,6:16,7:10}	9.143	9.193
-dff	{6:26,6:20,6:16,8:11}	9.144	9.164
g	{6:26,6:20,6:16,7:11,8:10}	9.144	9.151
-hrd	{6:26,6:20,6:16,7:11,8:9}	9.144	9.164
-dff	{6:26,6:20,6:16,7:11,9:10}	9.144	9.129
h	{6:26,6:20,6:16,7:11,8:10,8:10}	9.144	9.152
-hrd	{6:26,6:20,6:16,7:11,8:10,8:9}	9.144	9.147
-dff	{6:26,6:20,6:16,7:11,8:10,9:10}	9.144	9.151

Table 6.2. The influence of the higher angular momenta functions on the dipole polarizability of Rb^+ at the nonrelativistic HF and MP2 level, employing $\beta = 2.3$. All values are in a.u.

In order to demonstrate that these five exponents offer the most compact basis set, one high and one diffuse exponent was removed at a time, giving a *f*-type sub-set with i = 7-10 and i = 8-11, respectively. The resulting dipole polarizabilities were 9.193 and 9.164 a.u., respectively. These values deviate from the converged dipole polarizability by 0.022 and 0.007 a.u. This confirms that all of the five *f*-type exponents from i = 7-11 are necessary to reach convergence of the dipole polarizability with respect to the basis set expansion of *f*-type functions. It is desirable to show that additional functions do not significantly alter the dipole polarizability of Rb^+. This will be shown (in Table 6.3) in conjunction with *g*-type functions.

The influence of the *g*-type functions is evident from Table 6.2 as the dipole polarizability is reduced by 0.002 a.u. at the MP2 level, with the three optimum *g*-type exponents ranging from i = 8-10. The next two entries in Table 6.2 show the dipole polarizabilities of Rb^+ upon removal of one high and one diffuse *g*-type function, as was done for the *f*-type functions. The deviation from the optimum i = 8-10 *g*-type sub-set is large enough (0.013 and 0.022 a.u. for i = 8-9 and i = 9-10, respectively) to confirm that all three *g*-type exponents are necessary.

The influence of *h*-type function was tested by adding three *h*-type functions, the exponents of which were taken from the *g*-type sub-set. As can be

seen from Table 6.2, the *h*-type functions do not contribute significantly to the dipole polarizability and can therefore be ignored. This leads to the final basis set of {6:26,6:20,6:16,7:11,8:10}.

As a final test, this basis set was further augmented by first one high exponent and then one diffuse exponent for all angular momentum types. Table 6.3 summarizes the resulting dipole polarizabilities, together with the dipole polarizability from the final {6:26,6:20,6:16,7:11,8:10} set. The data in Table 6.3 confirm that further augmentation of the final set by either an additional high or low exponent function makes no significant difference in the dipole polarizability.

Basis set	NRHF	NRMP2
{6:26,6:20,6:16,7:11,8:10}	9.144	9.151
{6:27,6:21,6:17,7:12,8:11}	9.144	9.147
{5:26,5:20,5:16,6:11,7:10}	9.144	9.151

Table 6.3. Basis set effects on the Rb^+ dipole polarizability at the nonrelativistic HF and MP2 level, employing β= 2.3. All values are in a.u.

6.1.6 Summary of the test case : Rb^+

In the previous sections, a basis set optimization in an even-tempered manner was demonstrated for Rb^+. The nonrelativistic HF dipole polarizabilities confirm that once a sufficient number of *f*-type functions are added, the dipole polarizability is converged to 9.144 a.u. and is unaffected by higher angular momenta functions. At the MP2 level, however, it is evident that *g*-type functions are necessary. Moreover, the sensitive nature of the dipole polarizability to the inclusion of polarization functions makes it difficult to predict the changes incurred by the higher angular momenta functions. For example, the dipole polarizability seems to increase upon addition of *f*-type functions, then a decrease in the dipole polarizability is observed with addition of *g*-type functions. Nonetheless, the basis set limit is reached within the margin of error ($\Delta\alpha_D$ = 0.01 a.u.) with the inclusion of *f*- and *g*-type functions as the next higher angular momentum functions cause no significant changes in the dipole polarizability.

6.1.7 Even-Tempered Basis Sets for the Remainder of the Alkali Ions

The procedure for the generation of the even-tempered basis sets for all the other singly charged group 1 elements follows that for Rb^+. As was the case for Rb^+, all the basis sets generated were carefully tested for the convergence of dipole polarizabilities with respect to the basis sets.

The optimized even-tempered basis sets together with the nonrelativistic numerical HF limit and finite basis set total electronic energies are summarized in Table 6.4. The even-tempered basis set notation was used in Table 6.4 to clearly show the range of exponents used.

For these extensive basis sets, tests cannot be performed for the highly correlated methods. Therefore, an assumption is made that the basis sets with small errors at the HF and in particular at the correlated MP2 level, offer similar accuracies for the more advanced correlation methods. A similar trend in correlation effects between the MP2 and CCSD(T) method indicates the validity of this assumption. (see section 6.2.2)

Relativistic basis sets were designed according to the principles of the present nonrelativistic even-tempered basis sets, ensuring that the convergence threshold is met within a threshold, $\Delta\alpha_D$. This may serve as a measure for the estimated error bars if desired.

		Total electronic energies	
	Basis set	NR numerical	NR finite basis
Li^+	{6:26.6:20.7:13.8:12}	-7.23641520	-7.23641416
Na^+	{6:26.6:20.7:13.8:12}	-161.67696261	-161.67690968
K^+	{6:26.6:20.7:13.8:12}	-599.01757942	-599.01703333
Rb^+	{6:26.6:20.6:16.7:11.8:10}	-2938.21993123	-2938.20787859
Cs^+	{6:26.6:22.6:18.7:13.8:10}	-7553.81032852	-7553.75508721
Fr^+	{6:28.6:24.6:20.6:16.6:12}	-22475.74115378	-22475.49810209
$E119^+$	{6:28.6:26.6:20.5:17.3:11}	-47258.33924516	-47257.07306259

Table 6.4. A comparison between the calculated numerical and finite basis set total electronic energies at the nonrelativistic level of theory. All values are in a.u.

The basis set convergence threshold for the dipole polarizability at both the nonrelativistic and relativistic HF and MP2 level was as follow: $\Delta\alpha_D$ of less than 0.002 a.u. for Li^+ to K^+, less than 0.01 a.u. for Rb^+, less than 0.05 a.u. for Cs^+ and Fr^+, and $\Delta\alpha_D = 0.1$ a.u. for $E119^+$.

All basis sets were generally contracted. The final optimized basis sets described in Table 6.4 are written in a more conventional notation in Table 6.5 to clearly show the basis set contraction schemes used. The basis exponents and the contraction coefficients are summarized in appendix B.

	Basis set
Li^+	(21*s*15*p*7*d*5*f*)
Na^+	(21*s*15*p*7*d*5*f*)
K^+	(21*s*15*p*7*d*5*f*)
Rb^+	(21*s*15*p*11*d*5*f*3*g*)
Cs^+	(21*s*17*p*13*d*7*f*3*g*)/[12*s*11*p*10*d*7*f*3*g*]
Fr^+	(23*s*19*p*15*d*11*f*7*g*)/[13*s*12*p*11*d*11*f*7*g*]
$E119^+$	(23*s*21*p*15*d*13*f*9*g*)/[11*s*10*p*9*d*9*f*9*g*]

Table 6.5. The basis sets and contraction schemes for the singly charged group 1 elements.

The basis sets described in Table 6.5 were both for the nonrelativistic and the relativistic calculations. Usually, the relativistic basis sets require more hard functions than the nonrelativistic ones, especially for the *p* sub-set in the case of the singly charged group 1 elements. The hard functions are necessary to properly describe relativistic contraction of the $p_{1/2}$ orbital. In order to eliminate any basis set effects in estimating relativistic effects on the dipole polarizabilities, the same range of exponents used for the relativistic calculations was used in the final nonrelativistic calculations, ensuring that the exponents cover the necessary range of exponents needed in both calculations. The only difference between the relativistic and the nonrelativistic basis sets is, therefore, the contraction coefficients which are obtained in a separate HF calculation. This way any discrepancy arising from the use of different basis sets in a nonrelativistic and a relativistic calculation is minimized and an objective comparison can be made between the two levels of theory.

6.1.8 The Influence of Higher Angular Momentum Functions

Before discussing various aspects of static dipole polarizabilities of the singly charged group 1 ions, it is demonstrated that the higher angular momenta functions i.e. *h*-type functions do not significantly contribute to the dipole polarizability.

For the heaviest ion $E119^+$, a decrease in the dipole polarizability of 0.03 a.u. was found, at the DKMP2 level, on addition of five *h*-type functions (i = 5-9). This change is well within the basis set convergence threshold of $\Delta\alpha_D = 0.1$ a.u. and therefore the *h*-type functions are not included in the present study.

For Fr^+, three *h*-type functions (i = 8-10) reduce the dipole polarizability by 0.04 a.u. at the DKMP2 level. This decrease is slightly larger than expected from the influence of *h*-type functions on the $E119^+$ dipole polarizability, but still within the basis set convergence threshold for this ion. Therefore the *h*-type functions were ignored.

For Cs^+, the change in the dipole polarizability on addition of *h*-type functions is less than 0.01 a.u at the DKMP2 level.

6.2 Static Dipole Polarizabilities of the Singly Charged Group 1 Elements

The static dipole polarizabilities of the singly charged group 1 elements are calculated with the even-tempered basis sets described in the previous section. The resulting values are presented in Table 6.6.

6.2.1 Scalar Relativistic Effects

The calculated dipole polarizabilities of the singly charged group 1 elements are depicted in Figure 6.2 at the nonrelativistic and scalar relativistic HF level. At the nonrelativistic level, a monotonic increase in the dipole polarizability from Li^+ to $E119^+$ is observed. Not surprisingly, this trend is continued at the scalar relativistic level.

		Li^+	Na^+	K^+	Rb^+	Cs^+	Fr^+	$E119^+$
NR	HF	0.189	0.946	5.460	9.144	16.120	20.996	28.882
	MP2	0.191	1.005	5.514	9.151	15.958	20.737	28.384
	CCSD	0.192	0.994	5.507	9.147	15.965	20.777	28.470
	CCSD(T)		1.007	5.513	9.214	16.063	20.844	28.559
DK	HF	0.189	0.946	5.457	9.067	15.725	19.558	25.247
	MP2	0.191	1.005	5.513	9.084	15.622	19.564	25.020
	CCSD	0.192	0.995	5.500	9.066	15.635	19.543	25.049
	CCSD(T)		1.001	5.515	9.096	15.687	19.628	25.148
DC	HF	0.189	0.946	5.457	9.076	15.805	20.409	32.593
	MP2	0.191	1.005	5.513	9.114	15.769	20.459	31.474

Table 6.6. The calculated static dipole polarizabilities of the singly charged group 1 elements. All values are in a.u.

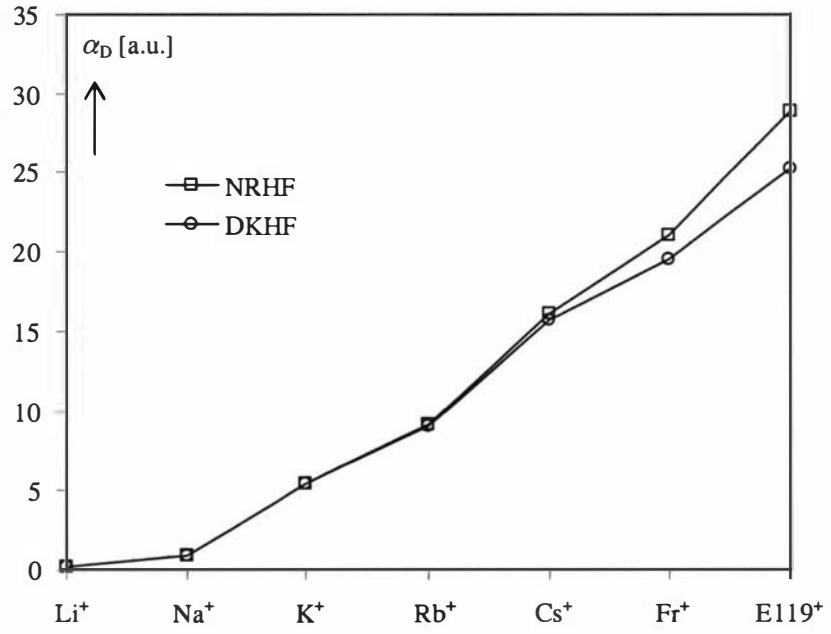

Figure 6.2. The dipole polarizabilities of the singly charged group 1 elements at the nonrelativistic and scalar relativistic HF level. All values are in a.u.

For light ions up to K^+, there are no significant scalar relativistic effects at the HF level. From Rb^+, however, scalar relativistic effects start to grow, causing a decrease in dipole polarizabilities in comparison with the nonrelativistic counterparts. Scalar relativistic effects for Rb^+ are small, 0.077 a.u., contributing less than 1% to the dipole polarizability at the HF level. Although this contribution is small, the change in the dipole polarizability due to relativity is far greater than the basis set convergence threshold set up in section 6.1.7 ($\Delta\alpha_D$ = 0.01 a.u. for Rb^+) and is therefore considered to be important.

For Cs^+, scalar relativistic effects become more noticeable, contributing 2.5% to the dipole polarizability. For Fr^+ and $E119^+$, the effects of scalar relativity continue to grow and cannot be neglected anymore. For the latter, this results in a decrease in the dipole polarizability by 12.6% from the nonrelativistic HF result.

The reduction in dipole polarizabilities at the scalar relativistic level is attributed to the direct relativistic stabilization of the spin-orbit averaged $(n\text{-}1)p$ shell. A relatively small relativistic $(n\text{-}1)p$ shell contraction does not lead to any anomalies in the trend of the dipole polarizabilities of the singly charged group 1

elements in contrast to the neutral group 1 atoms, where the large relativistic *ns* valence shell contraction for the heavier elements leads to an anomalous trend in the dipole polarizabilities, as discussed in chapter 5.

6.2.2 Electron Correlation Effects

The data in Table 6.6 show the results of various treatments of electron correlation on the dipole polarizability of the singly charged group 1 elements.

At the nonrelativistic level, the electron correlation contribution to the HF dipole polarizability is positive for ions from Li^+ to Rb^+ at all levels of treatment, thus the dipole polarizability at the correlated level is increased. For ions from Cs^+ to $E119^+$, however, a negative correlation contribution is observed, reducing the dipole polarizability.

At the relativistic level, the electron correlation contribution does not follow the trend observed at the nonrelativistic level as can be seen from Figure 6.3. Correlation effects at the relativistic level are less than one half of those at

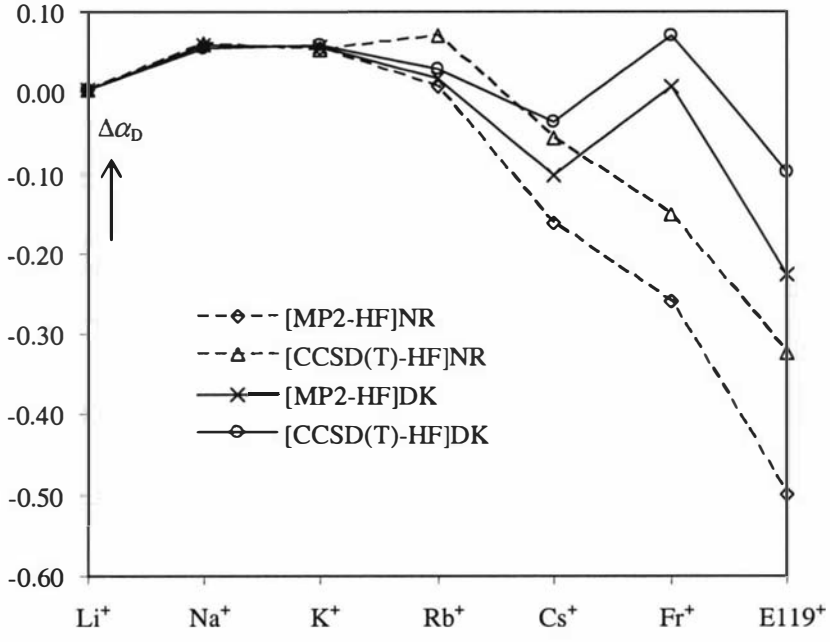

Figure 6.3. The electron correlation contribution to the dipole polarizabilities of the singly charged group 1 elements. All values are in a.u.

the nonrelativistic level for ions from Rb^+. This is because relativistic effects significantly reduce the correlation contribution since the dipole polarizability is already reduced by relativity. Electron correlation and relativistic effects are no longer additive [21]. The same trend is observed at the DCMP2 level as well.

In all cases, electron correlation effects in the dipole polarizability are small [22], contributing only 1% in the largest case of $E119^+$ at the nonrelativistic CCSD(T) level. This is attributed to the much larger HOMO-LUMO gap of the ions in comparison with the neutral atoms. For example, the HOMO-LUMO gap of Cs^+ is an order of magnitude larger than that of the neutral Cs atom [23].

A comparison between the MP2 and the CCSD(T) treatment of electron correlation shows that, in general, the MP2 method overestimates correlation effects compared to the CCSD(T) method, due to the well known slow convergence of the MP expansion. This is shown by more negative values of the MP2 correlation contribution than those of CCSD(T) in Figure 6.3. The overestimation of correlation effects at the MP2 level is more profound for the heavier ions as the effects of correlation become larger. The reliability of the MP2 method, however, seems more likely to be a quantitative problem rather than a qualitative one as the general trend in the MP2 correlation contribution follows closely that in the correlation contribution at the CCSD(T) level.

The importance of the perturbative triples is evident as the correlation contribution at the CCSD level is overestimated in comparison with the CCSD(T) level in both the nonrelativistic and scalar relativistic cases. For $E119^+$ for example, perturbative triple contributions account for 28% of the total correlation contribution at the nonrelativistic CCSD(T) level. At the relativistic level the contribution of the perturbative triples is the same order of magnitude as the total correlation contribution at the DKCCSD(T) level.

In order to test the incompleteness of the CCSD(T) expansion, full CI calculations were performed for Na^+ with a basis set of $(10s5p1d)$ contracted to $[4s4p1d]$ [24]. The dipole polarizability at the full CI level was found to be only 0.002 a.u. higher than that at the CCSD(T) level. This indicate that the CCSD(T) method offers a good approximation at least for this element. Here, the triples contributions account for 1.7% of the total correlation contribution at the CCSD(T) level.

6.2.3 Spin-Orbit Coupling Effects

The data shown in Table 6.6 highlight the effects of introducing spin-orbit (SO) coupling to the scalar relativistic wavefunctions.

The DCHF and DCMP2 results show a monotonic increase in the dipole polarizability from Li^+ to $E119^+$ as was the case at the scalar relativistic DK level. For the lighter ions up to K^+, spin-orbit coupling can be neglected. For Rb^+ to $E119^+$, however, spin-orbit effects lead to an increase in the dipole polarizability from their scalar relativistic counterparts.

Figure 6.4 depicts the electron correlation, scalar relativistic and spin-orbit coupling contributions to the dipole polarizability of the singly charged group 1

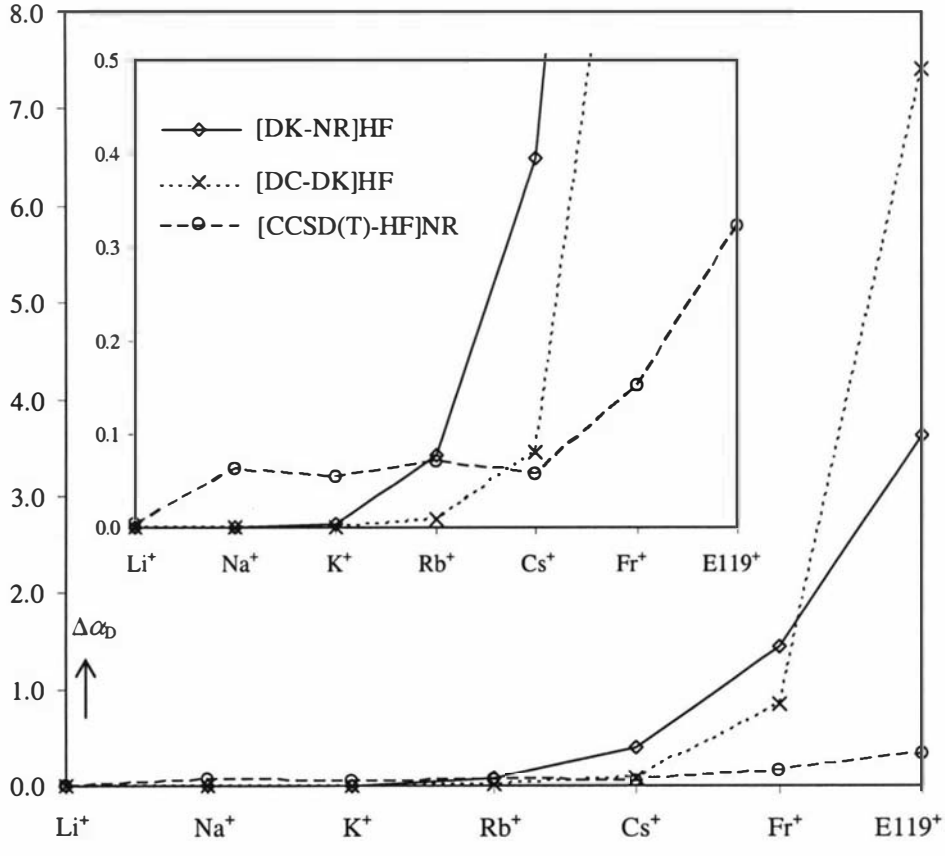

Figure 6.4. Electron correlation, scalar relativistic, and spin-orbit coupling contributions to the dipole polarizabilities of the singly charged group 1 elements. The electron correlation effects are taken from the nonrelativistic CCSD(T) results. All values are in a.u.

elements. Here, the correlation contribution is estimated at the nonrelativistic CCSD(T) level and spin-orbit effects by taking the difference between the DCHF and DKHF results. As shown in Figure 6.4, spin-orbit effects are very small for Rb^+. Electron correlation and scalar relativistic effects, which are of a similar magnitude, dominate over spin-orbit coupling effects. The magnitude of the spin-orbit contribution is about the same as the basis set convergence threshold ($\Delta\alpha_D$ = 0.01 a.u. for Rb^+), and is considered to be important in the present accuracy. The effects of spin-orbit coupling become non-negligible for Cs^+ and Fr^+. The spin-orbit contribution to the dipole polarizability grows by an order of magnitude from Cs^+ to Fr^+ and for the latter this contribution clearly dominates over electron correlation effects as shown in Figure 6.4. The largest contribution to the dipole polarizability of Cs^+ and Fr^+, however, still comes from scalar relativistic effects. For $E119^+$, spin-orbit effects again grow by an order of magnitude from Fr^+. In this case, the spin-orbit contribution accounts for 30% of the dipole polarizability and finally begins to dominate over scalar relativistic effects as well as correlation effects. This leads to a much larger dipole polarizability in comparison with the nonrelativistic value.

In the *j-j* coupling scheme, the $p_{1/2}$ orbital is more tightly bound and the $p_{3/2}$ more loosely bound than the spin-orbit averaged *p* orbital in the scalar relativistic LS coupled case. The $p_{3/2}$ shell expansion is an indirect relativistic effect caused by the increased screening of the nucleus by the relativistically contracted *s* and $p_{1/2}$ electrons. Neglecting spin-orbit coupling at the scalar relativistic DK level, therefore, leads to underestimated dipole polarizabilities. As expected, the splitting of these two orbitals is greatest for the heaviest ion in the group ($E(6p_{1/2})$ - $E(6p_{3/2})$ = -0.513 a.u.) and the fully relativistic DCHF and DCMP2 dipole polarizabilities of $E119^+$ clearly demonstrate the importance of spin-orbit effects for the accurate determination of dipole polarizabilities.

6.3. Recommended Static Dipole Polarizabilities

The recommended values of the static dipole polarizability of the singly charged group 1 elements are estimated by adding the scalar relativistic, the CCSD, the triples, and the spin-orbit contribution to the nonrelativistic HF result:

$$\alpha_D^{\text{Recomm.}} = \alpha_D^{\text{NRHF}} + \Delta\alpha_D^{\text{DKHF}} + \Delta\alpha_D^{\text{DKCCSD}} + \Delta\alpha_D^{\text{DKCCSD(T)}} + \Delta\alpha_D^{\text{DCMP2}}$$

The results are shown in Table 6.7, together with other theoretical and empirical values.

6.3.1 Comparison with other Results

For Li^+, there is a precise value of dipole polarizability (0.1924 a.u.) available by Johnson and Cheng [25]. The present value of 0.192 a.u. is in excellent agreement with their value. Bhatia and Drachman [26] determined relativistic and quantum electrodynamic effects to be only -4.52×10^{-5} a.u. for Li^+. (the present calculation gives -5.2×10^{-5} a.u. for relativistic effects)

The present values agree well with the numerical values of Mahan [30]. It is easy to see that the DKCCSD(T) values calculated by Miadoková and co-workers underestimate the dipole polarizability, mostly due to the neglect of spin-orbit effects. The present recommended values lie within the empirical values of Schmidt [27] *et al.*, Wilson and Curtis [1], and Coker [7].

Most importantly, the Cs^+ static dipole polarizability result is only slightly lower than 15.81 a.u., obtained by Derevianko *et al.* [28] by the relativistic random-phase approximation (RRPA) [29]. They have also estimated, in their high-precision calculations, the dipole polarizability of Fr^+ to be 20.41 a.u. [28]. This give great confidence in the present data.

	This work	Mahan [30]	Miadoková *et al.* [16]	Schmidt *et al.* [27]	Wilson & Curtis [1]	Coker [7]
Li^+	0.192	0.22	0.061	0.189	0.191	-
Na^+	1.001	1.06	0.829	0.965	0.999	-
K^+	5.515	5.60	5.05	5.216	5.473	5.736
Rb^+	9.110	9.25	8.32	8.665	9.245	9.515
Cs^+	15.76	15.93	14.98	15.096	15.59	16.33
Fr^+	20.38	-	19.19	-	-	-
$E119^+$	32.02	-	-	-	-	-

Table 6.7. The recommended dipole polarizabilities of the positively charged group 1 elements. The values are compared with other theoretical and empirical data. All values are in a.u.

6.4. Relationship with Ionization Potentials

As mentioned before, for one valence electron systems, there is a clear relationship between ionization potentials and static dipole polarizabilities as demonstrated by Fricke [31]. This originated from the use of the oscillator strength formula, Eq. 2.40.

Figure 6.5 shows a plot of the recommended dipole polarizabilities against the inverse square of the second ionization potentials from Li^+ to Cs^+. The second ionization potentials were obtained from Moore [23]. The following fit is obtained with a root mean square error of 0.032:

$$\alpha_D = 5.83 I_1^{-4} + 3.84 I_1^{-2} - 0.59 \qquad \text{Eq. 6.2}$$

where I_1 is the ionization potential. Interestingly, this implies that c_2 in Eq. 2.42 remains almost constant for the positively charged group 1 ions, which (in contrast to one-valence electron systems) is not immediately apparent.

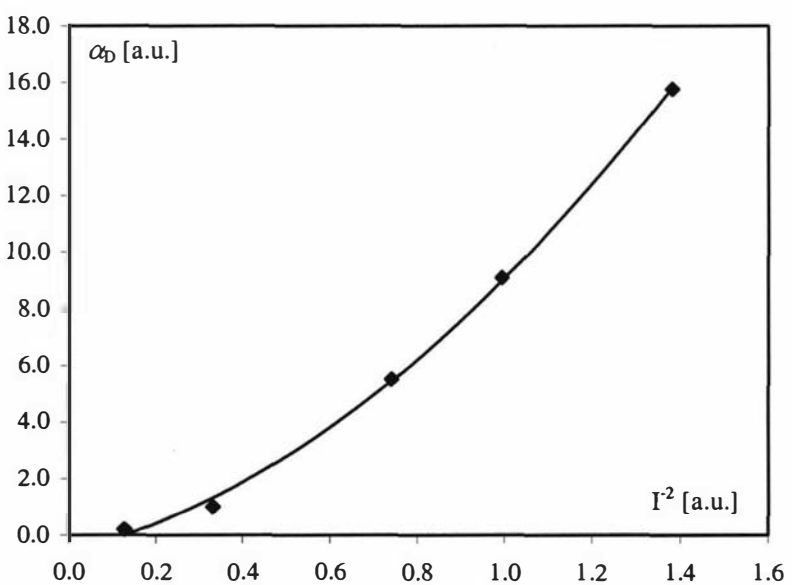

Figure 6.5. The dipole polarizabilities *vs.* inverse square of the second ionization potentials from Li^+ to Cs^+.

6.5 Pseudopotential Results

In this section, the static dipole polarizabilities calculated by using the present small-core scalar relativistic pseudopotentials (ARPP) are presented. These values are compared with the all-electron Douglas-Kroll [AE(DK)] values in Table 6.8. Core-polarization potentials (CPP) as detailed in chapter 4 were incorporated into the pseudopotential calculations for Cs^+ to $E119^+$ to account for core-valence correlation. The results are shown in Table 6.8.

6.5.1 Static Dipole Polarizabilities

For K^+, the ARPP slightly underestimates the dipole polarizability compared with the all-electron values. The agreement between the two methods is poor at the

		ARPP	ARPP+CPP	AE (DK)
K^+	HF	5.36	-	5.46
	CCSD	5.44	-	5.50
	CCSD(T)	5.46	-	5.52
Rb^+	HF	9.14	-	9.07
	CCSD	9.19	-	9.07
	CCSD(T)	9.21	-	9.10
Cs^+	HF	15.82	15.60	15.73
	CCSD	15.85	15.68	15.64
	CCSD(T)	15.89	15.72	15.69
Fr^+	HF	19.57	19.24	19.56
	CCSD	19.75	19.56	19.54
	CCSD(T)	19.81	19.62	19.63
$E119^+$	HF	27.30	26.86	25.25
	CCSD	27.15	26.87	25.05
	CCSD(T)	27.19	26.93	25.15

Table 6.8. The static dipole polarizabilities of the singly charged group 1 elements calculated by using the present scalar relativistic pseudopotentials, ARPP. The values are compared with the all-electron values at the Douglas-Kroll level [AE(DK)]. All values are in a.u.

HF level and begins to improve as correlation effects are accounted for. At the CCSD(T) level, the ARPP deviates from the AE(DK) by 1%.

For Rb^+ to $E119^+$, the ARPPs overestimate the dipole polarizabilities compared with the all-electron values. For the ions from Rb^+ to Fr^+, the overestimation is up to 0.2 a.u., which gives rise to a pseudopotential error of about 1%. For $E119^+$, however, the overestimation becomes larger by an order of magnitude, i.e. up to 2 a.u., yielding a pseudopotential error of 8%.

The use of core polarization potentials to account for core-valence correlation does bring down the dipole polarizabilities as shown in Table 6.8 for Cs^+ to $E119^+$. For Cs^+ and Fr^+ the discrepancy between the pseudopotential and the all-electron results becomes an order of magnitude smaller with the use of a CPP and the pseudopotential error reduces to 0.2% at the CCSD(T) level. For $E119^+$, however, core-valence correlation seems to help little in terms of the overall agreement between the pseudopotential and all-electron results. It is apparent that the overestimation of the ARPP is too large in the first place that the reduction of dipole polarizability by a CPP does not have much of an effect in the final result. It is likely that for $E119^+$, the core has to be chosen smaller than the nine-valence-electron and the ARPP needs to be re-adjusted.

References

[1] J. N. Wilson and R. M. Curtis, J. Phys. Chem. **74**, 187 (1970).

[2] P. W. Fowler and N. C. Pyper, Proc. R. Soc. Lond. A **398**, 377 (1985).

[3] T. M. Miller and B. Bederson, Adv. At. Mol. Phys. **25**, 37 (1988).

[4] K. Spangenberg, Z. Krist. **57**, 494 (1923).

[5] P. W. Fowler and P. A. Madden, Phys. Rev. B **29**, 1035 (1984).

[6] 0.192, 1.002 and 5.339 a.u. for Li^+, Na^+, and K^+, respectively. These values were coupled Hartree-Fock plus Møller-Plesset corrections and can be found in Ref. [2].

[7] H. Coker, J. Phys. Chem. **80**, 2078 (1976).

[8] M. J. Stott and E. Zasremba, Phys. Rev. A **21**, 12 (1980).

[9] M. K. Harbola, Phys. Rev. A **48**, 2696 (1993).

[10] T. K. Ghanty and S. K. Ghosh, J. Molc. Sturc. **366**, 139 (1996).

[11] G. A. Ruff, K. A. Safinta, and T. F. Gallagher, Phys. Rev. A **22**, 183 (1980).

[12] K. A. Safinta, T. F. Gallagher, and W. Sandner, Phys. Rev. A **22**, 2672 (1980).

[13] J. Lahiri and A. Mukherji, Phys Rev. **153**, 386 (1967); **155**, 24 (1967).

[14] R. M. Sternheimer, Phys Rev. **96**, 951 (1954); **107**, 1565 (1957); **115**, 1198 (1959).

[15] W. R. Johnson, D. Kolb, and K. N. Huang, At. Data Nucl. Data Tables **28**, 333 (1983).

[16] I. Miadoková, V. Kellö, and A. J. Sadlej, Theor. Chem. Acc. **96**, 166 (1997).

[17] A. J. Sadlej and M. Urban, J. Mol. Struct. (Theochem) **234**, 147 (1991).

[18] V. Kellö, A. J. Sadlej and K Fægri Jr., Phys. Rev. A **47**, 1715 (1993).

[19] G. Maroulis and D. M. Bishop, J. Phys. B: At. Mol. Phys. **19**, 369 (1986).

[20] C. Froese-Fischer, program MCHF (Pennsylvania: Pennsylvania State University) (1977).

[21] P. Schwerdtfeger and G. A. Bowmaker J. Chem. Phys. **100**, 4487 (1994).

[22] C. Pouchan and D. M. Bishop, Phys. Rev. A **29**, 1 (1984).

[23] C. E. Moore, *Atomic Energy Levels*, Natl. Bur. Stand. (U.S.) Circ. No. 467 (U.S. GPO, Washington, DC, 1958).

[24] This basis set was derived from a 6-31G* set using a *d* exponent of 0.525.

[25] W. R. Johnson and K. T. Cheng, Phys. Rev. A **53**, 1375 (1996).

[26] A. K. Bhatia and R. J. Drachman, Phys. Rev. A **55**, 1842 (1997); **58**, 4470 (1998).

[27] P. C. Schmidt, A. Weiss, and T. P. Das, Phys. Rev. B **19**, 5525 (1979).

[28] A. Derevianko, W. R. Johnson, M. S. Safronova, and J. F. Babb, Phys. Rev. Lett. **82**, 3589 (1999).

[29] D. Kolb, W. R. Johnson, and P. Shorer, Phys. Rev. A **26**, 19 (1982); W. R. Johnson, D. Kolb, and K. -N. Huang, At. Data Nucl. Data Tables **28**, 333 (1983).

[30] G. D. Mahan, Phys. Rev. A **22**, 1780 (1980).

[31] B. Fricke, J. Chem. Phys. **84**, 862 (1986).

Chapter 7

THE NEUTRAL GROUP 2 ELEMENTS

As for alkaline-earth metals, many of the theoretical studies have been limited to the evaluation of the dipole polarizabilities of open-shell M^+ ions [1-3] with a single valence electron. There is one set of purely *ab-initio* values of dipole polarizabilities available for the neutral alkaline-earth metals up to Ba [4, 5]. This study incorporated electron correlation at the coupled-cluster (CC) level of theory, and scalar relativistic effects approximated by the use of the Douglas-Kroll (DK) operator. These values, however, tend to depend on the basis set expansion as well as contraction schemes and neglect spin-orbit (SO) coupling. A study by Mahan [6] adopted a density functional formalism to modify the Sternheimer equation for atomic polarizabilities [7] in order to account for the self-consistent field. It was confirmed, in this study, that electron correlation reduces the dipole polarizabilities typically by 40% for closed shell atoms and ions.

On the semiempirical side are the calculations of dipole polarizabilities by summation of experimental oscillator strengths. In an early attempt, Altick [8] and Cohen [9] established the lower and upper bounds for the dipole polarizabilities of Sr and Ba with accuracies of about 16% in Altick's case and 6% in Cohen's case for both atoms. Their lower bounds coincided with one another whereas Altick's upper bound was much higher than that of Cohen's. It was noted that the semiempirical results are typically underestimated in the case of Ba but are overestimated for Ca [10].

On the experimental side, electric deflection studies have been a long standing method as has been for the alkali-metals. A study by Miller *et al.* [11] and Schwartz *et al.* [12] revealed that Cohen's semiempirical values were seriously underestimated and was able to reduce Altick's margin of error from 16% to about 8% for both Sr and Ba, yielding $\alpha_D(Sr) = 186.3 \pm 14.9$ and $\alpha_D(Ba)$

= 267.9 ± 21.6 a.u. They have later measured the dipole polarizability of Ca with a somewhat larger error at α_D(Ca) = 168.7 ± 16.9 a.u. [11].

So far, the static dipole polarizability of Ra is unknown (up to the write-up of this thesis). An accurate determination of α_D(Ra) will serve to better understand the large electron correlation and relativistic effects expected in static dipole polarizabilities of heavy elements.

In this chapter, the static dipole polarizabilities of the alkaline-earth elements from Ca to Ra are investigated using the scalar relativistic DK Hamiltonian within coupled-cluster (CC) theory. Spin-orbit coupling was tested by employing a fully relativistic four component Dirac-Coulomb-Hartree-Fock (DCHF) scheme followed by second-order many-body perturbation theory (DCMP2) in order to account for electron correlation.

	Basis set	Total electronic energies	
		DHF numerical	DHF finite basis
Ca	(20*s*15*p*8*d*)	-679.7101602882	-679.7052677615
Sr	(21*s*16*p*11*d*9*f*)	-3178.080046946	-3178.073284531
Ba	(26*s*22*p*17*d*13*f*)	-8135.645897280	-8135.636298367
Ra	(31*s*24*p*20*d*14*f*)	-25028.18780985	-25028.17080236

Table 7.1. A comparison between the calculated numerical and finite basis set total electronic energies at the Dirac-Coulomb-Hartree-Fock level of theory. All values are in a.u.

7.1 Basis Sets

The initial primitive Gaussian type orbital (GTO) basis set exponents for Ca and Sr were taken from Ref. [13] and for Ba from Ref. [4]. For Ra, the exponents were taken from Knut Faegri.

These exponents were re-optimized by energy minimization using the 4-component fully relativistic GRASP code [14]. These energy optimized basis sets were tested against the ground state energy at the numerical Dirac-Coulomb-Hartree-Fock limit as tabulated in Table 7.1. It is well known that the basis sets optimized with respect to the ground state HF energy only, may not be suitable for the calculation of polarizabilities. For example, some hard exponents

necessary in the energy minimization may be deleted without affecting the final value of the polarizability. Additional diffuse functions may be critical in correctly describing the polarization of valence orbitals. Furthermore, the basis exponents need to be tight enough to account for the core polarization. Therefore, it is necessary to carefully tailor the energy optimized basis sets to suit the calculation of the property of interest. The idea here is to devise small enough basis sets for high level calculations, which are, within a desired threshold, converged with respect to the basis set expansion and contraction schemes for the dipole polarizabilities. This is accomplished in a systematic manner by determining the upper and lower limits of the exponents for each angular momentum sub-set. The same is applied to polarization functions without which valence polarization cannot be described correctly. This gives us understanding of the convergence behavior of dipole polarizabilities with respect to the finite basis set expansion, which, in turn, enables us to estimate the errors caused by basis set deficiencies if desired.

A series of test calculations were performed at the DKMP2 level for each element monitoring the convergence behavior of the dipole polarizability. Typically, over 20 basis sets were tested until a desired convergence threshold was reached. The resulting basis sets were as follows: for Ca, Sr, Ba, and Ra, a (20*s*15*p*8*d*), (21*s*16*p*11*d*9*f*), (26*s*22*p*17*d*13*f*), and (31*s*24*p*20*d*14*f*) GTO set was used, respectively. For Sr to Ra, these GTO sets were generally contracted to a [15*s*12*p*10*d*9*f*], [17*s*16*p*13*d*13*f*], and [19*s*16*p*15*d*11*f*] CGTO set for the nonrelativistic calculations of Sr, Ba, and Ra, respectively. There were no changes made to the basis contraction for the relativistic calculation of Sr, but for Ba and Ra, a heavier contraction of respective [16*s*15*p*12*d*13*f*] and [18*s*15*p*14*d*10*f*] was used in order to improve on linear dependencies. For Ca there was no basis contraction used.

The influence of polarization functions was tested by expanding the above GTO/CGTO sets by five *f*-, three *g*-, ten *g*-, and eleven *g*-type functions for Ca, Sr, Ba, and Ra, respectively. All GTO/CGTO sets in the present study were of dual family type. The basis exponents and the contraction coefficients are summarized in appendix B.

		Nonrelativistic			Relativistic Douglas-Kroll		
		Basis set	NRHF	NRMP2	Basis set	DKHF	DKMP2
Ca	*d*	(20*s*15*p*8*d*)	185.45	142.57	(20*s*15*p*8*d*)	182.86	140.69
	*d**	(22*s*17*p*10*d*)	185.46	142.64	(22*s*17*p*10*d*)	182.87	140.70
	f	(20*s*15*p*8*d*5*f*)	185.45	143.06	(20*s*15*p*8*d*5*f*)	182.86	141.17
Sr	*uncntr*	(21*s*16*p*11*d*9*f*)	246.06	179.63	(21*s*16*p*11*d*9*f*)	232.88	170.51
	f	(21*s*16*p*11*d*9*f*)/ [15*s*12*p*10*d*9*f*]	246.06	179.67	(21*s*16*p*11*d*9*f*)/ [15*s*12*p*10*d*9*f*]	232.88	170.53
	*f**	(23*s*18*p*13*d*11*f*)/ [17*s*14*p*12*d*11*f*]	246.08	179.65	(23*s*18*p*13*d*11*f*)/ [17*s*14*p*12*d*11*f*]	232.92	170.57
	g	(21*s*16*p*11*d*9*f*3*g*)/ [15*s*12*p*10*d*9*f*3*g*]	246.06	178.30	(21*s*16*p*11*d*9*f*3*g*)/ [15*s*12*p*10*d*9*f*3*g*]	232.88	169.20

Table 7.2. The calculated nonrelativistic (NR) and scalar relativistic (DK) static dipole polarizabilities of the neutral group 2 elements at the HF and MP2 level. All values are in a.u. Continued on the following page.

Table 7.2. Continued from the previous page.

Ba	*uncntr*	(26*s*22*p*17*d*13*f*)	368.02	244.14	(26*s*22*p*17*d*13*f*)	324.67	217.11
	f	(26*s*22*p*17*d*13*f*)/ [17*s*16*p*13*d*13*f*]	368.02	244.13	(26*s*22*p*17*d*13*f*)/ [16*s*15*p*12*d*13*f*]	324.66	217.11
	*f**	(28*s*24*p*19*d*15*f*)/ [19*s*18*p*15*d*15*f*]	368.05	244.13	(28*s*24*p*19*d*15*f*)/ [18*s*17*p*14*d*15*f*]	324.68	217.12
	g	(26*s*22*p*17*d*13*f*10*g*)/ [17*s*16*p*13*d*13*f*10*g*]	368.02	243.75	(26*s*22*p*17*d*13*f*10*g*)/ [16*s*15*p*12*d*13*f*10*g*]	324.66	216.51
	*g**	(28*s*24*p*19*d*15*f*12*g*)/ [19*s*18*p*15*d*15*f*12*g*]	368.02	243.76	(28*s*24*p*19*d*15*f*12*g*)/ [18*s*17*p*14*d*15*f*12*g*]	324.66	216.52
Ra	*uncntr*	(31*s*24*p*20*d*14*f*)	440.85	279.75	(31*s*24*p*20*d*14*f*)	300.56	199.42
	f	(31*s*24*p*20*d*14*f*)/ [19*s*16*p*15*d*11*f*]	440.85	279.72	(31*s*24*p*20*d*14*f*)/ [18*s*15*p*14*d*10*f*]	300.56	199.44
	*f**	(33*s*26*p*22*d*16*f*)/ [21*s*18*p*17*d*13*f*]	440.87	279.75	(33*s*26*p*22*d*16*f*)/ [20*s*17*p*16*d*12*f*]	300.57	199.44
	g	(31*s*24*p*20*d*14*f*11*g*)/ [19*s*16*p*15*d*11*f*11*g*]	440.86	277.37	(31*s*24*p*20*d*14*f*11*g*)/ [18*s*15*p*14*d*10*f*11*g*]	300.57	196.31
	*g**	(33*s*26*p*22*d*16*f*13*g*)/ [21*s*18*p*17*d*13*f*13*g*]	440.86	277.42	(33*s*26*p*22*d*16*f*13*g*)/ [20*s*17*p*16*d*12*f*13*g*]	300.57	196.31

For the fully relativistic four component calculations, smaller, totally uncontracted basis sets, which include basis functions up to l = 3 (i.e. *f*-type functions), were used as the computational demand was very high. The large component exponents were taken from the above scalar relativistic basis sets, whereas the small component exponents were generated from the large components by a linear transformation and a projection [15] equivalent to the kinetic balance conditions [16]. A Gaussian nuclear model with nuclear exponents as given by Visscher and Dyall [17] was used.

All nonrelativistic and DK calculations were performed with the MOLCAS 5.2 program package [18]. All four-component calculations were performed with the DIRAC program package [19].

7.2 Basis Set Effects of the Dipole Polarizability

The static dipole polarizabilities of the neutral group 2 elements calculated with various basis sets are presented in Table 7.2 to demonstrate the choices of basis sets and their performances. For each element, the dipole polarizability resulting from the totally uncontracted basis set, labeled *uncntr*, is listed. (except for Ca since totally uncontracted basis sets were used through-out). Then the dipole polarizability following a basis set contraction is shown. These contracted basis sets are labeled l, where l denotes the highest angular momentum quantum number within that basis set. These CGTO's were further augmented by one high and one diffuse exponent in each angular momentum sub-set, giving set l^*. The dipole polarizabilities resulting from these l^* sets are listed to demonstrate that set l gives the converged dipole polarizability and no more functions are needed.

It is reminded that the convergence behavior of the dipole polarizability with respect to the basis set expansion was studied within a limitation of reasonable computational efforts. That is, high level correlation calculations were performed with basis sets which expand up to *g*-type functions only. A further expansion of the basis sets to *h*-type functions and beyond is unlikely to affect the overall quality of the present dipole polarizabilities, although it may serve as an indication for the margin of error associated with the use of a finite basis set, especially for the heavy element of Ra. Nevertheless, the influence of *h*- and *i*-type functions in the dipole polarizability of Ra is discussed in the following section.

7.2.1 Results

As shown in Table 7.2, the dipole polarizabilities remain virtually unchanged upon basis set contraction for all elements.

For Ca, a comparison between the dipole polarizabilities resulting from set *d* and *d** shows a negligible difference. This indicates that set *d* contains enough functions up to $l = 2$ and gives a converged value for the dipole polarizability. As for polarization functions, the influence of *f*-type functions is negligible as there is only a very small change in the dipole polarizability from set *d* to *f*. The influence of *g*-type functions was ignored for Ca because of the negligible influence of the *f*-type functions.

For elements from Sr to Ra, a comparison between set *f* and *f** reveals that the dipole polarizability is converged as a further augmentation of set *f* to *f** shows no significant change at all levels of theory.

The influence of *g*-type functions (compare set *f* and *g*) appears to be negligible for Sr and Ba, contributing less than 1% to the dipole polarizability. The final basis set for Sr and Ba are, therefore, the corresponding set *f* as shown in Table 7.2. For Ra, however, the influence of *g*-type functions is evident, as the dipole polarizability is reduced by a larger margin of 1.6% at the DKMP2 level. Further augmentation of set *g* to *g** shows no change in the dipole polarizability and this gives confidence that set *g* contains a sufficient number of basis set exponents for the dipole polarizability.

For Ra, it may be necessary to consider the influence of *h*-type functions. This was investigated by adding eight *h*-type functions to set *g* in Table 7.2. The resulting dipole polarizability at the DKMP2 level was 195.06 a.u., which is 1.3 a.u. lower than the dipole polarizability of set *g*. When this basis set is further augmented with five *i*-type functions, the dipole polarizability is reduced by 0.3 a.u. at the same level of theory. This means that the dipole polarizability of Ra is converged with respect to the basis set expansion to a level of less than 1 a.u. with the inclusion of the *h*-type functions. (as the influence of the *i*-type functions is well below 1 a.u.) Due to high computational demands, the influence of *h*-type functions was considered only at the MP2 level.

	Ca		Sr	Ba	Ra
NR	Basis set	(20*s*15*p*8*d*)	(21*s*16*p*11*d*9*f*)/ [15*s*12*p*10*d*9*f*]	(26*s*22*p*17*d*13*f*)/ [17*s*16*p*13*d*13*f*]	(31*s*24*p*20*d*14*f*11*g*)/ [19*s*16*p*15*d*11*f*11*g*]
	HF	185.45	246.06	368.02	440.86
	MP2	142.57	179.67	243.75	277.37
	CCSD	163.51	215.92	323.41	387.43
	CCSD(T)	160.94	211.34	316.21	378.46
DK	Basis set	(20*s*15*p*8*d*)	(21*s*16*p*11*d*9*f*)/ [15*s*12*p*10*d*9*f*]	(26*s*22*p*17*d*13*f*)/ [16*s*15*p*12*d*13*f*]	(31*s*24*p*20*d*14*f*11*g*)/ [18*s*15*p*14*d*10*f*11*g*]
	HF	182.85	232.88	324.66	300.57
	MP2	140.67	170.53	216.51	196.31
	CCSD	161.20	203.98	282.11	257.67
	CCSD(T)	158.68	199.54	273.85	248.56
DC	Basis set	(20*s*15*p*8*d*)	(21*s*16*p*11*d*9*f*)	(26*s*22*p*17*d*13*f*)	(31*s*24*p*20*d*14*f*)
	HF	182.79	232.66	323.82	299.59
	MP2	140.62	170.38	216.72	198.64

Table 7.3. The calculated dipole polarizabilities of the neutral group 2 elements at the nonrelativistic (NR), scalar relativistic Douglas-Kroll (DK), and relativistic Dirac-Coulomb (DC) level. All values are in a.u.

7.3 Static Dipole Polarizabilities

In order to obtain dipole polarizabilities of near basis set limit quality, the present final basis sets in section 7.2.1 were used in high level correlation calculations. The calculated dipole polarizabilities of the neutral group 2 elements from Ca to Ra are presented in Table 7.3.

7.3.1 Nonrelativistic Results

At the nonrelativistic level, the dipole polarizabilities show a monotonic increase from Ca to Ra both at the HF and correlated level. This increase is expected as the valence electrons are more effectively screened from the nucleus by the increasing number of core electrons.

The importance of electron correlation effects is evident as the dipole polarizabilities are significantly reduced at the correlated level. The reduction of the dipole polarizabilities at the correlated level is attributed to the valence shell contraction caused by electron correlation. As expected, correlation effects are more profound for heavier elements as depicted in Figure 7.1. At the MP2 level, the dipole polarizabilities are reduced by about 40% from the HF results. Due to a slow convergence of the MP expansion, however, electron correlation effects are overestimated at the MP2 level by at least a factor of two, in comparison with the CCSD/CCSD(T) results.

Also evident is the importance of perturbative triples effect, without which the correlation is underestimated. (Figure 7.1) The perturbative triples account for as much as 14% of the total electron correlation effects at the CCSD(T) level. This suggests that in order to further improve the results here, quadruple contributions may have to be included.

At the CCSD(T) level, the reduction of dipole polarizabilities from the uncorrelated HF results is found to be between 13 and 14% for all elements. This is significantly less than correlation effects in the neutral group 1 elements (at the same level of theory), where the dipole polarizabilities are reduced by, for example, over 40 % for Fr. A relatively smaller electron correlation contribution in the dipole polarizability of the group 2 elements is attributed to a stronger electron screening for the doubly occupied valence *ns* shell of the group 2 elements opposed to the singly occupied *ns* of the group 1 elements. As the two

valence electrons in the *ns* shell screen each other, the valence shell contraction caused by electron correlation for the group 2 elements is relatively smaller than for the singly occupied *ns* of the group 1 elements and hence a smaller correlation contribution is observed.

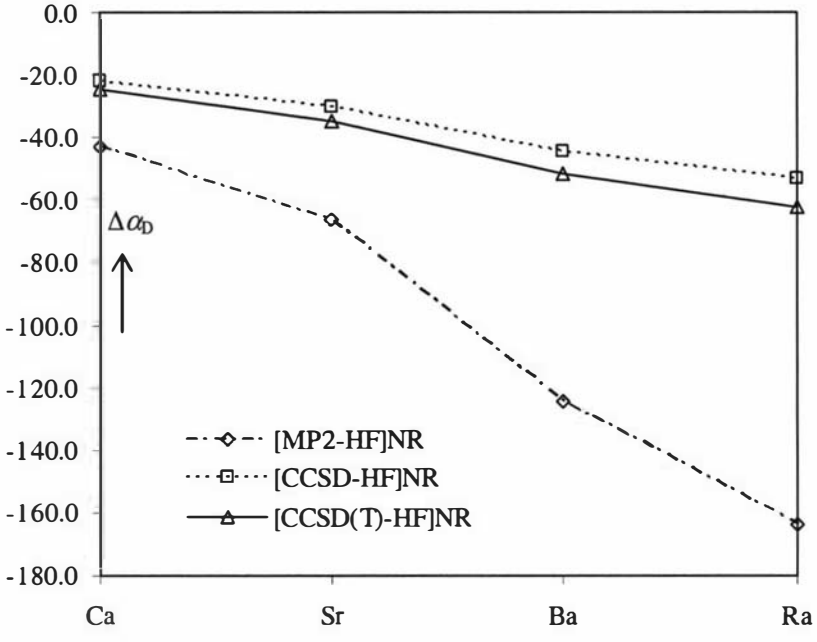

Figure 7.1. The electron correlation contribution to the dipole polarizabilities of the neutral group 2 elements at the nonrelativistic level. All values are in a.u.

7.3.2 Relativistic Results

The scalar relativistic DK results in Table 7.3 and Figure 7.2 demonstrate again the importance of scalar relativistic effects in the dipole polarizabilities. For a comparison, the scalar relativistic and electron correlation contributions to the dipole polarizabilities are depicted in Figure 7.3.

As shown in Figure 7.2, the relativistic valence *s* shell contraction leads to a smaller dipole polarizability in comparison with the nonrelativistic case for all elements. This effect is present even for a relatively light element of Ca with a

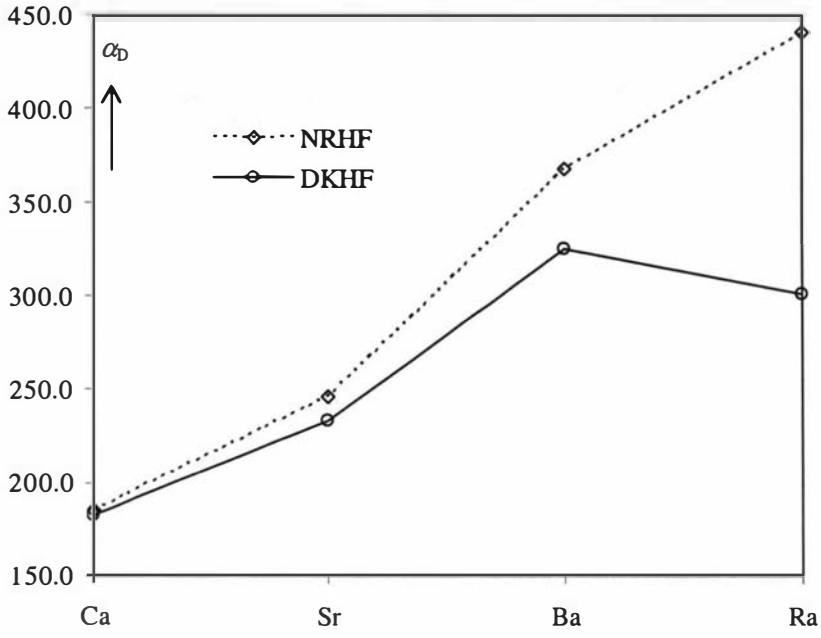

Figure 7.2. The nonrelativistic and scalar relativistic dipole polarizabilities of the neutral group 2 elements at the HF level. All values are in a.u.

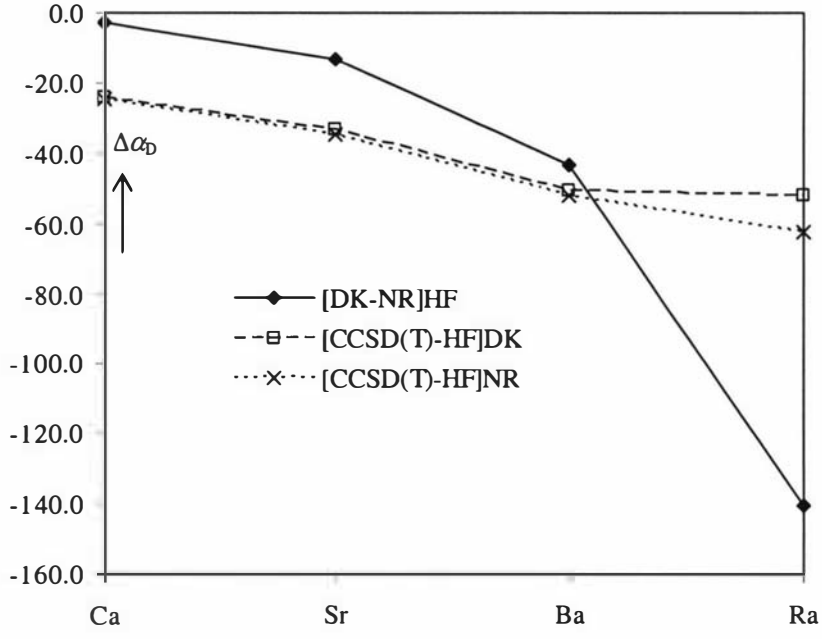

Figure 7.3. The electron correlation and relativistic contributions to the dipole polarizabilities of the neutral group 2 elements. All values are in a.u.

decrease in the dipole polarizability by 1.4%. Although it is quite negligible, the scalar relativistic contribution to Ca remains larger than the errors caused by the use a finite basis set of this study.

Scalar relativistic effects increase with the increasing nuclear charge and become non-negligible from the forth-row atom Sr with a 5.4% decrease in the dipole polarizability. For Ba, relativistic effects grow by two folds from Sr and become of a similar size as correlation effects as depicted in Figure 7.3.

Of particular interest is the scalar relativistic effect in the dipole polarizability of the sixth-row atom, Ra. For this element, relativistic effects begin to dominate over electron correlation. Here, the relativistic contribution is, in fact, more than twice as large as the correlation contribution. (See Figure 7.3) As shown in Figure 7.2, such large relativistic effects cause the dipole polarizability of Ra to drop below that of Ba and a monotonic increase in the nonrelativistic dipole polarizabilities is no longer observed at the relativistic level. This anomalous trend in the dipole polarizabilities, caused by a direct stabilization of the valence *s* orbital, is similar to the case of the neutral group 1 elements discussed in chapter 5. In that case, the dipole polarizability is the largest for the fifth-row atom Cs and becomes smaller thereon [20]. Even larger scalar relativistic effects are expected for element 120.

Electron correlation effects estimated by various methods at the scalar relativistic level are presented in Table 7.3 and in Figure 7.4. Electron correlation leads to a reduction in the dipole polarizabilities from the HF values at the scalar relativistic level, as was the case at the nonrelativistic level. As relativistic effects significantly alter electron correlation, the two effects are not additive and correlation effects at the relativistic level cannot be directly compared to those at the nonrelativistic level.

At the relativistic level, electron correlation is overestimated by the MP2 method as was the case at the nonrelativistic level. Electron correlation effects for Ra are smaller than for Ba at the MP2 level, whereas the CCSD/CCSD(T) method estimates electron correlation of Ra to be similar in size to that of Ba.

The well known Z^2 dependence of relativistic effects is depicted in Figure 7.5 at the CCSD(T) level. A polynomial fit gives

$$\alpha_D = -3\times10^{-6}\, Z^4 - 0.0145\, Z^2 - 0.1426$$

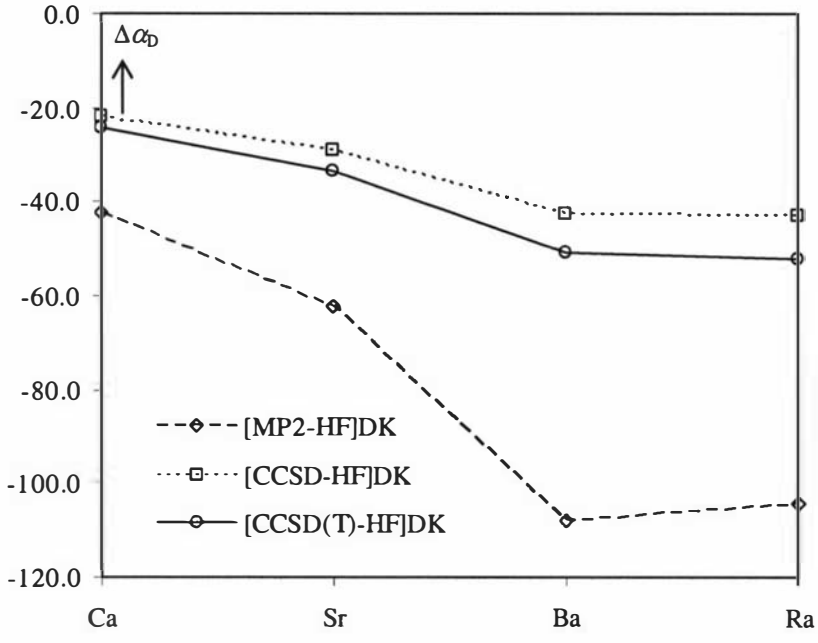

Figure 7.4. The correlation contribution to the dipole polarizabilities of the neutral group 2 elements at the scalar relativistic DK level. All values are in a.u.

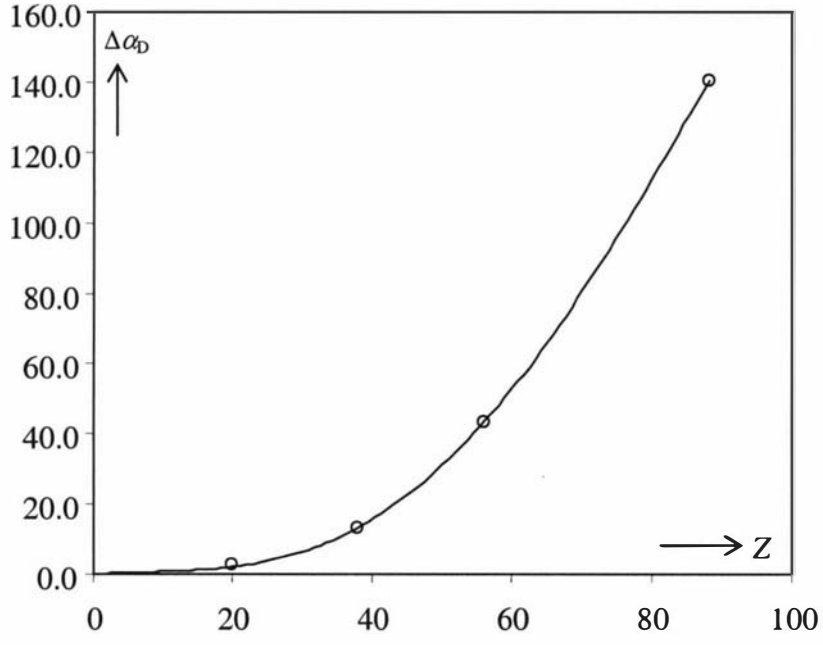

Figure 7.5. The relativistic contribution to the dipole polarizability of the neutral group 2 elements *vs.* nuclear charge, Z at the CCSD(T) level. In this plot $\Delta\alpha_D = \alpha_D^{NR} - \alpha_D^{R}$. All values are in a.u.

with a correlation coefficient of 0.9999 and a very small forth-order contribution.

7.3.3 Spin-Orbit Effects

In the scalar relativistic DK scheme, spin-orbit coupling effects are ignored. In order to test the influence of such effects, fully relativistic four-component DCHF and DCMP2 calculations were performed. Due to the extensiveness of the DHF and DMP2 calculations, the smaller, totally decontracted basis sets for heavy elements, which contain only up to l = 3 type functions (set *d* for Ca and set *uncntr* for Sr to Ra in Table 7.2) were used in the present calculation. As shown in Table 7.3, the effects of SO coupling are negligible for all elements. This is excepted as the consequences of the fine structure effects lie with the orbitals of angular momentum number greater than 1. That is, the p shell splits to $p_{1/2}$ and $p_{3/2}$ and d shell to $d_{3/2}$ and $d_{5/2}$ etc. As for the doubly occupied closed shell systems of the neutral group 2 elements, most of the dipole polarizability results from the polarization of the valence s shell and fine structure effects resulting from the next-to-valence shell have a negligible effect on the dipole polarizabilities. Therefore, SO coupling effects could be safely ignored for the dipole polarizabilities of the neutral group 2 elements.

7.3.4 Comparison with other Values

The DKCCSD(T) values of the dipole polarizabilities of the neutral group 2 elements are compared with the experimental and other theoretical values in Table 7.4.

In comparison with the present dipole polarizabilities, the experimental values of Hyman derived from the summation of oscillator strength [10] are systematically underestimated. The present values lie within the experimental uncertainties of Miller and Bederson [11, 12], which have been obtained by the electric deflection method.

The most direct comparison of the present values could be made with the DKCCSD(T) values of Sadlej *et al.* [4]. They have noted that the active space, in

	Ca	Sr	Ba	Ra
This work	158.68	199.54	273.85	248.56
Theor./DKCCSD(T)	152.0 [4]	194.0 [4]	277.1 [4]	-
Expt./Est.	167 ± 17 [11]	186 ± 15 [12]	268 ± 22 [12]	-
	154 [10]	192 [10]	242 [10]	
	155.9 [21]			

Table 7.4. The calculated static dipole polarizabilities of the neutral group 2 elements at the DKCCSD(T) level. The values are compared with other values. For the methods used, see text. All values are in a.u.

particular, freezing of electronic shells in the correlation step affected their final values. Also noted was the basis set contraction effect in the dipole polarizabilities. They have concluded, however, that their results may only be insignificantly improved by a basis set extension. On the contrary, the present study demonstrates that the dipole polarizabilities are extremely sensitive to the choice of basis sets and the errors caused by the use of finite basis sets could only be minimized by a systematic investigation of the convergence behavior of the dipole polarizabilities with respect to the basis set expansion. Such an investigation is computationally demanding and one must find a balance between the accuracy and the cost of calculations. Given the large experimental uncertainties, it is of a strong interest to obtain more accurate values of dipole polarizabilities which could serve as reference values. For this, however, calculations have to go beyond the CCSD(T) method.

7.4 Ionization Potentials

The ground state first ionization potentials of the neutral group 2 elements are presented in Table 7.5. These values are compared with experimental values [22, 24]. The basis sets for the ionization potential calculations were chosen to be the same as the final CCSD(T) dipole polarizability calculations.

At the nonrelativistic level, the ionization potentials show a monotonic decrease with increasing nuclear charge. This downward trend in the ionization potentials is in accordance with the upward trend in the dipole polarizabilities from Ca to Ra at the nonrelativistic level.

		Ca	Sr	Ba	Ra
NR	HF	5.121	4.677	4.135	3.908
	CCSD	6.002	5.522	4.947	4.701
	CCSD(T)	6.074	5.607	5.054	4.815
DK	HF	5.140	4.748	4.277	4.336
	CCSD	6.022	5.593	5.092	5.139
	CCSD(T)	6.093	5.678	5.194	5.238
Theor. [23]	RCC	-	-	5.327	5.369
Expt. [22, 24]		6.113	5.695	5.212	5.277

Table 7.5. The calculated ground state first ionization potentials of the neutral group 2 elements. All values are in eV.

The relativistic results estimated at the DK level demonstrate the importance of relativistic effects. Although the relativistic contribution for Ca is small, the discrepancy from the experimental value is halved by the consideration of relativistic effects. Relativistic effects grow with increasing nuclear charge and result in an increase in the ionization potentials from the nonrelativistic values at both the HF and correlated level. This is attributed to the relativistic contraction of the valence *s* orbital. As the relativistic valence *s* orbital contracts the electrons in this orbital are more tightly bound by the nucleus and in turn the energy required to remove the electron increases. As depicted in Figure 7.6, relativistic effects for Ra cause an anomaly in the trend of ionization potentials, where the downward trend of the nonrelativistic ionization potentials is no longer observed in the relativistic case.

Also shown in Table 7.5 and Figure 7.6 is the importance of electron correlation effects. Correlation effects are positive, leading to an increase in the ionization potentials at both the nonrelativistic and relativistic level. This is attributed to the shrinkage of the valence *s* orbital by electron correlation as was the case for the neutral group 1 elements. Electron correlation dominates over relativistic effects and accounts for up to 1 eV in ionization potentials at the CCSD(T) level (Figure 7.6). Correlation effects are slightly underestimated at the CCSD level.

In compared with experimental values, the present DKCCSD(T) values tend to be slightly underestimated. The agreement between the two sets of data is excellent, however, with a discrepancy of no more than 0.02 eV.

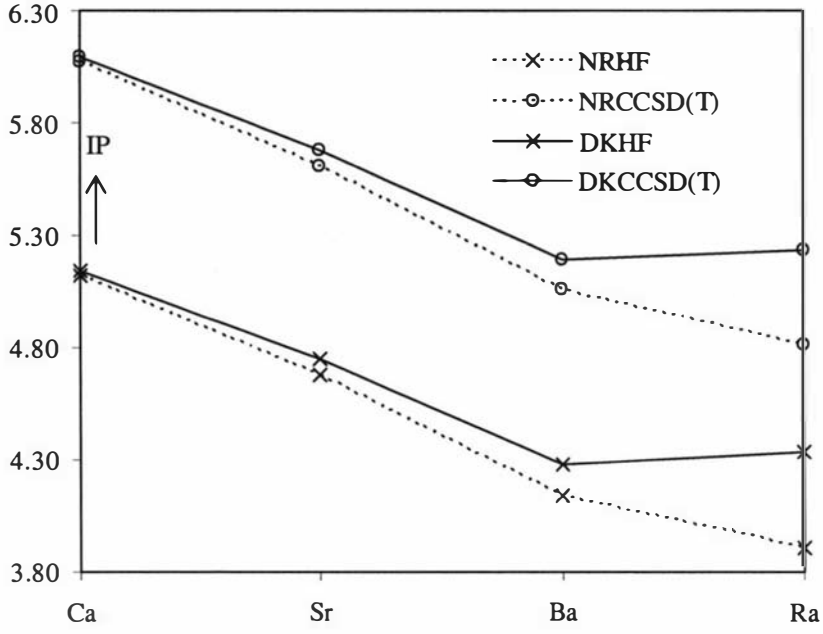

Figure 7.6. A plot of the ground state first ionization potentials of the neutral group 2 elements from Ca to Ra at the nonrelativistic and relativistic HF and CCSD(T) level. All values are in eV.

The theoretical values in Table 7.5 obtained by Kaldor *et al.*, which are Fock-space relativistic coupled-cluster (RCC) calculations [23], seem to overestimate the ionization potentials compared with experimental values. Another theoretical value of 5.278 eV for the ionization potential of Ra [25] favors the present result over Kaldor's. Kaldor *et al.* concluded that the overestimation of their results is most likely to be due to the basis set effects. This is rather uncertain as they have used an extremely large basis set (34*s*25*p*21*d*15*f*10*g*6*h*) including up to *h*-type functions. They also reported that correlation effects including the triples contribution could not be obtained with their large basis set. It is likely however that the triples contribution will be positive, increasing the ionization potential even further. Nevertheless, they have estimated an error of a few hundred wavenumbers in their ionization potentials, based on their earlier study. This amounts to about 0.09 eV and accounts for the major part of the discrepancy between Kaldor's and the present Ra ionization potential at the CCSD(T) level. The present ionization potential of Ra is believed to be highly accurate.

The relationship between the relativistic changes in the dipole polarizabilities and in the ionization potentials at the HF level is shown in Figure 7.7. (see Eq. 2.43) As shown, this linear relationship is almost perfectly satisfied with a correlation coefficient of 0.9997. A least square fit yields the following:

$$\frac{\alpha_D^{NR}}{\alpha_D^{R}} \cong 2.036 \frac{IP^2{}_R}{IP^2{}_{NR}} - 1.0407$$

The relativistic change in the ionization potential defined by $IP_R - IP_{NR}$ is always positive, (i.e. $IP_R - IP_{NR} > 0$) as shown by the increase in the ionization potential by relativistic effects. This implies that the ratio of relativistic to nonrelativistic ionization potential is always greater than unity, i.e. $IP_R/IP_{NR} > 1$, resulting in a even greater positive value of $IP^2{}_R/IP^2{}_{NR}$. The fact that the $\alpha_D{}^{NR}/\alpha_D{}^{R}$ is quadratically dependent on IP_R/IP_{NR} and is related to IP_R/IP_{NR} by a positive pre-factor greater than one means that the ratio $\alpha_D{}^{NR}/\alpha_D{}^{R}$ grows faster than the ratio $IP^2{}_R/IP^2{}_{NR}$, reinforcing the relativistic effects in the dipole polarizabilities.

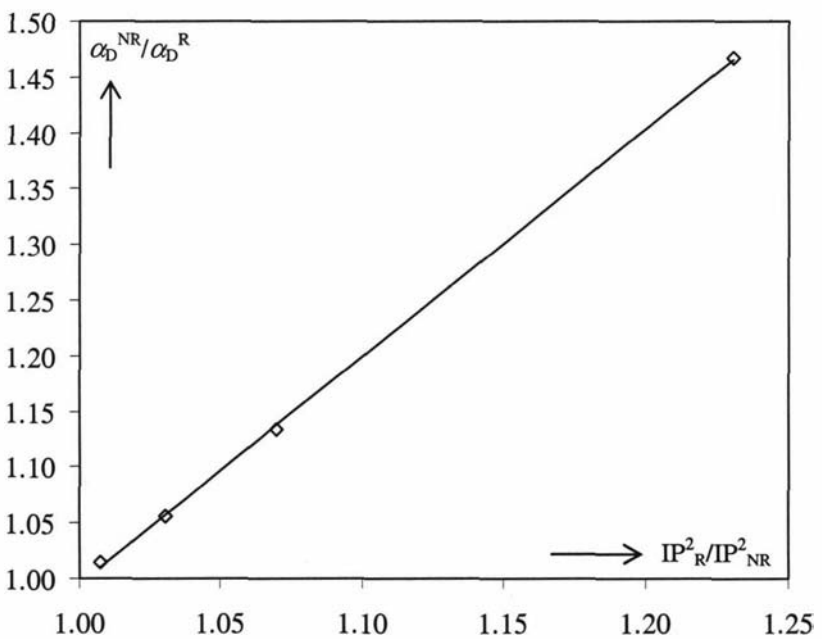

Figure 7.7. Relation between relativistic changes in dipole polarizabilities and in ionization potentials as $\alpha_D{}^{NR}/\alpha_D{}^{R}$ *vs.* $IP^2{}_R/IP^2{}_{NR}$ for Ca to Ra.

7.5 Pseudopotential Results

The 10-valence-electron pseudopotentials for the group 2 elements were tested for dipole polarizabilities and ionization potentials. The performance of the pseudopotentials is discussed in this section.

7.5.1 Static Dipole Polarizabilities

The calculated dipole polarizabilities of the neutral group 2 elements using the present scalar relativistic pseudopotentials are presented in Table 7.6. The values are compared with the all-electron values of this study. Also listed are the relative pseudopotential errors (ignoring signs) in the estimation of the dipole polarizabilities.

		ARPP	AE(DK)	% error
Ca	HF	181.98	182.85	0.5
	CCSD	160.04	161.20	0.7
	CCSD(T)	157.43	158.68	0.8
Sr	HF	232.81	232.88	0.0
	CCSD	203.70	203.98	0.1
	CCSD(T)	199.50	199.54	0.0
Ba	HF	323.62	324.66	0.3
	CCSD	283.94	282.11	0.7
	CCSD(T)	275.51	273.85	0.6
Ra	HF	299.52	300.57	0.4
	CCSD	259.88	257.67	0.9
	CCSD(T)	251.12	248.56	1.0

Table 7.6. The calculated dipole polarizabilities of the neutral group 2 elements estimated by the present scalar relativistic pseudopotentials, ARPP. The values are compared with the present all-electron Douglas-Kroll [AE(DK)]values. The percentage errors in pseudopotentials (ignoring signs) are listed. All values are in a.u.

The ARPP/HF values in Table 7.6 highlight scalar relativistic effects in the dipole polarizabilities. In comparison with the AE method, the ARPP method tends to slightly underestimate the dipole polarizabilities at the HF level. The deviation of the ARPP from the AE results, in the largest case is just over 1 a.u., amounting to no more than 0.5 %. This indicates that scalar relativistic effects are correctly incorporated into the ARPP.

At the correlated level, the pseudopotential errors increase slightly. At the CCSD(T) level, the deviations of the ARPP dipole polarizabilities from the AE results are 1.25, 0.04, 2.51, and 2.56 a.u. for Ca, Sr, Ba, and Ra, respectively. The maximum deviation, however, does not exceed 1 % at both the CCSD and CCSD(T) level. The pseudopotential error of this magnitude is considered acceptable. For the lighter elements, namely Ca and Sr, electron correlation effects are slightly overestimated by the ARPP at both the CCSD and CCSD(T) level. For the heavier elements, however, correlation effects are slightly underestimated by the ARPPs in comparison with the all-electron method, leading to a slight overestimation of the dipole polarizabilities. Generally, the discrepancy between the ARPP and the AE method at the correlated level is larger at the CCSD(T) level than at the CCSD level. Nevertheless, electron correlation effects are correctly described by the present small core (10-valence-electron) ARPPs.

The ARPP values of the dipole polarizabilities are compared with other theoretical values including results from other pseudopotentials in Table 7.7.

The pseudopotential results of ref. [3] in Table 7.7 were obtained by 2-valence-electron pseudopotentials. The description of these pseudopotentials are as follows: V denotes the Dirac-Fock adjusted 2-valence-electron pseudopotentials and V_{sp} is semi-empirical 2-valence-electron pseudopotentials including a polarization potential. The CI describes the valence correlation. Both V and V_{sp} include relativistic effects.

A comparison between the ARPP and the V values at the HF level reveals that the dipole polarizabilities are slightly overestimated by the V but the major relativistic effects are correctly estimated. The inclusion of valence correlation in the V + CISD, however, fails to correctly estimate electron correlation effects as shown by overestimated dipole polarizabilities. Only when core-valence correlation is included in the large core pseudopotential of Ref. [3] (V_{sp} + CISD), the dipole polarizabilities become comparable with those calculated by the small core ten-valence-electron ARPPs (without core-valence correlation).

The dipole polarizabilities estimated by a relativistic random-phase approximation (RRPA) at the coupled Hartree-Fock level agree well with the present ARPP/HF values, indicating once again the correct estimation of relativistic effects by the ARPP. The relativistic time-dependent local-density approximations (RTDLDA) give dipole polarizabilities which are too low.

Overall, the present pseudopotentials perform excellently in calculations of dipole polarizabilities and this serves as a good indication for the reliability of these pseudopotentials.

Method	Ref.	Ca	Sr	Ba	Ra
ARPP/HF	This work	181.98	232.81	323.62	299.52
ARPP/CCSD(T)	This work	157.43	199.50	276.36	251.12
V	[3]	185	237	324	-
V + CISD	[3]	171	230	332	-
V_{sp} + CISD	[3]	157	200	280	-
RRPA	[26]	182.8	232.6	324	-
RTDLDA	[27]	141	171	229	-

Table 7.7. The dipole polarizabilities of the neutral group 2 elements. The ARPP values are compared with other theoretical methods. V is the relativistic 2-valence-electron pseudopotential at the DCHF level, V + CISD is the relativistic pseudopotential plus valence correlation, and V_{sp} + CISD includes core-valence correlation. RRPA is the relativistic random-phase approximation at the coupled HF level and RTDLDA the relativistic time-dependent local-density approximation. All values are in a.u.

7.5.2 Ionization Potentials

The ground state first ionization potentials of the neutral group 2 elements calculated by the present scalar relativistic pseudopotentials are presented in Table 7.8. These values are compared with the scalar relativistic all-electron values of this study. The percentage pseudopotentials errors in the ionization potentials are also listed, ignoring signs.

At the HF level, the agreement between the ARPP and the AE method is excellent. The largest discrepancy is only 0.01 eV for Ca. This indicates that the

scalar relativistic effects are correctly estimated by the ARPPs and confirms the accuracy of the ARPPs as shown for the dipole polarizabilities. This is somewhat expected for the ionization potentials as the present pseudopotentials were energy adjusted. As was the case in the AE method, the smallest ionization potential is observed for Ba in accordance with the largest dipole polarizabilities for this element. The ionization potential increases thereon mainly for Ra, expected from the decrease in the dipole polarizability for this element.

At the correlated level, the discrepancies between the two methods are slightly larger than at the HF level. The relative pseudopotential error, however, is only 0.5% in the largest case at the CCSD(T) level. In comparison with the all-electron method, electron correlation effects are slightly underestimated, leading to smaller ionization potentials. Generally, the relative pseudopotential error is larger for the correlation treatment which includes perturbative triples. A comparison of the two methods confirms that electron correlation is correctly estimated by the ARPPs.

		ARPP	AE (DK)	% error
Ca	HF	5.151	5.140	0.2
	CCSD	6.008	6.022	0.2
	CCSD(T)	6.063	6.093	0.5
Sr	HF	4.750	4.748	0.0
	CCSD	5.593	5.593	0.0
	CCSD(T)	5.668	5.678	0.2
Ba	HF	4.281	4.277	0.1
	CCSD	5.079	5.092	0.3
	CCSD(T)	5.167	5.194	0.5
Ra	HF	4.338	4.336	0.0
	CCSD	5.130	5.139	0.2
	CCSD(T)	5.226	5.238	0.2

Table 7.8. The ground state first ionization potentials of the neutral group 2 elements estimated by the present scalar relativistic pseudopotentials. The values are compared with the all-electron Douglas-Kroll values of this study. The percentage errors in pseudopotentials are listed, ignoring signs. All values are in eV.

In Table 7.9, the ARPP ionization potentials are compared with other theoretical and experimental values. A comparison between the ARPP/HF and the relativistic 2-valence-electron V in Table 7.9 shows an excellent agreement. The data incorporating the valence correlation energy, V + CISD compares reasonably well with the ARPP/CCSD(T) results. The V + CISD values are, however, systematically smaller than the ARPP/CCSD(T) results due to an underestimation of correlation effects by the V + CISD. The deviation of the V + CISD results from the ARPP/CCSD(T) increases with increasing nuclear charge, up to 0.2 eV for Ba.

Method	Ref.	Ca	Sr	Ba	Ra
ARPP/HF	This work	5.151	4.750	4.281	4.338
ARPP/CCSD(T)	This work	6.063	5.668	5.167	5.226
V	[3]	5.151	4.757	4.280	-
V + CISD	[3]	5.970	5.510	4.985	-
V_{sp} + CISD	[3]	6.123	5.701	5.219	-
Expt.	[22]	6.113	5.695	5.212	5.277

Table 7.9. Comparison of the ground state first ionization potentials of the neutral group 2 elements. For explanation of the abbreviations see Table 7.7. All values are in eV.

A comparison between V + CISD and V_{sp} + CISD clearly demonstrate the importance of core-valence correlation in the large core pseudopotentials of Ref. [3]. The discrepancy between the pseudopotentials of Ref. [3] and the ARPP (without core-valence correction) is reduced by up to five folds with the inclusion of core-valence correlation in the V_{sp} + CISD.

In comparison with experimental values, the ionization potentials are underestimated by the ARPP/CCSD(T) and are overestimated by the V_{sp} + CISD. The deviation from the experimental values is significantly less for the V_{sp} + CISD than for the ARPP/CCSD(T). It seems that correlation effects are slightly underestimated in the ARPP/CCSD(T) calculations. In the case of V_{sp} + CISD, a proper account of core-valence correlation results in a larger correlation contribution than for the ARPP/CCSD(T) with ten valence electrons fully correlated. This leads to more comparable, but slightly overestimated ionization

potentials by the V_{sp} + CISD method in comparison with experimental values. Nevertheless, the pseudopotential error in the ARPP method at the CCSD(T) level remains below 1%.

Overall the present 10-valence-electron pseudopotentials perform well for both dipole polarizabilities and ionization potentials. This is a significant improvement on the pseudopotentials available up to now as these pseudopotentials offer sufficient accuracy without including core-valence correlation.

References

[1] S. H. Patil and K. T. Tang, J. Chem. Phys. **106**, 2298 (1997).

[2] S. H. Patil and K. T. Tang, Chem. Phys. Lett. **295**, 152 (1998).

[3] P. Fuentealba, L. von Szentpaly, H. Preuss, and H Stoll, J. Phys. B **18**, 1287 (1985).

[4] A. J. Sadlej and M. Urban, Phys. Rev. A **44**, 5547 (1991).

[5] I. Miadokova, V. Kellö, A. J. Sadlej, Theor. Chem. Acc. **96**, 166 (1997).

[6] G. D. Mahan, Phys. Rev. A **22**, 1780 (1980).

[7] R. M. Sternheimer, Phys. Rev. **96**, 951 (1954); **107**, 1565 (1957); **115**, 1198 (1959); **183**, 122 (1969); Phys. Rev. A **1**, 321 (1970).

[8] P. L. Altick, J. Chem. Phys. **40**, 238 (1964).

[9] M. Cohen, Can. J. Phys. **45**, 3387 (1967).

[10] H. A. Hyman, J. Chem. Phys. **61**, 4063 (1974).

[11] T. M. Miller and B. Bederson, Phys. Rev. A **14**, 1572 (1976).

[12] H. L. Schwartz, T. M. Miller, and B. Bederson, Phys. Rev. A **10**,1924 (1974).

[13] A. J. Sadlej and M. Urban, J. Mol. Struct (Theochem) **234**, 147 (1991).

[14] K. G. Dyall, I. P. Grant, C. T. Johnson, F. A. Parpia, E. P. Plummer, Comput. Phys. Commun **55**, 425 (1989).

[15] T. Saue, J. K. Laerdahl, L. Visscher, and H. J. Aa. Jensen (unpublished).

[16] K. G. Dyall and K. Faegri Jr., Chem. Phys. Lett. **174**, 25 (1990).

[17] L. Visscher and K. G. Dyall, At. Data. Nucl. Data Tables **67**, 207 (1997).

[18] *MOLCAS* Version 5.4, K. Andersson, M. Barysz, A. Bernhardsson, M. R. A. Blomberg, D. L. Cooper, M. P. Fülscher, C. de Graaf, B. A. Hess, G. Karlström, R. Lindh, P.-Å. Malmqvist, T. Nakajima, P. Neogrády, J. Olsen, B. O. Roos, B. Schimmelpfennig, M. Schütz, L. Seijo, L. Serrano-Andrés, P. E. M. Siegbahn, J. Stålring, T. Thorsteinsson, V. Veryazov, and P.-O. Widmark, Lund University, Sweden (2002).

[19] T. Saue, T. Enevoldsen, T. Helgaker, H. J. Aa. Jensen, J. K. Laerdahl, K. Ruud, J. Thyssen, and L. Vvisscher, Dirac, a relativistic *ab-initio* electronic structure program, Release 3.1 (1988) (Odense University, Denmark); see also: http://dirac.chem.sdu.dk; T. Saue, K. Faegri, Jr., T. Helgaker, and O. Gropen, Mol. Phys. **91**, 937 (1997); J. K. Laerdahl, T. Saue, and K. Faegri Jr., Theor. Chem. Acc. **97**, 177 (1997).

[20] I. S. Lim, M. Pernpointner, M. Seth, J. K. Laerdahl, and P. Schwerdtfeger, Phys. Rev. A **60**, 2822 (1999).

[21] D. R. Beck and C. A. Nicolaides, Chem. Phys. Lett. **49**, 357 (1977).

[22] R. C. Weast, M. J. Astle, *Handbook of Chemistry and Physics*. CRC Press, Boca Raton, p. E-64(1993).

[23] E. Eliav and U. Kaldor, Phys. Rev. A **53**, 3050 (1996).

[24] C. E. Moore, *Atomic Energy Levels*, Natl. Bur. Stand. (U.S.) Circ. No. 467 (U.S. GPO, Washington, DC, 1958), Vol. III.

[25] J. A. Armstrong, J. J. Wynne, and F. S. Tomkins, J. Phys. B **13**, L133 (1980).

[26] D. Kolb and W. R. Johnson, Phys. Rev. A **26**, 19 (1982).

[27] F. A. Parpia and W. R. Johnson, Phys. Lett. A **99**, 172 (1983).

Chapter 8
THE SINGLY CHARGED GROUP 2 ELEMENTS

The dipole polarizabilities and the ionization potentials of the singly charged group 2 elements have received special attention due to their easily approximated one-electron valence shell, much like the case in the neutral group 1 elements. In particular, Patil and Tang have calculated valence properties by treating the singly charged group 2 elements as a single valence electron problem by the use of pseudopotentials [1]. However, their earlier method for the determination of dipole polarizabilities by evaluating the multipolar matrix elements using simple wave functions based on the asymptotic behavior and the binding energies of the valence electron, seemed to offer a better agreement with the dipole polarizabilities of Sadlej and co-workers who have carried out purely *ab-initio* studies, including relativistic effects and high level electron correlation using the coupled-cluster approximation.

In this chapter, the dipole polarizabilities and the ionization potentials of the singly charged group 2 elements from Ca^+ to Ra^+ are presented.

8.1 Basis Sets

The basis set exponents for the singly charged group 2 elements were taken from the corresponding neutral elements. The range of the exponents, especially of the polarization functions as well as the contraction scheme, were modified slightly. The modifications were as follows: $(21s16p11d9f3g)/[15s12p10d9f3g]$ for both the nonrelativistic (NR) and scalar relativistic Douglas-Kroll (DK) calculations of Sr^+, $(25s21p16d8f5g)/[16s15p12d8f5g]$ for both the NR and DK of Ba^+, and $(31s24p20d12f8g)/[18s16p15d9f8g]$ for the NR calculations and $(31s24p20d12f8g)/[18s15p14d9f8g]$ for the DK calculations of Ra^+. Note that a

heavier contraction was used in the relativistic basis set for Ra^+ to improve on linear dependencies. In all cases, the contraction coefficients were obtained in separate nonrelativistic and relativistic Douglass-Kroll Hartree-Fock calculations.

For the spin-orbit (SO) calculations, totally uncontracted basis sets were used, which include basis functions up to l = 3 (i.e. *f*-type functions) as the computational demand was very high. The large component exponents were taken from the above basis sets for the DK calculations whereas the small component exponents were generated from the large components by a linear transformation and a projection [2] equivalent to the kinetic balance conditions [3]. Again, a Gaussian nuclear model with nuclear exponents as given by Visscher and Dyall [4] was used for the spin-orbit calculations.

8.1.1 Basis Set Effects

The calculated dipole polarizabilities of the singly charged group 2 elements resulting from various basis sets are presented in Table 8.1. As was the case for the neutral group 2 elements, the basis sets labeled l^* (l = maximum angular momentum function) contains one extra high and one extra diffuse function compared to the basis sets labeled l in Table 8.1.

For nonrelativistic Ca^+, a comparison between set *d* and *d** reveals that set *d* contains enough functions and the dipole polarizability is converged within 0.009 and 0.061 a.u. at the HF and MP2 level, respectively. The influence of *f*-type functions is clear when the dipole polarizability of set *d* is compared to that of set *f*. That is, the *f*-type functions reduce the dipole polarizability by 1.7 a.u. at the MP2 level. This change accounts for 2.4 % of the dipole polarizability at the MP2 level and more importantly is more than an order of magnitude higher than the basis set convergence within set *d*'s. Therefore, these *f*-type functions were included in the final basis set. In order to ensure that these five *f*-type functions of set *f* are sufficient, two additional functions were added in set *f**. As shown in Table 8.1, there is no significant change in the dipole polarizability and the basis set convergence is obtained at 0.009 and 0.037 a.u. at the HF and MP2 level, respectively. Set *f* was chosen as the final basis set for the nonrelativistic calculations. The relativistic dipole polarizabilities show a similar pattern where a reduction of the dipole polarizability is observed by the inclusion of *f*-type functions and the final basis set, set *f* contains enough functions, exhibiting a

		Nonrelativistic			Relativistic Douglas-Kroll		
		Basis set	HF	MP2	Basis set	HF	MP2
Ca^+	*d*	(20*s*15*p*8*d*)	98.64	73.84	(20*s*15*p*8*d*)	96.46	72.28
	*d**	(22*s*17*p*10*d*)	98.65	73.90	(22*s*17*p*10*d*)	96.47	72.34
	f	(20*s*15*p*8*d*5*f*)	98.64	72.16	(20*s*15*p*8*d*5*f*)	96.46	70.62
	*f**	(22*s*17*p*10*d*7*f*)	98.65	72.19	(22*s*17*p*10*d*7*f*)	96.47	70.66
Sr^+	*uncntr*	(21*s*16*p*11*d*9*f*)	132.15	87.06	(21*s*16*p*11*d*9*f*)	121.33	80.67
	f	(21*s*16*p*11*d*9*f*)/ [15*s*12*p*10*d*9*f*]	132.15	87.07	(21*s*16*p*11*d*9*f*)/ [15*s*12*p*10*d*9*f*]	121.33	80.68
	*f**	(23*s*18*p*13*d*11*f*)/ [17*s*14*p*12*d*11*f*]	132.16	87.07	(23*s*18*p*13*d*11*f*)/ [17*s*14*p*12*d*11*f*]	121.34	80.68
	g	(21*s*16*p*11*d*9*f*3*g*)/ [15*s*12*p*10*d*9*f*3*g*]	132.15	86.21	(21*s*16*p*11*d*9*f*3*g*)/ [15*s*12*p*10*d*9*f*3*g*]	121.33	79.89
	*g**	(23*s*18*p*13*d*11*f*5*g*)/ [17*s*14*p*12*d*11*f*5*g*]	132.16	86.26	(23*s*18*p*13*d*11*f*5*g*)/ [17*s*14*p*12*d*11*f*5*g*]	121.34	79.91

Table 8.1. The calculated static dipole polarizabilities of the singly charged group 2 elements from Ca^+ to Ra^+. All values are in a.u. Continued on the following page.

Ba^+	*uncntr*	(25*s*21*p*16*d*8*f*)	213.47	112.81	(25*s*21*p*16*d*8*f*)	174.64	96.69
	f	(25*s*21*p*16*d*8*f*)/ [16*s*15*p*12*d*8*f*]	213.47	112.82	(25*s*21*p*16*d*8*f*)/ [16*s*15*p*12*d*8*f*]	174.64	96.70
	*f**	(27*s*23*p*18*d*10*f*)/ [18*s*17*p*14*d*10*f*]	213.47	112.81	(27*s*23*p*18*d*10*f*)/ [18*s*17*p*14*d*10*f*]	174.65	96.68
	g	(25*s*21*p*16*d*8*f*5*g*)/ [16*s*15*p*12*d*8*f*5*g*]	213.47	110.60	(25*s*21*p*16*d*8*f*5*g*)/ [16*s*15*p*12*d*8*f*5*g*]	174.64	94.94
	g*	(27*s*23*p*18*d*10*f*7*g*)/ [18*s*17*p*14*d*10*f*7*g*]	213.47	110.56	(27*s*23*p*18*d*10*f*7*g*)/ [18*s*17*p*14*d*10*f*7*g*]	174.65	94.94
Ra^+	*uncntr*	(31*s*24*p*20*d*12*f*)	256.80	125.21	(31*s*24*p*20*d*12*f*)	145.46	82.61
	f	(31*s*24*p*20*d*12*f*)/ [19*s*16*p*15*d*9*f*]	256.80	125.25	(31*s*24*p*20*d*12*f*)/ [18*s*15*p*14*d*9*f*]	145.46	82.61
	*f**	(33*s*26*p*22*d*14*f*)/ [21*s*18*p*17*d*11*f*]	256.80	125.25	(33*s*26*p*22*d*14*f*)/ [20*s*17*p*16*d*11*f*]	145.47	82.60
	g	(31*s*24*p*20*d*12*f*8*g*)/ [19*s*16*p*15*d*9*f*8*g*]	257.00	123.23	(31*s*24*p*20*d*12*f*8*g*)/ [18*s*15*p*14*d*9*f*8*g*]	145.47	79.80
	*g**	(33*s*26*p*22*d*14*f*10*g*)/ [21*s*18*p*17*d*11*f*10*g*]	257.00	123.22	(33*s*26*p*22*d*14*f*10*g*)/ [20*s*17*p*16*d*11*f*10*g*]	145.47	79.81

Table 8.1. Continued form the previous page.

convergence in the dipole polarizability within 0.01 and 0.04 a.u. at the scalar relativistic HF and MP2 level, respectively.

For nonrelativistic Sr^+, the dipole polarizabilities resulting from a totally uncontracted basis set, *uncntr*, which includes up to *f*-type functions, give a starting point for the basis set study. As can be seen in Table 8.1, the dipole polarizabilities are unaffected (within 0.009 a.u. at the MP2 level) by the basis set contraction. In order to verify that the dipole polarizabilities are converged with respect to the basis set up to $l = 3$, set *f* was augmented by two additional functions as shown by set *f**. A comparison of resulting dipole polarizabilities reveals that indeed set *f* contains enough functions as the dipole polarizabilities are converged within 0.001 and 0.002 a.u. at the HF and MP2 level, respectively. The influence of *g*-type functions was tested by adding three such functions to set *f*. There is a slight decrease in the dipole polarizability at the MP2 level upon addition of *g*-type functions as shown by set *g*. This decrease is small, less than 1 a.u., but is significantly larger when compared to the basis convergence in the *f*-sets. The *g*-type functions were therefore included in the final basis set. When set *g* was augmented by two additional functions to set *g** the resulting dipole polarizabilities show no significant difference from those of set *g*. The final basis set was chosen to be set *g*.

The relativistic dipole polarizabilities show a similar trend to the nonrelativistic case in terms of the basis set expansion. Changes due to the basis set contraction are negligible for the dipole polarizabilities as shown by set *f*, which is sufficiently large as confirmed by an insignificant change in the dipole polarizabilities from a larger set *f**. The influence of *g*-type functions is once again significant as shown by a decrease in the dipole polarizability at the MP2 level. No more than three *g*-type functions were needed to obtain a convergence margin (i.e. $\Delta\alpha_D$ in set *g* and *g** = 0.03 a.u. at the MP2 level) smaller than the reduction in the dipole polarizability caused by the inclusion of *g*-type functions (i.e. $\Delta\alpha_D$ in set *f* and *g* = 0.8 a.u. at the MP2 level). Set *g* was chosen for the higher level correlation calculations.

For Ba^+ and Ra^+, the basis set effects on the dipole polarizabilities are similar to Sr^+. The basis set contraction scheme was carefully devised so that the dipole polarizabilities are unaffected by the basis set contraction as confirmed by a comparison between set *uncntr* and set *f* in Table 8.1. Basis sets that include up to *f*-type functions were converged in terms of the dipole polarizability as additional functions in set *f** show no significant deviation from set *f*. The influence of *g*-type functions is larger for Ba^+ and Ra^+ than for Sr^+, as expected

with increasing number of electrons. More precisely, the *g*-type functions reduce the dipole polarizability of Ba^+ by 2.2 and 1.8 a.u. at the nonrelativistic and relativistic MP2 level, respectively. For Ra^+, the influence of *g*-type functions amounts to 2.8 a.u. at the relativistic MP2 level. A sufficient number of *g*-type functions were, therefore, used to obtain converged values of the dipole polarizabilities, which included up to five and eight *g*-type functions for respective Ba^+ and Ra^+. The dipole polarizabilities of set *g** in each case confirm the final convergence in dipole polarizabilities with respect to the basis set expansion. (less than 0.1 a.u. in all cases) The final basis sets were set *g*. Note that for Ra^+ a slightly heavier contraction scheme was used for relativistic calculations to eliminate linear dependencies.

For Ra^+ the influence of *h*-type functions was tested by adding seven *h*-type functions to set *g*. The resulting dipole polarizability was 79.12 a.u. at the DKMP2 level. This is only 0.68 a.u. smaller than the dipole polarizability from set *g*. The *h*-type functions were therefore considered only at the MP2 level, which is a reasonable compromise between accuracy and computational demand.

8.2 Static Dipole Polarizabilities

In this section, the static dipole polarizabilities of the singly charged group 2 elements from Ca^+ to Ra^+ calculated in an all-electron approach are presented and discussed. The results are presented in Table 8.2.

8.2.1 Nonrelativistic Results

At the nonrelativistic level, the dipole polarizabilities increase monotonically from Ca^+ to Ra^+ at both the HF and correlated levels as shown in Table 8.2. It is of interest to compare the dipole polarizabilities of these singly charged ions with those of their neutral counterparts. Comparisons of data in Tables 7.3 and 8.2 show that the dipole polarizabilities of the singly charged ions are significantly smaller than those of the neutral atoms by up to 50 %. This is expected as the removal of one of the two electrons from the valence *s* shell means that the remaining valence *s* electron feels less screening from the nucleus. As a result,

		Ca^+	Sr^+	Ba^+	Ra^+
NR	Basis set	(20*s*15*p*8*d*5*f*)	(21*s*16*p*11*d*9*f*3*g*)/ [15*s*12*p*10*d*9*f*3*g*]	(25*s*21*p*16*d*8*f*5*g*)/ [16*s*15*p*12*d*8*f*5*g*]	(31*s*24*p*20*d*12*f*8*g*)/ [19*s*16*p*15*d*9*f*8*g*]
	HF	98.64	132.15	213.47	257.00
	MP2	72.16	86.21	110.60	123.23
	CCSD	79.65	101.58	144.93	186.00
	CCSD(T)	77.71	97.91	132.66	172.00
DK	Basis set	(20*s*15*p*8*d*5*f*)	(21*s*16*p*11*d*9*f*3*g*)/ [15*s*12*p*10*d*9*f*3*g*]	(25*s*21*p*16*d*8*f*5*g*)/ [16*s*15*p*12*d*8*f*5*g*]	(31*s*24*p*20*d*12*f*8*g*)/ [18*s*15*p*14*d*9*f*8*g*]
	HF	96.46	121.33	174.64	145.47
	MP2	70.62	79.89	94.94	79.80
	CCSD	77.75	94.31	129.92	110.48
	CCSD(T)	75.88	91.10	123.07	105.37

Table 8.2. The calculated static polarizabilities of the singly charged group 2 elements at the nonrelativistic and scalar relativistic Douglas-Kroll level of theory. All values are in a.u.

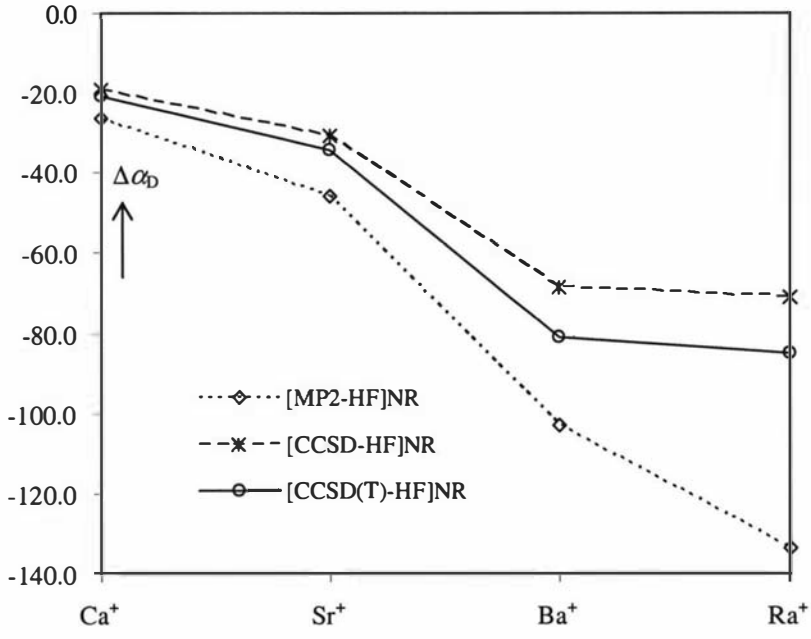

Figure 8.1. The electron correlation contribution to the dipole polarizabilities of the singly charged group 2 elements at the nonrelativistic level. All values are in a.u.

the diffuseness of the valence *s* shell is reduced, leading to smaller dipole polarizabilities for the ions.

The nonrelativistic dipole polarizabilities in Table 8.2 highlight the importance of electron correlation effects as depicted in Figure 8.1. Electron correlation causes the valence shell to contract as in the case of the neutral atoms. That is, for all ions, the electron correlation contribution is negative (Figure 8.1), resulting in smaller dipole polarizabilities than the HF values. As expected, the correlation contribution grows monotonically from Ca^+ to Ra^+ as shown in Figure 8.1. The MP2 method overestimates electron correlation, in this case too negative, for all ions. This overestimation is worst for the heaviest ion Ra^+, which amounts to 36% when compared with the CCSD(T) result. The importance of the perturbative triples is easily seen in Figure 8.1, as correlation effects are underestimated at the CCSD level.

Overall, electron correlation effects reduce the dipole polarizabilities by as much as 38% at the CCSD(T) level. This is larger than the case of neutral atoms where the correlation contribution only amounts to 14% as discussed in the

previous chapter. Interestingly, the magnitude of the relative correlation contribution to the dipole polarizabilities of the singly charged group 2 elements is similar to that of the neutral group 1 elements, both having the same valence electron configuration of ns^1.

8.2.2 Relativistic Effects

The data in Table 8.2 highlight relativistic effects in the static dipole polarizabilities of the singly charged group 2 elements at various levels of theory. As shown in Figure 8.2, relativistic effects cause a reduction in dipole polarizabilities for all ions. As discussed in previous chapters, the reduction of dipole polarizabilities by relativity is attributed to the relativistic contraction of the valence *s* orbital. This direct effect of relativity is present, though small, even for a light ion, Ca^+. In this case, the dipole polarizability is reduced by 2.1 a.u. at the HF level. This is larger than, for example, the basis set effects of *f*-type

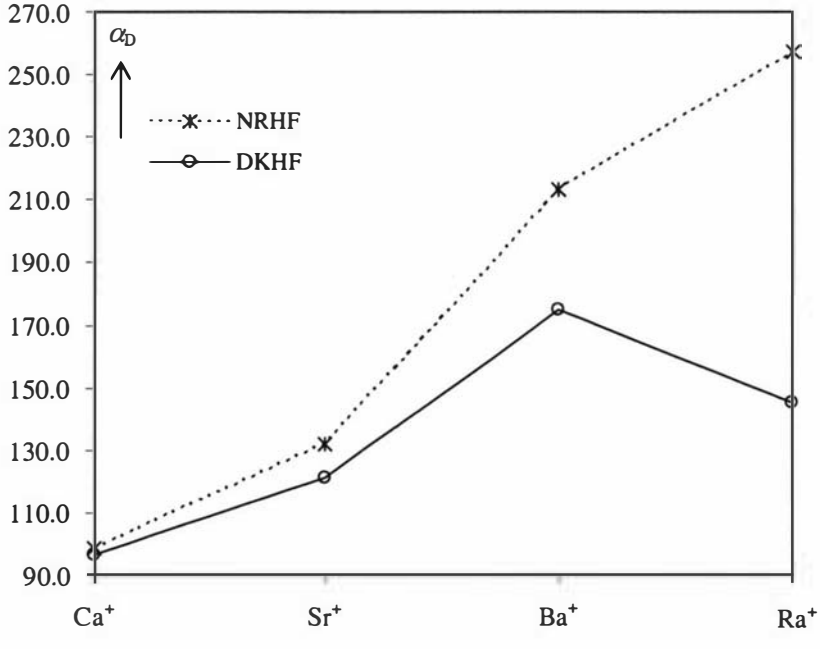

Figure 8.2. The nonrelativistic and scalar relativistic static dipole polarizabilities of the singly charged group 2 elements from Ca^+ to Ra^+ at the HF level. All values are in a.u.

functions (1.7 a.u. at the MP2 level, section 8.1.1) and is therefore considered non-negligible in an accurate determination of dipole polarizabilities. As one expects relativistic effects grow with increasing nuclear charge and become more visible for Sr^+ and Ba^+ as shown in Figure 8.2, where the dipole polarizability is reduced, respectively, by 11 and 39 a.u. at the HF level.

Relativistic effects are largest for the heaviest ion Ra^+. In fact, the effects of relativity are so big that the upward trend in the dipole polarizability at the nonrelativistic level is no longer continued at the relativistic level. That is, the dipole polarizability of Ra^+ is smaller than that of Ba^+ as depicted in Figure 8.2. Note that this anomalous trend in the dipole polarizability caused by relativity has been demonstrated for the neutral group 1 and 2 elements in previous chapters.

The relativistic contribution to the dipole polarizabilities at the DKHF level is compared with the electron correlation contribution at the nonrelativistic CCSD(T) level in Figure 8.3. Up to Ba^+, the largest contribution to the dipole polarizability comes from electron correlation effects, which dominate over relativistic effects. For Ra^+, however, relativistic effects become the most important contribution to the dipole polarizability and start to dominate over

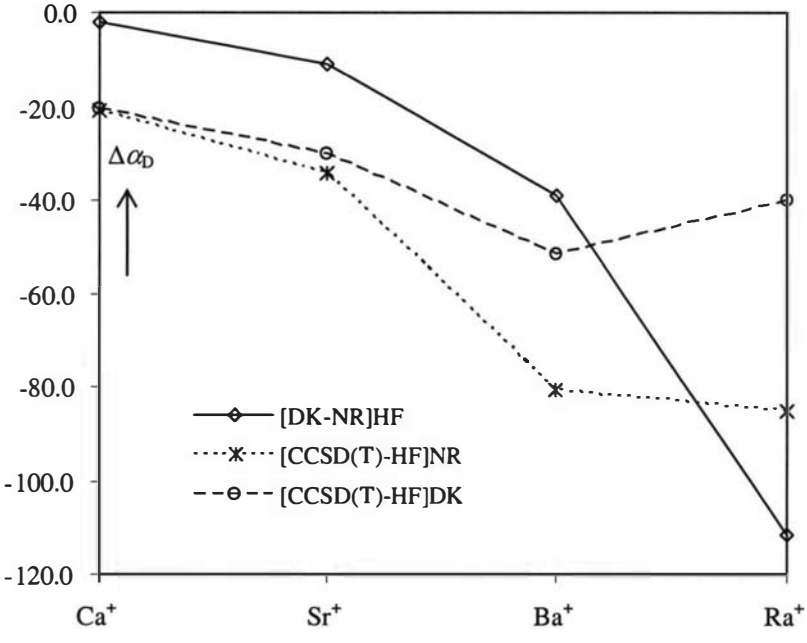

Figure 8.3. The relativistic and electron correlation contributions to the dipole polarizabilities of the singly charged group 2 elements. All values are in a.u.

correlation effects. In fact, the relativistic contribution accounts for as much as 43% of the dipole polarizability of Ra^+ at the HF level.

8.2.3 Electron Correlation Effects at the Relativistic Level

It has been discussed earlier that relativity significantly alters electron correlation effects. As shown in Figure 8.3, the correlation contribution to the dipole polarizabilities at the relativistic level starts to deviate from the nonrelativistic case with increasing effects of relativity.

Of particular interest is the correlation effects for Ba^+ and Ra^+. That is, Ra^+ experiences a smaller correlation contribution than Ba^+ at the relativistic level whereas an increasing correlation contribution from Ba^+ to Ra^+ is observed at the nonrelativistic level. This anomaly in the trend of correlation effects (at the relativistic level) is connected to relativity, in particular the direct stabilization of the valence *s* orbital. As the contraction of the valence orbital is already compensated for by relativistic effects in Ra^+, the extent to which the correlation causes the valence shell to contract is reduced and therefore smaller correlation effects are observed for Ra^+ compared to Ba^+. Interestingly, a similar trend of electron correlation effects is observed for the neutral group 1 elements where such effects at the relativistic level increase from K to Cs, but smaller correlation effects are observed for Fr and even smaller for E119 with increasing relativistic effects. (the correlation contributions are 275.5, 228.19, and 83.74 a.u for Cs, Fr, and E119 at the DKCCSD(T) level, respectively)

All in all, electron correlation effects act to reduce the dipole polarizabilities from the overestimated HF values. The MP2 method overestimates correlation effects as shown in Figure 8.4 but follows the trend of the CCSD/CCSD(T) method indicating that the overestimation by the MP2 method is more of a quantitative problem rather than a qualitative one. The perturbative triples play an important role as the CCSD method underestimates correlation effects compared to the CCSD(T) method.

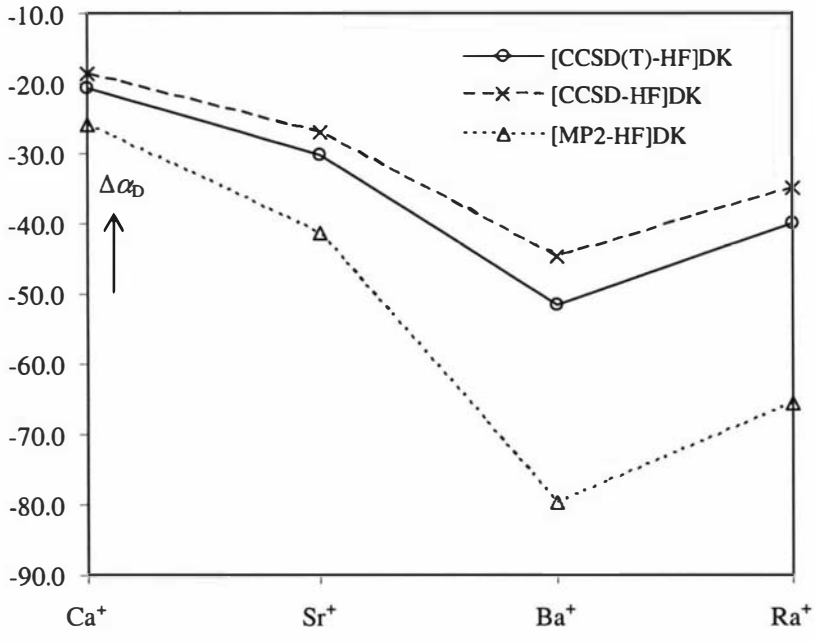

Figure 8.4. The electron correlation contributions to the dipole polarizabilities of the singly charged group 2 elements at the relativistic Douglas-Kroll level. All values are in a.u.

8.2.4 Spin-Orbit Effects

In order to test for spin-orbit (SO) effects in dipole polarizabilities of the singly charged group 2 elements, fully relativistic calculations were performed for Ba^+ and Ra^+. This was carried out with the totally uncontracted basis set denoted *uncntr* in Table 8.1.

For Ba^+, the Dirac-Coulomb-Hartree-Fock (DCHF) calculation results in a dipole polarizability of 174.28 a.u. This is 0.36 a.u. smaller than the scalar relativistic result of 174.64 a.u. with the same basis set. For Ra^+, DCHF calculations yield 144.73 a.u., 0.74 a.u. smaller than the DK counterpart. Such small effects are expected as the valence *s* shell experiences spin-orbit effect only at second order. Spin-Orbit coupling effects can, therefore, be ignored for dipole polarizabilities of the singly charged group 2 elements.

8.2.5 Comparison with other Values

The present dipole polarizabilities of the singly charged group 2 elements are compared with other values in Table 8.3. Sadlej and co-workers have used a similar method for the dipole polarizabilities calculations. They have estimated relativistic effects using the Douglas-Kroll scheme at the CCSD(T) level. As can be seen, the present values agree well with the values of Sadlej, except for Ba^+ where the dipole polarizability seems to be overestimated by Sadlej [5]. This is probably due to basis set deficiencies in Sadlej's results. They have also reported a dipole polarizability of Ba^+ which is further 3.4 a.u higher than quoted in Table 8.3, using a smaller basis set.

Tang *et al.* [6] have used a rather different approach to calculate dipole polarizabilities. They evaluated the multipolar matrix elements using simple wave functions based on the asymptotic behavior, and the binding energies of the valence electron of alkali atoms and their isoelectronic sequences. The present values are in good agreement with the values of Tang. This gives confidence on the dipole polarizability of Ra^+, which is determined in this study for the first time.

It is interesting to note that the dipole polarizabilities of the singly charged group 2 elements are almost one half of those of the neutral elements. It seems as if each electron in the valence shell contributes to the dipole polarizabilities in the same way regardless of the presence of the other electron. If one electron in the valence shell gives rise to a dipole polarizability of a magnitude, x, then approximately the same amount of dipole polarizability is added as another electron is added to the valence shell, so to speak. Although it is quite coincidental, it fits the picture of valence properties, where a whole chemical

	Ca^+	Sr^+	Ba^+	Ra^+
Recomm.	75.88	91.10	122.71	104.64
Sadlej *et al.*	75.71 [5]	91.58 [5]	126.2 [5]	-
Tang *et al.*	75.50 [6]	91.47 [6]	124.7 [6]	-

Table 8.3. Recommended dipole polarizabilities of the singly charged group 2 elements. Spin-Orbit effects for Ba^+ and Ra^+ are included at the DCHF level. The values are compared to other theoretical values. All values are in a.u.

system can be reduced to the electrons in the valence shell for a given property and can be related to another valence property such as ionization potentials. Any relation to this point will be discussed along with ionization potentials in the next section.

8.3 Ionization Potentials

The calculated second ionization potentials of the group 2 elements are presented in Table 8.4. The values are compared with other theoretical values.

At the nonrelativistic level, the ionization potentials show a monotonic decrease with increasing nuclear charge at the HF and correlated level. The downward trend in ionization potentials is in accordance with the upward trend in dipole polarizabilities. This relationship between ionization potentials and dipole polarizabilities noted by Dalgarno and Kingston, was formulated earlier in Eq. 2.42. Correlation effects are important as ionization potentials are underestimated at the HF level, due mostly to the neglect of valence orbital contraction by electron correlation. Note that electron correlation had opposite effects (i.e. causing a decrease) on the dipole polarizabilities, which is expected from Eq. 2.42.

Table 8.4 and Figure 8.5 highlight the importance of relativistic effects in ionization potentials. The effects of relativity increase the ionization potentials from the nonrelativistic counterparts. As said before, this is attributed to the relativistic contraction of the valence *s* orbital, upon which more energy is required to ionize the singly charged group 2 elements. Relativistic effects on Ca^+ are very small, an order of magnitude smaller than correlation effects. It is, however, considered non-negligible as the agreement between the present and the other value becomes much better with relativity taken into account. Relativistic effects grow by an order of magnitude for Ba^+. Due to large relativistic effects on Ra^+, the downward trend in ionization potentials is no longer observed and there is an increase in the ionization potential for Ra^+ as depicted in Figure 8.5. Relativistic effects are smaller than electron correlation effects for ions up to Ba^+. For Ra^+, it is relativistic effects that become larger in magnitude than correlation effects. As shown in Table 8.4, there is an excellent agreement between the present and other theoretical values.

		Ca^+	Sr^+	Ba^+	Ra^+
NR	HF	11.31	10.29	9.06	8.55
	CCSD	11.77	10.80	9.60	9.09
	CCSD(T)	11.81	10.85	9.66	9.16
DK	HF	11.35	10.44	9.36	9.42
	CCSD	11.82	10.97	9.93	10.04
	CCSD(T)	11.85	11.01	9.99	10.10
Theor. [7]	RCC	-	-	10.03	10.17
Expt. [8-10]		11.87	11.03	10.00	10.15

Table 8.4. The second ionization potentials of the group 2 elements. The values are compared with the other values obtained from references written in square brackets. All values are in eV.

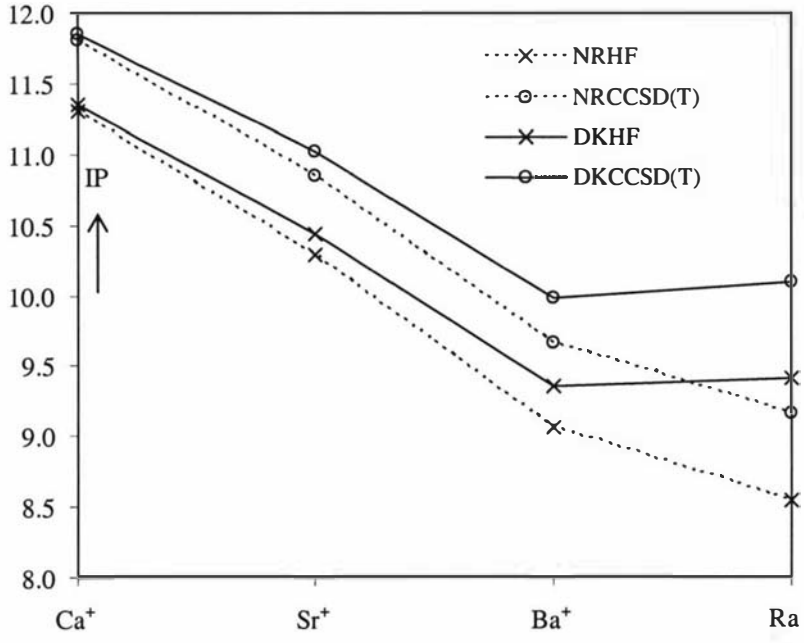

Figure 8.5. The second ionization potentials of the singly charged group 2 elements. All values are in eV.

It was noted in the previous section that the dipole polarizabilities of the singly charged group 2 elements are almost one half of those of the neutral elements. It is interesting to note that there is a similarity in ionization potentials.

That is, the second ionization potentials are almost double the first ionization potentials (see Table 7.5 for comparison). One can test the relationship between the dipole polarizabilities and ionization potentials as in Eq. 2.42, by taking the difference in the dipole polarizabilities and ionization potentials between the neutral and singly charged ions. That is, Eq. 2.42 is approximated by

$$\Delta\alpha_D = c_1\left(\frac{1}{IP_0^2} - \frac{1}{IP_1^2}\right) + c_2 \qquad \text{Eq. 8.1}$$

where $\Delta\alpha_D$ = α_D(neutral elements) - α_D(singly charged ions) and IP_0 and IP_1 are the first and second ionization potentials, respectively. Here, only two coefficients c_1 and c_2 were used for the fit.

The resulting plot is shown in Figure 8.6. There is an almost perfect linear relationship between the two valence properties. It confirms that the halving of dipole polarizabilities can be expected from a large increase in the ionization potentials from the neutral to singly charged elements.

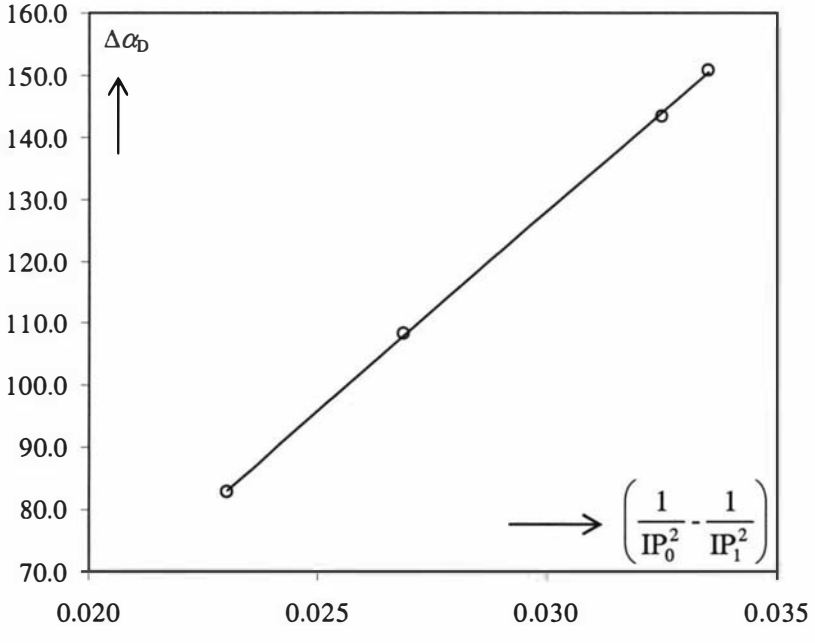

Figure 8.6. The plot of $\left(\frac{1}{IP_0^2} - \frac{1}{IP_1^2}\right)$ *vs.* $\Delta\alpha_D$ as in Eq. 8.1. All values are in a.u.

8.4 Pseudopotential Results

The static dipole polarizabilities of the singly charged group 2 elements are calculated using the present scalar relativistic pseudopotentials described in chapter 4. The resulting dipole polarizabilities are presented and compared with the all-electron values of this study in Table 8.5.

8.4.1 Static Dipole Polarizabilities

At the HF level, the dipole polarizabilities calculated by the scalar relativistic pseudopotentials (ARPP) agree well with the all-electron results at the Douglas-Kroll level [AE(DK)], except for Ba^+.

For Ba^+, there is a discrepancy of 5.8 a.u. between the two methods. Sadlej and co-workers [5] have calculated the dipole polarizability of Ba^+ to be 173.7 a.u., which includes relativistic effects by the DK scheme at the HF level.

		ARPP	AE (DK)	% error
Ca^+	HF	96.36	96.46	0.1
	CCSD	78.04	77.75	0.4
	CCSD(T)	76.20	75.88	0.4
Sr^+	HF	121.66	121.33	0.3
	CCSD	95.40	94.31	1.2
	CCSD(T)	92.50	91.10	1.5
Ba^+	HF	168.89	174.64	3.3
	CCSD	127.92	129.92	1.5
	CCSD(T)	122.35	123.07	0.6
Ra^+	HF	144.62	145.47	0.6
	CCSD	112.03	110.48	1.4
	CCSD(T)	107.42	105.37	1.9

Table 8.5. The static dipole polarizabilities of the singly charged group 2 elements calculated by the present scalar relativistic pseudopotentials (ARPP). The pseudopotential results are compared with the present all-electron results at the Douglas-Kroll level [AE(DK)]. The signs are ignored in the percentage pseudopotential errors. All values are in a.u.

Considering that Sadlej's value agrees very well with the AE(DK) value of 174.64 a.u., it is clearly the ARPP that underestimates the dipole polarizability of Ba^+ at the HF level, by 3.3%. This underestimation of the dipole polarizability by ARPP is rather puzzling as it seems to exist only for the singly charged Ba^+ ion and not for its neutral or doubly charged counterparts. (see chapter 9) Moreover, the discrepancy becomes much smaller at the correlated level, pointing towards a error compensation. In fact, the agreement between the ARPP and AE(DK) method is excellent at the CCSD(T) level. It is likely that the deviation of the ARPP value at the HF level for Ba^+ is caused by an artifact in the pseudopotential itself. Nevertheless, the anomalous trend in dipole polarizabilities caused by relativistic effects is reproduced by the ARPP with the dipole polarizability of Ra^+ becoming smaller than that of Ba^+.

At the correlated level, the agreement between the ARPP and AE(DK) becomes slightly worse than at the HF level, except for Ba^+ as mentioned above. The pseudopotential error grows up to 2% for Sr^+ and Ra^+ at the CCSD(T) level, as the dipole polarizabilities are slightly overestimated by the ARPP method.

Patil and Tang [1] have calculated the dipole polarizabilities by using one-valence-electron pseudopotentials. They obtained very accurate values of dipole polarizabilities of the neutral group 1 elements in such a way. For the singly charged group 2 elements, however, their values tend to be underestimated. (70.54, 83.55, and 109.6 a.u. for Ca^+, Sr^+ and Ba^+, respectively) This underestimation grows larger with increasing nuclear charge and results in a discrepancy of 15 a.u. for Ba^+ from their earlier calculations [6] by matrix elements (see Table 8.3). They have concluded that due to the lack of the availability of other data it is difficult to determine which method gives more reliable results. It seems as though it is their earlier method of matrix elements that gives more reliable dipole polarizabilities than their one-valence-electron pseudopotentials, as the former is in much better agreement with the present dipole polarizabilities as well as those determined by Sadlej [5]. Further, Tang's pseudopotential calculations utilized input data of ionization potentials, which could well influence the accuracy of their dipole polarizabilities.

Overall, the present ARPPs performs reasonably well in evaluation of dipole polarizabilities. The agreement with the all-electron results is satisfactory.

8.4.2 Ionization Potentials

The ionization potentials calculated by the present ARPPs are presented in Table 8.6 and are compared with the all-electron values of this study at the DK level.

The ionization potentials calculated by the ARPPs agree well with AE(DK) for all ions. At the HF level, the ARPP tends to overestimate the ionization potential slightly, but by no more than 0.02 eV. Relativistic effects for Ra^+ is correctly estimated, which cause an increase in the ionization potential from that of Ba^+.

At the correlated level, the ARPP method tends to underestimate the ionization potentials for all ions except for Ca^+. The deviation of ARPP values from the AE(DK) is no more than 0.04 eV.

According to the relationship between ionization potentials and the dipole polarizabilities discussed in the previous sections, the higher the dipole polarizabilities, the smaller the ionization potentials. This means that if one method of calculation, for example, ARPP, overestimates the dipole polarizability

		ARPP	AE (DK)	% error
Ca^+	HF	11.37	11.35	0.2
	CCSD	11.83	11.82	0.1
	CCSD(T)	11.86	11.85	0.1
Sr^+	HF	10.44	10.44	0.0
	CCSD	10.94	10.97	0.2
	CCSD(T)	10.98	11.01	0.3
Ba^+	HF	9.37	9.36	0.1
	CCSD	9.90	9.93	0.3
	CCSD(T)	9.95	9.99	0.4
Ra^+	HF	9.43	9.42	0.2
	CCSD	10.01	10.04	0.2
	CCSD(T)	10.07	10.10	0.3

Table 8.6. The second ionization potentials of the singly charged group 2 elements calculated by the present scalar relativistic pseudopotentials (ARPP). The values are compared with the all-electron values of this study at the Douglas-Kroll [AE(DK)] level. The signs are ignored in the percentage pseudopotential errors. All values are in eV.

due to some artifacts within the ARPP itself, then it is likely that these artifacts will give rise to an underestimated ionization potential. In order to test this, the data in Table 8.5 and Table 8.6 are compared. (Ca^+ is left out from this discussion as the pseudopotential error associated with this ion is rather small for both the dipole polarizability and ionization potential)

For Sr^+, the overestimated dipole polarizability is reflected in the ionization potential which is underestimated by the ARPP. The same is true for Ra^+, indicating small but some inaccuracies in the ARPP. Surprisingly, such a relationship is not found for Ba^+, where there is an underestimation of both the dipole polarizability and ionization potential at the correlated level. It is therefore difficult to conclude for Ba^+ what causes the deviation of ARPP data for the dipole polarizability at the HF level. It is possible that the overestimated correlation effects for the dipole polarizability of Ba^+ cancel out the pseudopotential error at the HF level, hence yielding a better agreement at the correlated level.

Nevertheless, the accuracies shown by the present ARPP in evaluating the second ionization potentials of the singly charged group 2 elements are satisfactory.

References

[1] S. H. Patil and K.T. Tang, Chem. Phys. Lett. **295**, 152 (1998).

[2] T. Saue, J. K. Laerdahl, L. Visscher, and H. J. Aa. Jensen (unpublished).

[3] K. G. Dyall and K. Faegri Jr., Chem. Phys. Lett. **174**, 25 (1990).

[4] L. Visscher and K. G. Dyall, At. Data. Nucl. Data Tables **67**, 207 (1997).

[5] I. Miadokova, V. Kello, and A. J. Sadlej, Theor. Chem. Acc. **96**, 166 (1997).

[6] S. H. Patil and K. T. Tang, J. Chem. Phys. **106**, 2298 (1997).

[7] E. Eliav and U. Kaldor, Phys. Rev. A **53**, 3050 (1996).

[8] J. Sugar and C. Corliss, J. Phys. Chem. Ref. Data **14**, Suppl. 2 (1985).

[9] C. E. Moore, *Atomic Energy Levels,* Natl. Bur. Stand. (U.S.) Circ. 467, Vol. II (1952); reprinted as Natl. Stand. Ref. Data Ser., Natl. Bur. Stand. (U.S.) **35** (1971); C. E. Moore, *Atomic Energy Levels,* Natl. Bur. Stand. (U.S.) Circ. 467. Vol. III (1958); reprinted as Natl. Stand. Ref. Data Ser., Natl. Bur. Stand. (U.S.) **35** (1971).

[10] H. Karlsson and U. Litzén, Phys. Scr. **60**, 321 (1999); S. G. Schmelling and G. O. Brink, Phys. Rev. A **12**, 2498 (1975); H. P. Palenius, Phys. Lett. **56A**, 451 (1976); J. R. Rubbmark, S. A. Borgstrom, and K. Bockasten, J. Phys. B **10**, 1803 (1977).

Chapter 9
THE DOUBLY CHARGED GROUP 2 ELEMENTS

In the previous two chapters, the dipole polarizabilities and the ionization potentials of the neutral and singly charged group 2 elements were presented and discussed. The discussion is continued in this chapter to the doubly charged group 2 ions. These ions are slightly different from their neutral and singly charged counterparts in that the valence *ns* electrons are no longer present and it is the $(n\text{-}1)p$ orbitals that contribute mostly to the dipole polarizability. Experiences from the singly charged group 1 elements with the same $(n\text{-}1)s^2p^6$ valence configuration predict certain aspects of electron correlation and relativistic effects in the dipole polarizability of these doubly charged ions. That is, electron correlation effects are predicted to be small in magnitude, though important for a precise dipole polarizability. The direct stabilization of the valence *s* orbital by relativity, which caused an anomalous trend in the dipole polarizability of M and M^+ (M = alkaline-earth elements), is absent and spin-orbit (SO) effects are expected to play a more important role.

As noted by Coker [1], free-ion polarizabilities are not susceptible to direct experimental measurements. However, his dipole polarizability data, based on empirical correlation of crystal polarizabilities, are referred to as experimental values by many authors. There are other sets of dipole polarizabilities available for the doubly charged group 2 elements, in particular, the density functional study of Harbola [2] and purely *ab-initio* study of Sadlej *et al.* [3].

In this chapter, precise values of dipole polarizabilities of the doubly charged group 2 elements are given, followed by a discussion on electron correlation and relativistic effects. The present pseudopotentials for the group 2 elements are tested for dipole polarizabilities.

9.1 Basis Set

The basis set exponents for the doubly charged group 2 elements were taken from the basis sets for the neutral group 2 elements, details of which are presented in chapter 7. The basis sets chosen for the doubly charged ions are as follows: no changes made for Ca^{2+} and Sr^{2+}, (25*s*21*p*16*d*8*f*5*g*)/[16*s*15*p*12*d*8*f*5*g*] for both the nonrelativistic (NR) and relativistic Douglas-Kroll (DK) calculations of Ba^{2+}, (31*s*24*p*20*d*12*f*8*g*)/[19*s*16*p*15*d*9*f*8*g*] and (31*s*24*p*20*d*12*f*8*g*)/[18*s*15*p*14*d*9*f*8*g*] for the NR and DK calculations of Ra^{2+}, respectively. A slightly heavier contraction was used for the relativistic Ra^{2+} calculations to improve on linear dependencies.

For the spin-orbit calculations, basis sets which include basis functions up to l = 3 only (i.e. *f*-type functions) were used as the computational demand was very high. These basis sets were totally decontracted. For comparisons, the DK calculations were performed with the same totally decontracted basis sets. The large component exponents were taken from the DK basis sets whereas the small component exponents were generated from the large components by a linear transformation and a projection [4] equivalent to the kinetic balance conditions [5] as before. A Gaussian nuclear charge distribution with nuclear exponents as given by Visscher and Dyall [6] was used.

All NR and DK calculations were performed with the MOLCAS 5.2/5.4 program package [7]. All four-component calculations were performed with the DIRAC program package [8].

9.1.1 Basis Set Effects

The static dipole polarizabilities of the doubly charged group 2 elements resulting from various basis sets are presented in Table 9.1. The values are shown to three decimal places to make small changes more transparent. The basis sets labeled *l** (l = maximum angular momentum function) contains, as before, one extra high and one extra diffuse function than the basis sets labeled *l* in Table 9.1.

For Ca^{2+}, set *d* contains enough functions, as set *d** shows no significant difference in the dipole polarizability both at the nonrelativistic and relativistic level. That is, the dipole polarizabilities are converged within 0.005 a.u. and 0.007 a.u. at the HF and the MP2 level, respectively. A comparison

		Nonrelativistic			Relativistic Douglas-Kroll		
		Basis set	HF	MP2	Basis set	HF	MP2
Ca^{2+}	*d*	(20*s*15*p*8*d*)	3.255	3.221	(20*s*15*p*8*d*)	3.248	3.216
	*d**	(22*s*17*p*10*d*)	3.260	3.215	(22*s*17*p*10*d*)	3.253	3.208
	f	(20*s*15*p*8*d*5*f*)	3.255	3.260	(20*s*15*p*8*d*5*f*)	3.248	3.260
	*f**	(22*s*17*p*10*d*7*f*)	3.253	3.254	(22*s*17*p*10*d*7*f*)	3.253	3.254
Sr^{2+}	*uncntr*	(21*s*16*p*11*d*9*f*)	5.866	5.845	(21*s*16*p*11*d*9*f*)	5.790	5.768
	f	(21*s*16*p*11*d*9*f*)/ [15*s*12*p*10*d*9*f*]	5.866	5.847	(21*s*16*p*11*d*9*f*)/ [15*s*12*p*10*d*9*f*]	5.790	5.768
	*f**	(23*s*18*p*13*d*11*f*)/ [17*s*14*p*12*d*11*f*]	5.868	5.845	(23*s*18*p*13*d*11*f*)/ [17*s*14*p*12*d*11*f*]	5.791	5.770
	g	(21*s*16*p*11*d*9*f*3*g*)/ [15*s*12*p*10*d*9*f*3*g*]	5.866	5.841	(21*s*16*p*11*d*9*f*3*g*)/ [15*s*12*p*10*d*9*f*3*g*]	5.790	5.761

Table 9.1. The calculated static dipole polarizabilities of the doubly charged group 2 elements from Ca^{2+} to Ra^{2+}. All values are in a.u. Continued on the following page.

Ba^{2+}	*uncntr*	(25*s*21*p*16*d*8*f*)	10.913	10.788	(25*s*21*p*16*d*8*f*)	10.559	10.475
	f	(25*s*21*p*16*d*8*f*)/ [16*s*15*p*12*d*8*f*]	10.913	10.788	(25*s*21*p*16*d*8*f*)/ [16*s*15*p*12*d*8*f*]	10.559	10.475
	*f**	(27*s*23*p*18*d*10*f*)/ [18*s*17*p*14*d*10*f*]	10.914	10.787	(27*s*23*p*18*d*10*f*)/ [18*s*17*p*14*d*10*f*]	10.559	10.477
	g	(27*s*23*p*18*d*10*f*5*g*)/ [16*s*15*p*12*d*8*f*5*g*]	10.913	10.764	(25*s*21*p*16*d*8*f*5*g*)/ [16*s*15*p*12*d*8*f*5*g*]	10.559	10.449
	g*	(25*s*21*p*16*d*8*f*7*g*)/ [18*s*17*p*14*d*10*f*7*g*]	10.913	10.762	(27*s*23*p*18*d*10*f*7*g*)/ [18*s*17*p*14*d*10*f*7*g*]	10.559	10.447
Ra^{2+}	*uncntr*	(31*s*24*p*20*d*12*f*)	14.628	14.480	(31*s*24*p*20*d*12*f*)	13.360	13.381
	f	(31*s*24*p*20*d*12*f*)/ [19*s*16*p*15*d*9*f*]	14.628	14.480	(31*s*24*p*20*d*12*f*)/ [18*s*15*p*14*d*9*f*]	13.360	13.379
	*f**	(33*s*26*p*22*d*14*f*)/ [21*s*18*p*17*d*11*f*]	14.628	14.487	(33*s*26*p*22*d*14*f*)/ [20*s*17*p*16*d*11*f*]	13.360	13.379
	g	(31*s*24*p*20*d*12*f*8*g*)/ [19*s*16*p*15*d*9*f*8*g*]	14.628	14.410	(31*s*24*p*20*d*12*f*8*g*)/ [18*s*15*p*14*d*9*f*8*g*]	13.360	13.314
	*g**	(33*s*26*p*22*d*14*f*10*g*)/ [21*s*18*p*17*d*11*f*10*g*]	14.628	14.403	(33*s*26*p*22*d*14*f*10*g*)/ [20*s*17*p*16*d*11*f*10*g*]	13.360	13.308

Table 9.1. Continued form the previous page.

between set *d* and set *f* in Table 9.1 reveals that the dipole polarizability is slightly increased upon addition of *f*-type functions at the correlated level. More precisely, the increase in the dipole polarizability amounts to 0.039 and 0.045 a.u. at the nonrelativistic and relativistic MP2 level, respectively. This contribution by the *f*-type functions is an order of magnitude larger than the basis set convergence within set *d*'s and is, therefore, considered to be important. A further augmentation of set *f* to set *f** shows no significant change in the dipole polarizabilities, indicating that set *f* bears a converged value for the dipole polarizability. The basis set convergence, therefore, remains below 0.01 a.u. for Ca^{2+} and the final basis set is chosen to be set *f*.

For Sr^{2+}, there is no significant change in the dipole polarizability following the basis set contraction. Upon the extension of set *f* to set *f**, the dipole polarizability remains unchanged at both the nonrelativistic and relativistic level. This confirms that the dipole polarizability of Sr^{2+} is converged with respect to the basis functions up to $l = 3$. The influence of *g*-type functions was considered by comparing the dipole polarizability of set *f* and set *g*. As shown in Table 9.1, the dipole polarizability is unaffected by the inclusion of *g*-type functions within 0.007 a.u. The basis set convergence remains well below 0.01 a.u. The final basis set for Sr^{2+} was chosen as set *f*.

For Ba^{2+} and Ra^{2+}, the results from the totally uncontracted basis sets and set *f* confirm that the dipole polarizabilities are virtually independent of the basis set contraction scheme. As was the case for Sr^{2+}, the dipole polarizability is converged within set *f* for these elements at all levels of theory as the more extensive set *f** shows no significant change. The influence of *g*-type functions is evident as the dipole polarizability is decreased by about 0.025 and 0.07 a.u. for respective Ba^{2+} and Ra^{2+} at the correlated level. As expected, the influence of *g*-type functions is more important for Ra^{2+} due to the occupied *f* orbitals. The dipole polarizability is converged, within the *g* sub-set (*g vs. g**) to 0.002 and 0.007 a.u. for Ba^{2+} and Ra^{2+}, respectively. The final basis sets for these elements are the corresponding sets *g*.

The influence of *h*-type functions was tested for Ra^{2+} at the DKMP2 level, by adding six *h*-type functions to set *g* in Table 9.1. The resulting dipole polarizability of 13.29 a.u. is virtually identical to that of set *g*. Therefore, *h*-type functions were ignored in the subsequent CCSD/CCSD(T) calculations.

		Ca^{2+}	Sr^{2+}	Ba^{2+}	Ra^{2+}
NR	Basis set	(20*s*15*p*8*d*5*f*)	(21*s*16*p*11*d*9*f*)/ [15*s*12*p*10*d*9*f*]	(25*s*21*p*16*d*8*f*5*g*)/ [16*s*15*p*12*d*8*f*5*g*]	(31*s*24*p*20*d*12*f*8*g*)/ [19*s*16*p*15*d*9*f*8*g*]
	HF	3.248	5.866	10.913	14.628
	MP2	3.260	5.847	10.764	14.410
	CCSD	3.259	5.859	10.797	14.471
	CCSD(T)	3.262	5.864	10.812	14.496
DK	Basis set	(20*s*15*p*8*d*5*f*)	(21*s*16*p*11*d*9*f*)/ [15*s*12*p*10*d*9*f*]	(25*s*21*p*16*d*8*f*5*g*)/ [16*s*15*p*12*d*8*f*5*g*]	(31*s*24*p*20*d*12*f*8*g*)/ [18*s*15*p*14*d*9*f*8*g*]
	HF	3.248	5.790	10.559	13.360
	MP2	3.260	5.768	10.449	13.314
	CCSD	3.259	5.787	10.474	13.328
	CCSD(T)	3.262	5.792	10.491	13.361
DC	Basis set	(20*s*15*p*8*d*5*f*)	(21*s*16*p*11*d*9*f*)	(25*s*21*p*16*d*8*f*)	(31*s*24*p*20*d*12*f*)
	HF	3.248	5.795	10.603	13.809
	MP2	3.256	5.780	10.516	13.779

Table 9.2. The calculated static dipole polarizabilities of the doubly charged group 2 elements at the nonrelativistic, scalar relativistic Douglas-Kroll, and fully relativistic four-component Dirac-Coulomb level. For the uncontracted DK results, see Table 9.1. All values are in a.u.

9.2 Static Dipole Polarizabilities

The static dipole polarizabilities of the doubly charged group 2 elements from Ca^{2+} to Ra^{2+} are presented in Table 9.2.

9.2.1 Nonrelativistic Results

The nonrelativistic results show that the dipole polarizability increases monotonically from Ca^{2+} to Ra^{2+} at both the HF and correlated levels. The magnitudes of the dipole polarizability are much smaller than those for the neutral or singly charged group 2 elements with the removal of all the valence *ns* electrons.

The electron correlation contribution at the nonrelativistic level is depicted in Figure 9.1. As shown, the electron correlation contribution to the dipole polarizability is negative, reducing the dipole polarizabilities from the HF values

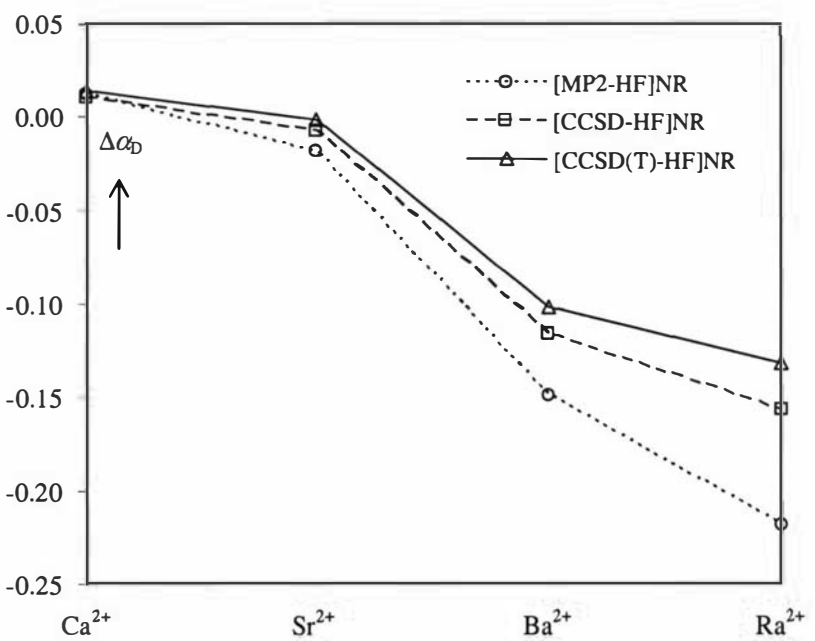

Figure 9.1. Electron correlation contributions to the dipole polarizabilities of the doubly charged group 2 elements at the nonrelativistic level. All values are in a.u.

for all ions, except for Ca^{2+}. For Ca^{2+}, there is an increase in the dipole polarizability. It is interesting to note that Sadlej's results [3] also show a positive correlation contribution to the dipole polarizability of Be^{2+} and Mg^{2+} as well as Ca^{2+}. This sign change in the correlation contribution was also noted in the singly charged group 1 elements in chapter 6, which have the same $(n\text{-}1)s^2p^6$ valence electron configuration. (see Figure 6.3)

As expected, electron correlation effects grow with increasing nuclear charge. Due to the well-known slow convergence of the MP expansion, electron correlation is overestimated at the MP2 level by as much as 65% compared with the CCSD(T) results for Ra^{2+}. The importance of the perturbative triples is evident as the CCSD method overestimates correlation effects compared with the CCSD(T) method.

Overall, the doubly charged group 2 elements show much smaller electron correlation effects than the neutral or singly charged group 2 elements. For example, correlation effects account for only 1% of the dipole polarizability of Ra^{2+} at the nonrelativistic CCSD(T) level. The small effect of electron correlation is attributed to the larger HOMO-LUMO gap for the doubly charged group 2 ions than in the neutral or singly charged cases. A similar effect was noted for the singly charged group 1 elements which share the same $(n\text{-}1)s^2p^6$ valence electron configuration.

9.2.2 Scalar Relativistic Results

A first look at the scalar relativistic results in Table 9.2 reveals that the dipole polarizabilities increase monotonically from Ca^{2+} to Ra^{2+} at both the HF and correlated levels. This is contrary to the case of the neutral atoms or the singly charged ions, where a relativistic contraction of the valence *ns* orbital leads to an anomalous trend in the dipole polarizabilities. Once again, this is attributed to the absence of the valence *ns* electrons.

Scalar relativistic effects and SO coupling effects at the HF level are depicted in Figure 9.2, together with electron correlation effects estimated at the nonrelativistic CCSD(T) level for comparison.

It is easy to see that for Ca^{2+} scalar relativistic effects are very small. For Sr^{2+}, scalar relativistic effects grow and act to reduce the dipole polarizability due to the overall relativistic contraction of the $(n\text{-}1)p$ shell. Although the scalar relativistic contribution to the dipole polarizability of Sr^{2+} is small, it dominates

over the electron correlation contribution by more than an order of magnitude and therefore cannot be ignored.

For Ba^{2+} and Ra^{2+}, scalar relativistic effects become increasingly more significant and account for up to 9% of the dipole polarizability at the HF level. This is relatively small, however, in comparison with the scalar relativistic contributions for the neutral and singly charged group 2 elements. This is due to a relatively small contraction of the spin-orbit averaged $(n\text{-}1)p$ shell compared to that of the ns shell by relativity. Such small relativistic effects do not cause any anomaly in the dipole polarizability trend. A monotonically increasing scalar relativistic dipole polarizability from Ca^{2+} to Ra^{2+} is in line with the trend in the dipole polarizability of the singly charged group 1 elements at the scalar relativistic level.

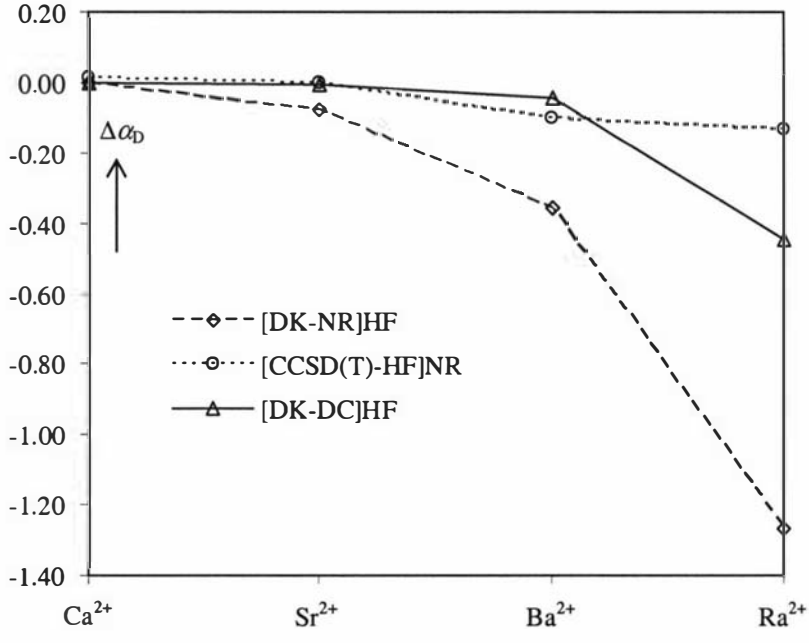

Figure 9.2. Scalar relativistic and SO coupling effects in the dipole polarizability of the doubly charged group 2 elements from Ca^{2+} to Ra^{2+}. Electron correlation effects at the nonrelativistic CCSD(T) level are also plotted. Note that spin-orbit effects are taken as $\alpha_D^{DK} - \alpha_D^{DC}$ at the HF level for better comparison with other results. All values are in a.u.

9.2.3 Fully Relativistic Results

The results in Table 9.2 and Figure 9.2 highlight the spin-orbit (SO) coupling contribution to the dipole polarizability of the doubly charged group 2 elements. Note that the DCHF and DCMP2 calculations were performed with the (totally decontracted) basis sets which contain only up to $l = 3$ only, (i.e. the *f*-type functions) for reasons of computational savings. Therefore, the SO contribution is estimated by comparing the dipole polarizabilities resulting from the basis set denoted *uncntr* in Table 9.1.

SO coupling effects are negligible for Ca^{2+} and also for Sr^{2+}, though present. SO effects for Ba^{2+} are more visible, where an increase in the dipole polarizability is observed from the spin-free DK scheme. The effects are small and it is still electron correlation effects that dominate over SO coupling effects. (See Figure 9.2) The SO coupling contribution is, however, almost twice as large as the basis set effects of *g*-type functions discussed in section 9.1.1 and is, therefore, considered important in an accurate determination of the dipole polarizability.

For Ra^{2+}, SO coupling effects grow by an order of magnitude from Ba^{2+} and finally start to dominate over electron correlation effects. The largest contribution to the dipole polarizability, however, still comes from scalar relativistic effects, which dominate over the SO and correlation contributions.

As shown in Table 9.2 and Figure 9.2, the SO contribution to the dipole polarizability is positive, leading to an increase in the dipole polarizability from the spin-free DK counterpart. (Note that the SO contribution is meant as $\alpha_D^{DC} - \alpha_D^{DK}$. Figure 9.2 shows values of $\alpha_D^{DK} - \alpha_D^{DC}$, which is negative, for better comparison with other results on the plot.) The positive contribution of the SO effects to the dipole polarizability is attributed to the fine structure splitting of the valence *p* orbital. As mentioned before, the $p_{3/2}$ shell experiences an increased screening from the nucleus by the relativistically contracted *s* and $p_{1/2}$ orbitals. This explains the increase in the dipole polarizability at the fully relativistic four-component DCHF and DCMP2 levels from the spin-free DK counterparts. As expected, SO coupling effects are greatest for the heaviest ion and the fully relativistic DCHF and DCMP2 results for Ra^{2+} clearly demonstrate the importance of such effects.

9.2.4 Electron Correlation at the Relativistic Level

It is mentioned earlier that relativistic and correlation effects are not additive. In order to show the effects of electron correlation at the relativistic level, the difference in the dipole polarizability resulting from the uncorrelated DKHF and correlated calculations at various levels of theory is depicted in Figure 9.3.

Correlation effects at the scalar relativistic level show a clear difference from those at the nonrelativistic level shown in Figure 9.1. At the nonrelativistic level, the electron correlation contribution to the dipole polarizability shows a monotonic increase with increasing nuclear charge. At the relativistic level, however, the correlation contribution increases only up to Ba^{2+} and then decreases for Ra^{2+}. Furthermore, the electron correlation contribution to the dipole polarizability is negative up to Ba^{2+}. However, a sudden change in the trend of electron correlation effects results in a much less negative contribution for Ra^{2+} than for Ba^{2+}. In fact, the correlation contribution for Ra^{2+} is slightly positive at the DKCCSD(T) level, leading to an increase in the dipole

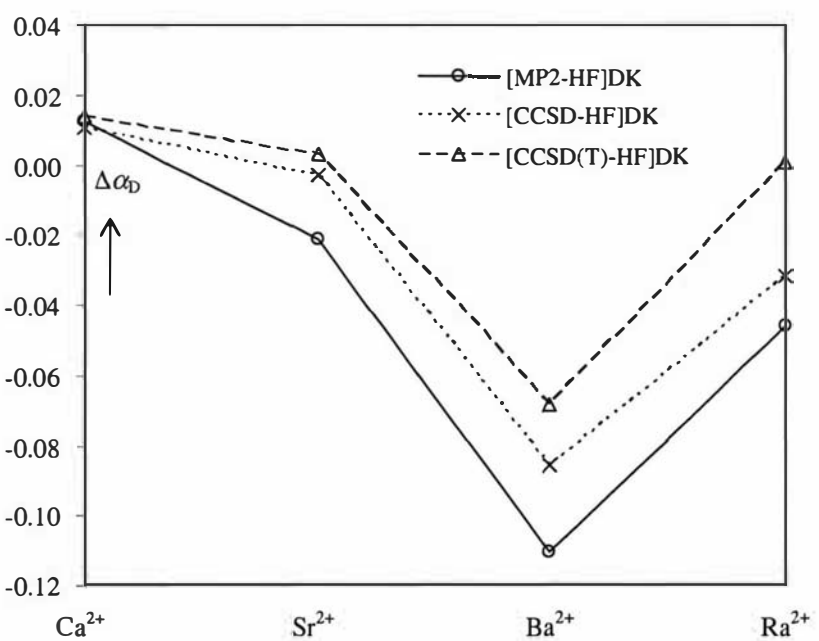

Figure 9.3. The electron correlation contribution to the dipole polarizability of the doubly charged group 2 elements at the MP2, CCSD, and CCSD(T) levels within the scalar relativistic DK level of theory. All values are in a.u.

polarizability. Interestingly, the biggest 'jump' in relativistic effects (estimated at the DKHF level) is observed from Ba^{2+} to Ra^{2+}, which coincides with the change in the behavior of correlation effects for these ions. A similar behavior in electron correlation at the relativistic level has been reported for the (n-1) valence system of the singly charged group 1 elements in chapter 6. That is, at the relativistic level, the electron correlation contribution is monotonic and becomes more negative up to Cs^+ and then it reverses to a positive contribution for Fr^+.

It is interesting to note such an anomaly in the electron correlation contribution caused by relativity as the situation only arises with a complete removal of the valence *ns* shell such as in the dipole polarizability of the respective singly and doubly charged group 1 and 2 ions. It is certainly related to the large relativistic change from the fifth-row element to the sixth-row element (Cs^+ to Fr^+ for group 1 and Ba^{2+} to Ra^{2+} for group 2) and clearly demonstrates the non-additivity of electron correlation and relativistic effects.

9.2.5 Recommended Values and Comparison with other Values

The recommended static dipole polarizabilities of the doubly charged group 2 elements are estimated by adding the SO contribution at the DCMP2 level to the DKCCSD(T) values of the dipole polarizability. The recommended values are presented and compared with other theoretical values in Table 9.3.

The recommended dipole polarizabilities show an excellent agreement with the numerical values of Mahan [9]. This gives confidence for the dipole polarizability of Ra^{2+}. The dipole polarizabilities of Sadlej *et al.* [3] tend to be underestimated. Their study, however, neglects SO coupling effects and was primarily focused on devising standardized basis sets for molecular application rather than on the accuracy of the dipole polarizability. The estimated (experimental) values in Table 9.3 depend on the crystalline environment as mentioned earlier in this chapter.

	Method	Ca^{2+}	Sr^{2+}	Ba^{2+}	Ra^{2+}
Recomm.	DK(CCSDT)+SO	3.258	5.804	10.532	13.735
Theor. [9]	[a]Sternheimer eq.	3.307	5.871	10.528	-
Theor. [3]	DKCCSD(T)	3.05	5.52	9.97	-
Est. [1, 10]		3.523	5.669	11.675	-

[a]Numerical results obtained from the modified Sternheimer equation to account for self-consistent field.

Table 9.3. Recommended dipole polarizabilities of the doubly charged group 2 elements. The values are compared to other theoretical and estimated experimental values. All values are in a.u.

9.3 Pseudopotential Results

The static dipole polarizabilities of the doubly charged group 2 elements are calculated using the scalar relativistic pseudopotentials described in chapter 4. The resulting dipole polarizabilities are presented and compared with all-electron results of this study in Table 9.4.

9.3.1 Static Dipole Polarizabilities

The ARPP results at the HF level show a good agreement with the AE(DK) HF results. This indicates that scalar relativistic effects are correctly described by the ARPPs.

The largest deviation between the ARPP and the AE(DK) method is observed for Ca^{2+}. When a different set of pseudopotential parameters was used, namely the relativistic 10-valence-electron Stuttgart pseudopotentials [11], the calculated dipole polarizabilities were 3.164 a.u. and 3.171 a.u. at the respective HF and CCSD(T) level. In other words, the agreement becomes even worse. It is not easy to say where this deviation comes from but one possible explanation could be the nodeless structure of the pseudoorbitals. The unoccupied *d* orbitals in Ca^{2+} may offer another explanation for this deviation, which causes a convergence problem in the pseudopotential fitting procedure. (Note also that the pseudopotential error for K was larger than that for Rb, for example, with K

		ARPP	AE (DK)	% error
Ca^{2+}	HF	3.198	3.248	1.5
	CCSD	3.210	3.259	1.5
	CCSD(T)	3.214	3.262	1.5
Sr^{2+}	HF	5.776	5.790	0.2
	CCSD	5.783	5.787	0.1
	CCSD(T)	5.787	5.792	0.1
Ba^{2+}	HF	10.582	10.559	0.2
	CCSD	10.525	10.474	0.5
	CCSD(T)	10.528	10.491	0.4
Ra^{2+}	HF	13.362	13.360	0.0
	CCSD	13.354	13.328	0.2
	CCSD(T)	13.374	13.361	0.1

Table 9.4. The static dipole polarizabilities of the doubly charged group 2 elements obtained from scalar relativistic pseudopotentials (ARPP). The pseudopotential results are compared with the all-electron results at the Douglas-Kroll level [AE(DK)]. Note that the signs are ignored in the relative pseudopotential errors. All values are in a.u.

being the first element of the group with the unoccupied *d* orbital. See chapter 5.) For all other ions, the pseudopotential error remains below 1%. A slightly larger pseudopotential error associated with Ca^{2+} seems to be consistent with the case of the neutral Ca atom, where the pseudopotential error for Ca lies on the high side, close to 1%. For Ca^{2+} and Sr^{2+}, the ARPP underestimates the dipole polarizabilities compared with the AE(DK) results. This trend is reversed for the heavier ions, where the dipole polarizabilities are overestimated for Ba^{2+} and Ra^{2+}.

As discussed in section 9.2.1, electron correlation effects in dipole polarizabilities of the doubly charged group 2 elements are small. In fact, they are too small to be directly compared across different methods of calculation. Moreover, the present ARPP dipole polarizabilities already incorporate relativistic effects, which further hampers direct comparisons of correlation effects. Therefore, the adequacy of the present ARPP in estimating correlation

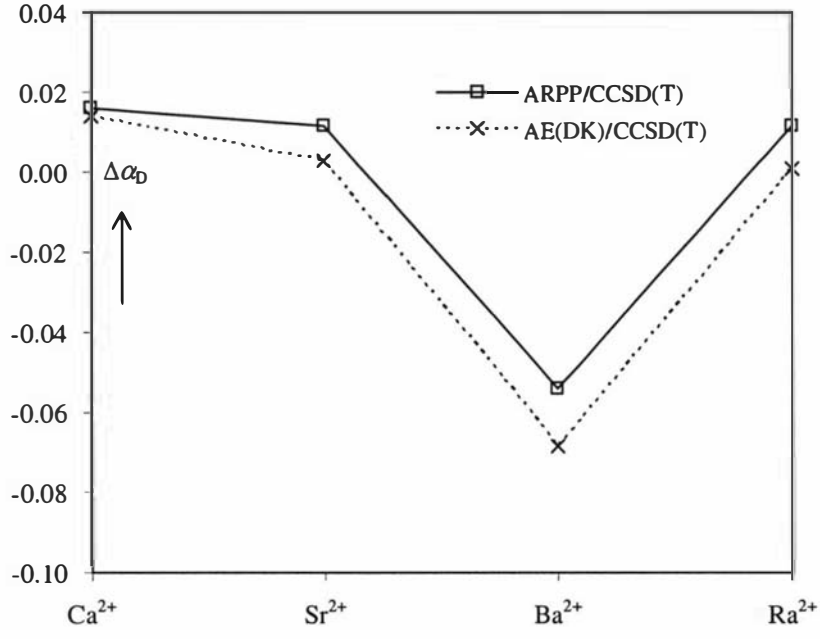

Figure 9.4. A plot of electron correlation contribution to the dipole polarizabilities at the CCSD(T) level ($\alpha_D^{CCSD(T)}$ - α_D^{HF}), estimated by the ARPP and AE(DK) methods. All values are in a.u.

effects is viewed by comparing the correlation contribution to the dipole polarizability within a given method of choice rather than the actual values of the dipole polarizability at the correlated level. This is done in a graphical representation similar to that of Figure 9.3, which depicts the electron correlation contribution to the dipole polarizability as ($\alpha_D^{correlated}$ - α_D^{HF}). If the ARPPs accurately describe electron correlation effects then ($\alpha_D^{correlated}$ - α_D^{HF}) of the ARPP method should follow the trend in the all-electron method at the DK level. This is shown in Figure 9.4.

As can be seen, the earlier mentioned anomalous trend in correlation effects due to relativity is correctly reproduced by the present ARPP. For all ions, the correlation contribution estimated by the ARPP is more positive than that by the AE(DK). This deviation is, however, small enough to retain the correct sign in $\alpha_D^{CCSD(T)}$ - α_D^{HF}, i.e. positive for ions Ca^{2+}, Sr^{2+} and Ra^{2+} and negative for Ba^{2+}. Nevertheless, Figure 9.4 is indicative of overestimated correlation effects by the ARPP in the case of positive correlation contributions (Ca^{2+}, Sr^{2+}, and Ra^{2+}) and

of underestimated correlation effects in the case of a negative correlation contribution (Ba^{2+}) at the CCSD(T) level.

Overall, the dipole polarizabilities at the CCSD(T) level, estimated by the present ARPP is accurate within 1% of the all-electron values at the DKCCSD(T) level as reported in Table 9.4, with the exception of Ca^{2+}.

References

[1] H. Coker, J. Phys. Chem. **80**, 2078 (1976).

[2] M. Harbola, Phys. Rev. A, **48**, 2696 (1992).

[3] I. Miadokova, V. Kellö, and A. J. Sadlej, Theor. Chem. Acc. **96**, 166 (1997).

[4] T. Saue, J. K. Laerdahl, L. Visscher, and H. J. Aa. Jensen (unpublished).

[5] K. G. Dyall and K. Faegri Jr., Chem. Phys. Lett. **174**, 25 (1990).

[6] L. Visscher and K. G. Dyall, At. Data. Nucl. Data Tables **67**, 207 (1997).

[7] *MOLCAS* Version 5.4, K. Andersson, M. Barysz, A. Bernhardsson, M. R. A. Blomberg, D. L. Cooper, M. P. Fülscher, C. de Graaf, B. A. Hess, G. Karlström, R. Lindh, P.-Å. Malmqvist, T. Nakajima, P. Neogrády, J. Olsen, B. O. Roos, B. Schimmelpfennig, M. Schütz, L. Seijo, L. Serrano-Andrés, P. E. M. Siegbahn, J. Stålring, T. Thorsteinsson, V. Veryazov, and P.-O. Widmark, Lund University, Sweden (2002).

[8] T. Saue, T. Enevoldsen, T. Helgaker, H. J. Aa. Jensen, J. K. Laerdahl, K. Ruud, J. Thyssen, and L. Vvisscher, *Dirac, a relativistic ab initio electronic structure program*, Release 3.1 (1988) (Odense University, Denmark); see also: http://dirac.chem.sdu.dk; T. Saue, K. Faegri, Jr.,T. Helgaker, and O. Gropen, Mol. Phys. **91**, 937 (1997); J. K. Laerdahl, T. Saue, and K. Faegri Jr., Theor. Chem. Acc. **97**, 177 (1997).

[9] G. D. Mahan, Phys. Rev. A **22**, 1780 (1980).

[10] R. R. Teachout and R. T. Pack, At. Data **3**, 195 (1971).

[11] M. Kaupp, P. v. R. Schleyer, H. Stoll, and H. Preuss, J. Chem. Phys. **94**, 1360 (1991).

Chapter 10
GROUND-STATE PROPERTIES AND STATIC DIPOLE POLARIZABILITIES OF THE ALKALI DIMERS

The simulation of metallic clusters is one of the main challenges in quantum chemistry today. In particular, all alkali-metals are known to form dimers [1-3]. These alkali dimers have been documented for a few decades. The rather weak metal-metal bond results from the overlap of the diffuse valence *ns* orbitals, especially for the heavier elements. Consequently, many attempts have been made to treat the atomic core as a closed shell system and reduce the valence contribution to one *ns* electron for each atom by employing pseudopotential methods. Pseudopotential methods are, however, associated with significant errors for systems with easily polarizable cores [4-10]. For example, one-valence-electron pseudopotentials derived from HF calculations lead to larger bond lengths (e.g. for K_2, R_e = 4.13 Å with a full CI treatment for valence correlation, compared with 3.92 Å by experiment). As the atomic ion core becomes increasingly more polarizable with increasing nuclear charge, core-valence correlation and core-polarization contribution cannot be neglected anymore [11] (See Figure 10.1). In fact, studies show that molecular properties of alkali dimers are significantly affected by core-valence correlation [12, 13].

The importance of core-valence correlation has been long recognized by Bottcher and Dalgarno [14] and has been demonstrated via an all-electron calculation of LiNa by Rosmus and Meyer [13]. In order to compute core-valence interactions, Jeung *et al.* developed a second order perturbative treatment within the effective core potential framework [15, 16]. This was, however, not fully satisfactory, attributed to the basis set dependent treatment of core-valence

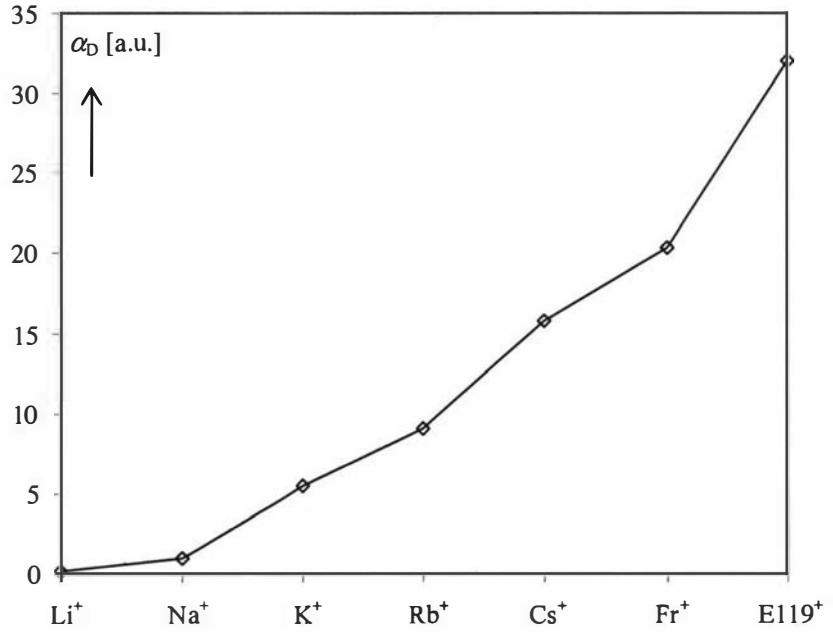

Figure 10.1. The dipole polarizabilities of the atomic core, M^+ where M = Li to E119. All values are in a.u.

correlation. Müller *et al.* [17, 26] employed a different approach by adding a semiempirical core polarization potential (CPP) to the valence Hamiltonian, restricted to the static dipole polarizability of the core.

As for all-electron methods, calculations which include core-valence correlation effects typically involve large basis sets and are thus very demanding in computational efforts. Further, the accuracy of such calculations is generally limited by the basis set incompleteness [7, 18].

As usual, the main attention on alkali dimers has been focused on the energetic aspects of these molecules such as spectroscopic constants. Electric properties such as dipole polarizabilities have also been investigated both in experimental and theoretical studies. In particular, the Fr dimer is of interest as the effects of core polarization and relativity in molecular bonding become more important.

In this chapter, the spectroscopic constants and the static dipole polarizabilities of alkali dimers from K_2 to Fr_2 determined by the use of the present small-core scalar relativistic pseudopotentials are presented. This addresses not only the accuracy and the transferability of the present

pseudopotentials but also the adequacy of the pseudopotentials without the use of a core polarization potential for the remaining small core.

10.1 Alkali Dimers

Selective spectroscopic constants of alkali dimers are presented in Tables 10.1 to 10.3. The methods of calculation are as follows: The results were obtained by the use of the relativistic nine-valence-electron pseudopotentials of this study with valence correlation treated at the CCSD(T) level. All nine electrons outside the core were correlated. Patil's results were all-electron values which include core-valence correlation and valence CISD treatment. (CISD, configuration interaction with single and double excitation. In this case, excitation was out of the same space, i.e. *ns*, *np*, and the $(n+1)s$ orbitals.) All the other results were obtained by the use of relativistic one-valence-electron pseudopotentials. In these cases, electron correlation effects were considered for the core-valence as well as the valence only part by the use of core polarization potentials for the former and by CISD for the latter. Only the present calculations omit core-valence correlation. For the bond lengths and dissociation energies, the present values are shown to three decimal places. For some of the other values quoted in the tables, no more than two significant figures were available. Whenever possible, three decimal places were used for these quantities.

10.1.1 Spectroscopic Constants

The calculated bond lengths, R_e from K_2 to Fr_2 are presented and compared with other theoretical and experimental values in Table 10.1.

As shown, the bond length increases from K_2 to Cs_2 as the valence *ns* orbital becomes more diffuse. This is expected as the size of the atom increases from K to Cs. An interesting feature is the bond distance of Fr_2, where the upward trend in the bond distance is no longer continued. In fact, for Fr_2 there is a decrease in the bond distance compared with Cs_2. This decrease in the bond distance is consistent with the decreasing atomic radius from Cs to Fr due to the relativistic stabilization of the valence *ns* orbital of Fr. The shorter bond distance of Fr_2 in comparison with that of Cs_2 has not been reported before.

	K_2	Rb_2	Cs_2	Fr_2
This work	3.920	4.184	4.641	4.593
Stoll [23]	3.91	4.19	4.61	-
Daudey [19]	-	4.18	4.58	-
Krauss [11]	3.94	4.16	4.63	-
Patridge [24]	3.91	4.35	4.97	-
Expt.[20-22]	3.924	4.18	4.646	-

Table 10.1. The calculated equilibrium bond lengths, R_e of the alkali dimers at the CCSD(T) level. The values are compared with other theoretical and experimental values. For the methods used, see text. All values are in Å.

	K_2	Rb_2	Cs_2	Fr_2
This work	0.537	0.469	0.428	0.433
Stoll [23]	0.53	0.48	0.43	-
Daudey [19]	-	0.49	0.46	-
Krauss [11]	0.529	0.50	0.44	-
Expt. [20-22]	0.520	0.485	0.452	-

Table 10.2. The calculated dissociation energies, D_e of the alkali dimers. The values are compared with other theoretical and experimental values. For the methods used, see text. All values are in eV.

	K_2	Rb_2	Cs_2	Fr_2
This work	92.3	58.3	42.4	33.5
Stoll [23]	92	57	42	-
Daudey [19]	-	58	44	-
Krauss [11]	88.4	59.2	41.0	-
Expt. [20-22]	92.0	57.8	42.0	-

Table 10.3. The calculated vibrational frequencies, ω_e of the alkali dimers. The values are compared with other theoretical and experimental values. For the methods used, see text. All values are in cm^{-1}.

In comparison with other pseudopotential results in Table 10.1, the calculated equilibrium bond lengths are in good agreement. It is therefore evident that the present scalar relativistic pseudopotentials correctly estimate equilibrium bond lengths even without the inclusion of a core polarization potential for the small core.

In one-valence-electron pseudopotentials, omitting core-valence correlation for the large core typically leads to an overestimated bond length, e.g. by 0.27 Å for K_2 and 0.37 Å for Cs_2 [15].

The underestimation of the equilibrium bond length in Stoll's calculation is explained in part by an overestimation of the valence correlation contribution together with the neglect of the repulsive core overlap interaction especially in the heavy alkali dimers [23].

All-electron results of Patridge *et al.* [24], which include core-valence correlation for K_2 and Rb_2, are in good agreement with the present results for K_2 but become worse for Rb_2. These authors have noted that inclusion of core-valence correlation as a perturbation up to the second order [25] leads to a much larger contribution than a direct CPP method as noted by Müller earlier [26]. For Cs_2, the deviation from experimental value remains at 0.27 Å [18] even with eighteen electrons correlated in the CISD scheme, partly due to the neglect of relativistic effects. They have reported that when a relativistic contraction of the bond length is estimated (by twice the Cs(6*s*) atomic contraction) this deviation reduces to 0.1 Å.

The equilibrium bond lengths of this study are in very good agreement with the known experimental values and therefore the accuracy limit is practically reached in the present calculations.

It has been shown for the dipole polarizability of Fr that core-valence correlation may play an important role. In order to test the influence of core-valence correlation, the equilibrium bond length of Fr_2 was calculated by including the core polarization potential (CPP) for Fr. (see appendix A) The inclusion of CPP yields a bond distance of 4.543 Å at the CCSD(T) level, only 1% smaller than the result of valence correlation only. Typically, omission of CPP was found to lead to overestimated bond lengths by more than 7%. It is therefore evident that although neglecting core-valence correlation leads to an overestimation of bond length, the error introduced by such an omission is rather small in these small-core pseudopotentials.

The calculated dissociation energies of the alkali dimers are collected in Table 10.2 along with other theoretical and experimental values.

The present values are in good agreement with the results of Ref. [23], which include core-valence correlation. This is not surprising, however, since the core-valence correlation contribution is much less important for dissociation energies than for bond lengths. It was found that inclusion of core-valence correlation causes a decrease in the dissociation energy of Fr_2 by 0.003 eV.

Daudey and co-workers [19] reported that saturation of basis sets by inclusion of higher angular momentum functions (e.g. *f*-type functions for Rb_2 and Cs_2) would lead to an overestimation of dissociation energies. For example, following inclusion of *f*-type functions, their dissociation energy was increased from 0.480 to 0.485 eV for Rb_2 and from 0.452 to 0.464 eV for Cs_2. This increase resulted in their dissociation of Rb_2 becoming more agreeable with the experimental value while the same effect caused an overestimation in the dissociation energy of Cs_2. No such overestimation in dissociation energies was found in this study although inclusion of *g*-type function did increase the dissociation energy of Cs_2 from 0.423 to 0.428 eV.

A recent relativistic all-electron study by Edvardsson *et al.* [27] on the potential energy curve for Rb_2 overestimates the dissociation energy (0.529 eV) even though their bond distance (4.20 Å) was longer than the experimental value.

In comparison with experimental values, the present dissociation energies are accurate within 0.025 eV. It has been noted by Müller and Meyer that the experimental dissociation energy of K_2 is too low [17].

Relativistic effects in Fr_2 cause the dissociation energy of Fr_2 to be slightly higher than that of Cs_2 as shown in Table 10.2. This leads to an anomalous trend in the dissociation energies of the alkali dimers as was in the equilibrium bond lengths.

The calculated harmonic vibrational frequencies of the alkali dimes are listed and compared with other theoretical and experimental values in Table 10.3. As shown, the vibrational frequencies calculated with the small-core pseudopotentials are in excellent agreement with the experimental values as well as other large-core pseudopotential results which incorporate core-valence correlation. This emphasizes that small-core pseudopotentials are capable of achieving accuracies better than the large-core pseudopotentials accompanied by a core-polarization potential. With these small-core pseudopotentials, some of the core-valence correlation contribution treated approximately in large-core pseudopotential calculations can be treated directly in a valence correlation procedure without relying on the use of core polarization potentials. Further, the frozen-core approximation is less severe in using small-core pseudopotentials and

core overlap contributions are reduced. Also, different methods of treating core-valence correlation can lead to sizable errors as noted by Daudey *et al.* For example, treating core-valence correlation by perturbative methods leads to an error of up to 10 cm^{-1} in vibrational frequencies of alkali dimers [25].

10.1.2 Static Dipole Polarizabilities

The static dipole polarizabilities of the alkali dimers are presented in Table 10.4 and Table 10.5 for the perpendicular and the parallel component, respectively. These values are compared with the all-electron calculations of Sadlej [30] and Meyer [31]. In Sadlej's calculation, relativistic effects were included by using a quasirelativistic scalar (i.e. mass-velocity Darwin terms) approximation. Electron correlation was treated at the CCSD(T) level. In Meyer's case, the polarizabilities were obtained from all-electron HF + valence CI calculations, including core-polarization effects by the use of an effective potential. Relativistic effects were neglected. Both Sadlej and Meyer used experimental bond distances for their dipole polarizability calculations. The present dipole polarizabilities were calculated with the optimized bond distances which are identical to experimental values within 0.01 Å.

As can be seen from Table 10.4, the perpendicular component of the dipole polarizability agrees well with Sadlej's values. Meyer's calculation seems to overestimate correlation effects shown by an underestimated dipole polarizability at the correlated level. The present values tend to be slightly smaller than Sadlej's values at all levels of theory.

Electron correlation effects reduce the dipole polarizabilities for all dimers. This negative contribution can be linked to the contraction of the electron distribution by correlation effects [28]. As expected, relativistic effects cause the perpendicular component of the Fr_2 dipole polarizability to drop down below that of Cs_2.

Interestingly, the magnitude of the perpendicular component of the dipole polarizability is smaller than the sum of the atomic dipole polarizabilities. This can be explained in terms of a dipole-induced-dipole model [29]. This model predicts a decrease in the perpendicular component and an increase in the parallel component of the dipole polarizability of the dimer compared with the dipole polarizabilities of individual atoms. Further, the perpendicular component of the dipole polarizabilities is primarily determined by the orbital excitation from the

strongly stabilized bonding σ-orbital to the unoccupied valence π-orbital as a counterpart of the atomic *ns-np* excitation for atoms. It is confirmed in a CIS calculation on the oscillator strengths that indeed the $\sigma \rightarrow \pi$ is the most intense transition, contributing mostly to the perpendicular component of the dipole polarizability.

The parallel component of the dipole polarizability shows a somewhat larger difference between the present and Sadlej's values. As was the case for the perpendicular component, Sadlej's values for the parallel components are overestimated compared with the present values. The discrepancy in the parallel components is, however, larger than in the perpendicular components, amounting

		Method	HF	CCSD	CCSD(T)
K_2	This work	ECP/CCSD(T)	456.1	385.0	374.0
	Sadlej [30]	AE/CCSD(T)	457.6	385.7	376.2
	Meyer [31]	AE/CI+CPP	465.0	-	348.0
Rb_2	This work	ECP/CCSD(T)	538.0	437.2	419.9
	Sadlej [30]	AE/CCSD(T)	549.3	479.1	445.4
Cs_2	This work	ECP/CCSD(T)	715.7	566.0	536.9
Fr_2	This work	ECP/CCSD(T)	655.9	511.2	480.4

Table 10.4. The calculated perpendicular component of the dipole polarizability of the alkali dimers. The values are compared with other theoretical values. For a detailed description of the methods used, see text. All values are in a.u.

		Method	HF	CCSD	CCSD(T)
K_2	This work	ECP/CCSD(T)	727.3	711.5	711.2
	Sadlej [30]	AE/CCSD(T)	726.9	766.6	753.6
	Meyer [31]	AE/CI+CPP	748.9	-	691.9
Rb_2	This work	ECP/CCSD(T)	879.4	826.8	815.2
	Sadlej [30]	AE/CCSD(T)	920.9	962.6	916.1
Cs_2	This work	ECP/CCSD(T)	1198.0	1095.9	1073.7
Fr_2	This work	ECP/CCSD(T)	1149.5	991.9	948.2

Table 10.5. The calculated parallel component of the dipole polarizability of the alkali dimers. The values are compared with other theoretical values. For a detailed description of the methods used, see text. All values are in a.u.

to as much as 100 a.u. for Rb_2 at the CCSD(T) level. As a result, the present values of the parallel component of the dipole polarizability for K_2 agree better with the Meyer's value than with Sadlej's. Note that both Sadlej and Meyer have used the same bond distance (taken from experimental values) for their calculation of the K_2 dipole polarizability.

Meyer has noted that electron correlation in the parallel component of the dipole polarizability has different signs for valence only and core-valence contribution [31]. That is, valence correlation has a positive correlation contribution while core-valence correlation is negative. For example, the dipole polarizability of K_2 increases from the HF value of 748.9 a.u. to 839.5 a.u. upon valence correlation then decreases to 691.9 a.u. upon the inclusion of core-valence correlation. The negative contribution from the core-valence correlation dominates over the positive valence only contribution with increasing nuclear charge as the core becomes more polarizable. Overall, this results in a spatial contraction of the valence shell. This is supported by the present case with increasing negative correlation contribution from 2% for K_2 to 18% for Fr_2.

In Sadlej's case, there seems to be an inconsistency in the estimation of correlation effects. This is first shown by a positive overall correlation contribution for K_2 at the CCSD(T) level. In fact for all dimers, the CCSD results of Sadlej show a positive correlation contribution. This is followed by a negative correlation contribution from the perturbative triples excitation. As the negative triples contribution is much smaller than the positive singles and doubles, the combined effects lead to a dipole polarizability too large for Rb_2 at the CCSD(T) level. This, in turn, gives rise to an overestimated average dipole polarizability of Rb_2. (See Table 10.6). Note that the same Rb_2 bond distance was used in Sadlej's and the present dipole polarizability calculations.

As was the case for the perpendicular component of the dipole polarizability, relativistic effects take charge for Fr_2, where the parallel component of the dipole polarizability also decreases from that of Cs_2, leading to a familiar relativistic anomaly in the trend of dipole polarizabilities.

The average dipole polarizability is obtained from Eq. 2.6 where the xx and the yy components of the dipole polarizability result from the perpendicular component and the zz component from the parallel component when the external electric field is applied along the z-direction (bonding axis). The resulting values are listed in Table 10.6.

Perhaps one of the most interesting features, though expected, is the decrease in the dipole polarizability from Cs_2 to Fr_2 due to relativity. A graphical

depiction of this effect is provided in Figure 10.2. This anomalous trend is attributed to the relativistic contraction of the valence *ns* shell of Fr.

It is clear from Table 10.6 and Figure 10.2 that the present average dipole polarizabilities are within the experimental uncertainties. The agreement between the present and experimental values is better than the all-electron calculations of Sadlej.

	Method	K_2	Rb_2	Cs_2	Fr_2
This work	DK/CCSD(T)	486.4	551.7	715.8	636.3
Sadlej [30]	MVD/CCSD(T)	502.1	602.0	-	-
Expt. [32]	Beam	499.4	533.1	701.8	-
	deflection	± 40.5	± 40.56	± 54.0	

Table 10.6. The average dipole polarizabilities of the alkali dimers. All values are in a.u. (1 a.u. = 0.14818 Å^3).

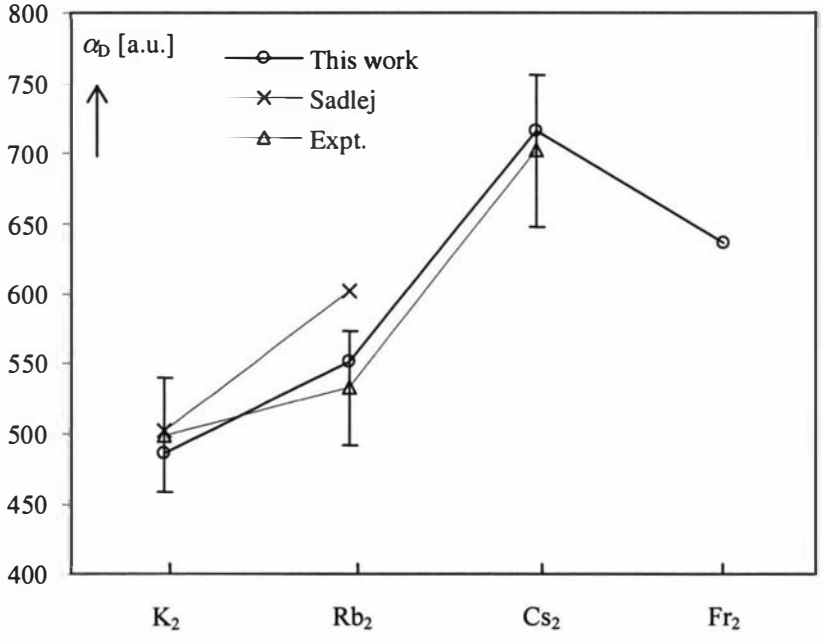

Figure 10.2. The average dipole polarizabilities of the alkali dimers from K_2 to Fr_2. The values from Sadlej and experimental data including error bars are also plotted. All values are in a.u.

10.2 Singly Charged Alkali Dimers

The calculated equilibrium bond lengths, dissociation energies, and vibrational frequencies of the singly charged alkali dimers are presented in Tables 10.7, 10.8, and 10.9, respectively. These are compared with other theoretical values.

The methods of calculation were as follows: The present values were obtained by the use of relativistic nine-valence-electron pseudopotentials of this study with valence correlation treated at the CCSD(T) level. Core-valence correlation was omitted unless stated otherwise. For comparison, the results of Stoll [36, 37], Krauss [11], Preuss [38], Daudey [15] are listed, which were obtained by the use of relativistic one-valence-electron pseudopotentials including core-valence correlation by the use of a CPP. Patil's results [39] were obtained by their one-valence-electron model potentials.

10.2.1 Spectroscopic Constants

In general, the present values agree well with other theoretical values. The best agreement is observed between the present and Stoll's values which include core-valence correlation. This indicates that the small-core pseudopotentials of this study perform extremely well without the need for core-polarization potentials.

Preuss *et al.* have noted that the difference between Stoll's [36, 37] and their [38] values are mainly due to different basis sets used rather than the spin-orbit splitting considered in their study. In fact, they have concluded that there is not a noticeable difference induced by their *j*-dependent pseudopotentials in comparison with Stoll's results. The present dissociation energies agree well with the experimental values of 0.74 ± 0.05 for Rb_2^+ [33] and 0.68 ± 0.05 eV for Cs_2^+ [34].

A recent potential energy curve calculation for Rb_2^+ by Aubert-Frécon *et al.* [35] support the present values. Their one-valence-electron pseudopotential calculation including core-valence correlation yielded $R_e(Rb_2^+)$ = 4.79 Å, $D_e(Rb_2^+)$ = 0.765 eV and $\omega_e(Rb_2^+)$ = 46.0 cm^{-1}.

	K_2^+	Rb_2^+	Cs_2^+	Fr_2^+
This work	4.509	4.802	5.269	5.239
Stoll [36, 37]	4.49	4.78	5.23	-
Krauss [11]	-	4.73	5.24	-
Preuss [38]	-	4.82	5.36	-
Daudey [15]	4.50	-	5.22	-
Patil [39]	4.39	4.60	5.03	-

Table 10.7. The calculated equilibrium bond lengths, R_e of the singly charged alkali dimers. The values are compared with other theoretical values. For the method of calculation, see text. All values are in Å.

	K_2^+	Rb_2^+	Cs_2^+	Fr_2^+
This work	0.822	0.753	0.712	0.682
Stoll [36, 37]	0.823	0.762	0.707	-
Krauss [11]	-	0.784	0.726	-
Preuss [38]	-	0.789	0.789	-
Daudey [15]	0.82	-	0.70	-
Patil [39]	0.883	0.865	0.830	-

Table 10.8. The calculated dissociation energies, D_e of the singly charged alkali dimers. The values are compared with other theoretical. For the method of calculation, see text. All values are in eV.

	K_2^+	Rb_2^+	Cs_2^+	Fr_2^+
This work	72.9	46.3	34.0	26.5
Stoll [36, 37]	72	47	33	-
Krauss [11]	-	46.5	33.7	-
Preuss [38]	-	44.5	32.4	-
Daudey [15]	74	-	38	-

Table 10.9. The calculated vibrational frequencies, ω_e of the singly charged alkali dimers. The values are compared with other theoretical values. For the method of calculation, see text. All values are in cm^{-1}.

The largest deviation from the present values of equilibrium bond lengths and dissociation energies are with Patil's results. Their model potential approach seems to suffer from an inaccurate description of core-valence correlation. As noted by Meyer *et al.* [17] this typically results in bond lengths too short and dissociation energies too large. The deviation of Patil's results from the present case grows with increasing nuclear charge i.e. from K_2^+ to Cs_2^+, with increasing polarizability of the core. It is believed that Daudey's results are affected by error cancellation resulting from too large core-valence correlation as pointed out by Meyer *et al.* [17].

An interesting feature is the equilibrium bond distance of Fr_2^+. Here, a monotonic increase in the bond distance from K_2^+ to Cs_2^+ is discontinued and there is a decrease in the bond distance from Cs_2^+ to Fr_2^+ due to a relativistically contracted valence *ns* shell of Fr. Inclusion of a core-polarization potential reduces the bond distance for Fr_2^+ to 5.186 Å. This is again about 1 %. This contribution from core-valence correlation for small-core pseudopotentials, is much smaller than previously reported for large-core pseudopotentials. For example, Stoll and co-workers have reported a reduction of up to 0.26 Å in the bond length of K_2^+ using their one-valence-electron pseudopotential [36].

In contrast to the bond distances, the dissociation energies of the positively charged alkali dimers show no anomaly in the trend. That is, the dissociation energies are monotonically decreasing from K_2^+ to Fr_2^+. As expected, the CPP does not significantly contribute to the dissociation energy of Fr_2^+, which causes an increase in the dissociation energy by only 0.0004 eV.

Overall, the present nine-valence-electron pseudopotentials perform extremely well for the alkali dimer ions. One of the nicest features of the these small-core pseudopotentials is that one can safely avoid the use of core-polarization potentials without scarifying the accuracy within 1 %.

References

[1] J. M. Walter and S. Barratt, Proc. R. Soc. London Ser. A **119**, 257 (1928).

[2] E. J. Breford, F. Engelke, G. Ennen, and K. H. Meiwes, Faraday Discuss. Chem. Soc. **71**, 233 (1981).

[3] H. P. Huber and G. Herzberg, *Molecular Spectra and Structure* (Van Nostrand-Reinhold, New York, 1978), Vol. 4.

[4] R. N. Dixon and J. M. V. Hugo, Mol. Phys. **29**, 953 (1975).

[5] L. R. Kahn, P. Baybutt, and D. C. Truhlar, J. Chem. Phys. **65**, 3826 (1976).

[6] J. C. Barthelat and Ph. Durand, Gazz. Chim. Ital. **108**, 225 (1978).

[7] D. Maynau and J. P. Daudey, Chem. Phys. Lett. **81**, 273 (1981).

[8] T. C. Chang, P. Habitz, B. Pittel, and W. H. E. Schwarz, Theoret. Chim. Acta. **34**, 263 (1973); **44**, 61 (1977).

[9] J. Flad, H. Stoll, and H. Preuss, J. Chem. Phys. **71**, 3042 (1979).

[10] H. Preuss, H. Stoll, U. Wedig, and Th. Krüger, Int. J. Quantum Chem. **19**, 113 (1981).

[11] M. Krauss and W. J. Stevens, J. Chem. Phys. **93**, 4236 (1991).

[12] W. Meyer and P. Rosmus, J. Chem. Phys. **63**,2356 (1975).

[13] P. Rosmus and W. Meyer, J. Chem. Phys. **65**,492 (1976).

[14] C. Bottcher and A. Dalgarno, Proc. R. London. Ser. A **340**, 187 (1974).

[15] G. H. Jeung, J. P. Malrieu, and J. P. Daudey, J. Chem. Phys. **77**, 3571 (1982).

[16] G. H. Jeung, J. P. Daudey, and J. P. Malrieu, J. Phys. B **16**, 699 (1983).

[17] W. Müller and W. Meyer, J. Chem. Phys. **80**, 3311 (1984).

[18] S. P. Walch, C. W. Bauschlicher Jr., P. E. M. Siegbahn, and H. Patridge, Chem. Phys. Lett. **92**, 54 (1982).

[19] M. Foucrault, Ph. Millie, and J. P. Daudey, J. Chem. Phys. **96**, 1257 (1991).

[20] F. Engelke, H. Hage, and U. Schühle, Chem. Phys. Lett. **106**, 535 (1984).

[21] C. D. Caldwell, F. Engelke, and H. Hage, Chem. Phys. **54**, 21 (1980).

[22] W. Weickenmeier, U. Diemer, M. Wahl, M. Rabb, W. Demtröder, and W. Müller, J. Chem. Phys. **82**, 5354 (1985).

[23] G. Igel-Mann, U. Wedig, P. Fuentealba, and H. Stoll, J. Chem. Phys. **84**, 5007 (1986).

[24] H. Patridge, C. W. Bauschlicher Jr., S. P. Walch, and B. Liu, J. Chem. Phys. **79**, 1866 (1983).

[25] G. H. Jeung, F. Spiegelmann, J. P. Daudey, and J. P. Malrieu, J. Phys. B **16**, 2659 (1983).

[26] W. Müller, J. Flesch, and W. Meyer, J. Chem. Phys. **80**, 3297 (1984).

[27] D. Edvardsson, S. Lunell, and C. M. Marian, Mol. Phys. **101**, 2381 (2003).

[28] H.-J. Werner and W. Meyer, Phys. Rev. A **13**, 13 (1976).

[29] L. Frommhold, Adv. Chem. Phys. **46**, 1 (1981).

[30] M. Urban and A. J. Sadlej, J. Chem. Phys. **103**, 9692 (1995).

[31] W. Müller and W. Meyer, J. Chem. Phys. **85**, 953 (1986).

[32] V. Tarnovsky, M. Bunimovicz, L. Vušković, B. Stumpf, and B. Bederson, J. Chem. Phys. **98**, 3894 (1993).

[33] C. L. Beckel and R. Engelke, J. Mol. Spectrosc. **42**, 578 (1972).

[34] G. V. Marr and S. R. Wherett, J. Phys. B **5**, 1735 (1972).

[35] A. Jraij, A. R. Allouche, M. Korek, and M. Aubert-Frécon, Chem. Phys. **290**, 129 (2003).

[36] P. Fuentealba, H. Preuss, H. Stoll, and L. von Szentpály, Chem. Phys. Lett. **89**, 418 (1982).

[37] L. von Szentpály, P. Fuentealba, H. Preuss, and H. Stoll, Chem. Phys. Lett. **93**, 555 (1982).

[38] H. Silberbach, P. Schwerdtfeger, H. Stoll, and H. Preuss, J. Phys. B **19**, 501 (1986).

[39] S. H. Patil and K. T. Tang, J. Chem. Phys. **113**, 676 (2000).

Chapter 11
AMMONIA COMPLEXES OF ALKALI-METALS

The reactions of alkali-metals with liquid water and ammonia are well known in chemistry [1]. These reactions are highly exothermic, attributed to the high solvation of the alkali cation [2]. In the gas phase, however, the reactivity is greatly reduced. *Ab-initio* SCF calculations predict the binding energy of 14.5 kcal/mol for Li-NH_3 and 6.0 kcal/mol for K-NH_3 [3, 4]. For the molecular ion of Li^+-NH_3 and K^+-NH_3, it was found by high-pressure mass spectroscopy that the binding energy increases to 33 and 29 kcal/mol, respectively [5]. The increase in the binding energy for the molecular ions is consistent with the shorter bond length for the ionic complexes. Moreover, the downward trend in the binding energy is expected to continue down the group for the larger alkali-metals.

An experimental infrared spectroscopic study by Süzer and Andrews provides some insight to the ammonia-alkali atom pair interaction of Li, Na, K, and Cs [2]. They carried out a careful analysis of the infrared spectra of these complexes in solid argon matrix and provided evidence for the existence of 1:1 molecular complexes in contrast to the well-known ionic solutions in liquid ammonia. This study was a big step forward since the only available data up to this point were for small alkali-metals. They have noted the lack of theoretical data on these molecules.

Early calculations on the alkali-ammonia complexes seemed to be limited to the positively charged molecular ionic species, owing to the simplicity arising from the closed shell structure of molecular ions. Furthermore, most studies have focused on the determination of the binding energies of these alkali-ammonia complexes because of the earlier suggestion that the neutral species may not be significantly bound partly due to the lack of charge transfer. More recently, Chalasinski and co-workers have reported van der Waals coefficients for small alkaline-earth metal bound to ammonia or water [6].

Recent advances include *ab-initio* studies on Na-$(NH_3)_n$ complexes [7, 8] for structure, binding energies and vibrational frequencies as well as anionic Na-NH_3 complexes [9]. A more comprehensive study on the positive and dipositive ions of M-$(H_2O)_n$ and M-$(NH_3)_n$ (M = Mg, Ca, Sr and n = 1 - 3) has been given by Partridge and co-workers [10].

To the author's knowledge, there are still no calculations available for the larger alkali-ammonia complexes. In particular, the dipole polarizabilities of these complexes remain unexplored. In view of this, the neutral and positively charged ammonia complexes of the alkali-metals from K to Fr are investigated in this chapter. The focus is placed on the periodic trend in the geometries, dissociation energies and the dipole polarizabilities as well as the vibrational frequencies of these complexes.

11.1 Method and Computational Details

For ammonia, augmented triple zeta type basis sets were used. For the alkali-metals, the scalar relativistic pseudopotentials and the corresponding valence basis sets of this study were used. Ammonia is of a C_{3v} symmetry and the optimized parameters were the (N-H) bond length and (H-N-H) bond angle. On formation of the complexes, the two parameters of the NH_3 geometry were allowed to vary along with the (M-N) bond length and the (M-N-H) bond angle. The (M-N) bond was placed along the C_3 axis which was chosen as the z-axis i.e. parallel with the applied external electric field in all dipole polarizability calculations. All calculations including the dipole polarizabilities were performed at the MP2 level using the Gaussian 03 program package [11].

11.2 Optimal Geometry

The calculated equilibrium geometries (MP2 level) of the neutral and the positively charged alkali-ammonia complexes are presented in Tables 11.1 and 11.2, respectively.

	R_e(M-N)	R_e(N-H)	∠(H-N-H)	∠(M-N-H)
NH_3	-	1.010	107.04	-
K-NH_3	2.855	1.013	106.47	112.33
Rb-NH_3	3.008	1.013	106.49	112.31
Cs-NH_3	3.170	1.013	106.50	112.30
Fr-NH_3	3.281	1.012	106.61	112.20

Table 11.1. The optimized equilibrium geometry of the alkali-ammonia complexes at the MP2 level. The bond lengths are in Å and the bond angles are in degrees.

	R_e(M-N)	R_e(N-H)	∠(H-N-H)	∠(M-N-H)
NH_3	-	1.010	107.04	-
$(K\text{-}NH_3)^+$	2.762	1.013	104.91	113.72
$(Rb\text{-}NH_3)^+$	2.921	1.013	104.95	113.68
$(Cs\text{-}NH_3)^+$	3.129	1.013	105.04	113.61
$(Fr\text{-}NH_3)^+$	3.194	1.013	105.09	113.56

Table 11.2. The optimized equilibrium geometry of the singly charged alkali-ammonia complexes at the MP2 level. The equilibrium bond lengths are in Å and the bond angles are in degrees.

Briefly, the calculated NH_3 geometry at the MP2 level (Table 11.1) is compared with the experimental geometry to gain knowledge on the accuracy of the MP2 method. In comparison with the experimental values [12] of R_e(N-H) = 1.012 Å and ∠(H-N-H) = 106.68 °, the present MP2 values suffer only a slight overestimation, far less than 1 % in magnitude. These small errors can be improved by the use of a more sophisticated electron correlation treatment. As this study is not aimed at high accuracies but rather understanding of periodic trends emerging from the complexation of alkali-metals to ammonia, the inaccuracy of less than 1% is accepted.

Evident from the data in Table 11.1 and Table 11.2 is the general trend in the equilibrium geometry of the ammonia complexes. On formation of the neutral complexes with all alkali-metals, the NH_3 geometry changes slightly. The (N-H) bond is lengthened and the (H-N-H) bond angle is decreased. As

expected, the change in the NH_3 geometry upon complexation is larger for strongly bound species such as K, then decreases down the group to Fr.

The change in the NH_3 geometry is a little more enhanced upon complexation of the singly charged molecular ions as shown in Table 11.2. It is not surprising, however, as the singly charged alkali ions are more strongly bound to ammonia than the neutral atoms. This is supported by the shorter (M-N) bond lengths for the singly positive molecular ions. The shorter (M-N) bond lengths of the positively charged complexes are attributed to the stronger electrostatic force between the alkali cation and the lone-pair of electrons in ammonia, characterized by a base → metal charge transfer.

As far as the metal-ammonia interactions are concerned, a straightforward trend emerges from the (M-N) bond length. That is, the (M-N) bond length increases with increasing nuclear charge of the metal for both the neutral and cationic complexes. As the (M-N) interaction weakens the NH_3 geometry tends back toward free ammonia geometry, with decreasing (N-H) distance and increasing (H-N-H) bond angle.

11.3 Dissociation Energies

The calculated dissociation energies of the neutral and positively charged alkali-ammonia complexes at the MP2 level are presented in Table 11.3. It can be seen from Table 11.3. that the dissociation energies are monotonically decreasing from K- to Fr-NH_3 for both the neutral and the positively charged complexes. This is reasonable with increasing bond distances as nuclear charge increases from K to Fr. The dissociation energies of the positively charged complexes are more than

	Dissociation Energy	
	Neutral	Positively charged
K-NH_3	0.259	0.863
Rb-NH_3	0.237	0.773
Cs-NH_3	0.213	0.681
Fr-NH_3	0.206	0.663

Table 11.3. The calculated dissociation energies of the neutral and positively charged alkali-ammonia complexes at the MP2 level. All values are in eV.

three times higher than those of the neutral species. Hence, the positively charged complexes are more strongly bound, again confirming the shorter bond distances for the charged complexes.

Experimental dissociation energies of theses complexes are not available. Although the accuracy of the present results is sacrificed by the use of the MP2 method for the correlation treatment, the present study provides useful data on these complexes.

11.4 Relativistic Effects in the M-N Interaction

Particular attention is drawn to the ammonia complex of Fr. It is well known that atomic Fr experiences large relativistic effects. Such large effects of relativity affect properties such as the dipole polarizability and the ionization potential, which can lead to an anomalous trend in molecular properties as given in previous chapters. Based on such findings, one might expect similar effects in the properties of Fr-NH_3 in comparison with those of Cs-NH_3. That is, relativistic effects in Fr are expected to stabilize the M-N interaction, causing a decrease in the (M-N) distance from Cs- to Fr-NH_3. However, this is not the case. Here, the (M-N) bond distance increases from Cs- to Fr-NH_3 and there is no anomaly in the straightforward upward trend in the (M-N) distance from K- to Fr-NH_3 as shown in Table 11.1.

In order to provide a qualitative explanation for the monotonic increase in the (M-N) distance, the orbital energies of the anti-bonding and the bonding orbitals of the complexes are compared in Table 11.4. A graphical depiction of this is provided in Figure 11.1 and Figure 11.2.

The data in Table 11.4 and Figure 11.1 show that the orbital energy of the anti-bonding orbital increases from K- to Cs-NH_3 and then decreases for Fr-NH_3.

	K-NH_3	Rb-NH_3	Cs-NH_3	Fr-NH_3
Anti-bonding	-0.12795	-0.12229	-0.11392	-0.11653
Bonding	-0.48469	-0.47902	-0.47343	-0.46723

Table 11.4. The calculated HF orbital energies of the bonding and anti-bonding orbitals of ammonia complexes of alkali-metals from K to Fr. All values are in a.u.

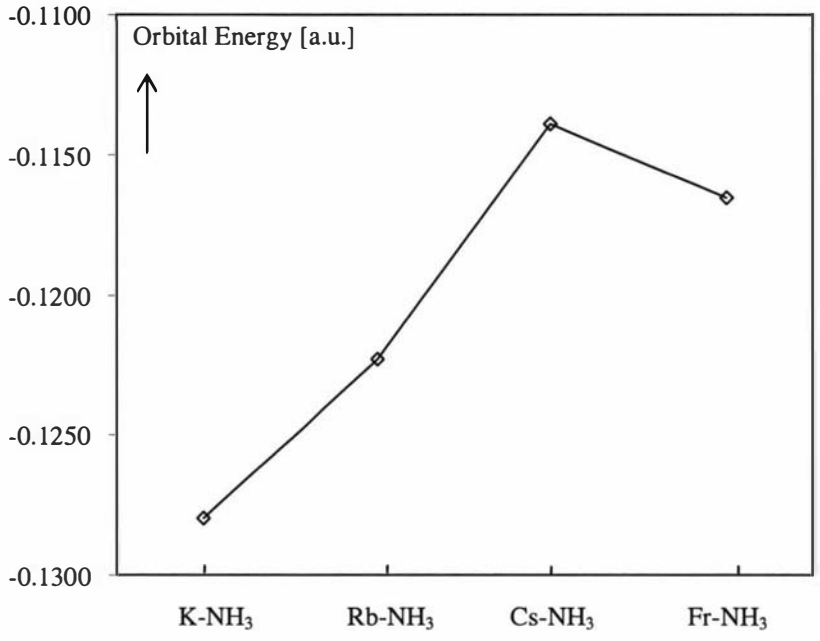

Figure 11.1. A graphical representation of the anti-bonding orbital energies of alkali-ammonia complexes. All values are in a.u.

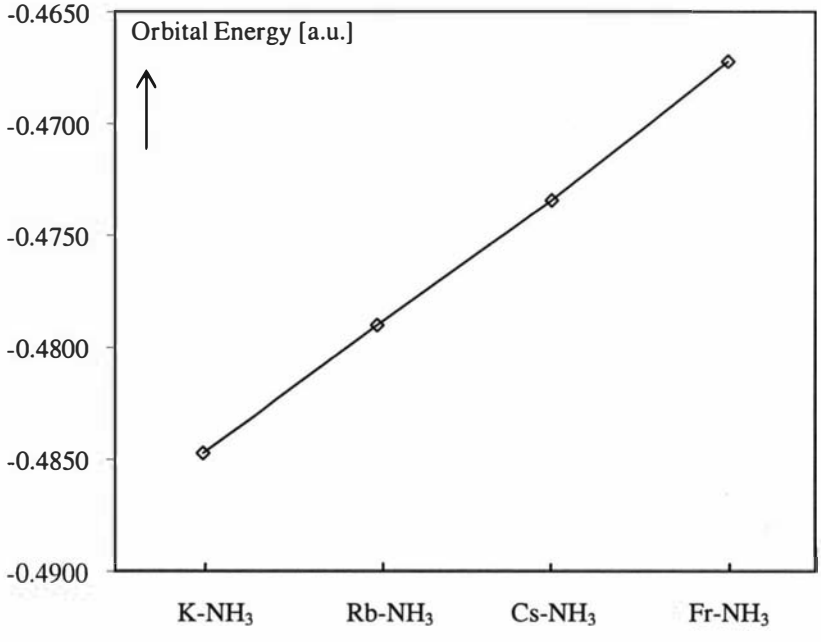

Figure 11.2. A graphical representation of the bonding orbital energies of alkali-ammonia complexes. All values are in a.u.

This decrease in the orbital energy of Fr-NH_3 arises from the relativistic stabilization of the valence *ns* orbital of Fr. As for the bonding orbital, a different picture emerges. (Table 11.4 and Figure 11.2) That is, the orbital energy increases monotonically without any anomaly from K- to Fr-NH_3. This is reasonable as the bonding orbital largely remains NH_3 like in character and relativistic effects that govern atomic properties of alkali-metals are not reflected in the bonding of M-NH_3. The consequences of this is such that the trend in the (M-N) bond distance exhibits the same trend as in the orbital energy of the bonding orbital. This explains the monotonic upward trend in the (M-N) bond distance from K- to Fr-NH_3.

It can also be deduced from the above qualitative description that the HOMO of these complexes are largely characterized by the atomic valence *ns* orbital of the metal.

11.5 Vibrational Frequencies

The vibrational frequencies and the corresponding infrared (IR) intensities of the alkali-ammonia complexes are presented in Table 11.5. Note that the Nakamoto convention for vibrational modes are used [13]. There are a few key features that can be seen from this table.

Firstly, the two bands, $\nu_1(A_1)$ and $\nu_3(E)$ around 3500 - 3700 cm^{-1} for NH_3, correspond to the very week N-H symmetric and anti-symmetric stretching mode of NH_3, respectively. The bending modes occur at much lower frequencies as expected.

One of the most striking features from Table 11.5 is the enhancement of the symmetric (N-H) stretching mode, $\nu_1(A_1)$ on complex formation. For example, in K-NH_3, the IR intensity of the $\nu_1(A_1)$ vibration is intensified by 120 times from free ammonia. In fact, this band is the strongest of all modes in all alkali-ammonia complexes. The IR intensity enhancement of the band from uncomplexed ammonia grows with increasing nuclear charge of the alkali-metal up to Cs-NH_3. Then a familiar anomaly appears for Fr-NH_3 where the IR intensity of the band suddenly decreases from the Cs-NH_3 counterpart. This is attributed to relativistic effects involving the Fr atom.

	$\nu_1(A_1)$ NH sym. str.		$\nu_2(A_1)$ HNH sym. bent.		$\nu_3(E)$ NH asym. str.		$\nu_4(E)$ HNH asym. bent.	
	ν	I	ν	I	ν	I	ν	I
NH_3	3535	3	1026	144	3666	9	1668	15
K-NH_3	3492	360	1114	216	3621	18	1661	10
Rb-NH_3	3492	384	1108	215	3622	13	1660	9
Cs-NH_3	3491	479	1105	208	3621	7	1660	7
Fr-NH_3	3494	310	1092	210	3625	8	1659	10

Table 11.5. The calculated vibrational frequencies (ν, cm^{-1}) and infrared intensities (I, km/mol) of ammonia and its complexes of the alkali-metals. Sym. and asym. denote symmetric and anti-symmetric, respectively. Str. is stretching mode and bent. is bending mode.

In line with the intensification of the $\nu_1(A_1)$ mode is the perturbation on $\nu_1(A_1)$. That is, the shift in the stretching $\nu_1(A_1)$ mode on complexation follows the same trend as the intensification of the $\nu_1(A_1)$ mode. For example, the red shift in $\nu_1(A_1)$ for K-NH_3 amounts to 42.7 cm^{-1}. This shift grows to 43.9 cm^{-1} for Cs-NH_3 and then decreases for Fr-NH_3 to 40.5 cm^{-1}.

As for the bending mode of $\nu_2(A_1)$, a familiar blue shift [14] is observed for the complexes. This amounts to 88, 82, 79 and 66 cm^{-1} for K-, Rb-, Cs-, and Fr-NH_3, respectively. The decrease in the blue shift of the $\nu_2(A_1)$ mode from K- to Fr-NH_3 may be explained by the increasing (M-N) bond distance. As the (M-N) bond distance increases a weaker repulsion between the ammonia hydrogen and the metal is expected and hence the smaller blue shift in the $\nu_2(A_1)$ mode.

Finally, the anti-symmetric stretching mode, $\nu_3(E)$ is found to shift from the uncomplexed $\nu_3(E)$ mode by the same amount as the $\nu_1(A_1)$ mode. Although experimental studies suggest little perturbation on the $\nu_3(E)$ mode for larger alkali-metal complexes, it is found in this study that perturbation on the $\nu_3(E)$ mode remains similar to that on the $\nu_1(A_1)$ mode with the difference being the relative level of IR intensity enhancement on complex formation. That is, the intensification of the $\nu_3(E)$ mode is observed only for the strongly bound complexes such as K-NH_3, and Rb-NH_3 to a lesser degree. For the larger alkali-metal complexes, the IR intensity remains similar to the unperturbed case, which may contribute to the experimental difficulties in assigning this vibrational mode

[2]. The anti-symmetric bending mode, $\nu_4(E)$ remains rather featureless on complexation.

In Table 11.6, the dipole moments of the alkali-ammonia complexes are listed. There is a straight forward decrease in the dipole moments from K- to Fr-NH_3 in line with the increasing bond lengths from K- to Fr-NH_3. As for the enhancements of IR intensities, it is rather difficult to quantify the intensification of a specific mode as the IR intensity is determined by the derivative of the dipole moment not the moments themselves.

	K-NH_3	Rb-NH_3	Cs-NH_3	Fr-NH_3
Dipole moment	4.728	4.352	3.794	3.670

Table 11.6. The dipole moments of the alkali-ammonia complexes. All values are in Debye.

The vibrational frequencies of the positively charged complexes shown in Table 11.7 reveal somewhat different features from the neutral species. The intensification of the $\nu_1(A_1)$ mode is not present for the charged complexes, rather it is the anti-symmetric $\nu_3(E)$ mode that experiences enhancement on complex formation. It is difficult to explain the absence of $\nu_1(A_1)$ mode intensification in the charged complexes. One possible explanation could be that in the charged complexes, the (M-N) bond is by far more ionic in nature. This means that the vibrations involving the (M-N) bond are expected to show little charge fluctuation and hence little enhancement in the IR intensity.

The intensification of the anti-symmetric $\nu_3(E)$ mode, on the other hand, may be attributed to the shorter (M-N) bond distance in the charged complexes than in the neutral counterpart. The more rigid (M-N) structure in the cationic complexes means that the vibrations involving the motion of the nitrogen atom are more likely to affect the overall charge distribution about the (M-N) bond. This results in a more noticeable enhancement of the IR intensity in the cationic complexes compared with the neutral species for the $\nu_3(E)$ mode.

The band intensification, however, is by no means an easy phenomenon to interpret especially for the charged systems due to difficulties arising from the analysis of the dipole moment.

	$\nu_1(A_1)$ NH sym. str.		$\nu_2(A_1)$ HNH sym. bent.		$\nu_3(E)$ NH asym. str.		$\nu_4(E)$ HNH asym. bent.	
	ν	I	ν	I	ν	I	ν	I
NH_3	3535	3	1026	144	3666	9	1668	15
$(K\text{-}NH_3)^+$	3507	5	1227	128	3608	32	1673	19
$(Rb\text{-}NH_3)^+$	3507	5	1218	128	3610	30	1673	19
$(Cs\text{-}NH_3)^+$	3508	4	1206	129	3613	27	1672	19
$(Fr\text{-}NH_3)^+$	3507	4	1199	129	3613	26	1671	19

Table 11.7. The calculated vibrational frequencies (ν, cm^{-1}) and infrared intensities (I, km/mol) of the ammonia and its singly positive complexes of the alkali-metals. Sym. and asym. denote symmetric and anti-symmetric, respectively. Str. is stretching mode and bent. is bending mode.

11.6 Static Dipole Polarizabilities

The static dipole polarizabilities of the alkali-ammonia complexes calculated at the MP2 level of theory are presented in Table 11.8.

The dipole polarizabilities of NH_3 at the MP2 level compare reasonably well with the experimental values of 13.86 - 13.96 a.u. for the perpendicular and 15.74 - 15.95 a.u. for the parallel component of the dipole polarizability [15]. A slight underestimation by the present MP2 values is expected for the dipole polarizability as the MP2 method typically overestimates correlation effects as discussed in previous chapters.

The data compiled in Table 11.8 reveal some surprising aspects of the dipole polarizability for these complexes. The perpendicular component of the dipole polarizability shows a monotonic decrease from K- to $Fr\text{-}NH_3$. Considering the trend in the atomic dipole polarizability from K to Fr, this monotonic downward trend for the ammonia complexes is rather unexpected. As for the parallel component of the dipole polarizability, a rather familiar trend emerges. That is, the dipole polarizability increases from K- to $Cs\text{-}NH_3$ then starts to decrease for $Fr\text{-}NH_3$, following the same trend as the atomic dipole polarizability for the alkali-metals.

	Dipole polarizabilities		
	Perpendicular	Parallel	Average
NH_3	13.6	15.3	14.2
K-NH_3	404.7	438.9	416.1
Rb-NH_3	391.8	461.8	415.1
Cs-NH_3	378.6	516.2	424.5
Fr-NH_3	284.1	398.3	322.1

Table 11.8. The calculated perpendicular and parallel component of the static dipole polarizabilities of the alkali-metal ammonia complexes at the MP2 level. All values are in a.u.

It has been discussed in the last chapter that for alkali dimers the perpendicular component of the dipole polarizability is largely determined by the orbital excitation from the bonding σ-orbital to the unoccupied π-orbital whereas the parallel component comes from the excitation of bonding σ to anti-bonding σ^*-orbital. This line of argument is based on the sum-over-states formula. For approximate dipole polarizabilities, the sum-over-states formula can be truncated using only the most intense transitions which result in large oscillator strengths. It has been shown that the sum-over-states formula works well for the well defined systems such as alkali-metals with a single valence electron outside the core, which contribute mostly to the dipole polarizability. This approximation also works well for alkali dimers and has been used to qualitatively describe the trend in the dipole polarizabilities.

The present case, however, seems to be complicated by the occupation of the anti-bonding orbital. That is, according to the CIS (configurational interaction with single excitation) calculations, the most intense transition involves the anti-bonding orbital rather than the bonding orbital. The excitation from the anti-bonding to the unoccupied π-orbital (i.e. $\sigma^* \rightarrow \pi$) contribute mostly to the perpendicular component of the dipole polarizability whereas the excitation from the anti-bonding to the unoccupied σ-orbital (i.e. $\sigma^* \rightarrow \sigma$) determines mostly the parallel component of the dipole polarizability. By this argument, the perpendicular component of the dipole polarizability is expected to increase from K- to Cs-NH_3 and decrease for Fr-NH_3, exhibiting the same trend as in the parallel component. This is rather obvious as the trend in the anti-bonding orbital energy follows the same pattern. Although it might be obvious, it

is contradictory to the trend reported in this study where the perpendicular component is found to be monotonically decreasing. Interestingly, the trend observed in the dipole polarizabilities of the alkali-ammonia complexes fits the argument involving the bonding orbital, i.e. $\sigma \rightarrow \pi$ for the perpendicular and $\sigma \rightarrow \sigma^*$ for the parallel component of the dipole polarizability though these transitions do not exhibit large oscillator strengths.

It must be said that the CIS approximation is rather crude and should be excluded from quantitative description. For example, it predicts larger oscillator strength for the perpendicular component than for the parallel component, which is wrong. It should be at least able to offer correct qualitative description though. However it does not seem to be the case in the present study.

It is a difficult matter to explain the decreasing perpendicular component of the dipole polarizability from K- to Fr-NH_3. One may consider higher level calculations including multi-reference CISD as well as CCSD(T) calculations for evaluating more accurate electron correlation effects in dipole polarizabilities. Currently CCSD(T) calculations on these complexes with large basis sets are extremely time consuming.

Nevertheless, the perpendicular component of the dipole polarizability is larger than the sum of individual dipole polarizabilities. (Here, the atomic dipole polarizabilities were taken as 267.4, 273.1, 296.3 and 238.2 a.u. for K, Rb, Cs, and Fr, respectively. These values were obtained in a separate calculation which best models the dipole polarizability calculation for the complexes.) This can be explained by the occupation of the anti-bonding orbital in the complexes. As the valence orbitals of the free metal and ammonia combine into a bonding/anti-bonding pair, the result is such that the bonding orbital is lowered in energy and the anti-bonding orbital is raised. As a result, occupying the anti-bonding orbital leads to a larger net dipole polarizability than the sum of the individual dipole polarizabilities as is the case here. The same line of argument can be used for the parallel component too, where the parallel component of the dipole polarizability is larger than the sum of the individual dipole polarizabilities due to the occupied anti-bonding orbital.

The average dipole polarizabilities show a somewhat more familiar trend. Apart from a slight decrease in the average dipole polarizability from K- to Rb-NH_3, the dipole polarizability increases up to Cs-NH_3 and then decreases for Fr-NH_3 due to relativistic effects.

The dipole polarizabilities of the singly charged complexes are presented in Table 11.9. The singly charged complexes have a bonding σ-HOMO and an anti-

bonding σ^*-LUMO as opposed to a σ^*-HOMO for the neutral complexes. As shown in Table 11.9, both the perpendicular and parallel component of the dipole polarizability shows a monotonic increase from K- to Fr-NH_3. This trend is the same as the monotonically increasing atomic dipole polarizability of the positively charged alkali-metals.

Both components of the dipole polarizability are smaller than the sum of the individual dipole polarizabilities (i.e. $\alpha_D(M^+) + \alpha_D(NH_3)$), due to the lowering of the valence σ-orbital on formation of these complexes.

	Dipole polarizabilities		
	Perpendicular	Parallel	Average
NH_3	13.6	15.3	14.2
$(K\text{-}NH_3)^+$	17.5	21.4	18.8
$(Rb\text{-}NH_3)^+$	21.0	26.4	22.8
$(Cs\text{-}NH_3)^+$	27.4	34.9	29.9
$(Fr\text{-}NH_3)^+$	31.2	39.5	34.0

Table 11.9. The calculated perpendicular and parallel component of the dipole polarizability for the singly charged alkali-ammonia complexes at the MP2 level of theory. All values are in a.u.

There seems to be a lot of work needed to fully understand the behavior of the dipole polarizabilities for alkali-ammonia complexes. As mentioned earlier improvements can be made in calculating oscillator strengths, which may be used to qualitatively describe the decreasing perpendicular component of the dipole polarizability of the neutral alkali-ammonia complexes.

Chapter 12
CONCLUSION

The study of atomic dipole polarizabilities has long been an active and a challenging field of research. Although today's advances in computing power certainly help to carry out high level calculations, it is by no means an easy task to obtain highly accurate dipole polarizabilities. Lack of experimental data makes it even more difficult to judge the accuracy in the calculated dipole polarizabilities.

In this thesis, the static electric dipole polarizabilities and the ionization potentials of the neutral and singly charged group 1 elements and the neutral, singly and doubly charged group 2 elements were presented. The basis sets for such calculations were devised in a 4-component scheme.

Basis set requirements are severe for the calculation of the dipole polarizabilities. Usually, the basis sets for dipole polarizability calculations requires more diffuse functions than energy optimized basis sets typically offer. Electron correlation effects are large especially for the neutral group 1 and the neutral and singly charged group 2 elements and must be considered at the highest level of approximation possible. Relativistic effects must be included even for light elements such as K or Ca. The relativistic contraction of the valence *ns* shell leads to an anomaly in the trend of the dipole polarizabilities for the neutral group 1 and 2 elements as well as the singly charged group 2 elements. Fine structure effects such as spin-orbit coupling become important for the singly charged group 1 and the doubly charged group 2 elements. For superheavy elements such as E119, spin-orbit effects dominate over both electron correlation and scalar relativistic effects.

The dipole polarizabilities of the group 1 and group 2 elements are summarized in Tables 12.1 and 12.2, respectively. These values are the final recommended values which include all contributions including electron

correlation and relativistic effects as well as basis set effects. The values are very accurate and should be considered as future reference values.

	Alkali-metals	
M	$\alpha_D(M)$	$\alpha_D(M^+)$
K	291.1	5.52
Rb	316.2	9.11
Cs	396.0	15.76
Fr	315.2	20.38
E119	163.8	32.02

Table 12.1. Recommended dipole polarizabilities of the group 1 elements. All values are in a.u.

	Alkaline-earth metals		
M	$\alpha_D(M)$	$\alpha_D(M^+)$	$\alpha_D(M^{2+})$
Ca	158.6	75.9	3.26
Sr	199.4	91.1	5.80
Ba	273.5	122.7	10.53
Ra	246.2	104.0	13.74

Table 12.2. Recommended dipole polarizabilities of the group 2 elements. All values are in a.u.

Energy-adjusted scalar relativistic small-core pseudopotentials for the group 1 and group 2 elements with accompanying valence basis sets were presented. The performance of these pseudopotentials was tested for dipole polarizabilities and ionization potentials. Except for a few cases, the pseudopotential error remains below 1%.

Following atomic calculations, applications were made to molecular systems, utilizing these small-core pseudopotentials.

Selected spectroscopic constants of the alkali dimers from K_2 to Fr_2 clearly demonstrate the large relativistic contraction of the bonding σ-orbital for Fr_2. That is, the equilibrium bond length is monotonically increasing from K_2 to Cs_2 then it decreases for Fr_2. Also, the dissociation energy of Fr_2 is larger than that of

Cs_2, leading to an anomalous trend as was the case in the bond lengths. This is attributed to the relativistic contraction of valence *ns* orbital of Fr. The dipole polarizabilities of the dimers reflect such relativistic effects as well, where a monotonically increasing average dipole polarizability from K_2 to Cs_2 is followed by a decrease in the dipole polarizability for Fr_2. The dipole polarizabilities calculated in this thesis provide the most accurate theoretical values so far for the alkali dimers.

The properties of the M-NH_3 (M = K to Fr) complexes reveal more interesting aspects for these molecules. There is no anomaly in the trend of the (M-N) bond lengths caused by relativity. Rather, a straightforward upward trend in (M-N) bond lengths and a downward trend in dissociation energies were observed at the MP2 level of theory. As a qualitative description, this monotonic trend in both properties was related to the trend emerging from the orbital energy of the bonding σ- and the anti-bonding σ*-orbital. Relativistic effects were, however, evident in the vibrational frequencies of these complexes, where the red shift of the $\nu_1(A_1)$ stretching mode increases from K- to Cs-NH_3 while there is a decrease for Fr-NH_3. Also, the average dipole polarizabilities of these complexes show an increase from K- to Cs-NH_3 and a decrease for Fr-NH_3.

There is no question that the study of dipole polarizabilities for atoms and molecules is currently an active area of research. Many authors are now extending their interest in dipole polarizabilities to the main *p*-group elements including the rare gases. An interesting topic of research includes the dipole polarizabilities of open shell systems of the main group elements, which would require multi-reference techniques. Further work includes dipole polarizabilities of metallic clusters such as Cs_n and more precise calculation [CCSD(T)] of the dipole polarizabilities of the ammonia complexes.

Appendix A

Pseudopotential Parameters
Valence Basis sets
Core Polarization Potentials

		ARPP		SOPP	
l	j	C_{ljk}	γ_{ljk}	B_{ljk}	β_{ljk}
s	1/2	91.1449309562	6.8827987246		
p	1/2	9.6747284044	4.7268609354	-19.3494568087	4.7268609354
	3/2	20.5691419447	4.8452670859	20.5691419447	4.8452670859
d	3/2	-2.5426460757	8.7075426957	2.5426460757	8.7075426957
	5/2	-3.4640466626	8.3108395261	-2.3093644417	8.3108395261
	3/2	-2.5426460757	8.7075426957	2.5426460757	8.7075426957
	5/2	-3.4640466626	8.3108395261	-2.3093644417	8.3108395261
f	5/2	-16.5552815369	13.9396691527	11.0368543579	13.9396691527
	7/2	-36.6211530998	16.6295514183	-18.3105765499	16.6295514183

Table A.1. The pseudopotential parameters for K.

s exp.	coeff.	p exp.	coeff.	d exp.	f exp.
180.901	1.1900E-03	65.912	1.3160E-03	1.556	0.612
71.218	-5.0300E-04	24.599	2.4760E-03	0.612	0.223
29.384	2.6850E-03	9.882	1.4056E-02	0.223	0.081
8.699	6.9043E-02	4.117	-6.7812E-02	0.081	
3.473		1.556		0.030	
0.815		0.612			
0.319		0.223			
0.070		0.081			
0.035		0.030			
0.016		0.011			
0.008		0.004			

Table A.2. The valence basis set for K.

		ARPP		SOPP	
l	j	C_{ljk}	γ_{ljk}	B_{ljk}	β_{ljk}
s	1/2	89.5039495866	5.0316833770		
	1/2	0.4379036054	2.0151854344		
p	1/2	19.5204701963	4.3835444589	-39.0409403927	4.3835444589
	3/2	39.0389553574	4.3326592801	39.0389553574	4.3326592801
	1/2	0.1706093411	1.3742880878	-0.3412186822	1.3742880878
	3/2	0.4184998756	1.2257723910	0.4184998756	1.2257723910
d	3/2	10.4826612392	3.4156013715	-10.4826612392	3.4156013715
	5/2	15.7240602781	3.4128633664	10.4827068521	3.4128633664
	3/2	0.2660828384	1.0305048989	-0.2660828384	1.0305048989
	5/2	0.4088021844	1.0198721631	0.2725347896	1.0198721631
f	5/2	-4.4782844280	3.5744034088	2.9855229520	3.5744034088
	7/2	-5.9569075093	3.5657105906	-2.9784537546	3.5657105906

Table A.3. The pseudopotential parameters for Rb.

s exp.	coeff.	p exp.	coeff.	d exp.	f exp.	g exp.
240.217	1.5440E-03	46.598	3.0550E-03	0.859	2.432	0.722
106.111	-3.2750E-03	20.619	-8.2620E-03	0.608	0.722	
40.822	1.2417E-02	8.546	3.5584E-02	0.211	0.211	
18.695	-3.7286E-02	3.728	-1.2865E-01	0.071		
7.851	1.5438E-01	1.626		0.025		
3.946	-2.0471E-01	0.608				
1.844		0.211				
0.692		0.073				
0.277		0.025				
0.079		0.009				
0.039						
0.020						
0.010						

Table A.4. The valence basis set for Rb.

		ARPP		SOPP	
l	j	C_{ljk}	γ_{ljk}	B_{ljk}	β_{ljk}
s	1/2	84.5477223303	4.0811192132		
	1/2	16.6540349697	2.4215223834		
p	1/2	52.3496307434	5.5339726442	-104.6992614868	5.5339726442
	3/2	104.6994131784	5.5067943837	104.6994131784	5.5067943837
	1/2	8.8065577246	2.2809615797	-17.6131154493	2.2809615797
	3/2	17.6166111065	2.1034905048	17.6166111065	2.1034905048
d	3/2	5.2689855127	1.8131494101	-5.2689855127	1.8131494101
	5/2	7.9036419222	1.8077216837	5.2690946148	1.8077216837
	3/2	1.3364312806	0.8729040305	-1.3364312806	0.8729040305
	5/2	2.0056513277	0.8587202788	1.3371008851	0.8587202788
f	5/2	-16.4976542980	5.2170838603	10.9984361987	5.2170838603
	7/2	-23.3081313394	5.1481964790	-11.6540656697	5.1481964790
	5/2	-2.2368273458	1.5805994689	1.4912182305	1.5805994689
	7/2	-2.2269419523	1.3478959235	-1.1134709761	1.3478959235
g	7/2	-2.5041987223	1.8077398221	1.2520993612	1.8077398221
	9/2	-3.1382445239	1.8050613093	-1.2552978096	1.8050613093

Table A.5. The pseudopotential parameters for Cs.

s exp.	coeff.	p exp.	coeff.	d exp.	f exp.	g exp.
132.350	-5.8900E-04	38.617	3.2600E-04	0.916	0.916	0.916
67.030	2.5130E-03	18.515	-1.3410E-03	0.347	0.347	0.347
33.465	-6.2360E-03	9.139	1.8140E-03	0.134	0.134	
14.569	1.7078E-02	4.129	4.3747E-02	0.050		
7.459	-3.1642E-02	1.929		0.020		
3.001		0.812				
1.461		0.347				
0.402		0.134				
0.176		0.052				
0.046		0.020				
0.020		0.008				
0.009						

Table A.6. The valence basis set for Cs.

		ARPP		SOPP	
l	j	C_{ljk}	γ_{ljk}	B_{ljk}	β_{ljk}
s	1/2	84.5180870726	4.1883216710		
	1/2	16.0791763225	2.0327157095		
p	1/2	52.3518105852	5.2754619363	-104.7036211703	5.2754619363
	3/2	104.7051043940	5.0844250530	104.7051043940	5.0844250530
	1/2	8.8773326590	2.1469841485	-17.7546653179	2.1469841485
	3/2	18.0916927840	1.7332116980	18.0916927840	1.7332116980
d	3/2	5.2947750025	2.0791488560	-5.2947750025	2.0791488560
	5/2	7.9504027975	1.8864281963	5.3002685317	1.8864281963
	3/2	1.6324230520	0.6446109973	-1.6324230520	0.6446109973
	5/2	2.6241859029	0.6435923033	1.7494572686	0.6435923033
f	5/2	-6.9234644253	4.4144958812	4.6156429502	4.4144958812
	7/2	-9.0218190158	4.5020024499	-4.5109095079	4.5020024499
	5/2	-1.2584633859	0.9012335172	0.8389755906	0.9012335172
	7/2	-1.6392402167	0.8750939606	-0.8196201084	0.8750939606
g	7/2	-4.1273705712	1.5924322369	2.0636852856	1.5924322369
	9/2	-5.0045495613	1.5625770064	-2.0018198245	1.5625770064

Table A.7. The pseudopotential parameters for Fr.

s exp.	coeff.	p exp.	coeff.	d exp.	f exp.	g exp.
205.233	3.1500E-04	71.292	5.8500E-04	2.610	0.361	0.347
103.067	-1.4370E-03	36.898	-2.5770E-03	1.219	0.135	0.134
46.537	5.1380E-03	18.716	7.4880E-03	0.512	0.053	0.050
24.831	-1.1684E-02	9.524	-2.1315E-02	0.361	0.022	
11.069	3.2420E-02	4.832	6.7796E-02	0.135		
5.942	-6.5536E-02	2.292		0.053		
2.282		1.085		0.022		
1.192		0.361		0.010		
0.338		0.135				
0.152		0.047				
0.047		0.022				
0.022		0.010				
0.010		0.005				
0.005						

Table A.8. The valence basis set for Fr.

		ARPP		SOPP	
l	j	C_{ljk}	γ_{ljk}	B_{ljk}	β_{ljk}
s	1/2	100.4116127692	3.4495227720		
p	1/2	62.9679339001	4.2178270150	-125.9358678003	4.2178270150
	3/2	107.7414670032	3.0505335922	107.7414670032	3.0505335922
	1/2	9.1235910628	3.7548575042	-18.2471821255	3.7548575042
	3/2	17.9693197428	1.5368642497	17.9693197428	1.5368642497
d	3/2	4.1566008829	0.7342461002	-4.1566008829	0.7342461002
	5/2	3.0362451866	0.4999237513	2.0241634578	0.4999237513
	3/2	2.1258152423	3.3801573898	-2.1258152423	3.3801573898
	5/2	3.5012168352	3.8837295763	2.3341445568	3.8837295763
f	5/2	1.0308932630	2.9305938562	-0.6872621753	2.9305938562
	7/2	1.9993664340	2.4601922125	0.9996832170	2.4601922125
	5/2	-0.2683039020	0.1977099322	0.1788692680	0.1977099322
	7/2	-0.3650353169	0.1971938855	-0.1825176584	0.1971938855
g	7/2	-96.7309309556	10.8946707624	48.3654654778	10.8946707624
	9/2	-124.0113520081	10.8802972889	-49.6045408032	10.8802972889
	7/2	-8.1619529005	1.5826469575	4.0809764503	1.5826469575
	9/2	-9.4553677586	1.5095826843	-3.7821471035	1.5095826843

Table A.9. The pseudopotential parameters for E119.

s exp.	coeff.	p exp.	coeff.	d exp.	f exp.	g exp.
326.050	-5.0300E-04	160.473	4.0500E-04	9.562	3.000	3.000
170.985	2.2330E-03	85.590	-1.9150E-03	4.900	1.000	1.000
84.216	-6.9910E-03	45.796	5.5650E-03	2.316	0.300	0.300
45.853	1.3680E-02	24.795	-1.3085E-02	1.095	0.100	0.100
20.198	-3.4946E-02	13.490	2.7637E-02	0.460	0.030	0.030
11.063	7.1871E-02	7.083	-6.4908E-02	0.193		
5.057	-1.5261E-01	3.769		0.081		
2.114		1.757		0.040		
1.095		0.856		0.015		
0.266		0.291		0.005		
0.137		0.113				
0.038		0.044				
0.013		0.017				
0.005		0.005				
0.002		0.002				

Table A.10. The valence basis set for E119.

	α_D	δ
Cs	0.69	1.4702
Fr	1.25	1.1636
E119	2.25	0.5726

Table A.11. The core polarization potentials parameters for Cs, Fr, and E119.

		ARPP		SOPP	
l	j	C_{ljk}	γ_{ljk}	B_{ljk}	β_{ljk}
s	1/2	138.8327287452	10.5560584024		
	1/2	16.7548245987	5.2931549074		
p	1/2	27.6616076106	12.7145714450	-55.3232152213	12.7145714450
	3/2	55.2978625759	12.8785160568	55.2978625759	12.8785160568
	1/2	4.2109743066	4.1479236216	-8.4219486132	4.1479236216
	3/2	7.6274825862	3.8412874573	7.6274825862	3.8412874573
d	3/2	-0.5143247165	4.7032641363	0.5143247165	4.7032641363
	5/2	-0.7651847993	4.7079758980	-0.5101231996	4.7079758980
	3/2	-6.4906215843	13.6961514500	6.4906215843	13.6961514500
	5/2	-9.7355555579	13.6981651075	-6.4903703720	13.6981651075
f	5/2	-14.0001482366	14.8200191370	9.3334321578	14.8200191370
	7/2	-61.6160663319	22.0008032389	-30.8080331659	22.0008032389

Table A.12. The pseudopotential parameters for Ca.

s exp.	p exp.	d exp.
113.083	87.341	3.108
44.702	38.552	1.045
16.203	17.862	0.414
7.133	8.496	0.213
3.108	4.112	0.070
1.045	1.911	0.030
0.414	0.891	0.018
0.213	0.407	
0.070	0.171	
0.030	0.068	
0.018	0.030	
0.007	0.015	

Table A.13. The valence basis set for Ca.

		ARPP		SOPP	
l	j	C_{ljk}	γ_{ljk}	B_{ljk}	β_{ljk}
s	s:	135.2710429087	6.9334609897		
	s:	17.9440714020	4.1140038325		
p	1/2	29.4380813451	7.2168166232	-58.8761626902	7.2168166232
	3/2	58.8806748628	7.1736961720	58.8806748628	7.1736961720
	1/2	4.9362826922	3.0227988173	-9.8725653845	3.0227988173
	3/2	9.7233520709	2.8656990305	9.7233520709	2.8656990305
d	3/2	11.9072391870	6.3215146002	-11.9072391870	6.3215146002
	5/2	17.8595514400	6.3914994947	11.9063676267	6.3914994947
	3/2	2.1991802261	1.7697265969	-2.1991802261	1.7697265969
	5/2	2.8935708661	1.6367716651	1.9290472441	1.6367716651
f	5/2	-5.5093332540	4.2441983960	3.6728888360	4.2441983960
	7/2	-7.3046416929	4.2291644711	-3.6523208464	4.2291644711

Table A.14. The pseudopotential parameters for Sr.

s exp.	coeff.	p exp.	coeff.	d exp.	f exp.	g exp.
328.348	-5.6000E-05	49.173	1.2050E-03	1.429	2.130	1.429
140.488	5.6900E-04	23.367	-5.2230E-03	0.471	0.807	
63.335	-1.6420E-03	10.429	2.8513E-02	0.166	0.311	
27.720	6.0270E-03	4.892	-9.7735E-02	0.077	0.127	
12.767	-4.4662E-02	2.130		0.032		
6.370	3.3289E-01	0.807				
3.404	-7.3847E-01	0.311				
1.429		0.127				
0.471		0.047				
0.166		0.018				
0.077		0.008				
0.032						
0.016						
0.007						

Table A.15. The valence basis set for Sr.

		ARPP		SOPP	
l	j	C_{ljk}	γ_{ljk}	B_{ljk}	β_{ljk}
s	1/2	84.7854575830	4.1779315870		
	1/2	17.3727090408	2.5226327996		
p	1/2	52.5122257430	6.2941193507	-105.0244514859	6.2941193507
	3/2	105.0226686473	6.4764577461	105.0226686473	6.4764577461
	1/2	8.7070149366	2.2843266466	-17.4140298731	2.2843266466
	3/2	17.1654588321	2.0915552007	17.1654588321	2.0915552007
d	3/2	5.3465356794	1.9252917446	-5.3465356794	1.9252917446
	5/2	8.0257207417	1.8785341179	5.3504804945	1.8785341179
	3/2	1.3462950814	0.9070887265	-1.3462950814	0.9070887265
	5/2	2.0637104527	0.9100609530	1.3758069685	0.9100609530
f	5/2	-20.0032234715	6.2563216686	13.3354823143	6.2563216686
	7/2	-26.1182147485	6.1341358367	-13.0591073742	6.1341358367
	5/2	-2.3444579892	1.6413827845	1.5629719928	1.6413827845
	7/2	-2.9808674802	1.5993433158	-1.4904337401	1.5993433158
g	7/2	-3.3166027586	2.1423810008	1.6583013793	2.1423810008
	9/2	-4.2756470183	2.1599811094	-1.7102588073	2.1599811094

Table A.16. The pseudopotential parameters for Ba.

s exp.	coeff.	p exp.	coeff.	d exp.	f exp.	g exp.
114.075	1.8680E-03	51.225	-8.8000E-05	1.304	1.365	0.565
52.874	-8.7520E-03	24.862	4.6400E-04	0.565	0.642	0.252
25.187	2.9840E-02	12.277	-3.4090E-03	0.252	0.273	
12.287	-8.6380E-02	5.959	3.2871E-02	0.105	0.106	
5.951	2.1877E-01	2.811		0.046		
2.808		1.365		0.020		
1.304		0.642				
0.565		0.273				
0.252		0.106				
0.105		0.028				
0.046		0.011				
0.020		0.005				
0.008						

Table A.17. The valence basis set for Ba.

		ARPP		SOPP	
l	j	C_{ljk}	γ_{ljk}	B_{ljk}	β_{ljk}
s	1/2	84.5539661355	4.0507301896		
	1/2	16.5708711741	2.1831253933		
p	1/2	52.3551054236	4.9122574939	-104.7102108472	4.9122574939
	3/2	104.7052976899	5.0286256617	104.7052976899	5.0286256617
	1/2	8.9451694396	2.2745077053	-17.8903388792	2.2745077053
	3/2	18.1068641548	1.7766526853	18.1068641548	1.7766526853
d	3/2	5.3001157565	1.8635297993	-5.3001157565	1.8635297993
	5/2	7.9705701222	1.6039711060	5.3137134148	1.6039711060
	3/2	1.6804663600	0.6904072503	-1.6804663600	0.6904072503
	5/2	2.8245100599	0.7327167503	1.8830067066	0.7327167503
f	5/2	6.5196913540	8.1031058777	-4.3464609027	8.1031058777
	7/2	9.5105813792	7.8694467660	4.7552906896	7.8694467660
	5/2	-2.9220600625	1.3940555886	1.9480400417	1.3940555886
	7/2	-3.6573636695	1.3371451524	-1.8286818347	1.3371451524
g	7/2	-5.3359111934	1.8579397932	2.6679555967	1.8579397932
	9/2	-6.4501248892	1.8216095858	-2.5800499557	1.8216095858

Table A.18. The pseudopotential parameters for Ra.

s exp.	coeff.	p exp.	coeff.	d exp.	f exp.	g exp.
212.705	-5.4900E-04	85.158	6.2000E-04	3.098	1.139	0.597
103.894	3.2790E-03	43.001	-2.8030E-03	1.431	0.418	0.254
52.166	-1.0178E-02	21.623	8.2660E-03	0.597	0.156	0.110
26.452	2.5662E-02	10.784	-2.3706E-02	0.254	0.071	
13.233	-5.8675E-02	5.342	7.2636E-02	0.110		
6.604	1.0225E-01	2.471		0.048		
3.098		1.139		0.021		
1.431		0.418		0.009		
0.597		0.156				
0.254		0.071				
0.110		0.029				
0.048		0.013				
0.021		0.006				
0.009		0.003				
0.004						

Table A.19. The valence basis set for Ra.

Appendix B

All-electron Basis Sets

s exp.	coeff.			p exp.	coeff	
151351.900	-8.7454E-04	2.5386E-04	8.3635E-05	868.390	2.6765E-03	-8.2093E-04
22745.910	-3.2878E-03	9.5247E-04	3.1459E-04	205.577	1.9471E-02	-5.9683E-03
5227.166	-1.2346E-02	3.6426E-03	1.1981E-03	65.912	8.7854E-02	-2.7788E-02
1500.188	-4.3425E-02	1.2820E-02	4.2593E-03	24.599	2.5129E-01	-8.1424E-02
495.470	-1.3084E-01	4.1675E-02	1.3754E-02	9.882		
180.901	-3.0021E-01	1.0401E-01	3.5369E-02	4.117		
71.218	-4.1559E-01	2.0564E-01	7.0296E-02	1.556		
29.384	-2.3340E-01	1.2868E-01	5.0153E-02	0.612		
8.699				0.223		
3.473				0.081		
0.815				0.030		
0.319				0.011		
0.070				0.004		
0.035				0.002		
0.016						
0.008						
0.003						

Tabel B.1. The relativistic basis set for K.

d exp.	f exp.
4.117	4.117
1.556	1.556
0.612	0.612
0.223	0.223
0.081	0.081
0.030	
0.011	

Tabel B.1. The relativistic basis set for K continued.

s exp.	coeff.			
1843444.800	7.5265E-04	2.4529E-04	-9.9694E-05	3.3725E-05
307240.800	2.1720E-03	7.1060E-04	-2.8888E-04	9.7718E-05
61448.160	7.3853E-03	2.4261E-03	-9.8740E-04	3.3416E-04
15362.040	2.2319E-02	7.4539E-03	-3.0368E-03	1.0273E-03
4506.950	6.5755E-02	2.2458E-02	-9.1959E-03	3.1167E-03
1533.262	1.6782E-01	6.1817E-02	-2.5483E-02	8.6302E-03
581.096	3.3034E-01	1.3887E-01	-5.8657E-02	2.0005E-02
240.217	3.8043E-01	2.2503E-01	-9.8758E-02	3.3700E-02
106.111	1.7669E-01	9.1990E-02	-4.4260E-02	1.5748E-02
40.822	1.5266E-02	-4.8092E-01	3.1246E-01	-1.1537E-01
18.695	-2.3595E-03	-5.7636E-01	5.3980E-01	-2.0723E-01
7.851				
3.946				
1.844				
0.692				
0.277				
0.079				
0.039				
0.020				
0.010				
0.003				
0.001				

Tabel B.2. The relativistic basis set for Rb.

p exp.	coeff.			d exp.	coeff.	f exp.	g exp.
3772.360	3.6635E-03	-1.5286E-03	4.5698E-04	132.333	2.0199E-02	17.659	17.659
896.850	2.1685E-02	-9.0863E-03	2.7070E-03	38.801	1.1910E-01	6.360	6.360
291.177	9.3412E-02	-4.0634E-02	1.2237E-02	14.105	3.2811E-01	2.432	2.432
111.167	2.6328E-01	-1.1901E-01	3.5772E-02	5.537		0.722	0.722
46.598	4.3340E-01	-2.1528E-01	6.6527E-02	2.240		0.211	0.211
20.619	3.1698E-01	-9.1340E-02	2.2294E-02	0.859		0.071	
8.546				0.608		0.025	
3.728				0.211		0.009	
1.626				0.071			
0.608				0.025			
0.211				0.009			
0.073							
0.025							
0.009							
0.003							

Tabel B.2. The relativistic basis set for Rb continued.

s exp.	coeff.				p exp.	coeff.		
25325100000.000	3.5024E-06	-1.2243E-06	5.5204E-07	-2.5439E-07	141690.346	2.7905E-04	1.3252E-04	-5.9585E-05
3088422749.000	1.2032E-05	-4.2060E-06	1.8966E-06	-8.7392E-07	28338.069	1.1205E-03	5.3432E-04	-2.4008E-04
428947604.000	4.9586E-05	-1.7333E-05	7.8154E-06	-3.6014E-06	7084.517	5.0472E-03	2.4180E-03	-1.0904E-03
68086921.270	1.3983E-04	-4.8898E-05	2.2051E-05	-1.0161E-05	2299.177	1.9015E-02	9.2261E-03	-4.1548E-03
14379440.230	4.6106E-04	-1.6132E-04	7.2750E-05	-3.3526E-05	877.156	6.4025E-02	3.1697E-02	-1.4409E-02
2579050.047	1.4489E-03	-5.0801E-04	2.2920E-04	-1.0561E-04	370.648	1.7313E-01	8.9574E-02	-4.0820E-02
614059.535	3.4460E-03	-1.2121E-03	5.4693E-04	-2.5213E-04	167.623	3.3619E-01	1.8401E-01	-8.5773E-02
173927.900	8.0075E-03	-2.8370E-03	1.2825E-03	-5.9095E-04	79.458	3.8317E-01	2.1263E-01	-9.7149E-02
56739.082	1.7204E-02	-6.1524E-03	2.7810E-03	-1.2835E-03	38.617	1.8698E-01	-6.7149E-02	5.3156E-02
20481.202	3.7847E-02	-1.3832E-02	6.2888E-03	-2.8978E-03	18.515	2.3242E-02	-5.2781E-01	3.6966E-01
7896.413	7.9672E-02	-2.9995E-02	1.3640E-02	-6.3154E-03	9.139	3.3173E-04	-4.5289E-01	2.9175E-01
3310.821	1.5694E-01	-6.3316E-02	2.9293E-02	-1.3513E-02	4.129			
1442.310	2.7635E-01	-1.2446E-01	5.8033E-02	-2.7115E-02	1.929			
654.023	3.4120E-01	-1.9572E-01	9.6491E-02	-4.4840E-02	0.812			
304.041	2.2556E-01	-1.4542E-01	7.1782E-02	-3.4982E-02	0.347			
132.350	3.9953E-02	2.3706E-01	-1.5542E-01	8.1492E-02	0.134			
67.030	-3.4561E-03	5.7695E-01	-5.4704E-01	2.8700E-01	0.052			
33.465	1.5782E-03	3.3651E-01	-3.1196E-01	1.9921E-01	0.020			
14.569					0.008			
7.459								
3.001								
1.461								
0.402								
0.176								
0.046								
0.020								
0.009								

Tabel B.3. The relativistic basis set for Cs. Continued on the following page.

d exp.	coeff.		f exp.	g exp.
638.157	-7.4957E-03	3.2541E-03	30.342	5.623
191.608	-5.1962E-02	2.2934E-02	13.239	2.373
72.488	-1.9658E-01	8.7971E-02	5.623	0.916
30.342	-4.1117E-01	1.8392E-01	2.373	0.347
13.239	-4.2581E-01	1.3772E-01	0.916	0.134
5.623	-1.3577E-01	-2.8272E-01	0.347	
2.373			0.134	
0.916			0.050	
0.347			0.020	
0.134			0.008	
0.050				
0.020				
0.008				

Tabel B.3. The relativistic basis set for Cs. Continued from the previous page.

s exp.	coeff.				
358861000000.000	-6.6731E-06	-2.6970E-06	1.3081E-06	6.6992E-07	-3.1780E-07
44857600000.000	-2.0503E-05	-8.2830E-06	4.0170E-06	2.0572E-06	-9.7589E-07
6144876662.000	-7.3109E-05	-2.9522E-05	1.4317E-05	7.3321E-06	-3.4782E-06
903658332.600	-2.3202E-04	-9.3664E-05	4.5418E-05	2.3260E-05	-1.1034E-05
150609722.100	-6.8672E-04	-2.7723E-04	1.3445E-04	6.8852E-05	-3.2663E-05
28416928.700	-1.7719E-03	-7.1587E-04	3.4717E-04	1.7780E-04	-8.4342E-05
6458392.886	-4.1596E-03	-1.6843E-03	8.1731E-04	4.1861E-04	-1.9860E-04
1655998.176	-8.8478E-03	-3.5978E-03	1.7465E-03	8.9473E-04	-4.2442E-04
501817.629	-1.7352E-02	-7.1144E-03	3.4605E-03	1.7732E-03	-8.4151E-04
163704.385	-3.4008E-02	-1.4124E-02	6.8776E-03	3.5268E-03	-1.6729E-03
59092.583	-6.0936E-02	-2.5911E-02	1.2695E-02	6.5142E-03	-3.0945E-03
23042.147	-1.0819E-01	-4.7590E-02	2.3364E-02	1.2015E-02	-5.6965E-03
9552.227	-1.7960E-01	-8.4125E-02	4.2061E-02	2.1663E-02	-1.0321E-02
4161.732	-2.6770E-01	-1.3710E-01	6.8842E-02	3.5695E-02	-1.6899E-02
1888.067	-3.0600E-01	-1.8154E-01	9.6157E-02	4.9989E-02	-2.4052E-02
881.063	-2.0472E-01	-9.3806E-02	4.0637E-02	2.0972E-02	-9.3319E-03
405.734	-4.4577E-02	2.6128E-01	-1.9790E-01	-1.1643E-01	5.5480E-02
205.233	1.1714E-03	5.5226E-01	-5.8601E-01	-3.5941E-01	1.8305E-01
103.067	-9.6204E-04	3.1911E-01	-2.4073E-01	-1.6018E-01	7.3596E-02
46.537	5.3807E-04	2.2888E-02	8.2455E-01	9.6570E-01	-5.4853E-01
24.831	-3.0663E-04	8.0751E-04	4.8651E-01	5.5915E-01	-3.7776E-01
11.069					
5.942					
2.282					
1.192					
0.338					
0.152					
0.047					
0.022					
0.010					
0.005					

Tabel B.4. The relativistic basis set for Fr. Continued on the following page.

p exp.	coeff.				d exp.	coeff.	
492909.300	7.2627E-04	-3.8148E-04	-1.9563E-04	8.8755E-05	26669.612	7.2452E-05	3.9484E-05
98581.860	2.1811E-03	-1.1522E-03	-5.9163E-04	2.6840E-04	7408.226	9.5667E-04	5.2165E-04
25277.400	7.3566E-03	-3.9138E-03	-2.0134E-03	9.1461E-04	1852.056	7.4017E-03	4.0708E-03
8154.385	2.1276E-02	-1.1472E-02	-5.9190E-03	2.6865E-03	724.226	3.0983E-02	1.7168E-02
3117.418	5.8509E-02	-3.2133E-02	-1.6664E-02	7.5925E-03	321.815	1.0537E-01	5.9616E-02
1322.346	1.4364E-01	-8.1755E-02	-4.2748E-02	1.9442E-02	154.434	2.4899E-01	1.4212E-01
602.971	2.8308E-01	-1.6824E-01	-8.9111E-02	4.0892E-02	77.502	3.8482E-01	2.1160E-01
289.498	3.7513E-01	-2.2934E-01	-1.2194E-01	5.5396E-02	40.092	3.1823E-01	8.0209E-02
143.958	2.5668E-01	-4.4389E-02	-1.2147E-03	-1.1618E-03	20.710	1.1095E-01	-3.0393E-01
71.292	5.9317E-02	4.2796E-01	3.5549E-01	-1.8368E-01	10.586	9.4963E-03	-5.1783E-01
36.898	-3.5414E-04	5.2562E-01	4.3828E-01	-2.1529E-01	5.390		
18.716	1.1036E-03	1.5993E-01	-2.7312E-01	2.0322E-01	2.610		
9.524	-7.3006E-04	4.4073E-03	-7.1430E-01	6.0554E-01	1.219		
4.832					0.512		
2.292					0.361		
1.085					0.135		
0.361					0.053		
0.135					0.022		
0.047					0.010		
0.022							
0.010							

Tabel B.4. The relativistic basis set for Fr. Continued on the following page.

f exp.	coeff.	g exp.
635.258	-1.8644E-03	13.239
222.351	-1.4678E-02	5.623
95.785	-6.4510E-02	2.373
45.079	-1.8216E-01	0.916
22.206		0.347
10.996		0.134
5.390		0.050
2.610		
1.219		
0.512		
0.361		
0.135		
0.053		
0.022		

Tabel B.4. The relativistic basis set for Fr. Continued from the previous page.

s exp.	coeff.				
1080933000.000	-2.6563E-03	1.3150E-03	-6.5742E-04	-3.5671E-04	-1.9682E-04
216186600.000	-3.6644E-03	1.8146E-03	-9.0731E-04	-4.9231E-04	-2.7165E-04
51473000.000	-8.6479E-03	4.2833E-03	-2.1418E-03	-1.1622E-03	-6.4126E-04
13359000.000	-1.4098E-02	6.9920E-03	-3.4973E-03	-1.8978E-03	-1.0472E-03
4329700.000	-2.2091E-02	1.0983E-02	-5.4965E-03	-2.9832E-03	-1.6461E-03
1510600.000	-3.5400E-02	1.7680E-02	-8.8560E-03	-4.8075E-03	-2.6532E-03
558770.000	-5.5132E-02	2.7743E-02	-1.3918E-02	-7.5586E-03	-4.1715E-03
213270.000	-8.5595E-02	4.3595E-02	-2.1923E-02	-1.1913E-02	-6.5772E-03
83861.000	-1.2873E-01	6.6785E-02	-3.3704E-02	-1.8335E-02	-1.0122E-02
33798.000	-1.8648E-01	9.9280E-02	-5.0363E-02	-2.7424E-02	-1.5156E-02
13953.000	-2.4827E-01	1.3570E-01	-6.9087E-02	-3.7683E-02	-2.0804E-02
5899.500	-2.7559E-01	1.4521E-01	-7.2444E-02	-3.9171E-02	-2.1648E-02
2565.800	-2.0452E-01	3.4868E-02	6.7345E-04	3.4248E-03	2.6098E-03
1145.800	-6.5862E-02	-2.8751E-01	2.4773E-01	1.5545E-01	8.9147E-02
537.560	-2.4870E-03	-5.2490E-01	5.2875E-01	3.4722E-01	2.0476E-01
262.870	-1.0693E-03	-2.6542E-01	1.6381E-01	8.7190E-02	4.3294E-02
132.780	8.2433E-04	-2.2087E-02	-7.3710E-01	-8.9941E-01	-6.2963E-01
68.405	-5.7668E-04	-1.8682E-03	-5.4704E-01	-7.4748E-01	-5.8796E-01
35.201	4.0673E-04	1.2256E-03	-4.4426E-02	9.4379E-01	1.2491E+00
18.468					
9.386					
4.692					
2.173					
0.985					
0.403					
0.172					
0.078					
0.039					
0.020					
0.009					

Tabel B.5. The relativistic basis set for E119. Continued on the following page.

p exp.	coeff.				d exp.	coeff.		
49075000.000	1.3228E-04	-7.3500E-05	-4.0875E-05	-2.2237E-05	213270.000	2.9224E-05	1.8051E-05	9.6875E-06
14407000.000	1.6006E-04	-8.9057E-05	-4.9547E-05	-2.6953E-05	83861.000	6.4544E-05	3.9988E-05	2.1215E-05
4537700.000	4.5455E-04	-2.5318E-04	-1.4089E-04	-7.6665E-05	33798.000	2.6564E-04	1.6458E-04	8.8581E-05
1521500.000	8.5286E-04	-4.7617E-04	-2.6516E-04	-1.4428E-04	13953.000	9.7241E-04	6.0524E-04	3.2229E-04
535880.000	1.8741E-03	-1.0498E-03	-5.8504E-04	-3.1854E-04	5899.500	3.7097E-03	2.3152E-03	1.2462E-03
196240.000	3.9170E-03	-2.2041E-03	-1.2300E-03	-6.6954E-04	2565.800	1.4356E-02	9.0356E-03	4.8364E-03
74207.000	8.6771E-03	-4.9172E-03	-2.7488E-03	-1.4984E-03	1145.800	5.0696E-02	3.2246E-02	1.7427E-02
28894.000	1.9542E-02	-1.1177E-02	-6.2654E-03	-3.4139E-03	537.560	1.4606E-01	9.4557E-02	5.1035E-02
11658.000	4.4771E-02	-2.5997E-02	-1.4626E-02	-7.9923E-03	262.870	3.0764E-01	1.9842E-01	1.0782E-01
4903.400	1.0043E-01	-5.9515E-02	-3.3694E-02	-1.8403E-02	132.780	3.9726E-01	2.2326E-01	1.1269E-01
2154.600	2.0555E-01	-1.2556E-01	-7.1619E-02	-3.9336E-02	68.405	2.4558E-01	-8.1708E-02	-9.2030E-02
987.430	3.3658E-01	-2.1007E-01	-1.2071E-01	-6.6082E-02	35.201	5.0974E-02	-5.1587E-01	-4.0998E-01
469.550	3.4704E-01	-1.7851E-01	-9.2636E-02	-4.9701E-02	18.468			
229.880	1.5640E-01	1.9084E-01	1.9024E-01	1.2246E-01	9.386			
114.890	1.5658E-02	5.8384E-01	5.5439E-01	3.4777E-01	4.692			
57.947	8.5502E-04	3.2978E-01	7.1232E-02	-9.6788E-03	2.173			
29.643	-7.2713E-04	2.8623E-02	-7.6548E-01	-8.3192E-01	0.985			
15.300					0.403			
7.849					0.172			
3.926					0.078			
1.790					0.039			
0.869					0.020			
0.366					0.009			
0.160								
0.067								
0.033								
0.016								
0.008								
0.004								

Tabel B.5. The relativistic basis set for E119. Continued on the following page.

f exp.	g exp.
11658.000	132.780
4903.400	68.405
2154.600	35.201
987.430	18.468
469.550	9.386
229.880	4.692
114.890	2.173
57.947	0.985
29.643	0.403
15.300	0.172
7.849	0.078
3.926	
1.790	
0.869	
0.366	
0.160	
0.067	

Tabel B.5. The relativistic basis set for E119. Continued from the previous page.

s exp.	p exp.	d exp.	f exp.
1104576.757	7461.547	21.915	9.528
480250.764	3244.151	9.528	4.143
208804.680	1410.500	4.143	1.801
90784.643	613.261	1.801	0.783
39471.584	266.635	0.783	0.340
17161.558	115.928	0.340	
7461.547	50.404	0.148	
3244.151	21.915		
1410.500	9.528		
613.261	4.143		
266.635	1.801		
115.928	0.783		
50.404	0.340		
21.915	0.148		
9.528	0.064		
4.143			
1.801			
0.783			
0.340			
0.148			
0.064			

Tabel B.6. The nonrelativistic and relativistic basis sets for Li^+, Na^+, and K^+.

s exp.	p exp.	d exp.	f exp.	g exp.
1104576.757	7461.547	266.635	4.143	1.801
480250.764	3244.151	115.928	1.801	0.783
208804.680	1410.500	50.404	0.783	0.340
90784.643	613.261	21.915	0.340	
39471.584	266.635	9.528	0.148	
17161.558	115.928	4.143		
7461.547	50.404	1.801		
3244.151	21.915	0.783		
1410.500	9.528	0.340		
613.261	4.143	0.148		
266.635	1.801	0.064		
115.928	0.783			
50.404	0.340			
21.915	0.148			
9.528	0.064			
4.143				
1.801				
0.783				
0.340				
0.148				
0.064				

Tabel B.7. The nonrelativistic and relativistic basis sets for Rb^+.

s exp.	coeff.				p exp.	coeff.		
1104576.757	-2.7018E-04	8.8224E-05	-3.9466E-05	1.8228E-05	39471.584	1.2308E-04	5.8304E-05	-2.6421E-05
480250.764	-8.9435E-05	2.7965E-05	-1.3236E-05	5.9576E-06	17161.558	2.8158E-04	1.2999E-04	-5.7277E-05
208804.680	-1.1910E-03	3.9208E-04	-1.7389E-04	8.0647E-05	7461.547	1.4628E-03	6.9674E-04	-3.1655E-04
90784.643	-2.3284E-03	7.5104E-04	-3.4310E-04	1.5699E-04	3244.151	5.8315E-03	2.7437E-03	-1.2248E-03
39471.584	-7.5421E-03	2.5028E-03	-1.1102E-03	5.1521E-04	1410.500	2.2959E-02	1.1077E-02	-5.0222E-03
17161.558	-1.9879E-02	6.5432E-03	-2.9824E-03	1.3683E-03	613.261	8.1933E-02	4.0363E-02	-1.8249E-02
7461.547	-5.3934E-02	1.8560E-02	-8.2969E-03	3.8508E-03	266.635	2.3406E-01	1.2256E-01	-5.6443E-02
3244.151	-1.3294E-01	4.7779E-02	-2.2005E-02	1.0132E-02	115.928	4.3757E-01	2.4663E-01	-1.1485E-01
1410.500	-2.7773E-01	1.1591E-01	-5.3342E-02	2.4904E-02	50.404	3.3986E-01	1.3027E-01	-5.3589E-02
613.261	-3.9358E-01	2.1407E-01	-1.0544E-01	4.9158E-02	21.915			
266.635	-2.3573E-01	1.9355E-01	-9.9728E-02	4.8563E-02	9.528			
115.928	-2.0940E-02	-3.3511E-01	2.1732E-01	-1.1149E-01	4.143			
50.404	-2.6973E-03	-7.0259E-01	7.4012E-01	-4.0483E-01	1.801			
21.915					0.783			
9.528					0.340			
4.143					0.148			
1.801					0.064			
0.783								
0.340								
0.148								
0.064								

Tabel B.8. The nonrelativistic basis set for Cs^+. Continued on the following page.

d exp.	coeff.		f exp.	g exp.
1410.500	8.7291E-04	3.7151E-04	21.915	1.801
613.261	3.8364E-03	1.7057E-03	9.528	0.783
266.635	2.1375E-02	9.2741E-03	4.143	0.340
115.928	9.0865E-02	4.0806E-02	1.801	
50.404	2.7115E-01	1.2188E-01	0.783	
21.915			0.340	
9.528			0.148	
4.143				
1.801				
0.783				
0.340				
0.148				
0.064				

Tabel B.8. The nonrelativistic basis set for Cs^+. Continued from the previous page.

s exp.	coeff.				p exp.	coeff.		
1104576.757	4.4997E-03	-1.5780E-03	7.1173E-04	3.2802E-04	39471.584	9.3510E-04	4.4538E-04	2.0063E-04
480250.764	-1.6885E-03	5.8924E-04	-2.6490E-04	-1.2213E-04	17161.558	4.9651E-04	2.3588E-04	1.0456E-04
208804.680	9.0729E-03	-3.2010E-03	1.4433E-03	6.6549E-04	7461.547	3.7600E-03	1.8068E-03	8.1845E-04
90784.643	5.6130E-03	-2.0051E-03	9.1248E-04	4.2021E-04	3244.151	9.0151E-03	4.3356E-03	1.9416E-03
39471.584	2.1350E-02	-7.6863E-03	3.4676E-03	1.6008E-03	1410.500	3.0944E-02	1.5176E-02	6.8971E-03
17161.558	3.4489E-02	-1.2615E-02	5.7604E-03	2.6548E-03	613.261	9.4421E-02	4.7368E-02	2.1448E-02
7461.547	7.9031E-02	-3.0022E-02	1.3625E-02	6.3039E-03	266.635	2.4864E-01	1.3162E-01	6.0735E-02
3244.151	1.5555E-01	-6.2338E-02	2.8903E-02	1.3357E-02	115.928	4.3474E-01	2.4446E-01	1.1340E-01
1410.500	2.8815E-01	-1.3196E-01	6.1544E-02	2.8672E-02	50.404	3.2049E-01	9.9346E-02	3.6550E-02
613.261	3.6627E-01	-2.1038E-01	1.0406E-01	4.8657E-02	21.915			
266.635	2.0519E-01	-1.3477E-01	6.6812E-02	3.2140E-02	9.528			
115.928	1.6106E-02	4.1106E-01	-2.8596E-01	-1.4672E-01	4.143			
50.404	2.8716E-03	6.5193E-01	-7.0539E-01	-3.9182E-01	1.801			
21.915					0.783			
9.528					0.340			
4.143					0.148			
1.801					0.064			
0.783								
0.340								
0.148								
0.064								

Tabel B.9. The relativistic basis set for Cs^+. Continued on the following page.

d exp.	coeff.		f exp.	g exp.
1410.500	-1.2516E-03	-5.3498E-04	21.915	1.801
613.261	-4.4095E-03	-1.9555E-03	9.528	0.783
266.635	-2.3149E-02	-1.0033E-02	4.143	0.340
115.928	-9.3255E-02	-4.1791E-02	1.801	
50.404	-2.7210E-01	-1.2164E-01	0.783	
21.915			0.340	
9.528			0.148	
4.143				
1.801				
0.783				
0.340				
0.148				
0.064				

Tabel B.9. The relativistic basis set for Cs^+. Continued from the previous page.

s exp.	coeff.				
5843211.046	1.0651E-04	3.5547E-05	-1.7065E-05	8.7595E-06	4.1138E-06
2540526.542	3.5009E-05	1.2173E-05	-5.6599E-06	2.6458E-06	1.2914E-06
1104576.757	4.7009E-04	1.5596E-04	-7.5274E-05	3.9187E-05	1.8300E-05
480250.764	9.1970E-04	3.1214E-04	-1.4813E-04	7.3548E-05	3.5010E-05
208804.680	3.0011E-03	9.9855E-04	-4.8244E-04	2.5152E-04	1.1740E-04
90784.643	8.0070E-03	2.7300E-03	-1.3007E-03	6.5112E-04	3.0898E-04
39471.584	2.2434E-02	7.6188E-03	-3.6860E-03	1.9152E-03	8.9560E-04
17161.558	5.9321E-02	2.1060E-02	-1.0117E-02	5.0945E-03	2.4143E-03
7461.547	1.4559E-01	5.4502E-02	-2.6743E-02	1.3911E-02	6.5182E-03
3244.151	2.9603E-01	1.3020E-01	-6.4770E-02	3.2923E-02	1.5632E-02
1410.500	3.9394E-01	2.3224E-01	-1.2334E-01	6.5725E-02	3.0896E-02
613.261	2.0453E-01	1.6724E-01	-9.6369E-02	4.8783E-02	2.3870E-02
266.635	1.0597E-02	-4.5670E-01	3.5707E-01	-1.9852E-01	-9.7972E-02
115.928	3.1450E-03	-6.7134E-01	8.3441E-01	-5.7284E-01	-2.8492E-01
50.404	-2.2998E-03	-8.4236E-02	-5.8369E-01	6.2319E-01	3.3474E-01
21.915					
9.528					
4.143					
1.801					
0.783					
0.340					
0.148					
0.064					

Tabel B.10. The nonrelativistic basis set for Fr^+. Continued on the following page.

p exp.	coeff.				d exp.	coeff.		
208804.680	3.5280E-05	1.8658E-05	9.0741E-06	4.2044E-06	7461.547	2.1628E-04	-1.1786E-04	-4.6760E-05
90784.643	7.9710E-05	3.7452E-05	2.0982E-05	9.0768E-06	3244.151	1.0519E-03	-5.6161E-04	-2.3487E-04
39471.584	4.2473E-04	2.2665E-04	1.0936E-04	5.0890E-05	1410.500	6.2962E-03	-3.4402E-03	-1.3870E-03
17161.558	1.7135E-03	8.4996E-04	4.4948E-04	2.0002E-04	613.261	3.3576E-02	-1.8397E-02	-7.5878E-03
7461.547	7.1308E-03	3.7491E-03	1.8690E-03	8.5719E-04	266.635	1.3783E-01	-7.7748E-02	-3.1847E-02
3244.151	2.7937E-02	1.4448E-02	7.5165E-03	3.3855E-03	115.928	3.7898E-01	-2.1645E-01	-8.9895E-02
1410.500	9.8213E-02	5.3812E-02	2.7499E-02	1.2574E-02	50.404	4.7751E-01	-2.1710E-01	-8.2028E-02
613.261	2.7330E-01	1.5727E-01	8.3469E-02	3.7940E-02	21.915			
266.635	4.6122E-01	2.9352E-01	1.5568E-01	7.1987E-02	9.528			
115.928	2.8109E-01	1.0284E-02	-2.0215E-02	-1.4457E-02	4.143			
50.404	1.9748E-02	-6.9626E-01	-6.0783E-01	-3.0747E-01	1.801			
21.915					0.783			
9.528					0.340			
4.143					0.148			
1.801					0.064			
0.783								
0.340								
0.148								
0.064								

f exp.	g exp.
266.635	9.528
115.928	4.143
50.404	1.801
21.915	0.783
9.528	0.340
4.143	0.148
1.801	0.064
0.783	
0.340	
0.148	
0.064	

Tabel B.10. The nonrelativistic basis set for Fr^+. Continued from the previous page.

s exp.	coeff.				
5843211.046	8.4279E-03	3.4046E-03	1.6512E-03	8.4586E-04	-4.0132E-04
2540526.542	-3.8180E-03	-1.5342E-03	-7.4288E-04	-3.8099E-04	1.8067E-04
1104576.757	1.5627E-02	6.3420E-03	3.0771E-03	1.5777E-03	-7.4840E-04
480250.764	5.6681E-03	2.3567E-03	1.1518E-03	5.8739E-04	-2.7933E-04
208804.680	2.8487E-02	1.1748E-02	5.7110E-03	2.9349E-03	-1.3917E-03
90784.643	3.3780E-02	1.4247E-02	6.9778E-03	3.5630E-03	-1.6942E-03
39471.584	7.3063E-02	3.1377E-02	1.5340E-02	7.9190E-03	-3.7536E-03
17161.558	1.1638E-01	5.2190E-02	2.5871E-02	1.3208E-02	-6.2894E-03
7461.547	2.0685E-01	9.8821E-02	4.9141E-02	2.5608E-02	-1.2139E-02
3244.151	2.9986E-01	1.6054E-01	8.2548E-02	4.2202E-02	-2.0176E-02
1410.500	3.1423E-01	1.9075E-01	9.8468E-02	5.2991E-02	-2.5072E-02
613.261	1.3053E-01	-4.2551E-02	-4.0683E-02	-2.8551E-02	1.3579E-02
266.635	6.8450E-03	-5.9333E-01	-5.4464E-01	-3.1669E-01	1.5788E-01
115.928	8.2975E-04	-4.6952E-01	-5.1072E-01	-3.6599E-01	1.8374E-01
50.404	-6.2794E-04	-1.6622E-02	9.0280E-01	1.0405E+00	-5.9215E-01
21.915					
9.528					
4.143					
1.801					
0.783					
0.340					
0.148					
0.064					

Tabel B.11. The relativistic basis set for Fr^+. Continued on the following page.

p exp.	coeff.				d exp.	coeff.		
208804.680	1.4803E-03	-7.7953E-04	-3.9940E-04	-1.8133E-04	7461.547	6.9433E-04	3.7913E-04	1.5131E-04
90784.643	3.0128E-04	-1.5771E-04	-8.3121E-05	-3.7219E-05	3244.151	1.8535E-03	1.0134E-03	4.1326E-04
39471.584	4.1211E-03	-2.1946E-03	-1.1224E-03	-5.1092E-04	1410.500	9.3659E-03	5.1633E-03	2.0651E-03
17161.558	6.4854E-03	-3.4355E-03	-1.7840E-03	-8.0613E-04	613.261	4.0440E-02	2.2487E-02	9.1321E-03
7461.547	1.9894E-02	-1.0815E-02	-5.5433E-03	-2.5288E-03	266.635	1.4913E-01	8.4685E-02	3.4221E-02
3244.151	5.0753E-02	-2.7648E-02	-1.4437E-02	-6.5409E-03	115.928	3.8309E-01	2.1821E-01	8.9017E-02
1410.500	1.3680E-01	-7.8086E-02	-4.0532E-02	-1.8537E-02	50.404	4.6642E-01	2.0251E-01	7.4027E-02
613.261	3.0736E-01	-1.8142E-01	-9.6778E-02	-4.4077E-02	21.915			
266.635	4.3820E-01	-2.6673E-01	-1.3935E-01	-6.4154E-02	9.528			
115.928	2.2837E-01	1.0633E-01	1.0422E-01	5.5724E-02	4.143			
50.404	1.2518E-02	7.0186E-01	6.1333E-01	3.1099E-01	1.801			
21.915					0.783			
9.528					0.340			
4.143					0.148			
1.801					0.064			
0.783								
0.340								
0.148								
0.064								

f exp.	g exp.
266.635	9.528
115.928	4.143
50.404	1.801
21.915	0.783
9.528	0.340
4.143	0.148
1.801	0.064
0.783	
0.340	
0.148	
0.064	

Tabel B.11. The relativistic basis set for Fr^+. Continued from the previous page.

s exp.	coeff.				
5843211.046	2.3300E-04	-7.9236E-05	3.9175E-05	2.2342E-05	-1.3796E-05
2540526.542	7.7589E-05	-2.4835E-05	1.3768E-05	9.2085E-06	-5.5840E-06
1104576.757	1.0262E-03	-3.5272E-04	1.7127E-04	9.4815E-05	-5.8767E-05
480250.764	2.0145E-03	-6.7232E-04	3.4687E-04	2.1088E-04	-1.2924E-04
208804.680	6.5102E-03	-2.2546E-03	1.0940E-03	6.0393E-04	-3.7450E-04
90784.643	1.7266E-02	-5.8804E-03	3.0125E-03	1.8074E-03	-1.1098E-03
39471.584	4.7053E-02	-1.6832E-02	8.2544E-03	4.6022E-03	-2.8525E-03
17161.558	1.1823E-01	-4.3698E-02	2.2574E-02	1.3500E-02	-8.3071E-03
7461.547	2.5536E-01	-1.0910E-01	5.5218E-02	3.1146E-02	-1.9356E-02
3244.151	3.9200E-01	-2.1260E-01	1.1792E-01	7.2277E-02	-4.4754E-02
1410.500	2.7216E-01	-2.2951E-01	1.2998E-01	7.2470E-02	-4.6044E-02
613.261	3.3710E-02	2.8848E-01	-2.0809E-01	-1.1913E-01	7.8052E-02
266.635	1.5404E-03	7.4714E-01	-9.3408E-01	-7.4763E-01	5.0474E-01
115.928	-1.4852E-03	1.8400E-01	2.9444E-01	4.8414E-01	-3.6961E-01
50.404	1.0503E-03	-7.8673E-03	1.1009E+00	1.6917E+00	-1.6562E+00
21.915	-7.0408E-04	2.4811E-03	-2.5625E-02	-1.6593E+00	3.0722E+00
9.528	4.6585E-04	-1.0005E-03	5.4727E-02	-3.4230E-01	-9.8629E-01
4.143					
1.801					
0.783					
0.340					
0.148					
0.064					

Tabel B.12. The nonrelativistic basis set for E119$^+$. Continued on the following page.

p exp.	coeff.				d exp.	coeff.		
1104576.757	-5.7124E-06	-3.0030E-06	2.2514E-06	1.6137E-06	7461.547	1.0284E-03	-6.4643E-04	3.7832E-04
480250.764	-1.4010E-05	-7.6531E-06	2.1858E-06	2.7921E-07	3244.151	4.3084E-03	-2.9379E-03	1.9819E-03
208804.680	-6.8822E-05	-3.6114E-05	2.8223E-05	2.0644E-05	1410.500	2.6208E-02	-1.7089E-02	1.0427E-02
90784.643	-2.9636E-04	-1.5980E-04	7.3900E-05	3.6314E-05	613.261	1.1346E-01	-7.8488E-02	5.1418E-02
39471.584	-1.2236E-03	-6.5073E-04	4.3247E-04	2.8979E-04	266.635	3.5246E-01	-2.4500E-01	1.5504E-01
17161.558	-5.1981E-03	-2.8109E-03	1.5129E-03	8.6759E-04	115.928	5.0853E-01	-3.0470E-01	1.8956E-01
7461.547	-2.0470E-02	-1.1150E-02	6.9150E-03	4.4222E-03	50.404	1.8721E-01	4.6513E-01	-5.3324E-01
3244.151	-7.5479E-02	-4.2609E-02	2.4374E-02	1.4624E-02	21.915	-3.9562E-03	6.6263E-01	-3.4544E-01
1410.500	-2.2502E-01	-1.3462E-01	8.3836E-02	5.3266E-02	9.528	4.6037E-03	2.0246E-02	1.0368E+00
613.261	-4.4423E-01	-2.9261E-01	1.7562E-01	1.0725E-01	4.143			
266.635	-3.5210E-01	-1.3561E-01	7.8664E-02	5.2529E-02	1.801			
115.928	-4.5563E-02	6.6511E-01	-7.4259E-01	-5.7783E-01	0.783			
50.404	-1.2833E-03	4.9139E-01	-1.4154E-01	6.8538E-02	0.340			
21.915	1.6499E-03	-1.7351E-02	1.1119E+00	1.3991E+00	0.148			
9.528	-1.1942E-03	1.9752E-02	6.5557E-02	-1.2859E+00	0.064			
4.143								
1.801								
0.783								
0.340								
0.148								
0.064								

Tabel B.12. The nonrelativistic basis set for E119^{+}. Continued on the following page.

f exp.	coeff.		g exp.
613.261	9.9930E-03	5.4030E-03	4.143
266.635	5.1519E-02	2.8435E-02	1.801
115.928	2.1928E-01	1.2041E-01	0.783
50.404	4.7843E-01	2.4734E-01	0.340
21.915	4.0776E-01	3.2661E-02	0.148
9.528	7.4376E-02	-5.3568E-01	0.064
4.143			0.028
1.801			0.012
0.783			0.005
0.340			
0.148			
0.064			
0.028			

Tabel B.12. The nonrelativistic basis set for $E119^{+}$. Continued from the previous page.

s exp.	coeff.				
5843211.046	2.3300E-04	-7.9236E-05	-3.9174E-05	-2.2342E-05	-1.3796E-05
2540526.542	7.7589E-05	-2.4835E-05	-1.3768E-05	-9.2083E-06	-5.5836E-06
1104576.757	1.0262E-03	-3.5272E-04	-1.7127E-04	-9.4814E-05	-5.8765E-05
480250.764	2.0145E-03	-6.7232E-04	-3.4687E-04	-2.1087E-04	-1.2924E-04
208804.680	6.5102E-03	-2.2546E-03	-1.0940E-03	-6.0393E-04	-3.7449E-04
90784.643	1.7266E-02	-5.8804E-03	-3.0125E-03	-1.8074E-03	-1.1098E-03
39471.584	4.7053E-02	-1.6832E-02	-8.2544E-03	-4.6021E-03	-2.8524E-03
17161.558	1.1823E-01	-4.3698E-02	-2.2574E-02	-1.3500E-02	-8.3068E-03
7461.547	2.5536E-01	-1.0910E-01	-5.5218E-02	-3.1145E-02	-1.9355E-02
3244.151	3.9200E-01	-2.1260E-01	-1.1792E-01	-7.2275E-02	-4.4752E-02
1410.500	2.7216E-01	-2.2951E-01	-1.2998E-01	-7.2469E-02	-4.6042E-02
613.261	3.3710E-02	2.8848E-01	2.0808E-01	1.1913E-01	7.8050E-02
266.635	1.5405E-03	7.4714E-01	9.3408E-01	7.4761E-01	5.0471E-01
115.928	-1.4852E-03	1.8400E-01	-2.9443E-01	-4.8411E-01	-3.6957E-01
50.404	1.0503E-03	-7.8673E-03	-1.1009E+00	-1.6917E+00	-1.6562E+00
21.915	-7.0409E-04	2.4813E-03	2.5621E-02	1.6592E+00	3.0719E+00
9.528	4.6586E-04	-1.0008E-03	-5.4726E-02	3.4236E-01	-9.8593E-01
4.143					
1.801					
0.783					
0.340					
0.148					
0.064					

Tabel B.13. The relativistic basis set for E119+. Continued on the following page.

p exp.	coeff.				d exp.	coeff.		
1104576.757	-6.4010E-05	-3.3612E-05	2.6126E-05	1.9041E-05	7461.547	1.0284E-03	-6.4641E-04	3.7831E-04
480250.764	1.4750E-05	8.0537E-06	-2.2958E-06	-2.9647E-07	3244.151	4.3084E-03	-2.9378E-03	1.9817E-03
208804.680	1.1749E-04	6.1673E-05	-4.8210E-05	-3.5230E-05	1410.500	2.6208E-02	-1.7089E-02	1.0426E-02
90784.643	2.9636E-04	1.5977E-04	-7.3854E-05	-3.6332E-05	613.261	1.1346E-01	-7.8486E-02	5.1414E-02
39471.584	1.2236E-03	6.5081E-04	-4.3258E-04	-2.8972E-04	266.635	3.5245E-01	-2.4499E-01	1.5503E-01
17161.558	5.1981E-03	2.8106E-03	-1.5126E-03	-8.6768E-04	115.928	5.0853E-01	-3.0470E-01	1.8955E-01
7461.547	2.0469E-02	1.1151E-02	-6.9156E-03	-4.4216E-03	50.404	1.8721E-01	4.6510E-01	-5.3316E-01
3244.151	7.5480E-02	4.2608E-02	-2.4372E-02	-1.4625E-02	21.915	-3.9555E-03	6.6264E-01	-3.4550E-01
1410.500	2.2502E-01	1.3462E-01	-8.3840E-02	-5.3260E-02	9.528	4.6038E-03	2.0266E-02	1.0367E+00
613.261	4.4423E-01	2.9260E-01	-1.7560E-01	-1.0725E-01	4.143			
266.635	3.5210E-01	1.3564E-01	-7.8702E-02	-5.2509E-02	1.801			
115.928	4.5568E-02	-6.6515E-01	7.4265E-01	5.7773E-01	0.783			
50.404	1.2750E-03	-4.9128E-01	1.4133E-01	-6.8353E-02	0.340			
21.915	-1.6357E-03	1.7139E-02	-1.1113E+00	-1.3993E+00	0.148			
9.528	1.1706E-03	-1.9382E-02	-6.6662E-02	1.2862E+00	0.064			
4.143								
1.801								
0.783								
0.340								
0.148								
0.064								

Tabel B.13. The relativistic basis set for E119^{+}. Continued on the following page.

f exp.	coeff.		g exp.
613.261	1.3786E-02	7.3588E-03	4.143
266.635	5.8836E-02	3.1925E-02	1.801
115.928	2.3052E-01	1.2384E-01	0.783
50.404	4.7487E-01	2.3713E-01	0.340
21.915	3.9819E-01	2.3834E-02	0.148
9.528	7.5232E-02	-5.1758E-01	0.064
4.143			0.028
1.801			0.012
0.783			0.005
0.340			
0.148			
0.064			
0.028			

Tabel B.13. The relativistic basis set for E119+. Continued from the previous page.

s exp.	p exp.	d exp.
1081067.783	1993.800	7.133
360355.928	591.661	3.108
47703.660	214.227	1.045
10085.764	87.341	0.414
2719.595	38.552	0.213
855.621	17.862	0.070
299.455	8.496	0.030
113.083	4.112	0.018
44.702	1.911	
16.203	0.891	
7.133	0.407	
3.108	0.171	
1.045	0.068	
0.414	0.030	
0.213	0.015	
0.070		
0.030		
0.018		
0.007		
0.003		

Tabel B.14. The nonrelativistic and relativistic basis sets for Ca.

Tabel B.15. The nonrelativistic basis set for Sr.

s exp.	coeff.			p exp.	coeff.		d exp.	coeff.	f exp.
228929.439	-7.1965E-04	2.2755E-04	-9.3056E-05	4736.515	1.3934E-03	-5.7714E-04	140.488	1.5122E-02	49.173
57429.512	-2.6583E-03	8.4462E-04	-3.4475E-04	1525.948	6.8443E-03	-2.9028E-03	63.335	4.3753E-02	23.367
16983.750	-1.1655E-02	3.7144E-03	-1.5221E-03	571.363	3.1295E-02	-1.3207E-02	27.720		10.429
5615.232	-3.9677E-02	1.2953E-02	-5.3019E-03	236.499	1.0268E-01	-4.5640E-02	12.767		4.892
2036.275	-1.1696E-01	3.9923E-02	-1.6526E-02	105.446	2.4764E-01	-1.1302E-01	6.370		2.130
793.685	-2.6556E-01	1.0298E-01	-4.3057E-02	49.173	3.9017E-01	-1.9788E-01	3.404		0.807
328.348	-4.0116E-01	1.9973E-01	-8.7440E-02	23.367			1.429		0.311
140.488	-2.7160E-01	2.1198E-01	-9.8036E-02	10.429			0.471		0.127
63.335	-3.5489E-02	-1.8831E-01	1.0029E-01	4.892			0.166		0.047
27.720				2.130			0.077		
12.767				0.807			0.032		
6.370				0.311					
3.404				0.127					
1.429				0.047					
0.471				0.018					
0.166				0.008					
0.077									
0.032									
0.016									
0.007									
0.003									

Tabel B.16. The relativistic basis set for Sr.

s exp.	coeff.			p exp.	coeff.		d exp.	coeff.	f exp.
228929.439	3.7952E-03	1.2460E-03	-5.1118E-04	4736.515	2.5910E-03	-1.0853E-03	140.488	1.5821E-02	49.173
57429.512	6.1874E-03	2.0501E-03	-8.4155E-04	1525.948	8.4705E-03	-3.6185E-03	63.335	4.3823E-02	23.367
16983.750	2.0383E-02	6.8057E-03	-2.8003E-03	571.363	3.5735E-02	-1.5227E-02	27.720		10.429
5615.232	5.0880E-02	1.7481E-02	-7.2044E-03	236.499	1.0827E-01	-4.8478E-02	12.767		4.892
2036.275	1.3126E-01	4.7193E-02	-1.9638E-02	105.446	2.5328E-01	-1.1616E-01	6.370		2.130
793.685	2.7246E-01	1.1093E-01	-4.6722E-02	49.173	3.8846E-01	-1.9710E-01	3.404		0.807
328.348	3.9201E-01	2.0132E-01	-8.8464E-02	23.367			1.429		0.311
140.488	2.5504E-01	1.9211E-01	-8.8914E-02	10.429			0.471		0.127
63.335	3.2878E-02	-2.2424E-01	1.2499E-01	4.892			0.166		0.047
27.720				2.130			0.077		
12.767				0.807			0.032		
6.370				0.311					
3.404				0.127					
1.429				0.047					
0.471				0.018					
0.166				0.008					
0.077									
0.032									
0.016									
0.007									
0.003									

s exp.	coeff.			p exp.	coeff.	
29226833.650	-5.2819E-06	1.7214E-06	7.7554E-07	48859.030	1.0758E-04	-5.0738E-05
4586662.126	-4.0148E-05	1.3090E-05	5.8971E-06	13391.306	7.6159E-04	-3.5980E-04
996100.266	-2.3514E-04	7.6655E-05	3.4537E-05	4599.757	4.0824E-03	-1.9386E-03
259063.657	-1.1278E-03	3.6822E-04	1.6591E-04	1844.854	1.6353E-02	-7.8502E-03
76980.918	-4.6395E-03	1.5190E-03	6.8482E-04	805.870	5.5501E-02	-2.7272E-02
25361.499	-1.6753E-02	5.5425E-03	2.5020E-03	381.464	1.3535E-01	-6.9323E-02
9070.612	-5.3315E-02	1.8083E-02	8.1946E-03	196.503	2.5489E-01	-1.3790E-01
3469.522	-1.4409E-01	5.2137E-02	2.3841E-02	101.193	3.6869E-01	-2.1254E-01
1403.966	-3.0237E-01	1.2646E-01	5.9124E-02	51.225		
592.874	-3.9927E-01	2.2761E-01	1.1167E-01	24.862		
256.816	-2.1034E-01	1.6520E-01	8.9468E-02	12.277		
114.075	-1.2879E-02	-3.5427E-01	-2.4497E-01	5.959		
52.874				2.811		
25.187				1.365		
12.287				0.642		
5.951				0.273		
2.808				0.106		
1.304				0.053		
0.565				0.028		
0.252				0.011		
0.105				0.005		
0.046				0.002		
0.020						
0.008						
0.004						
0.002						

Tabel B.17. The nonrelativistic basis set for Ba. Continued on the followin page.

d exp.	coeff.	f exp.	g exp.
3469.522	-1.3804E-04	101.193	52.874
1403.966	-7.8001E-04	51.225	25.187
592.874	-4.7914E-03	24.862	12.287
256.816	-2.4692E-02	12.277	5.951
114.075	-9.4625E-02	5.959	2.808
52.874		2.811	1.304
25.187		1.365	0.565
12.287		0.642	0.252
5.951		0.273	0.105
2.808		0.106	0.046
1.304		0.053	
0.565		0.028	
0.252		0.011	
0.105			
0.046			
0.020			
0.008			

Tabel B.17. The nonrelativistic basis set for Ba. Continued from the previous page.

s exp.	coeff.			p exp.	coeff.	
29226833.650	-4.0806E-04	1.4327E-04	6.4851E-05	48859.030	7.9601E-04	-3.8062E-04
4586662.126	-1.0347E-03	3.6392E-04	1.6477E-04	13391.306	2.1172E-03	-1.0173E-03
996100.266	-2.7721E-03	9.7778E-04	4.4289E-04	4599.757	7.6937E-03	-3.7196E-03
259063.657	-6.6606E-03	2.3630E-03	1.0712E-03	1844.854	2.2835E-02	-1.1176E-02
76980.918	-1.5573E-02	5.5793E-03	2.5332E-03	805.870	6.7119E-02	-3.3588E-02
25361.499	-3.5643E-02	1.3010E-02	5.9229E-03	381.464	1.4804E-01	-7.6968E-02
9070.612	-8.0691E-02	3.0443E-02	1.3932E-02	196.503	2.6336E-01	-1.4358E-01
3469.522	-1.7245E-01	6.9601E-02	3.2173E-02	101.193	3.6188E-01	-2.0634E-01
1403.966	-3.1063E-01	1.4321E-01	6.7666E-02	51.225	2.5747E-01	-6.3938E-02
592.874	-3.6899E-01	2.2043E-01	1.0878E-01	24.862		
256.816	-1.7999E-01	9.8412E-02	5.0138E-02	12.277		
114.075	-1.0180E-02	-4.2573E-01	-3.1147E-01	5.959		
52.874	-3.8593E-03	-5.9845E-01	-6.3454E-01	2.811		
25.187				1.365		
12.287				0.642		
5.951				0.273		
2.808				0.106		
1.304				0.053		
0.565				0.028		
0.252				0.011		
0.105				0.005		
0.046				0.002		
0.020						
0.008						
0.004						
0.002						

Tabel B.18. The relativistic basis set for Ba. Continued on the following page.

d exp.	coeff.	f exp.	g exp.
3469.522	-1.2970E-04	101.193	52.874
1403.966	-5.0907E-04	51.225	25.187
592.874	-2.8041E-03	24.862	12.287
256.816	-1.3132E-02	12.277	5.951
114.075	-4.8159E-02	5.959	2.808
52.874	-1.2227E-01	2.811	1.304
25.187		1.365	0.565
12.287		0.642	0.252
5.951		0.273	0.105
2.808		0.106	0.046
1.304		0.053	
0.565		0.028	
0.252		0.011	
0.105			
0.046			
0.020			
0.008			

Tabel B.18. The relativistic basis set for Ba. Continued from the previous page.

s exp.	coeff.				p exp.	coeff.		
303780712.740	8.3086E-07	2.7825E-07	-1.3347E-07	-6.8357E-08	1106448.313	2.2659E-06	-1.1580E-06	-5.9391E-07
54615913.610	5.2252E-06	1.7478E-06	-8.3815E-07	-4.2913E-07	304836.785	1.7660E-05	-8.9902E-06	-4.5731E-06
13644310.630	2.4323E-05	8.1511E-06	-3.9105E-06	-2.0030E-06	92710.067	1.3277E-04	-6.7851E-05	-3.4736E-05
4219580.991	9.4941E-05	3.1746E-05	-1.5223E-05	-7.7933E-06	30701.983	8.4141E-04	-4.3001E-04	-2.1933E-04
1412175.855	3.5015E-04	1.1745E-04	-5.6355E-05	-2.8868E-05	11019.292	4.5364E-03	-2.3351E-03	-1.1963E-03
504524.424	1.1996E-03	4.0169E-04	-1.9266E-04	-9.8634E-05	4275.164	2.0320E-02	-1.0590E-02	-5.4306E-03
188914.813	3.8888E-03	1.3101E-03	-6.2908E-04	-3.2231E-04	1780.816	7.3696E-02	-3.9635E-02	-2.0520E-02
73701.679	1.1950E-02	4.0443E-03	-1.9429E-03	-9.9510E-04	787.396	2.0336E-01	-1.1556E-01	-6.0553E-02
29665.559	3.4766E-02	1.2024E-02	-5.7973E-03	-2.9734E-03	365.047	3.7539E-01	-2.3195E-01	-1.2466E-01
12219.053	9.3752E-02	3.3768E-02	-1.6382E-02	-8.4108E-03	175.495	3.6492E-01	-2.0424E-01	-1.0533E-01
5143.375	2.1560E-01	8.6131E-02	-4.2492E-02	-2.1920E-02	85.158	1.2476E-01	2.4158E-01	2.0325E-01
2222.378	3.6358E-01	1.7935E-01	-9.1639E-02	-4.7656E-02	43.001			
988.070	3.2866E-01	2.3931E-01	-1.3185E-01	-7.0001E-02	21.623			
449.738	9.1211E-02	-1.5155E-02	1.2675E-02	7.3884E-03	10.784			
212.705	1.1324E-03	-5.7201E-01	5.0985E-01	3.0485E-01	5.342			
103.894	7.8590E-04	-4.9571E-01	6.4735E-01	4.4473E-01	2.471			
52.166					1.139			
26.452					0.418			
13.233					0.156			
6.604					0.071			
3.098					0.029			
1.431					0.013			
0.597					0.006			
0.254					0.003			
0.110								
0.048								
0.021								
0.009								
0.004								
0.002								
0.001								

Tabel B.19. The nonrelativistic basis set for Ra. Continued on the following page.

d exp.	coeff.		f exp.	coeff.	g exp.
12219.053	7.9017E-05	-4.2566E-05	787.396	-1.2768E-05	103.894
5143.375	4.1485E-04	-2.2563E-04	365.047	-3.6934E-05	52.166
2222.378	2.5293E-03	-1.3734E-03	175.495	-3.0553E-04	26.452
988.070	1.3351E-02	-7.3335E-03	85.158	-8.9441E-04	13.233
449.738	5.6595E-02	-3.1506E-02	43.001		6.604
212.705	1.7460E-01	-9.9783E-02	43.001		3.098
103.894	3.5243E-01	-2.0154E-01	21.623		1.431
52.166			10.784		0.597
26.452			5.342		0.254
13.233			2.471		0.110
6.604			1.139		0.048
3.098			0.418		
1.431			0.156		
0.597			0.071		
0.254			0.029		
0.110					
0.048					
0.021					
0.009					
0.004					

Tabel B.19. The nonrelativistic basis set for Ra. Continued from the previous page.

s exp.	coeff.				p exp.	coeff.		
303780712.740	6.0958E-04	2.4727E-04	1.2008E-04	-6.1670E-05	1106448.313	3.7175E-04	1.9541E-04	1.0054E-04
54615913.610	1.1342E-03	4.6045E-04	2.2362E-04	-1.1485E-04	304836.785	6.3170E-04	3.3324E-04	1.7161E-04
13644310.630	2.4725E-03	1.0050E-03	4.8817E-04	-2.5075E-04	92710.067	2.0258E-03	1.0725E-03	5.5276E-04
4219580.991	4.4414E-03	1.8098E-03	8.7953E-04	-4.5179E-04	30701.983	5.2963E-03	2.8217E-03	1.4565E-03
1412175.855	8.6813E-03	3.5524E-03	1.7276E-03	-8.8765E-04	11019.292	1.5171E-02	8.1657E-03	4.2258E-03
504524.424	1.5696E-02	6.4687E-03	3.1498E-03	-1.6187E-03	4275.164	4.1996E-02	2.2961E-02	1.1928E-02
188914.813	2.8866E-02	1.2036E-02	5.8723E-03	-3.0199E-03	1780.816	1.0997E-01	6.1907E-02	3.2403E-02
73701.679	5.1629E-02	2.1932E-02	1.0736E-02	-5.5235E-03	787.396	2.4172E-01	1.4189E-01	7.5065E-02
29665.559	9.2748E-02	4.0651E-02	2.0004E-02	-1.0312E-02	365.047	3.7761E-01	2.3205E-01	1.2437E-01
12219.053	1.6193E-01	7.4660E-02	3.7085E-02	-1.9144E-02	175.495	3.1720E-01	1.3039E-01	5.6820E-02
5143.375	2.5900E-01	1.3049E-01	6.5864E-02	-3.4192E-02	85.158	9.4319E-02	-3.3470E-01	-2.7803E-01
2222.378	3.2468E-01	1.8623E-01	9.6525E-02	-5.0302E-02	43.001	1.8630E-03	-5.8158E-01	-5.0477E-01
988.070	2.3386E-01	1.2604E-01	6.3561E-02	-3.3218E-02	21.623			
449.738	5.3609E-02	-2.4251E-01	-1.9248E-01	1.1256E-01	10.784			
212.705	1.0136E-03	-5.9361E-01	-5.9764E-01	3.6883E-01	5.342			
103.894	-9.7985E-05	-3.0305E-01	-2.8810E-01	1.9506E-01	2.471			
52.166	2.1135E-04	-2.1669E-02	7.7439E-01	-8.5219E-01	1.139			
26.452					0.418			
13.233					0.156			
6.604					0.071			
3.098					0.029			
1.431					0.013			
0.597					0.006			
0.254					0.003			
0.110								
0.048								
0.021								
0.009								
0.004								
0.002								
0.001								

Tabel B.20. The relativistic basis set for Ra. Continued on the following page.

d exp.	coeff.		f exp.	coeff.	g exp.
12219.053	3.3497E-04	-1.8372E-04	787.396	-6.8570E-04	103.894
5143.375	8.8982E-04	-4.8874E-04	365.047	-2.6727E-03	52.166
2222.378	4.3336E-03	-2.3933E-03	175.495	-1.4400E-02	26.452
988.070	1.7712E-02	-9.8455E-03	85.158	-4.9796E-02	13.233
449.738	6.5332E-02	-3.6838E-02	43.001	-1.2884E-01	6.604
212.705	1.8433E-01	-1.0581E-01	21.623		3.098
103.894	3.5406E-01	-2.0122E-01	10.784		1.431
52.166	3.8480E-01	-1.7054E-01	5.342		0.597
26.452			2.471		0.254
13.233			1.139		0.110
6.604			0.418		0.048
3.098			0.156		
1.431			0.071		
0.597			0.029		
0.254					
0.110					
0.048					
0.021					
0.009					
0.004					

Tabel B.20. The relativistic basis set for Ra. Continued from the previous page.